Ministry of Higher Education and Scientific Research

Syrian Virtual University

Program Master of BIMM

PHOTOGRAMMETRY-DRIVEN HBIM: Improving Accuracy and Efficient Integration in Construction and Heritage Documentation - A Study on Data Accuracy, Usability, and Workflow Optimization

- *Pilot Case Study – Al-Takiyya Al-Rifa'aia Al-Ikhlasia, Al-Bayyada, Aleppo, Syria*
- *Main Case Study – Jami' Al-Tunbugha, Sahet Al-Melh, Aleppo, Syria*

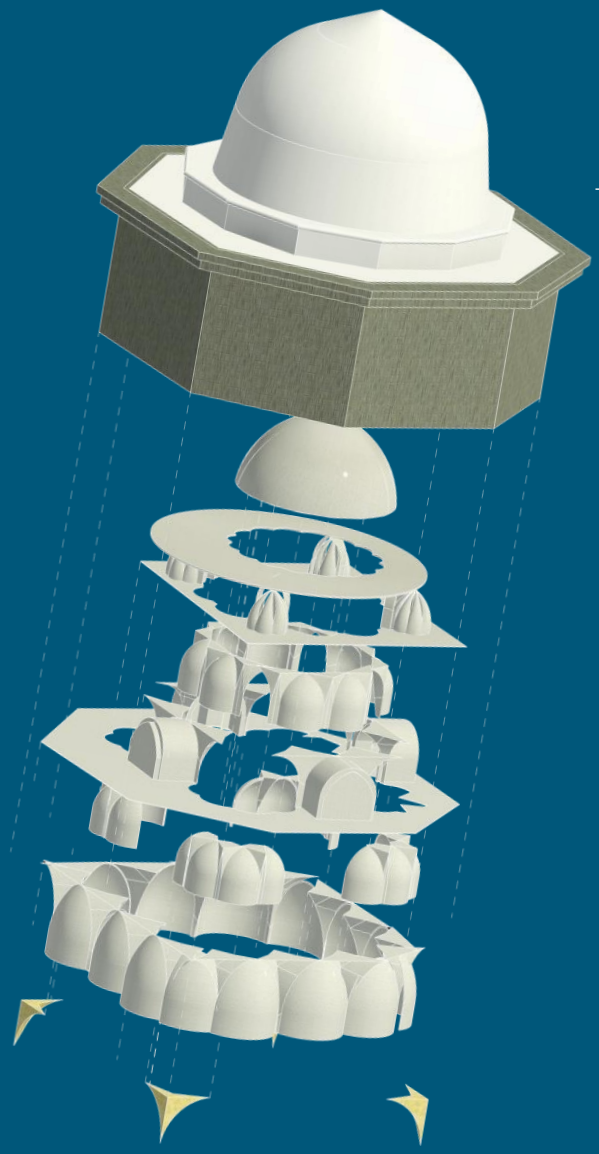

Thesis Submitted for the Degree of Master of Qualification and Specialization in Building Information Modeling and Management (BIMM)

RESEARCHER NAME

Eyyas Abras

RESEARCHER ID

213192

SUPERVISOR NAME

Dr. Eng. Ahmad Yasser Tachouli

YEAR

2025-2025

[English Version]

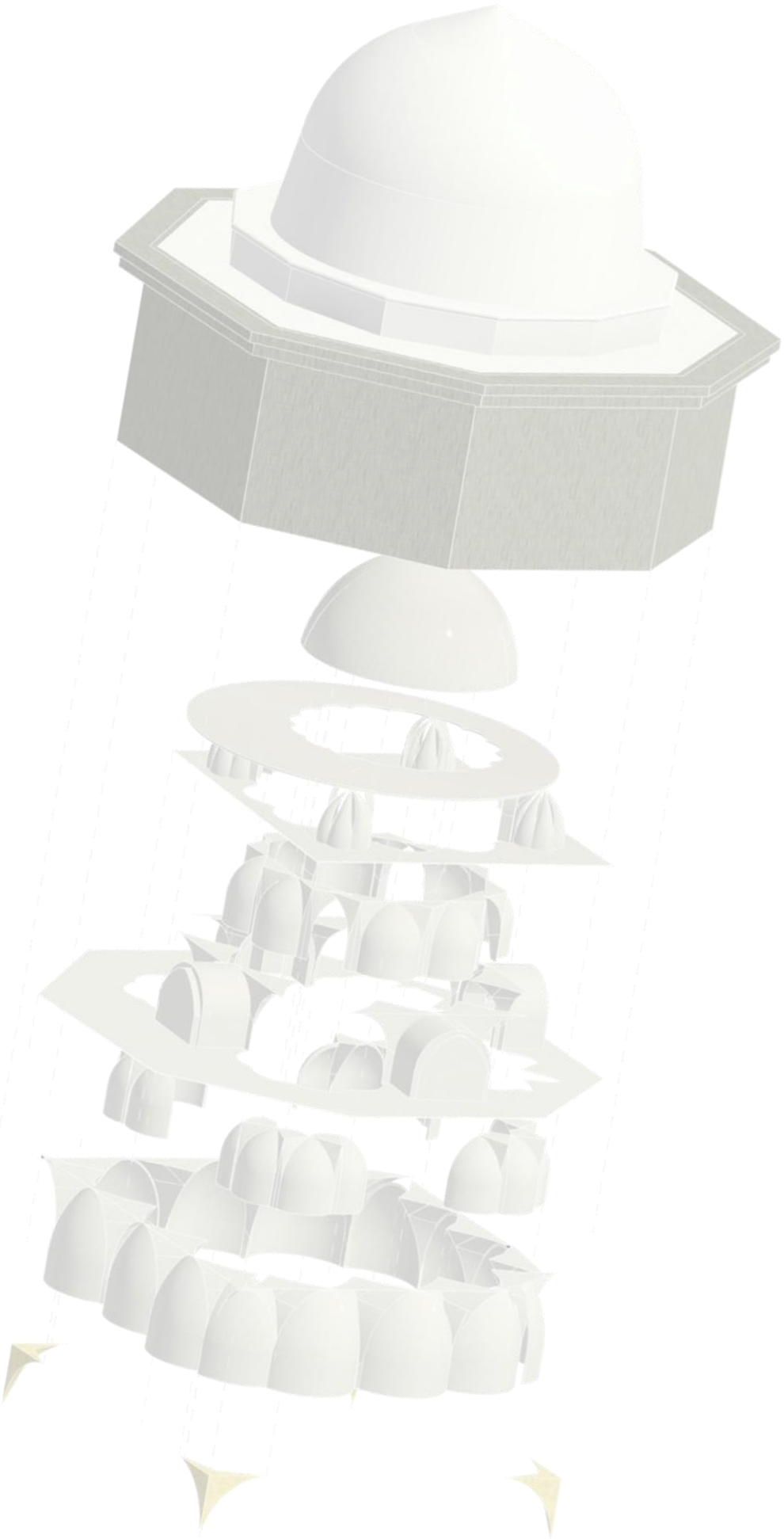

ACKNOWLEDGEMENT

The researcher wishes to express profound gratitude to **Professor Ahmad Yasser Tachouli**, whose expert guidance, insightful feedback, and unwavering support were indispensable to the successful completion of this thesis. His academic rigor, patience, and invaluable advice have left a lasting impact on the researcher's scholarly development.

Appreciation is also extended to the Master's Programme Staff of **Building Information Management and Modeling, Syrian Virtual University**, for their constructive comments and intellectual guidance throughout the course of this research and throughout the entire Master's programme. Particular thanks are due to **Professor Sonia Ahmed**, **Ms. Walaa Al-Janan,** and **Professor Muslim Shamia** whose contributions and assistance were of great significance during the preparation of this work.

The researcher also wishes to extend sincere appreciation to **UNICEF** for providing the necessary support and flexibility that enabled the timely completion of this thesis. The opportunity to balance professional responsibilities with academic pursuits was made possible through the organization's understanding and encouragement, for which the author is deeply grateful.

The researcher further wishes to acknowledge **ICCROM** (International Centre for the Study of the Preservation and Restoration of Cultural Property) as the first institution to provide support in the pursuit of a professional career and academic knowledge in the field of cultural heritage preservation. The training opportunities, guidance, and encouragement received from ICCROM have been instrumental in shaping the author's academic path and professional aspirations.

The researcher also extends gratitude to the **Directorate of Tourism** and **Directorate of Awqaf** for their valuable cooperation in granting approval and facilitating access to public heritage buildings. Their support was essential in enabling the collection of relevant

data and the advancement of this research. Particular thanks are due to **Arch. Nayla Chahoud**, and **Professor Wasila Sammani.**

The researcher is further indebted to colleagues and peers, whose discussions and collaboration provided an enriching academic environment that greatly enhanced the quality of this study; Special thanks to **Arch. Hoor Al-Mahlool, Eng. Abdulla Attar, Eng. Saria Hindawi**, and **Asst. Eng. Ahmad Kelzia**. Also, special thanks to the owner of Al-Takiyya Al-Rifa'aia Al-Ikhlasia, **Mr. Mohammed Mo'utasem Al-Rifai**, and the guard of the Tunbugha Mosque, **Mr. Mohammed Dammamet Al-Lolo.**

Above all, the researcher highly acknowledges with deep appreciation the unwavering technical and administrative support, on-site work, team coordination, encouragement, and patience of **Eng. Alaa Doghan,** who has been an enduring source of strength inspiration, , and a bridge that eased the challenges of being frequently away from Aleppo throughout this academic journey.

Eyyas Abras

ABSTRACT

The destruction of cultural heritage in conflict-affected regions presents an urgent challenge for conservation, recovery, and the safeguarding of collective memory. In Aleppo, Syria, monuments such as Al-Takiyya Al-Rifa'aia and Al-Tunbugha Mosque have suffered severe damage, underscoring the need for accurate, efficient, and sustainable documentation methods. This research responds to that need by developing, applying, and evaluating a methodological framework that integrates photogrammetry and Heritage Building Information Modeling (HBIM), benchmarked against surveying standards.

The study adopts a two-stage case study design. A pilot case (Al-Takiyya al-Rifaʿia al-Ikhlasia) tested photogrammetry-to-HBIM workflows, identified limitations, and guided methodological refinements. The main case (Al-Tunbugha Mosque) applied the refined approach, enhanced dense point clouds, incorporating UAV-based image acquisition and HBIM modeling at varying Levels of Detail (LoD 300–500). Accuracy was evaluated through comparisons with ground control points, using metrics such as coordinate deviations (ΔX, ΔY, ΔZ), distance deviations (Δd), 3D errors (Δ3D), angular deviations (Δθ), and statistical measures (bias, MAE, RMSE, P95). Performance indicators—time, cost, computational resources, and visualization quality—were also systematically assessed.

Results demonstrate that photogrammetry can achieve sub-centimetric to centimetric accuracy when validated against survey benchmarks, producing models suitable for conservation planning. HBIM added semantic richness and long-term management potential but required compromises between geometric fidelity and modeling effort. In this study, all architectural elements and components were modeled at LoD 500, ensuring maximum geometric and semantic detail, particularly valuable for conservation of fragile inscriptions and fine features. The comparative analysis of the pilot and main studies revealed trade-offs between accuracy and efficiency, highlighting the practical value of combining photogrammetry and HBIM within a unified workflow.

The research makes three contributions. Methodologically, it offers a validated workflow that integrates photogrammetry and HBIM, tested under post-conflict conditions. Practically, it provides a digital record of Aleppo's heritage, supporting conservation planning and future reconstruction. Academically, it addresses a gap in Syrian heritage studies by providing systematic evidence of accuracy and performance, linking international documentation standards (CIPA/ICOMOS, BIM tolerances) to local application.

This study demonstrates that digital workflows, when rigorously validated, can deliver both accuracy and usability for heritage documentation in fragile contexts. It proposes a replicable framework for Syrian and other post-conflict heritage sites, contributing to the international discourse on digital heritage, conservation, and the creation of sustainable "digital twins" of cultural monuments at risk.

TABLE OF CONTENTS

LIST OF FIGURES

LIST OF TABLES

LIST OF ACRONYMS

Acronym	Full Form
2.5D	Two-and-a-Half Dimensional
AI	Artificial Intelligence
BIM	Building Information Modeling
CAD	Computer-Aided Design
CIPA	International Committee for Architectural Photogrammetry (ICOMOS Scientific Committee)
CSV	Comma-Separated Values
DEM	Digital Elevation Model
DTM	Digital Terrain Model
DSM	Digital Surface Model
EO	Exterior Orientation
GCP	Ground Control Point
GIS	Geographic Information System
GNSS	Global Navigation Satellite System
GPS	Global Positioning System
HBIM	Historic Building Information Modeling
ICCROM	International Centre for the Study of the Preservation and Restoration of Cultural Property
ICOMOS	International Council on Monuments and Sites
IFC	Industry Foundation Classes (open BIM format)
IR	Infrared
LAS	LiDAR Point Cloud Format
LiDAR	Light Detection and Ranging
LOA	Level of Accuracy
LOD	Level of Detail
MAE	Mean Absolute Error
NDVI	Normalized Difference Vegetation Index
OBJ	Object File Format
OUV	Outstanding Universal Value
P95	95th Percentile
RGB	Red-Green-Blue (Color Model)
REVIT	Autodesk Revit (BIM software)
RMSE	Root Mean Square Error

Acronym	Full Form
SD	Standard Deviation
TLS	Terrestrial Laser Scanning
UAS	Unmanned Aerial System
UAV	Unmanned Aerial Vehicle
UNESCO	United Nations Educational, Scientific and Cultural Organization

LIST OF DEFINITIONS (GLOSSARY)

Term / Acronym	Definition
2.5D	A surface model that represents height values but does not capture full 3D volume; often used in terrain modeling.
AI (Artificial Intelligence)	The simulation of human intelligence by computer systems, including tasks such as learning, reasoning, and problem-solving.
Algorithm	A step-by-step procedure for solving a problem or performing a computation.
BIM (Building Information Modeling)	A digital representation of the physical and functional characteristics of a facility, enabling data-rich, multi-disciplinary collaboration.
CAD (Computer-Aided Design)	The use of software to create precision drawings or models of buildings, structures, or objects.
CIPA	International Committee for Architectural Photogrammetry (ICOMOS Scientific Committee), focusing on heritage documentation standards.
CSV (Comma-Separated Values)	A simple file format used for tabular data exchange, where values are separated by commas.
DEM (Digital Elevation Model)	A digital representation of terrain elevations, typically depicting the bare-earth surface.
Documentation	A systematic and detailed record (reports, drawings, photographs, maps, etc.) of an artifact or building, created before, during, and after interventions, serving as a permanent reference.
DSM (Digital Surface Model)	A digital model that represents the Earth's surface including objects such as buildings, vegetation, and infrastructure.
DTM (Digital Terrain Model)	A digital representation of the ground surface that excludes objects like vegetation and buildings.
EO (Exterior Orientation)	The external orientation of a camera refers to the position and orientation of the camera in 3D space at the moment an image is captured, expressed relative to a defined coordinate system (usually the object or ground reference system).
GCP (Ground Control Point)	A known geographic location measured precisely (often with a total station or GNSS), used to georeference and scale photogrammetric models.
Georeferencing	Aligning spatial data (images, maps) with geographic coordinates.
Geomatics	A broad field integrating technologies and sciences for collecting, analyzing, managing, and visualizing spatial (georeferenced) data.
GIS (Geographic Information System)	A framework for managing, analyzing, and visualizing spatial and geographic data.
GNSS (Global Navigation Satellite System)	A general term for satellite systems that provide positioning, navigation, and timing (includes GPS, GLONASS, Galileo).
GPS (Global Positioning System)	A GNSS operated by the United States, widely used for positioning and navigation.
HBIM (Historic Building Information Modeling)	The application of BIM specifically for documenting, analyzing, and managing cultural heritage buildings.

Term / Acronym	Definition
Heritage	Our legacy from the past, what we live with today, and what we pass on to future generations. Cultural and natural heritage are both irreplaceable sources of life and inspiration.
ICCROM	International Centre for the Study of the Preservation and Restoration of Cultural Property.
ICOMOS	International Council on Monuments and Sites.
IFC (Industry Foundation Classes)	An open standard file format for exchanging BIM data across software platforms.
Immovable Tangible Heritage	Architectural monuments, groups of buildings, and sites with historical, aesthetic, or scientific value.
Inspection	The first step in studying a heritage building, based on visual observation and/or scientific tools, to assess construction materials, structure, and signs of damage.
Intangible Heritage	Traditions or living expressions inherited from ancestors and passed to descendants (e.g., oral traditions, performing arts, rituals, festive events, knowledge, and traditional crafts).
IR (Infrared)	Electromagnetic radiation with longer wavelengths than visible light, often used in remote sensing.
LAS	A standard file format for storing LiDAR point cloud data.
LiDAR (Light Detection and Ranging)	A remote sensing method that uses laser light to measure distances and generate 3D point clouds of surfaces.
LoA (Level of Accuracy)	A measure that defines the expected deviation or tolerance of geometric data.
LoD (Level of Detail)	The degree of completeness or granularity in a digital model, ranging from coarse outlines to highly detailed representations.
MAE (Mean Absolute Error)	A statistical measure representing the average magnitude of absolute deviations between computed and reference values.
Movable Tangible Heritage	Cultural items of artistic, historical, or archaeological significance (e.g., art, manuscripts, books) that are not fixed to a location.
NDVI (Normalized Difference Vegetation Index)	An index calculated from visible and near-infrared light, used to assess vegetation health.
OBJ	A standard 3D file format used to store geometry and surface attributes of models.
Outstanding Universal Value (OUV)	Cultural and/or natural significance so exceptional that it transcends national boundaries and is of common importance for present and future generations of humanity.
P95 (95th Percentile)	A statistical metric indicating the value below which 95% of observed errors fall.
Photogrammetry	The science of making measurements from photographs, often used in 3D modeling of buildings and landscapes.
Projection System	A one-to-one mathematical relationship between points on the Earth's curved surface (geographic coordinates) and their representation on a plane (projected coordinates).
RGB (Red-Green-Blue)	A color model in which colors are represented as combinations of red, green, and blue light.

Term / Acronym	Definition
REVIT	A BIM software developed by Autodesk, used for parametric modeling and HBIM applications.
RMSE (Root Mean Square Error)	A statistical measure representing the square root of the average of squared deviations between computed and reference values.
SD (Standard Deviation)	A measure of the dispersion of data points from their mean value.
TLS (Terrestrial Laser Scanning)	A ground-based method of laser scanning used to capture high-resolution 3D point clouds of surfaces and structures.
UAV (Unmanned Aerial Vehicle)	An aerial platform (drone) used for image capture in photogrammetry.
UAS (Unmanned Aerial System)	The UAV together with its ground control equipment and communication system.
UNESCO	United Nations Educational, Scientific and Cultural Organization.

LIST OF ONLINE SUPPLEMENTARY MATERIALS

No.	File Name / Description	Link
Pilot Case Study - Al-Takiyya Al-Refa'aia Al-Ikhalsia		Open here
00	**Data Acquisition** ▪ 00 GCPs ▪ 01 DWG Surveying Docs ▪ 02 Raw Photos ▪ 03 Raw Videos and Photos (Drone)	Download here
01	**Data Processing (Photogrammetry)** ▪ Agisoft .psx files and associated files.	Download here
02	**Photogrammetry Outputs** ▪ 00 Orthomosaic ▪ 01 Point Clouds (RCP) ▪ 02 Dense Point Clouds (Medium) ▪ 03 3D Model Videos	Download here
03	**CAD Outputs** ▪ 00 Orthomosaic-Derived CAD Drawings ▪ 02 PDFs and JPEGs ▪ 03 Total Station-Derived CAD Drawings	Download here
04	**HBIM Outputs** ▪ 00 Revit Working Files ▪ 01 HBIM Output Sheets ▪ 02 Supporting Documents	Download here
05	**Accuracy Analysis**	Download here
Main Case Study - Al-Tunbugha Mosque		Open here
00	**Data Acquisition** ▪ 00 GCPs ▪ 01 DWG Surveying Docs ▪ 02 Raw Photos ▪ 03 Raw Videos and Photos (Drone)	Download here
01	**Data Processing (Photogrammetry)** ▪ Agisoft .psx files and associated files.	Download here
02	**Photogrammetry Outputs** ▪ 00 Orthomosaic ▪ 01 Point Clouds (RCP) ▪ 02 Dense Point Clouds (Medium) ▪ 03 3D Model Videos	Download here

03	**CAD Supporting Outputs (Not Used)** ▪ 00 Orthomosaic-Derived CAD Drawings ▪ 02 PDFs and JPEGs ▪ 03 Total Station-Derived CAD Drawings	Download here
04	**HBIM Outputs** ▪ 00 Revit Working Files ▪ 01 HBIM Output Sheets ▪ 02 HBIM Output Rendered Scenes ▪ 03 HBIM Output Rendered Videos ▪ 04 Supporting Documents	Download here
05	**Accuracy Analysis**	Download here
Bibliography and References		Open here

CHAPTER 1. INTRODUCTION

1.1 BACKGROUND AND RATIONALE

The documentation of cultural heritage is a critical endeavor, particularly in regions affected by armed conflict. Historical monuments and traditional urban fabrics represent not only architectural achievements but also bearers of cultural identity and collective memory. When these assets are damaged or destroyed, the loss extends beyond material fabric, impacting community resilience, cultural continuity, and prospects for post-conflict recovery. In such contexts, systematic documentation becomes essential, both as a safeguard for irreplaceable knowledge and as a foundation for conservation, reconstruction, and future scholarship.

In recent decades, digital technologies have transformed the field of heritage documentation. Photogrammetry has enabled the rapid generation of metrically accurate 3D models from images, while CAD platforms have supported the production of detailed drawings and orthographic representations. More recently, **Heritage Building Information Modeling (HBIM)** has emerged as a powerful tool, integrating geometric accuracy with semantic data, enabling not only visualization but also conservation planning, condition monitoring, and lifecycle management. These technologies collectively respond to the urgent need for accurate, reliable, and sustainable records in fragile contexts.

The city of **Aleppo**, with its rich heritage, has been severely affected by conflict, resulting in extensive damage to monuments, mosques, and traditional urban structures. Among these, the **heritage of both Al-Takiyya Al-Refa'aia and Al-Tunbugha Mosque** stands as cases of both architectural significance and vulnerability. Documenting such monuments in the aftermath of conflict poses specific challenges: limited site access, structural instability, and resource constraints. At the same time, it presents an opportunity to test and refine digital workflows that balance accuracy, efficiency, and usability for heritage at risk.

Against this backdrop, this research is motivated by the dual imperative of safeguarding endangered heritage and advancing methodological approaches for digital documentation in post-conflict settings. By applying and evaluating a photogrammetry-to-HBIM workflow, the study aims to contribute both to the academic discourse on digital heritage and to the practical needs of documentation and conservation in Syria.

1.2 PROBLEM STATEMENT

Traditional documentation methods—such as manual surveying and CAD-based drafting—have long been used to record architectural heritage. While reliable, these approaches are time-consuming, labor-intensive, and often limited in precision, particularly when applied to complex or irregular historic geometries. Their dependence on selective measurements can also result in partial representations that fail to capture the full dimensional and material complexity of heritage structures.

In contrast, photogrammetry and HBIM offer the potential for greater efficiency, accuracy, and semantic richness. Photogrammetry can generate dense point clouds and textured models rapidly and at relatively low cost, while HBIM provides an integrated environment for structuring geometric and non-geometric information. Yet, these digital methods are not without challenges. Their outputs must be validated against established survey benchmarks (e.g., total station measurements, international accuracy standards) to ensure that they meet the tolerances required for conservation and reconstruction.

Despite international advances, there is a notable lack of systematic studies in the Syrian heritage context that evaluate digital workflows through both accuracy and performance metrics. Existing initiatives often emphasize visual results or emergency recording, without rigorous assessment of deviations (ΔX, ΔY, ΔZ, Δd, $\Delta 3D$, angular errors) or analysis of processing time, cost, and usability. This gap is particularly critical in post-conflict Aleppo, where reliable documentation is urgently needed to guide conservation and rebuilding efforts.

Accordingly, the research problem addressed in this study is the absence of validated, performance-tested digital workflows for heritage documentation in Syria—a gap that

limits both immediate conservation actions and the development of replicable methodologies for cultural heritage at risk.

1.3 RESEARCH AIM AND OBJECTIVES

1.3.1 Research Aim

The aim of this study is to develop, apply, and evaluate a methodological framework for heritage building documentation that integrates photogrammetry and Heritage Building Information Modeling (HBIM), validated against surveying standards. The framework seeks to balance accuracy, efficiency, and usability, with specific application to the documentation of conflict-affected heritage in Aleppo.

1.3.2 Research Objectives

To achieve this aim, the study pursues the following objectives:

i. To conduct a pilot study of Al-Takiyya Al-Refa'aia testing photogrammetric documentation workflows and identifying initial challenges and opportunities.

ii. To refine the workflow methodology for application in the main case study of Al-Tunbugha Mosque.

iii. To evaluate spatial accuracy—including linear deviations (Δd), 3D positional errors (Δ3D), relative error, and angular deviation—against international documentation thresholds (CIPA/ICOMOS standards, BIM LoD tolerances, and surveying benchmarks).

iv. To assess performance indicators, including time, cost, computational resources, and visualization quality, as measures of workflow efficiency and usability.

v. To synthesize findings into a methodological framework tailored for heritage documentation in Syria, with potential for replication in other post-conflict or at-risk contexts.

1.4 RESEARCH QUESTIONS

This study is guided by a set of interrelated research questions that address both the technical and practical dimensions of heritage documentation in post-conflict contexts:

i. **Accuracy** – How accurate are photogrammetric and HBIM outputs when benchmarked against independent survey data (total station measurements)?

ii. **Level of Detail** – To what extent can HBIM models represent architectural complexity and decorative elements at different Levels of Detail (LoD 300–500)?

iii. **Performance Trade-offs** – What are the comparative strengths and limitations of photogrammetry-Driven HBIM in terms of time, cost, resources, and visualization quality?

iv. **Framework Development** – How can integrated accuracy and performance evaluation frameworks support reliable, replicable heritage documentation in conflict-affected regions such as Aleppo?

1.5 SIGNIFICANCE OF THE STUDY

This research holds significance at methodological, practical, and academic levels.

Methodological contribution. The study develops and validates a workflow that combines photogrammetry, CAD, and HBIM, benchmarked against survey standards. By systematically integrating accuracy assessment (Δd, Δ3D, angular deviations, RMSE, P95) with performance evaluation (time, cost, visualization), the research offers a replicable framework for balancing fidelity, efficiency, and usability in digital heritage documentation.

Practical contribution. Applied to Aleppo's heritage, specifically Al-Takiyya Al-Refa'aia and Al-Tunbugha Mosque, the research provides a digital record that supports conservation planning in a post-conflict context. The outputs serve not only as accurate references for restoration but also as tools for risk management and decision-making in fragile environments where heritage is under threat.

Academic contribution. The study enriches the literature on digital heritage by providing comparative evidence of accuracy and performance across photogrammetry and HBIM. It addresses a major gap in research on Syrian heritage sites, where systematic accuracy/performance evaluations are scarce. In doing so, it positions the Al-Takiyya Al-

Refa'aia and Al-Tunbugha cases as both a local intervention and a model with broader relevance for post-conflict heritage documentation worldwide.

1.6 RESEARCH ASSUMPTIONS

The present study rests on a set of underlying assumptions that shape the methodological framework and guide the interpretation of results. These assumptions were necessary to define the scope of inquiry, ensure methodological coherence, and enable meaningful comparison between survey, photogrammetric, and HBIM outputs. The key assumptions are as follows:

i. **Survey control accuracy.** Total station measurements are assumed to represent the most reliable reference, or "ground truth," with millimeter-level precision sufficient for benchmarking photogrammetric and HBIM outputs.

ii. **Software consistency.** Photogrammetric processing software (Agisoft Metashape) and modeling platforms (AutoCAD, Revit) are assumed to perform calibration, adjustment, and coordinate transformations consistently, without introducing systematic distortions beyond their documented accuracy limits.

iii. **Environmental stability.** The architectural structures under study are assumed to have remained geometrically stable during the data acquisition period, with no measurable deformations, displacements, or alterations between the survey and photogrammetry campaigns.

iv. **Data interoperability.** Exported datasets (point clouds, meshes, orthophotos, CAD drawings) are assumed to be interoperable across different software environments, with any discrepancies arising from file conversions or format specifications considered negligible.

v. **Standards applicability.** International documentation accuracy standards—particularly CIPA/ICOMOS guidelines and BIM Level of Development (LoD)

tolerances—are assumed to be relevant and transferable to the Syrian heritage context.

These assumptions establish the foundation upon which the evaluation of accuracy and performance is conducted. They also define the conditions under which the findings of this study can be interpreted, compared, and generalized to other heritage documentation contexts.

1.7 SCOPE AND LIMITATIONS

Geographic scope. The study focuses on the city of Aleppo, with both a pilot and a main case study undertaken on historic heritage.

Methodological scope. The research evaluates a workflow that integrates photogrammetry and Heritage Building Information Modeling (HBIM). Levels of Development (LoD) ranging from 300 to 500 are considered, with selective application of higher LoDs for elements of architectural or conservation significance. The analysis emphasizes accuracy evaluation (Δd, Δ3D, angular deviation, relative error) and performance assessment (time, cost, visualization, and usability).

Limitations. Several constraints shaped the conduct of the study:

i. **Restricted field access:** Security conditions, limited permits, and structural instability of monuments restricted the duration and extent of on-site data collection.

ii. **Equipment and software constraints:** The reliance on available cameras, UAVs, total stations, and processing software limited the achievable resolution and processing speed, influencing model fidelity and efficiency.

iii. **Contextual challenges:** Working in a post-conflict environment presented logistical and geopolitical difficulties, including limited site accessibility, scarce resources, and the urgency of documentation under fragile conditions.

1.8 STRUCTURE OF THE THESIS

The thesis is organized into **eight chapters**, supported by supplementary lists and appendices. Each chapter addresses a specific stage of the research process, while together they contribute to the development and validation of a photogrammetry-to-HBIM workflow for post-conflict heritage documentation in Aleppo.

Chapter 1 – Introduction

Establishes the background and rationale, outlines the research problem, aims, objectives, and questions, and sets out the significance, assumptions, scope, and limitations of the study.

Chapter 2 – Literature Review

Examines key themes in heritage documentation, including international definitions and values of cultural heritage, methods of inspection and recording, photogrammetry, geomatics, and HBIM. It also reviews accuracy and performance evaluation approaches, analytical frameworks, and previous studies, identifying gaps that this research seeks to address.

Chapter 3 – Methodology

Describes the overall research design and framework, including an exploratory review, the case study approach, and site selection. It details instruments, software, data acquisition and processing, and outlines the accuracy, performance, and analytical frameworks applied to both the pilot and main case studies.

Chapter 4 – Pilot Case Study Results: Al-Takiyya al-Rifaʿia al-Ikhlasia

Presents the results of the pilot study, including historical background, data acquisition, photogrammetry outputs, CAD and HBIM processes, and accuracy/performance evaluation. The chapter concludes with lessons learned that inform refinements to the main case study.

Chapter 5 – Main Case Study Results: Al-Tunbugha al-Nasiri Mosque

Applies the refined methodology to the main case study, providing historical context, data acquisition, photogrammetry and HBIM outputs, and detailed accuracy and performance analyses. Comparative observations are drawn between the pilot and main studies.

Chapter 6 – Conclusions and Recommendations

Summarizes the findings of both case studies and their comparative analysis. It outlines the methodological, practical, and academic contributions of the research, acknowledges its technical, methodological, and contextual limitations, and provides recommendations for future research.

Chapter 7 – Bibliography

Lists all sources referenced throughout the thesis in accordance with academic conventions.

Chapter 8 – Appendices

Provides supplementary material, including detailed damage mapping, classification of alteration phenomena, and categories of building damage that support the main analysis.

CHAPTER 2. LITERATURE REVIEW

2.1 INTRODUCTION

The purpose of this literature review is to situate the research within the broader field of cultural heritage documentation and to identify the theoretical and methodological foundations that inform the study. By engaging with existing scholarship, international standards, and applied case studies, the chapter clarifies both the opportunities and the limitations of current practices, while highlighting the gaps that this thesis aims to address.

Three key themes guide the discussion. The **first is heritage documentation**, including its objectives, evolution, and the frameworks established by international organizations for safeguarding architectural and cultural assets. **The second is the role of digital technologies—notably photogrammetry and Heritage Building Information Modeling (HBIM)**—that have transformed the ways in which historic structures are recorded, analyzed, and managed. The third theme focuses on **accuracy and performance evaluation**, a critical dimension that determines whether digital documentation can be trusted for conservation, reconstruction, and long-term management.

By organizing the literature around these themes, the chapter provides a foundation for the methodological choices in this study. It also establishes the context for the two cases of Al-Takiyya Al-Refai'a and Al-Tunbugha Mosque, where photogrammetry-to-HBIM workflows are tested against rigorous accuracy thresholds and performance measures in a post-conflict Syrian heritage setting.

2.2 HERITAGE DOCUMENTATION IN POST-CONFLICT CONTEXTS

The documentation of architectural heritage in post-conflict contexts presents a unique set of challenges. Sites affected by war are often unstable, inaccessible, and at high risk of further deterioration. Structural instability, the presence of unexploded ordnance, and restricted access due to security concerns complicate data collection. Moreover, the urgency of post-conflict environments frequently demands rapid recording methods, creating tensions between the need for speed and the requirement for accuracy. In such conditions, traditional surveying approaches are often impractical, leading to increased

reliance on digital tools such as photogrammetry, UAV-based surveys, and, where possible, laser scanning.

International guidelines emphasize the critical importance of heritage documentation as both an emergency measure and a foundation for long-term recovery. UNESCO advocates for safeguarding cultural heritage as a component of peacebuilding and sustainable development, while ICCROM has highlighted documentation as a core principle in conservation planning. ICOMOS, through its charters and scientific committees such as CIPA, has set forth standards on accuracy, transparency, and methodological rigor, insisting that records produced under crisis conditions must remain scientifically credible and verifiable. These international frameworks provide not only technical guidance but also an ethical mandate: documentation should safeguard cultural value, ensure reproducibility, and remain usable for future interventions.

Accuracy and reliability acquire heightened importance in post-conflict reconstruction efforts. Digital records often serve as the only surviving references for monuments that have been partially or entirely destroyed. Inaccurate documentation risks distorting architectural knowledge and may undermine authenticity in reconstruction projects. Conversely, precise and reliable datasets enable conservation professionals to develop effective stabilization, restoration, and adaptive reuse strategies that respect historical integrity. Within the Syrian context, the careful application of photogrammetry-to-HBIM workflows responds directly to these imperatives, ensuring that documentation serves not only as an academic exercise but as a practical tool for safeguarding and recovering endangered heritage.

2.2.1 Heritage Definition

Heritage is our legacy from the past, what we live with today, and what we pass on to future generations. Our cultural and natural heritage are both irreplaceable sources of life and inspiration.[1]

[1] (Tandon, 2018)

Because of their exceptional qualities, they can be considered to be of Outstanding Universal Value and as such worthy of special protection against the dangers which increasingly threaten them.

2.2.2 Types of Cultural Heritage

2.2.2.1 *Intangible Heritage*

Includes traditions or living expressions inherited from our ancestors and passed on to our descendants, such as oral traditions, performing arts, social practices, rituals, festive events, knowledge and practices concerning nature and the universe or the knowledge and skills to produce traditional crafts.

2.2.2.2 *Movable Tangible Heritage*

Physically existing cultural items of artistic, historical, archaeological, or documentary significance—such as works of art, manuscripts, books, and other objects—that are not fixed to a location and can be transported, thereby forming an essential part of humanity's cultural heritage.

2.2.2.3 *Immovable Tangible Heritage*

Monuments: architectural works, works of monumental sculpture and painting, elements or structures of an archaeological nature, inscriptions, cave dwellings and combinations of features, which has values from the point of view of history, art or science.

Groups of buildings (ensembles): groups of separate or connected buildings which, because of their architecture, their homogeneity or their place in the landscape, have values from the point of view of history, art or science.

Sites: works of man or the combined works of nature and man, and areas including archaeological and under water archaeological sites which has values from the historical, aesthetic, ethnological or anthropological point of view

2.2.3 Values, Significances and OUV

The term "value" refers to the significance or worth attributed to an object, practice, or phenomenon, arising from its use, rarity, utility, importance, or uniqueness.

2.2.3.1 *Values and Significances*[2]

- Artistic value
- Historic and Archaeological value
- Typological value
- Aesthetic Value
- Architectural value
- Symbolism value
- Scientific value
- Social or spiritual/ religious value
- …etc.

2.2.3.2 *Outstanding Universal Values related to World Heritage sites*

Outstanding: For properties to be of Outstanding Universal Value they should be exceptional, or superlative they should be the most remarkable places on earth.

Universal: Properties need to be outstanding from a global perspective. World Heritage does not aim to recognize properties that are remarkable only from a national or regional perspective. Countries are encouraged to develop other approaches to recognize these places.

Value: What makes a property outstanding and universal is its "value", or the natural and/or cultural worth of a property.

2.2.4 The Significance of Cultural Heritage and the Causes of Its Degradation

Cultural heritage in general—and architectural heritage in particular—constitutes a defining expression of the cultural and civilizational depth of society. It embodies a value of enduring significance, not only for the present but also for successive generations, as it plays a vital role in shaping economic, social, and human development. Heritage is also woven into the fabric of daily life, reflected in diverse practices, methods, and traditions. Despite this, the recognition of its importance for individuals and communities is often lacking, leading to its marginalization. In Syria, the causes of this deterioration can be summarized as follows:

[2] (Torre, 2002)

A. ***Natural factors****:* including humidity, wind, erosion, and other environmental conditions, as well as natural disasters such as earthquakes and floods.

B. ***Human and industrial factors****:* most notably the destructive impacts of wars and their long-term consequences.

C. ***Lack of awareness****:* limited recognition of heritage values at both the individual and societal levels, accompanied by insufficient cultural consciousness.

D. ***Deficiencies in preservation practices****:* the absence of a clear and systematic understanding of how to properly safeguard heritage, resulting in ineffective or inappropriate conservation efforts due to:

a) Absence of a clear working methodology in the field of heritage preservation.

b) Insufficient budgetary allocations within state institutions dedicated to safeguarding cultural heritage.

c) Limited support for private owners of archaeological properties, preventing proper restoration and sustainable investment.

d) Underutilization of modern scientific methods and technologies in documentation and conservation processes.

e) Inadequate scientific approaches to restoration, compounded by the disappearance of traditional crafts, skills, and techniques essential for high-quality artistic restoration.

f) Lack of systematic preventive and corrective maintenance, leading to gradual structural and aesthetic deterioration.

2.3 INSPECTION AND DOCUMENTATION OF HERITAGE SITES

2.3.1 Definitions

The ***inspection of the building*** constitutes the first step in its study and serves as a fundamental basis for any future intervention. It provides an essential means of gaining a thorough understanding of the structure, whether through direct visual observation or with the aid of modern scientific methods and specialized equipment. By employing diverse

inspection techniques, it becomes possible to conduct a comprehensive assessment of the building, including its construction materials, structural systems, and the condition of its various elements, as well as identifying manifestations of damage and existing deterioration problems.

Documentation is a process that complements and extends the inspection stage, with both often considered integral to one another. It constitutes a systematic and detailed record—typically in the form of reports—that provides comprehensive information about the artifact or building. This record may include written descriptions, architectural drawings, maps, photographs, and other forms of visual or textual data. Documentation is not a one-time activity but an ongoing process that begins prior to any restoration work, continues throughout the intervention, and extends beyond its completion, serving as a permanent reference throughout the lifetime of the artifact or structure.

2.3.2 The Significance of Heritage Documentation

The importance of the documentation process can be summarized in the following points:

a) **Transmission of cultural heritage**: ensuring the transfer of heritage to future generations through precise photographic and digital recording of buildings and sites.

b) **Provision of accurate data**: generating reliable information on the condition of a building from architectural, structural, and physical perspectives to support informed future planning.

c) **Monitoring deterioration**: systematically documenting structural and architectural changes or deformations to identify and address problems affecting the site.

d) **Dissemination of historical knowledge**: preserving and communicating the historical significance of the building as an integral component of the documentation process.

2.3.3 Documentation Methods

Each historical element possesses unique characteristics, and the choice of documentation method must be tailored to its physical condition, the required level of

accuracy, and the overall project objectives. Accordingly, the selection of the most appropriate documentation technique is influenced by several key factors:

1) Historical and scientific significance of the heritage building.
2) Required level of accuracy in the documentation outputs.
3) Available budget allocated for the documentation process.
4) Timeframe designated for conducting the work.
5) Qualifications and expertise of the personnel involved.

According to one of the referenced sources[3], documentation methods can be classified as follows:

1) **Manual Measurement**: This method is applied to objects with dimensions not exceeding a few meters, as it becomes impractical and time-consuming for larger structures. The outputs are typically ***simplified two-dimensional plans*** with limited detail and accuracy.
2) **Topographic Surveying**: employed primarily for ***preliminary documentation***, without extensive focus on architectural or structural details. It is generally used to define the ***internal and external boundaries of a building*** and determine the ***dimensions of openings***. The results are ***basic two-dimensional plans*** with acceptable levels of accuracy.
3) **Photogrammetry**: utilizes photographic images to obtain ***comprehensive and precise measurements*** of buildings and archaeological sites. This technique captures both overall geometry and fine details, producing ***detailed two-dimensional plans*** and ***high-resolution three-dimensional models***.
4) **Laser Scanning**: represents one of the most advanced and efficient documentation methods, generating ***highly accurate 3D models*** in a short time through the creation of a **dense point cloud** surrounding the object. The

[3] (A'akeeli, 2013)

outputs include ***detailed 2D drawings*** and ***high-resolution 3D models***, making them particularly suitable for complex or large-scale structures.

According to another referenced source[4], documentation methods can be classified as follows:

2.3.3.1 *Image-based Techniques*

Photography is widely recognized as a fundamental tool for heritage documentation, as systematic production and archiving photographic records are vital for meeting future preservation needs. In this regard, the photographic image functions as the primary source of information, providing accurate data about the target building. Within the field of documentation, this technique is commonly classified into following main categories:

A. Photogrammetry[5]

1) Panorama
2) Close-range Photogrammetry
3) Unmanned Aerial Vehicle (UAV)

B. IR Cameras

All objects emit infrared (IR) energy, commonly referred to as a heat signature. An infrared camera (also known as a thermograph) detects and measures this radiation and converts it into an electronic image that represents the apparent surface temperature of the object. This capability makes IR cameras particularly valuable in the documentation of cultural heritage, the study of artworks, and the preservation of historical artifacts.

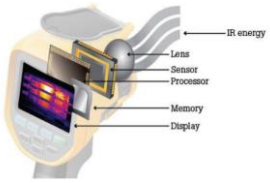

Figure 1: IR Camera

Infrared imaging reveals the heat distribution across surfaces, which can be influenced by factors such as relative humidity, material

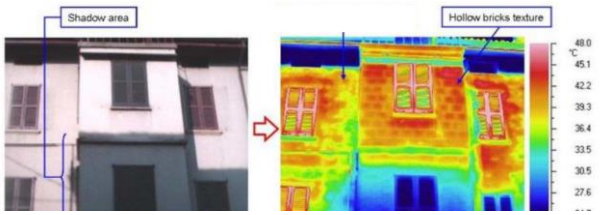

Figure 2: Example of IR documentation

[4] (Saleh & Winterstein, 2022) and (Abras, 2020)
[5] This classification will be further elaborated and analyzed in detail as a central pillar of this research.

composition, and physical condition. These cameras are considered highly effective for identifying hidden defects in historic buildings and are completely safe for both structures and movable heritage objects. Their applications include detecting moisture infiltration, locating cracks, and assessing other structural vulnerabilities.

Moreover, infrared images can be ***integrated with digital photography and 3D models*** to support ***quantitative damage analysis***, enhancing the precision of conservation planning.

Table 1: Advantages and Limitations of IR Cameras

Advantages	Limitations
Non-invasive and does not cause any damage to the target object.	Requires a relatively high level of expertise to operate and interpret results accurately.
Effective for detecting moisture, cracks, and other forms of deterioration.	
Capable of producing high-resolution thermal images.	

2.3.3.2 *Non-Image-based Techniques*

A. Traditional Terrestrial Survey

Surveying encompasses a set of techniques used to determine the precise location of one or more points on the Earth's surface, as well as to calculate the distances and angles between them. In the context of cultural heritage documentation, surveying methods can be broadly classified into manual and automated approaches.

1) Manual Surveying

Manual surveying relies on simple measuring tools such as measuring tapes, rulers, mercury bubble level, or water level. Measurements are recorded on a preliminary sketch drawn prior to the survey and later processed to generate

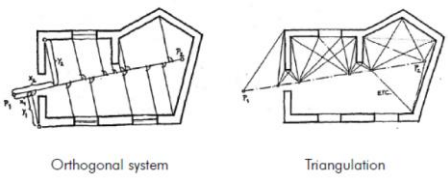

Figure 3: Manual Surveying Techniques

accurate representations using computer-aided design (CAD, BIM, …etc.) software.

This method is particularly useful in situations where modern technologies are unavailable or prohibitively expensive, or where spatial constraints prevent the use of advanced surveying equipment. Despite its limitations, manual surveying can still provide sufficiently detailed building drawings.

Table 2: Advantages and Limitations of Manual Terrestrial Surveying

Advantages	Limitations
Low cost	Low accuracy compared to modern methods.
Simple to implement and requires minimal expertise.	Time-consuming and labor-intensive.
Equipment is inexpensive and readily available.	Difficulty in documenting curved, intricate, or hard-to-reach elements.
Practical in areas with limited visibility.	Results are highly susceptible to human error.

2) Automated Surveying

Automated (digital) surveying employs topographic surveying instruments to determine point coordinates and generate polygons of the target building, including curved surfaces. In this method, angles and distances are measured simultaneously, and the resulting data can be processed with modeling and design software to produce a 3D digital model.

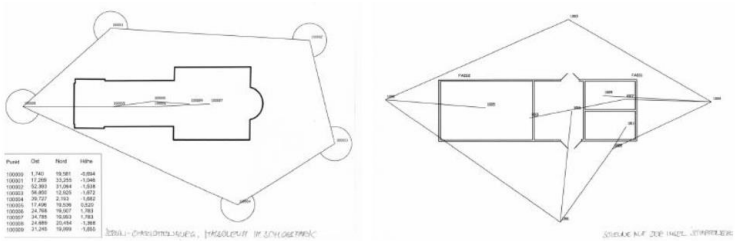

Figure 4: Automated Surveying Techniques

This technique is increasingly considered essential for cultural heritage documentation due to its accuracy and integration with digital workflows.

Table 3: Advantages and Limitation of Automated Terrestrial Surveying

Advantages	Limitations
High level of accuracy.	Extended fieldwork time may be required.
Cost-effective when a limited number of survey points are required.	Skilled operators are necessary.
Relatively straightforward operation once equipment is available.	Can not capture color or material properties.
	Inefficient for highly complex geometries or very large datasets.

B. Laser Scanner

1) Terrestrial Laser Scanner

A laser scanner functions as a robotic total station capable of capturing data from a target at very high speed. Unlike traditional surveying instruments, it measures distances without the need for a reflector, relying instead on precise calculations of distance and angle. This technology has a wide range of applications in cultural heritage documentation, from small-scale artifacts to large and complex architectural structures. Its key strengths include the ability to acquire data at a true scale, with exceptional accuracy, high speed, and the production of extremely dense point clouds.

Figure 5: Example of Terrestrial Laser Scanning Outputs

Workflow Stages

- Field survey and data collection
- Data processing
- Generation of final outputs

Table 4: Advantages and Limitation of Terrestrial Laser Scanner

Advantages	Limitations
High accuracy and rapid data acquisition.	Very high cost, with specialized operators and software required.
Ability to capture very large datasets.	Large datasets pose challenges for processing, storage, and management.
Effective for documenting irregular surfaces and complex geometries.	Data processing is time-consuming.

Functional in both dark and illuminated environments.	Limited efficiency in small or confined spaces.
	Reduced effectiveness in documenting fine details such as edges, cracks, and obstructed elements.

2) Light Detection and Ranging (LiDAR)

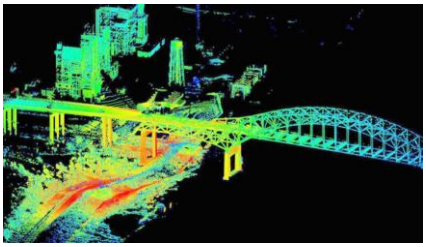

Figure 6: Example of LiDAR Outputs

LiDAR is one of the most advanced remote sensing technologies. It operates by emitting a laser beam in a specific direction, receiving the reflected light, and analyzing it to detect and identify the properties of the surfaces from which the light is reflected. By calculating the time difference between the transmission and reception of each laser pulse, the device determines the distance between the sensor and the observed object.

LiDAR sensors are capable of scanning hundreds of thousands of points per second, producing dense and highly accurate datasets. This makes LiDAR an ideal tool for archaeological site surveys, systematic studies of historic buildings, and the documentation of large-scale excavation areas. The variations in the reflected beam reveal critical information about the geometry and characteristics of the target surface.

Table 5: Advantages and Limitations of LiDAR

Advantages	Limitations
High accuracy and rapid data acquisition.	Very high cost, with specialized operators and software required.
Ability to collect very large datasets.	Processing and storing dense datasets can be challenging due to memory and computational demands.
Well-suited for documenting large structures, sites, and landscapes.	Limited effectiveness in documenting fine details such as edges and cracks.
Effective in environments with vegetation, allowing data acquisition even in areas with dense botanical cover.	

2.3.3.3 *Combinative Methods*

Combinative methods integrate the characteristics of both image-based and non-image-based approaches. They combine photogrammetry, which relies on image-based data acquisition, with scanning techniques that project laser or light beams onto a surface to capture geometric information. By merging these two approaches, combinative methods mitigate the limitations inherent in each individual technique and provide more robust, accurate, and comprehensive documentation of heritage structures.

Photo-Laser Scanner

Modern laser scanners are often equipped with digital cameras, enabling the integration of point cloud data with photographic imagery. In this process, once the target has been fully scanned and a dense point cloud generated, the mounted camera captures high-resolution images. These images are then merged with the point cloud, allowing the individual points to acquire their true color and texture. This integration enhances the geometric precision of laser scanning with the visual richness of photogrammetry, producing highly detailed and realistic documentation outputs.

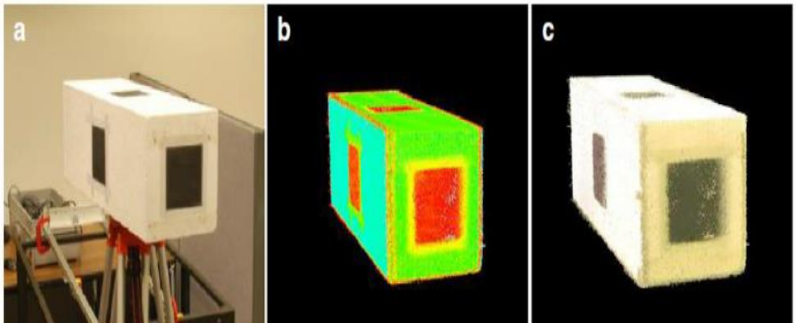

Figure 7: Photo-Laser Scanner-(a) Actual image of masonry block, (b) returned point cloud over fitted CAD object, (c) point cloud with masonry block images overlaid.

Table 6: Advantages and Limitations of Photo-Laser Scanners

Advantages	Limitations
High-resolution outputs.	Very high cost of equipment.

Reduced fieldwork time.	Requires skilled operators and specialized software.
Ability to capture large volumes of data.	Data processing is time-intensive.
Well-suited for documenting complex geometries and surfaces.	
Provides both texture and color information.	

2.4 PHOTOGRAMMETRY IN HERITAGE DOCUMENTATION

2.4.1 Definitions

Photogrammetry is a scientific discipline primarily concerned with determining the geometric characteristics of objects—such as size, shape, location, and dimensions—and producing accurate plans or models based on photographs of those objects. In simple terms, it is the science of making precise measurements from photographs.

According to the American Scientific Society, photogrammetry is "the art, science, and technology of obtaining reliable information about natural and artificial features on the Earth's surface by recording, measuring, and interpreting photographs of these features."

The term itself is derived from the Greek words:

- Photo (φωτός) meaning light.
- Gramma (γράμμα) meaning drawing or writing.
- Metron (μέτρον) meaning measurement.

Thus, photogrammetry literally translates to "measuring by drawing with light."

It is important to distinguish between photography and photogrammetry. While photography is primarily concerned with capturing images and exploring artistic or technical aspects of visual representation, photogrammetry focuses on the analytical use of photographs for measurement and mapping purposes.

Today, photogrammetry is regarded as one of the most significant applied sciences because of its interdisciplinary nature and wide-ranging applications. Its relevance extends far beyond engineering and surveying; it also plays an essential role in fields such as medicine, archaeology, architecture, and the documentation and preservation of cultural heritage.

2.4.2 Photogrammetry Applications[6]

A. **Image Rectification:** Photogrammetry enables the transformation of photographs taken with central perspective projection into a vertical or orthographic projection. This process, known as image rectification, corrects distortions and returns the image to its true geometric position, allowing for accurate measurement and mapping.

B. **Building Documentation:** One of the most prominent applications is in the field of architectural documentation. Photogrammetry supports the creation of precise 3D digital models of buildings, which are essential for restoration, conservation, and heritage preservation. These models provide both geometric accuracy and detailed texture information.

C. **3D City Modeling:** At the urban scale, photogrammetry contributes to 3D city modeling, where entire cityscapes are represented digitally. These models are widely used in urban planning, infrastructure development, virtual tourism, and simulation of environmental or disaster scenarios.

D. **Medical Modeling:** Beyond engineering and architecture, photogrammetry has valuable applications in the medical field. It is used for creating accurate 3D models of anatomical structures, supporting surgical planning, prosthetics design, and medical research.

2.4.3 Types of Photogrammetry

In general, photogrammetry is divided into two distinct categories:

I. **Terrestrial Photogrammetry**

Terrestrial photogrammetry refers to photographs captured from a camera mounted on or near the ground, typically placed on a tripod or a stable platform. The camera lens is generally oriented horizontally, although it can be tilted depending on the requirements of the survey. This method is commonly used for documenting buildings, monuments, and other objects where close-range, ground-based imaging provides high levels of detail and accuracy.

II. **Aerial Photogrammetry**

[6] (Othman P. I., 2013)

Aerial photogrammetry involves photographs taken from cameras mounted on aircraft, unmanned aerial vehicles (UAVs/drones), or other aerial platforms. The camera lens is usually oriented in a near-vertical position, although it can also be intentionally tilted to capture oblique views. This technique is extensively applied in topographic mapping, land-use analysis, agriculture, and large-scale environmental studies, as it allows coverage of wide areas with high geometric precision.

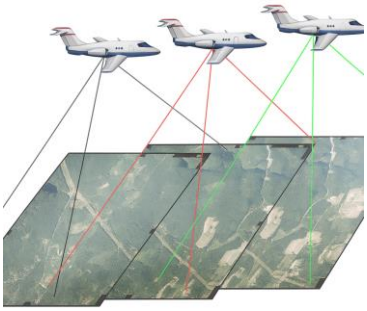

Figure 8: Airal Photogrammetry

As referenced in Section, *Image-based Techniques,* photogrammetry can be classified into the following categories[7]:

A. Panorama

Panorama photography represents a multi-image photogrammetry technique and serves as a prime example of image-based visualization as opposed to model-based visualization. Unlike traditional 3D modeling, this approach avoids many associated complexities. Its greatest advantage lies in its ability to document and store information about large objects using only a limited number of images. Panoramic images are widely applied in fields such as tourism, where they are used to showcase buildings, monuments, and cultural heritage sites.

B. Close-Range Photogrammetry (CRP)

Close-range photogrammetry requires at least two overlapping images of the same object to ensure accurate measurement and reconstruction. The primary goal is to streamline and accelerate both data acquisition and processing. This method is particularly effective for documenting texture, color, and fine details, while also accommodating objects of diverse size and complexity in relatively short

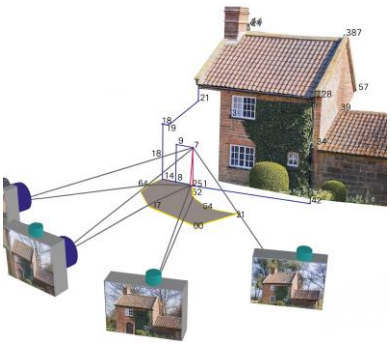

Figure 9: Close-Range Photogrammetry

[7] (Saleh & Winterstein, 2022)

timeframes. With the availability of high-resolution digital cameras, the process has become more accessible and cost-efficient. Outputs may include rectified photographs, orthophotos, or complete 3D models, which serve as valuable tools for creating digital archives and supporting various documentation objectives.

C. Unmanned Aerial Vehicle (UAV) Photogrammetry

UAV photogrammetry employs unmanned aerial platforms to capture aerial imagery for photogrammetric processing. UAVs can take different forms, including:

- Remotely Piloted Vehicles (RPVs)
- Remotely Operated Aircraft (ROAs)
- Remotely Controlled Helicopters (RC-Helicopters)

This approach provides flexible, cost-effective, and efficient means of surveying large areas, making it highly suitable for mapping, monitoring, and documentation tasks.

In the context of this research, both **close-range *photogrammetry*** and ***UAV-based photogrammetry*** have been employed as primary methods of data acquisition.

2.4.4 The Digital Image

The surface elements of an object reflect light at different intensities depending on their color and material properties. These variations in reflected light allow the photographed object to be distinguished and represented. A digital image captures this information by encoding the reflected light into discrete units called pixels. Each pixel corresponds to a numerical value representing a specific color, while its position in the image is determined by its row and column coordinates.

The process begins when light rays reflected from the object pass through the camera lens and optical filters before reaching the sensor. The sensor records the light intensity and spectral information, converting it into a digital signal composed of pixels. This digital data is then stored electronically in a memory unit or, in older systems, on photographic film.

In digital imaging, a channel refers to the portion of the light spectrum that the sensor is capable of recording. Based on the number of channels, images can be categorized into three main types:

A. **Binary Images:** Represented by a matrix containing only two values, 0 (black) and 1 (white).

B. **Grayscale Images (Ray-level Images):** A single-channel matrix where pixel values range from 0 to 255, corresponding to shades of gray.

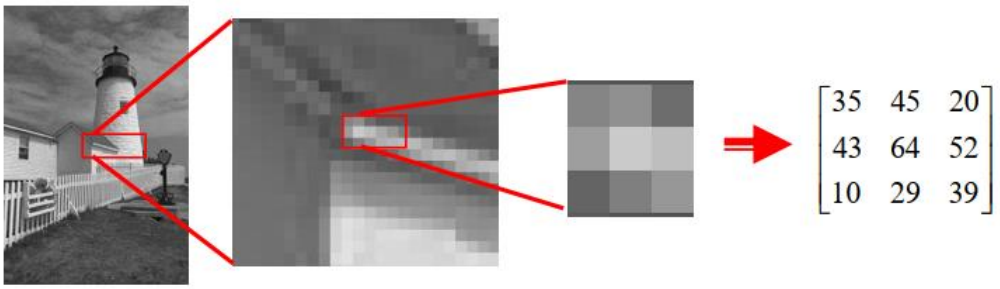

Figure 10: Grayscale Image

C. **Color Images (RGB Images):** Composed of three channels—Red, Green, and Blue. Each channel is represented as a matrix with values ranging from 0 to 255. A pixel's final color is formed by combining the three components: (R: 0–255, G: 0–255, B: 0–255).

Figure 11: RGB Image

2.4.5 Classification of Photogrammetry Methods in Heritage Documentation

Heritage documentation methods employing photogrammetry can be broadly classified into two principal categories:

2.4.5.1 *Two-Dimensional Documentation*

Two-Dimensional Documentation involves the production of corrected or rectified images from which both visual information and two-dimensional measurements can be extracted, eliminating the need for direct ground measurements for redrawing and documentation. This approach significantly reduces the time and cost of the documentation process. It is particularly effective for recording flat facades or surfaces where geometric

projections remain relatively simple and superficial.

The two-dimensional documentation process relies primarily on the removal of image distortions, which include both lens distortions introduced by the camera optics and perspective distortions resulting from the central projection of the image when captured at an oblique angle to the surface. Once these distortions are corrected, the resulting image preserves true-to-reality proportions. From this rectified image, accurate dimensions of architectural or heritage elements can be extracted and redrawn using computer-aided design (CAD) software.

A. Two-Dimensional Documentation Using Rectified Images

The use of rectified images is based on transforming one of the planes of a perspective view into an orthographic view. To achieve this rectification, the spatial coordinates of at least three points on the target plane must be known. While some lens distortions may persist if they are not explicitly removed, distortions arising from perspective projection are fully corrected. This process ensures that the resulting image reflects accurate geometry, as illustrated in the following example:

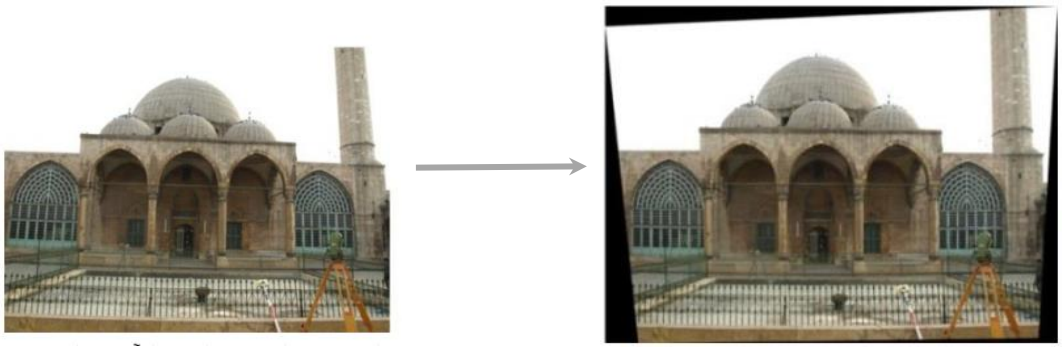

Figure 12: Rectified image of the southern facade of the Ottoman Mosque

This method is regarded as one of the simplest approaches to documentation. To correct a façade image, it is sufficient to determine the precise coordinates of three points lying on the façade plane, either using a surveying instrument or through manual measurement. Perspective distortions can then be removed directly, without requiring knowledge of the camera's internal parameters or specifications, provided that lens distortions are negligible.

For this reason, the use of cameras with pronounced lens distortions—such as wide-angle or fisheye lenses—is not recommended.

In cases where the facade comprises several adjacent planes or includes shallow protrusions, each plane can be corrected separately and later merged using computer-aided design (CAD) software.

Figure 13: Rectified Image of Mustafa al-Sami's house in Istanbul.

B. Two-Dimensional Documentation Using Orthorectified Images

Orthorectification is the projection of a real object onto a reference plane using the principles of parallel projection. In this process, all projection rays are parallel to one another and perpendicular to the projection plane, ensuring that parallel lines remain parallel and that scale is preserved regardless of distance. Consequently, the orthorectified image is free from perspective distortions and retains the same geometric properties as the actual object. It preserves dimensions and proportions, making accurate measurement directly possible.

Orthorectified images are widely used to capture detailed surface information and are also employed as textures in two- and three-dimensional modeling programs. By linking texture images to the surfaces of digital models, these programs enhance both the accuracy and the visual realism of the reconstructed objects.

Unlike simple rectified images (corrected images), which provide a distortion-free projection of only a single plane, orthorectified images ensure the accurate projection of multiple planes onto a single, unified reference plane.

It should be noted, however, that the production of orthorectified images requires prior determination of the camera's internal and external parameters, without which the rectification process cannot be completed reliably.

2.4.5.2 *Three-Dimensional Documentation*

Three-dimensional documentation enables the extraction of both two- and three-dimensional measurements, culminating in the generation of a 3D model. While widely applied in numerous disciplines beyond heritage documentation, it also represents the

second principal axis of photogrammetric heritage recording. This approach can be further classified according to the number of images employed, as follows:

A. Three-Dimensional Documentation Using a Single Image

This technique is particularly valuable in cases where historical monuments have been completely or largely destroyed and must be reconstructed or completed, but no recent photographs from multiple viewpoints are available. The fundamental principle of deriving a 3D model from a single image is based on:

- Aligning the edges and surfaces of the object along parallel and perpendicular directions.
- Establishing connections between these surfaces and edges through identifiable control points.

One of the essential properties of perspective projection is that straight edges remain straight within the image plane. However, parallel edges in reality are not preserved as parallel in the image; instead, they converge at a point known as the ***vanishing point***. As shown in the following figure, all lines that should be parallel in space appear to intersect at a single vanishing point within the image. By analyzing the directions of these edges (at least two), the orientation of the façade surface can be inferred. Information about perpendicular relationships further aids in determining orientation when parallel edges are insufficient.

Subsequently, groups of four edges can be connected to define planar surfaces. These surfaces are then integrated through the mathematical treatment of geometric constraints—such as parallelism, perpendicularity, and the convergence of parallel lines at a vanishing point—combined with topological relationships between surfaces (e.g., containment, adjacency). This process enables the representation of surfaces and the computation of the coordinates of the vertices that define them.

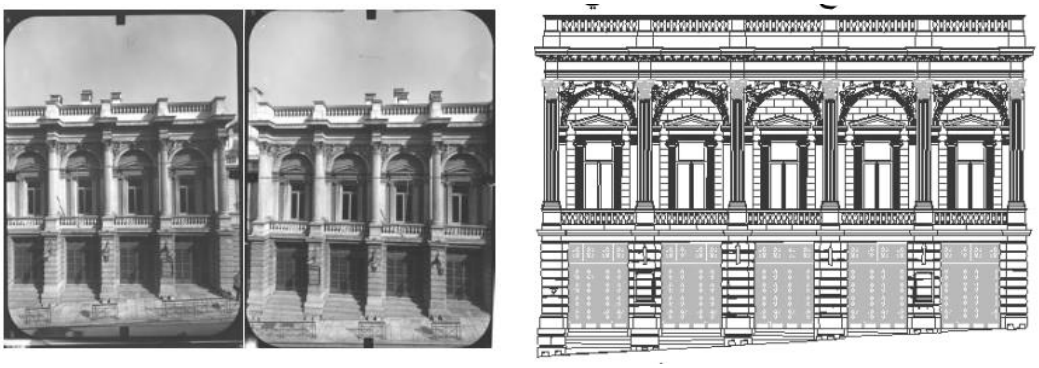

Figure 16: Two real-time photos of the facade of the National Theatre in Athens.

Figure 14: Three-Dimensional Documentation Using a Single Image

B. Three-Dimensional Documentation Using Two Images

This approach can be implemented through two primary methods:

Stereoscopic Vision:

A three-dimensional model is generated from a pair of overlapping images of the object. These images may be captured using a dual-lens camera that records both simultaneously, or with two separate cam eras positioned to capture overlapping views under controlled geometric conditions.

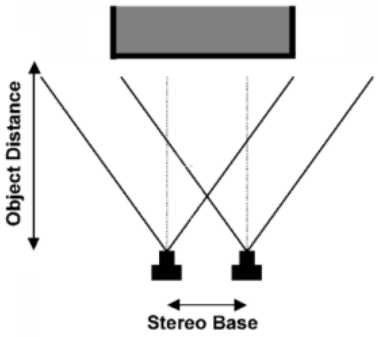

Figure 15: Stereographic Processing (Controlled geometric conditions)

The underlying principle is analogous to human binocular vision, where two slightly different perspectives of the same object are fused to create depth perception. Similarly, when two images of an object are acquired with sufficient overlap, a stereoscopic 3D reconstruction can be achieved.

The geometric foundation of this method lies in calculating the 3D coordinates of a point through the intersection of two projection rays in space. To ensure accurate results, several conditions must be observed during image acquisition:

- ***Visibility and overlap:*** The majority of the object's surfaces should be visible in both images, with a cross-sectional overlap ratio of at least 60%.
- ***Camera orientation:*** The camera axes should remain as parallel as possible to the object's facade in order to obtain high-quality stereoscopic views.
- ***Camera calibration:*** Calibrated photogrammetric cameras are generally required, with well-defined internal and external parameters and minimal lens distortion.
- ***Perpendicular alignment:*** Ideally, the camera axis should be oriented as close to perpendicular to the object's facade as possible.
- ***Baseline-to-distance ratio:*** The ratio between the baseline (distance between the two camera stations) and the camera-to-object distance should fall within the range of 1:5 to 1:15 to achieve reliable stereoscopic results.

Pair of Images:

The fundamental principle is that each three-dimensional point can be determined by the intersection of two projection rays in space. When two images of an object are acquired from different positions with sufficient overlap (typically around 60%), the corresponding rays intersect at the object's surface, thereby defining the precise 3D location of that point. By repeating this process for numerous points across the object, the complete set of three-dimensional coordinates can be calculated, resulting in the construction of a detailed 3D model, as illustrated in the following figure.

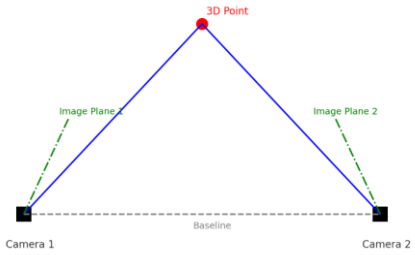

Figure 17: Principle of 3D Point Determination from Stereo Images

C. Three-Dimensional Documentation Using Multiple Images

In many cases, a single pair of images is insufficient for reconstructing a complex building or site containing numerous details. Therefore, a larger number of images is required to ensure full coverage of the structure or site.

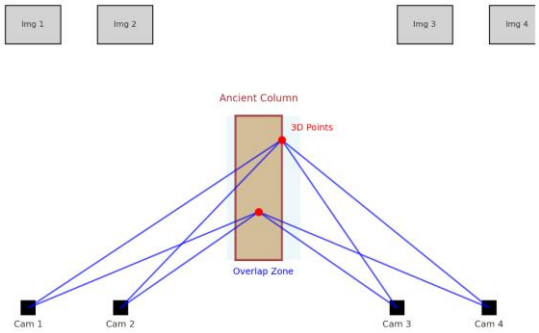

Figure 18: Principle of 3D Point Determination from Multiple Images

The foundation of 3D documentation lies in calculating the spatial coordinates of a point from its projections across multiple images. Projection rays are drawn from the image points through the projection centers of the cameras, intersecting at the actual object point in space. The accuracy of this process depends largely on the number and placement of the cameras.

In both two-image and multi-image cases, common points must be identified across overlapping images. The number of these points depends on the shape of the object, the number of levels it contains, and the level of detail required:

- For complex objects (e.g., statues, decorative stonework), this produces a dense point cloud.
- For simpler objects, only a limited number of points may be necessary.

2.4.5.3 *Criteria for Capturing Images:*

- ***Visibility and overlap:*** Most parts of the object must be visible in the images, which should overlap with at least 60% cross-sectional overlap. Unlike stereo pairs, the camera axes do not necessarily need to be parallel.
- ***Coverage:*** For multi-image documentation, it is recommended to acquire at least three images from different angles for each part or level of the object. The total number of images is not fixed but depends on the level of detail required and the processing capacity of the equipment and software.

- ***Distance:*** There is no fixed ratio between the baseline (camera separation) and the camera-to-object distance. The distance should be adjusted according to site conditions and the required level of detail.
- ***Angles:*** The angle between two adjacent shooting axes should ideally approach 90°, ensuring good geometric strength. Adequate variation between horizontal and vertical camera positions is also recommended, avoiding all stations being aligned on the same level.

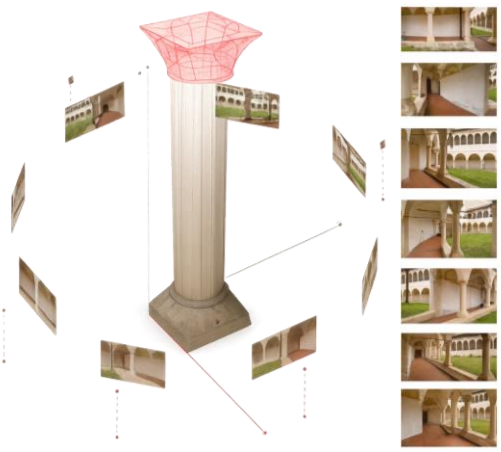

Figure 19: Multi-Image Photogrammetry for 3D Documentation

- ***Zoom ratio:*** Images should be captured with a consistent zoom setting to maintain scale consistency.
- ***Image selection:*** Capture multiple photographs from different stations, and then select the most suitable ones for processing.

Once the basic image-set has been acquired, additional steps can be taken to improve coverage and detail:

- **Approach the object** to capture fine details.
- **Increase the distance** to include the entire object or its surrounding context.
- **Capture supplementary images** between the planned stations, as well as from above and below them, to ensure comprehensive coverage.
- **Optimize lighting conditions** by photographing at times that minimize sharp contrasts and shadows, which are difficult to correct in post-processing. The most favorable conditions are during overcast weather or in the early morning before sunrise.

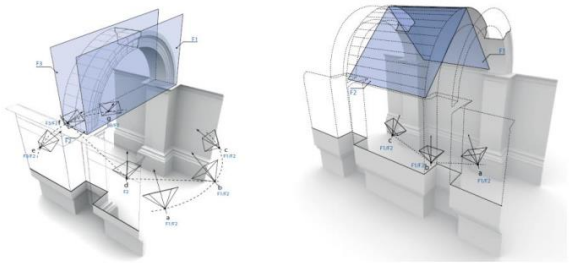

Figure 20: Relative locations of cameras to the object

2.4.5.4 *Type of Camera Used*

Digital cameras represent the primary tool in photogrammetric documentation. Cameras are generally classified into ***metric*** and ***non-metric***, each with distinct advantages and limitations that must be considered when selecting the appropriate device.

A. Metric Cameras

Metric cameras are designed specifically for photogrammetry, with internal parameters—such as ***focal length, lens distortion, sensor dimensions, and principal point location***—precisely defined by the manufacturer. In earlier film-based models, a network of fiducial marks was embedded inside the camera to allow accurate repositioning of the image during processing. With the advent of digital photography, such internal networks are no longer required.

B. Non-Metric Cameras

Non-metric cameras are standard commercial digital cameras, available in a wide range of models, from simple consumer devices to semi-professional and professional systems. Unlike metric cameras, their internal parameters are ***not pre-defined*** and may vary depending on usage.

Key Considerations in Camera Selection

- ***Cost***

  Metric cameras are relatively expensive compared to non-metric alternatives.
- ***Software Compatibility***
  - Metric cameras are typically supported by dedicated manufacturer software, designed to process only images captured with that specific camera and offering advanced calibration functions not available elsewhere.
  - Non-metric cameras, by contrast, are not tied to proprietary software, requiring the user to select general-purpose photogrammetric software compatible with their workflow.
- ***Zoom Capability***
  - Metric cameras generally employ a fixed focal length and therefore do not allow zooming.
  - Professional non-metric cameras often include zoom lenses, enabling adjustments to match the size of the object being documented. This flexibility reduces restrictions on camera-to-object distance.

- ***Calibration Requirements***
  - Metric cameras have pre-calibrated internal parameters provided by the manufacturer, eliminating the need for recalibration.
  - Non-metric cameras require careful calibration before use in 3D modeling, since parameters such as focal length and lens distortion may vary each time the camera is used.

Table 7: Comparison Between Metric and Non-Metric Cameras

Aspect	Metric Cameras	Non-Metric Cameras
Definition	Specially designed for photogrammetry with precisely defined internal parameters.	Commercial digital cameras (consumer, semi-professional, or professional models).
Internal Parameters	Predefined and stable (focal length, lens distortion, sensor dimensions, principal point).	Unknown and variable; must be determined through calibration.
Fiducial Marks	Older models included fiducial marks for image orientation.	No fiducial marks provided.
Calibration	Factory-calibrated; no recalibration required.	Requires frequent calibration before use in 3D modeling.
Zoom Capability	Fixed focal length; no zoom option.	Often includes zoom lenses, offering flexibility in object size and camera distance.
Software	Comes with proprietary software, usable only with images from that camera.	No dedicated software; relies on general photogrammetric programs.
Cost	Relatively high.	More affordable; available at a wide range of prices.
Applications	Precision surveying, engineering, and scientific documentation.	Widely used in heritage documentation, architecture, archaeology, and flexible fieldwork.

2.4.6 Fundamental Principles of Photogrammetric Calculations

Projection geometry forms the foundation of photogrammetry. The transition from digital images to accurate 3D models requires a solid understanding of perspective projection, homographic transformation, and the principles used in calculating three-dimensional coordinates. These calculations rely primarily on defining the camera's ***Intrinsic*** and ***Extrinsic*** parameters, which are described as follows:

2.4.6.1 *Intrinsic Parameters (Interior Orientation):*

Internal parameters define the geometry of the imaging process inside the camera. They describe how the image is projected onto the sensor and include:

- ***Focal length (f):*** the distance between the camera lens and the image plane.
- ***Principal point coordinates (c_x, c_y):*** the intersection of the optical axis with the image plane.
- ***Lens distortion coefficients:*** parameters accounting for radial and tangential distortions introduced by the lens.
- ***Pixel size and sensor resolution:*** which determine the precision of image measurements.

Together, these parameters ensure that the image geometry is accurately reconstructed.

2.4.6.2 *Extrinsic Parameters (Exterior Orientation):*

External parameters describe the position and orientation of the camera in space at the moment of exposure. They define the relationship between the object coordinate system (ground) and the image coordinate system (camera) and include:

- ***Camera position (X_c, Y_c, Z_c):*** the spatial coordinates of the projection center.
- ***Camera orientation (ω, φ, κ):*** the three rotation angles (omega, phi, kappa) describing how the camera is tilted relative to the object coordinate system.

These parameters are crucial for determining the transformation between image space and object space, enabling the accurate computation of 3D coordinates.

2.4.6.3 *Mathematical Framework for Camera Calibration and 2D-to-3D Transformation*

I. Camera Projection Model

The relationship between a 3D world point (X, Y, Z) and its 2D image projection (u, v) can be expressed as:

$$s\begin{bmatrix} u \\ v \\ 1 \end{bmatrix} = K[R|t]\begin{bmatrix} X \\ Y \\ Z \\ 1 \end{bmatrix}$$

Where:

- $P = K[R|t]$ camera projection 3×4 matrix
- s = scale factor (depth information)
- K = intrinsic matrix (internal parameters)
- R = rotation matrix (camera orientation in space)
- t = translation vector (camera position in space)
- $[X, Y, Z]^T$ = world point in 3D coordinates
- $[u, v]$ = pixel coordinates on the image plane

II. Intrinsic Parameters (Interior Orientation)

The intrinsic matrix K is:

$$K = \begin{bmatrix} f_x & 0 & c_x \\ 0 & f_y & c_y \\ 0 & 0 & 1 \end{bmatrix}$$

Where:

- $f_x = \frac{f}{p_x}, f_y = \frac{f}{p_y}$ (focal length in terms of pixel size)
- (c_x, c_y) = principal point (image center)
- p_x, p_y = pixel size in x and y directions

Lens distortion is also part of the calibration:

Radial distortion:

$$x_{corr} = x(1 + k_1 r^2 + k_2 r^4 + k_3 r^6)$$

$$y_{corr} = y(1 + k_1 r^2 + k_2 r^4 + k_3 r^6)$$

Tangential distortion:

$$x_{corr} = x + [2p_1 xy + p_2(r^2 + 2x^2)]$$

$$y_{corr} = y + [p_1(r^2 + 2y^2) + 2p_2 xy]$$

Where: $r^2 = x^2 + y^2$

III. Extrinsic Parameters (Exterior Orientation)

The extrinsic matrix $[R|t]$ converts from world coordinates to camera coordinates:

$$\begin{bmatrix} X_c \\ Y_c \\ Z_c \end{bmatrix} = R \begin{bmatrix} X \\ Y \\ Z \end{bmatrix} + t$$

- R = rotation matrix (described by Euler angles ω, φ, κ)
- t = translation vector (camera center in world coordinates)

IV. Steps in Camera Calibration

Step 1: Collect Calibration Data

- Capture images of a known calibration target (checkerboard or 3D control points).
- Detect feature points (e.g., checkerboard corners).

Step 2: Initial Estimation

- Use Direct Linear Transformation (**DLT**) to estimate projection matrix P

$$P = K[R|t]$$

The Direct Linear Transformation (DLT) is a method to estimate the camera projection matrix ***P*** that relates 3D world points (X, Y, Z) to their 2D image points (u, v). It's called direct because it solves the projection equations using a linear system, without requiring iterative non-linear optimization at the first step.

Step 3: Parameter Refinement

- Decompose P to extract intrinsic K and extrinsic $[R|t]$
- Estimate lens distortion coefficients.

Step 4: Optimization (Bundle Adjustment)

- Minimize the reprojection error:

$$Error = \sum_i \left\| (u_i, v_i)_{observed} - (u_i, v_i)_{projected} \right\|$$

This ensures maximum accuracy.

V. 2D to 3D Reconstruction

- A single image cannot recover full 3D coordinates (depth is lost).
- Using multiple images (stereo or multi-view photogrammetry), we can triangulate.

Triangulation (Geometric Principle)

If a 3D point is observed in two camera views:

$$s_1 \begin{bmatrix} u_1 \\ v_1 \\ 1 \end{bmatrix} = K[R_1|t_1] \begin{bmatrix} X \\ Y \\ Z \\ 1 \end{bmatrix}$$

$$s_2 \begin{bmatrix} u_2 \\ v_2 \\ 1 \end{bmatrix} = K[R_2|t_2] \begin{bmatrix} X \\ Y \\ Z \\ 1 \end{bmatrix}$$

Solving both equations gives the **3D coordinates** $(\boldsymbol{X}, \boldsymbol{Y}, \boldsymbol{Z})$

- Each 2D image point corresponds to a ray in 3D space (from the camera center through the pixel).
- With two images, we get two rays.
- The intersection (or closest point) of these rays gives the 3D coordinate.

Mathematically, triangulation is solved using linear least squares:

$$X = argmin\left\|(u,v)_{obs} - (u,v)_{proj}(X)\right\|$$

The ***external orientation parameters*** of the camera (i.e., transformation matrix values) are determined by the photogrammetric software during the modeling process. Through the automatic or manual identification of tie points across multiple images, the software simultaneously computes the transformation matrices for all images, thereby establishing their spatial relationships.

In ***aerial photogrammetry***, the determination of external orientation typically involves two distinct stages: ***relative orientation*** (which establishes the geometric relationship between overlapping images) and ***absolute orientation*** (which aligns the model to a ground coordinate system). By contrast, in ***terrestrial photogrammetry***, these two stages are often absent in the software workflow, as the process is more closely integrated with camera calibration. In such cases, certain aspects of the ***external orientation***

parameters may be incorporated directly into the calibration procedure.

After completing the camera calibration, it is essential to examine the ***error values (residuals)***. These are defined as the distance, measured in pixels, between the two-dimensional points identified in the image and the corresponding three-dimensional points computed by the software. The magnitude of these residuals reflects the accuracy of the calibration process and is directly influenced by the precision with which the calibration points were located in the images.

Example on Calibration Error Table (per point)

This shows the residuals for each calibration point:

Calibration Point	Image X (px)	Image Y (px)	Residual X (px)	Residual Y (px)	Total Residual (px)
P1	1024.55	768.43	-0.35	+0.28	0.45
P2	845.22	692.18	+0.12	-0.19	0.22
P3	930.14	800.67	-0.25	-0.31	0.40
…	…	…	…	…	…

- Root Mean Residual (RMS): 0.37 px (average overall error, computed using squared values to avoid positive/negative cancellation).
- Maximum Residual: 0.45 px (biggest error among all points).

The ***Total Residual (px)*** is usually calculated using the ***Euclidean distance*** formula, combining the residuals in the ***X*** and ***Y*** directions into one value.

$$Total\ Residual(r) = \sqrt{r_X^2 + r_Y^2}$$

$$RMS = \sqrt{\frac{\sum_{i=1}^{n}(r_i)^2}{n}}$$

An RMS error of ***0.37 px*** combined with a maximum residual of ***0.45 px*** demonstrates a ***high-quality camera calibration***, as both values fall well below the common acceptance threshold of ***1 pixel*** in photogrammetric applications.

2.4.7 Applications in cultural heritage worldwide

Over the past two decades, photogrammetry has become a cornerstone of cultural heritage documentation. It has been applied to diverse contexts ranging from UNESCO World Heritage sites to smaller-scale archaeological artifacts. International case studies

include the recording of monuments in Palmyra, Petra, and Angkor Wat, as well as post-disaster surveys in Nepal and Iraq. Its versatility allows documentation of sites that are inaccessible or at risk, enabling rapid recording, monitoring of deterioration, and even virtual reconstruction of destroyed structures.

Advantages: cost-effective, detailed, adaptable

Photogrammetry is recognized for its cost-effectiveness compared to laser scanning, requiring only a digital camera and processing software. It captures both geometry and texture, providing detailed 3D models enriched with photographic realism. The technique is highly adaptable, applicable to scales from small artifacts to entire landscapes, and easily combined with drones (UAVs) for inaccessible areas such as rooftops and domes. This flexibility makes it particularly well suited for heritage sites in conflict or post-conflict contexts, where rapid and affordable solutions are essential.

Limitations: dependency on image quality, environmental conditions

Despite its advantages, photogrammetry is subject to notable limitations. Accuracy is strongly dependent on image quality, overlap, and calibration. Lighting variations, shadows, and reflective or uniform surfaces can reduce tie-point detection, introducing errors into the reconstruction. Environmental conditions—such as weather, vegetation cover, or structural obstructions—may further compromise results. Moreover, very large datasets are computationally demanding, requiring significant processing power. These limitations necessitate careful planning of acquisition strategies and validation of outputs against independent survey data.

2.5 INTRODUCTION TO GEOMATICS

Geomatics is a broad field that integrates technologies and sciences for collecting, analyzing, managing, and visualizing spatial (georeferenced) data. Different sources classify it in slightly different ways, but in academic and professional practice, the core classifications of Geomatics can be grouped as follows:

- Geodesy
- Surveying (Topography)
- Photogrammetry & Remote Sensing
- GIS & Cartography
- Geoinformatics

2.5.1 Surveying (Topography)

Every country maintains an integrated geodetic network that covers its entire territory. This network is composed of numerous geodetic points interconnected through a series of triangles or polygons. Triangular networks are commonly employed, and the system is typically divided into four hierarchical levels. These levels differ in terms of baseline lengths as well as the precision of angle and side measurements. The specifications of this network are presented in the following table:

Table 8: Specifications of Geodetic Triangulation Networks

Level (Order)	Triangle Side Length (km)	MSE in Angle Measurement	Accuracy of Side Measurement	Permissible Triangle Misclosure (cc)	Purpose
First-order	Greater than 20	±2 cc	1:300,000	6	National framework, international connection
Second-order	7 – 20	±3 cc	1:250,000	10	Regional control, densification of primary network
Third-order	5 – 8	±6 cc	1:200,000	15	Local control, mapping at medium scales
Fourth-order	1 – 5	±10 cc	1:100,000	30	Engineering surveys, cadastral and detailed mapping

Geodetic points are interconnected within a coordinate network defined by (x, y) values. A designated point in the country is established as the coordinate origin, or zero point, i.e., $(x = 0, y = 0)$. Depending on the location of this origin, other points in the network may have positive or negative coordinate values. These points are fixed with high precision, and geodetic markers of various shapes are installed above them. To ensure visibility and reliable monitoring, such markers are typically placed in prominent locations, including hills, mountain peaks, and minarets.

2.5.2 The Geodetic Network in Syria

The Syrian national geodetic network is a four-order triangulation system developed in stages through the combined efforts of specialists from France, Russia, and Syria. These individual networks were later integrated into a unified framework and officially adopted as the geodetic reference network for the country, providing essential control for engineering and surveying projects. Today, this network serves as the fundamental basis for all topographic surveying activities, covering the entirety of Syrian territory.

In this system, the coordinate origin was established at a reference point located southeast of the city of Palmyra. As a result, Syrian maps display both positive and negative coordinate values depending on their position relative to this origin.

2.5.3 Types of Traverses

Traverses in surveying are classified according to the availability of known control points, the nature of the facility, and the size of the study area. The main types are:

Open Traverse:

This type is commonly applied in the surveying of linear features such as roads, railways, and oil or gas pipelines. An open traverse consists of a series of sequentially connected sides that begin from at least two known control points and extend to terminate at another set of at least two known control points.

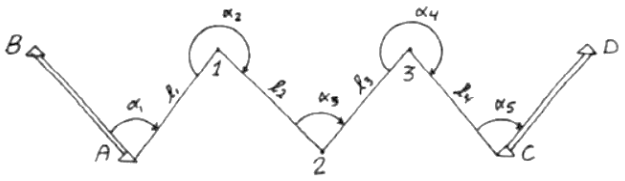

Figure 21: Open Traverse

Closed Traverse:

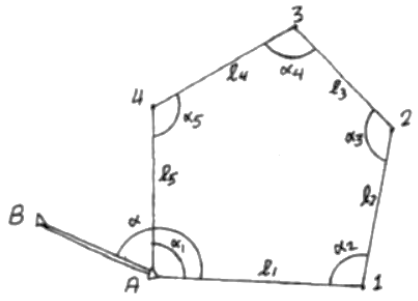

Figure 22: Closed Traverse

This type is typically used for relatively limited areas, particularly where the terrain or the nature of the facility does not allow the establishment of an open traverse. A closed traverse is formed by a sequence of connected sides that originate from a known point and return to the same point, thereby forming a closed loop. To ensure proper orientation,

the traverse must also be tied to a known azimuth by connecting the starting point with another control point.

Free Traverse:

This type begins from a point with known coordinates but does not close on another known point, often due to the absence of such control in the area or the nature of the facility being surveyed. Since closure and verification cannot be performed, this method is less reliable and is generally used only when unavoidable.

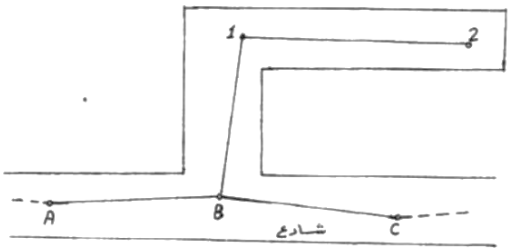

Figure 23: Free Traverse

Straight Traverse:

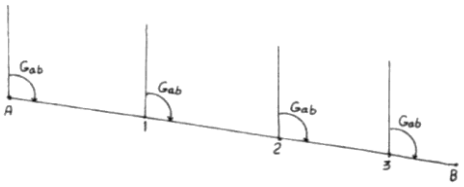

Figure 24: Straight Traverse

This type occurs when all known and unknown points lie along a single straight line. In this case, the azimuth at each station coincides with the azimuth of the line itself, which simplifies the process and provides flexibility in computing the coordinates of unknown points. Such traverses are commonly encountered when surveying long linear features, such as streets, or when establishing localized leveling networks arranged in rectangular or square patterns.

Traverse Network:

When the surveyed area is extensive, a single closed or open polygon is insufficient, and it becomes necessary to establish a polygon network. This network may consist of two or more interconnected closed polygons, or—if the terrain prevents forming closed loops—a system of intersecting open polygons. The intersections of these open traverses

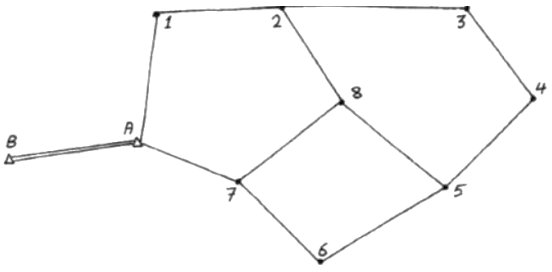

Figure 25: Traverse Network

are known as nodes. In some cases, a hybrid network is created, combining both closed and open polygons to ensure adequate coverage and connectivity of control points.

2.5.4 Overview of Projection Systems

Representing the Earth's curved surface on a plane would be straightforward if the surface of a sphere or ellipsoid could be directly transferred without distortion. However, since the ellipsoidal surface is bi-curved, it cannot be projected onto a plane without introducing tearing, stretching, or deformation.

It is well established that only mono-curved surfaces, such as the cylinder and the cone, can be developed onto a plane without distortion. This principle forms the basis of cylindrical and conical projection systems, in which the spherical (or ellipsoidal) surface is projected onto the surface of a cylinder, a cone, or a secant version of these surfaces. Once the projection is complete, the cylindrical or conical surface is mathematically "unwrapped" to form a plane representation. In addition, there are azimuthal projection systems, where the Earth's surface is projected directly onto a plane that is tangent to or secant with the sphere (or ellipsoid).

In general terms, a projection system may be defined as a one-to-one mathematical relationship between points on the Earth's surface—expressed by geographic coordinates (latitude ϕ and longitude λ)—and their corresponding points on the plane—expressed by projected coordinates X and Y.

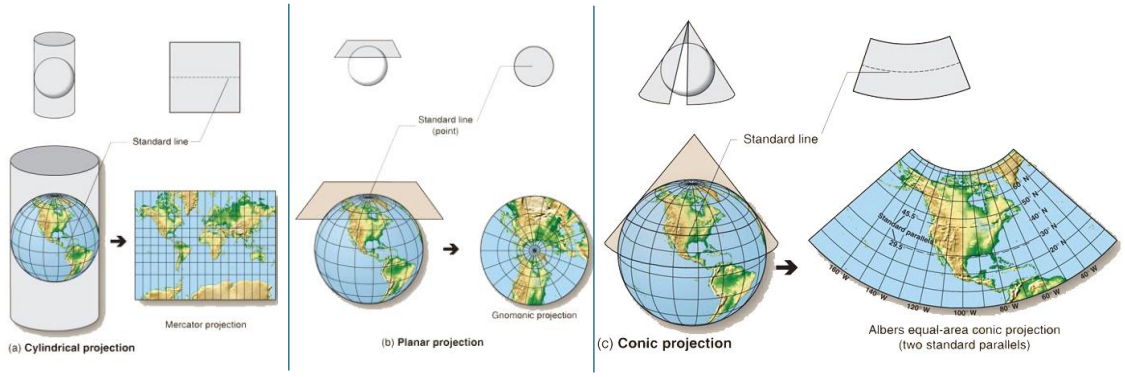

Figure 26: Projection main types

2.5.4.1 *Adopted Projection Systems in Syria: Properties and Applications*

A. Transverse Mercator Projection (STM)

- Type: Conformal, angle-preserving projection.
- Reference Ellipsoid: Hayford (1924).
- Zone Width: 3° longitude ($\lambda = 3°$).
- Special Adjustment: A quarter degree was added to the edges of the zones, so that each zone covers 3.5° in total. The overlap between adjacent zones is 0.5°.
- Coverage: Syria extends across three zones (IV, V, VI). Each has its own Cartesian coordinate system.
- Adoption Date: Introduced during the union of Syria and Egypt in 1958.
- Use: Applied mainly for small-scale mapping.

B. Lambert Conic Projection

- Type: Conformal conic projection.
- Reference Ellipsoid: Clarke (1880).
- Standard Parallels: $\varphi 1 = 36.75°$ and $\varphi 2 = 40.25°$. Distortion is zero along these two parallels, negative between them, and positive outside them ($K = 1$ on the standard parallels).
- Scale at Central Latitude: $K_o = 0.99962560$.
- Maximum Distortion: 1:2550 along the northern and southern boundaries of Syria, which is within accepted surveying accuracy.
- Adoption Date: Approved in 1920.
- Use: Applied in small- and medium-scale mapping, as well as in the establishment of first-order triangulation networks.

C. Oblique Stereographic Projection

- Type: Conformal azimuthal projection.
- Reference Ellipsoid: Clarke (1880).
- Isometric Circle Radius: 275 km, centered at the projection origin.
- Distortion Zone: Defined by two circles, with radii ±0.75 km relative to the zero-distortion circle.
- Scale Factor at Center: $K_o = 0.9995314$.
- Adoption Date: Established in 1920.
- Use: Developed to document real estate ownership. It was applied in calculating surveying base points, producing cadastral maps, urban plans, topographic maps, and engineering project datasets.

D. WGS84 / UTM System

- Type: Global system, using Universal Transverse Mercator (UTM) projection.
- Reference Ellipsoid: WGS84.
- Application: Provides satellite imagery and geospatial data through the Global Positioning System (GPS). Widely used by public and private organizations for monitoring and surveying projects.
- Official Status: Although widely utilized, it is not formally adopted as the national system in Syria.

*In the context of this research, as in most projects conducted in Syria, the **Oblique Stereographic Projection coordinate system** is used, which is also referred to in some engineering software as the Deir ez-Zor Projection.*

2.6 HBIM (HERITAGE BUILDING INFORMATION MODELING)

The development of Heritage Building Information Modeling (HBIM) represents an evolution of Building Information Modeling (BIM) from its original application in new construction to the domain of historic and complex buildings. While BIM was conceived as a design and project management tool for contemporary architecture, HBIM adapts its principles to accommodate the irregular geometries, material heterogeneity, and layered histories of cultural heritage assets. This transition has been driven by the need for digital platforms that can integrate diverse survey data, support conservation planning, and preserve documentation in sustainable digital formats.

The application of HBIM to historic buildings has proven both valuable and challenging. Unlike modern structures characterized by standardized elements, heritage architecture often contains unique, asymmetrical, or deteriorated features that resist parametric simplification. This requires hybrid modeling strategies that combine automated and manual processes, as well as semantic enrichment that records not only geometric detail but also historical, material, and conservation information. The resulting models provide

not just digital replicas but knowledge-based systems that can be queried, updated, and reused across conservation and management contexts.

Central to HBIM is the use of Levels of Detail (LoD), which define the degree of geometric and semantic precision represented in the model. LoD 300 provides accurate geometry suitable for architectural documentation at scales such as 1:50, while LoD 400 incorporates greater detail in construction and material representation. LoD 500 achieves the highest level of fidelity, approaching a digital twin of the building, but it demands significant time, effort, and computational resources. In practice, heritage HBIM often combines levels—using LoD 300 for large structural components while applying LoD 400–500 selectively to elements of high significance, such as decorated domes or minarets.

Integration of survey data is a defining feature of HBIM workflows. Photogrammetry contributes dense point clouds and textured models that capture fine surface details with sub-centimetric accuracy, while terrestrial laser scanning (TLS) provides highly precise geometric data over large areas. The combination of these methods ensures both accuracy and completeness: photogrammetry enriches the HBIM model with visual realism, and laser scanning anchors it with geometric rigor. Together, these data sources form the backbone of HBIM, enabling robust digital documentation of historic structures that balances fidelity, usability, and long-term conservation needs.

Table 9: Levels of Detail (LoD) in HBIM for Heritage Documentation

LoD	Description	Accuracy / Geometry	Effort & Cost	Typical Heritage Application
LoD 300	Accurate geometry of main structural elements; simplified representation of details.	~1:50 scale; sub-centimetric to centimetric accuracy.	Moderate effort; efficient processing.	General architectural documentation, conservation planning, base for drawings.
LoD 350	Geometry includes interfaces and connections between elements; greater detail than LoD 300 but not full material specification.	~1:20–1:50 scale; improved precision, especially at junctions and boundaries.	Higher effort than LoD 300; still less demanding than LoD 400.	Useful for documenting how historic elements interact (arches with walls, domes with drums) without modeling every material layer.

LoD	Description	Accuracy / Geometry	Effort & Cost	Typical Heritage Application
LoD 400	Detailed geometry with higher precision and richer semantic data (materials, construction).	~1:20–1:50 scale; sub-centimetric accuracy.	High effort and cost due to modeling complexity.	Selective modeling of important façades, decorated surfaces, or structural systems.
LoD 500	"As-built" digital twin, highest fidelity in both geometry and semantics; closely aligned to reality.	Approaches millimetric accuracy, depending on survey input.	Very high effort and computational demand; often impractical for full monuments.	Applied selectively to critical heritage elements (domes, inscriptions, damaged details).
LoD 600	Fully operational model including maintenance data, conservation history, and lifecycle management. Goes beyond geometry into asset management.	Geometry same as LoD 500, but enriched with ongoing monitoring and historical data.	Extremely resource-intensive; requires continuous updating and data integration.	Rare in heritage; theoretical level used for long-term conservation management or UNESCO World Heritage digital twins.

2.7 ACCURACY EVALUATION IN DIGITAL HERITAGE WORKFLOWS

The reliability of digital heritage documentation is closely linked to the ability to quantify and validate accuracy. A range of metrics are commonly employed to assess how closely digital models replicate measured reality. At the most basic level, deviations are expressed in Cartesian coordinates (ΔX, ΔY, ΔZ), measuring differences between model points and survey benchmarks. Distance deviations (Δd) and relative errors (%) are often calculated to contextualize the magnitude of discrepancies against the scale of the measured feature. In angular assessments, angular deviation (Δθ) quantifies differences in computed versus measured angles, typically expressed in degrees. Together, these metrics provide a multi-dimensional picture of spatial accuracy.

International guidelines provide benchmarks for acceptable tolerances. The CIPA/ICOMOS Principles on heritage documentation emphasize that all digital products should be accurate, reliable, and verifiable, with error margins stated explicitly. In heritage practice, tolerances are often set at the centimetric to sub-centimetric level depending on the scale of documentation. For instance, façade-level surveys may accept 1–2 cm deviations, while detailed element recording may require accuracy at the millimetric level.

These standards ensure that documentation outputs can serve as a credible basis for conservation and reconstruction.

Accuracy assessment also intersects with BIM and engineering tolerances, particularly when working at high Levels of Detail (LoD 400–500). At these levels, even small deviations can accumulate, affecting model usability for conservation planning. Engineering tolerances at LoD 400 typically demand sub-centimetric precision, while LoD 500 approaches "as-built" accuracy with millimetric fidelity. Heritage HBIM must therefore balance between achievable accuracy in photogrammetry or laser scanning and the representational limits of parametric modeling.

Previous studies demonstrate diverse approaches to accuracy evaluation. Fai et al. (2013) highlighted the challenges of modeling irregular heritage geometries within BIM platforms and the reliance on survey benchmarks for validation. Hichri et al. (2013) emphasized user expertise as a key factor in achieving accuracy, noting the interpretative role of operators in translating point clouds to BIM objects. Remondino et al. (2012, 2014) presented systematic comparisons of photogrammetry and laser scanning, underscoring that both can achieve sub-centimetric accuracy when acquisition and processing parameters are carefully optimized. Collectively, these works establish accuracy evaluation as both a technical exercise (quantifying deviations) and a methodological safeguard (ensuring reliability and reproducibility).

2.8 PERFORMANCE EVALUATION OF PHOTOGRAMMETRY AND HBIM

Indicators: time, cost, resource demands, visualization quality.

Comparative studies of photogrammetry vs. laser scanning vs. CAD.

Trade-offs between accuracy and efficiency.

2.9 ANALYTICAL FRAMEWORKS IN HERITAGE DOCUMENTATION RESEARCH

Analytical frameworks in heritage documentation research provide a structured means of evaluating the effectiveness of different recording methods. Comparative dimensions typically include ***accuracy*** (how closely outputs replicate reality), ***performance*** (efficiency

in terms of cost, time, and resource demands), visualization quality (clarity, interpretability, and capacity to support conservation decision-making), and applicability (the adaptability of methods to diverse heritage contexts). These dimensions enable a balanced assessment that moves beyond technical precision to consider usability and long-term value for heritage management.

Existing models have been adapted to heritage contexts from broader engineering and architectural research. Frameworks originally designed to evaluate survey or BIM performance are increasingly applied to cultural heritage, with emphasis on integrating diverse data sources—such as photogrammetry, terrestrial laser scanning, and archival records—into coherent evaluation structures. In HBIM research, these frameworks are often extended to include semantic enrichment and conservation-specific attributes, such as material information or condition assessment layers.

However, a critical gap remains in Syrian heritage documentation. Despite the urgent need created by conflict-related damage and risk, systematic evaluation of accuracy and performance is limited. Studies tend to focus either on the feasibility of using photogrammetry and UAVs for rapid documentation or on the production of visual models for awareness and education. Few works apply a rigorous analytical framework that combines accuracy validation, workflow efficiency, and conservation usability in an integrated way. Addressing this gap, the present research develops a structured methodology for evaluating photogrammetry-to-HBIM workflows at Al-Tunbugha Mosque, thereby contributing a replicable model for post-conflict heritage contexts in Syria.

2.10 SUMMARY OF LITERATURE REVIEW

The review of existing literature highlights **three key insights** that shape the present study. **First**, heritage documentation has evolved from manual surveying and CAD-based drafting to advanced digital methods such as photogrammetry, terrestrial laser scanning, and HBIM. These technologies provide new opportunities for recording cultural heritage with greater speed, detail, and integration, especially in post-conflict contexts where accuracy and reliability are vital for reconstruction.

Second, the literature shows that each method carries strengths and limitations. Photogrammetry offers cost-effective, adaptable, and visually rich models but is dependent on image quality and environmental conditions. Laser scanning provides exceptional geometric accuracy but at higher financial and technical costs. HBIM, while enabling parametric structuring and semantic enrichment, requires careful calibration of LoD to balance fidelity, resource demands, and conservation goals.

Third, accuracy and performance evaluation emerges as a critical but underdeveloped dimension in heritage documentation research. International standards from CIPA/ICOMOS emphasize transparency and explicit error reporting, yet many case studies focus on visual results without systematically quantifying deviations or benchmarking against survey data. Studies such as those by Fai, Hichri, and Remondino point to this need, underscoring the importance of combining technical validation with practical usability.

Despite these contributions, a significant gap remains in Syrian heritage documentation. Few studies have systematically integrated accuracy evaluation, workflow performance, and HBIM applicability in post-conflict settings. This research addresses that gap by developing and applying a structured methodology that moves from photogrammetry to HBIM, rigorously tested against survey benchmarks at Al-Tunbugha Mosque.

The insights from this literature review directly inform the methodology outlined in Chapter 3, which emphasizes accuracy and performance evaluation as central components of the workflow. By grounding the research in both international standards and local post-conflict needs, the methodology positions the study to contribute not only to academic discourse but also to practical heritage conservation in Syria.

CHAPTER 3. METHODOLOGY

3.1 RESEARCH DESIGN AND FRAMEWORK

This research adopts an ***Applied, Two-Stage Case Study–Based*** design that combines qualitative evaluation and quantitative analysis in order to assess the accuracy, usability, and workflow efficiency of integrating photogrammetry into Building Information Modeling for heritage documentation (HBIM).

The framework of the research is structured around the following components:

3.1.1 Exploratory Review

Prior to establishing the research methodology, an exploratory review was undertaken to examine the techniques, tools, and standards available for heritage documentation in Syria. The purpose of this review was not only to survey theoretical approaches but also to identify practical constraints and opportunities that would guide the design of the methodology.

First, different documentation approaches were assessed, with particular attention to photogrammetry. Although terrestrial laser scanning provides high accuracy and dense point clouds, its application in Syria is limited by high costs, restricted equipment availability, and the need for specialized operators. Photogrammetry, by contrast, proved more accessible, cost-effective, and adaptable to local field conditions, especially given the availability of non-metric digital cameras and UAV platforms. On this basis, photogrammetry was selected as the primary input and methodological driver leading into the HBIM process.

Second, software platforms were reviewed for their suitability in processing and integrating photogrammetric data. Agisoft Metashape and Autodesk ReCap were evaluated for image alignment, point cloud generation, and mesh reconstruction, while Autodesk Revit was considered for integration of the outputs into a BIM environment. Trial applications demonstrated that the chosen workflow—***Metashape for photogrammetry and Revit for BIM—offered the best balance of accuracy, usability, and interoperability.***

Third, the national geodetic context was analyzed, with attention to projection systems historically used in Syria. Among the available systems, the Oblique Stereographic Projection (commonly referred to as the "Deir ez-Zor Projection") was identified as the most relevant for this research. Its adoption ensured that all outputs were accurately georeferenced and consistent with local surveying standards.

Finally, preliminary field assessments, including the pilot documentation of *Al-Takiyya Al-Refa'aia Al-Ikhlasia*, confirmed the feasibility of the selected approach. This pilot exercise provided practical feedback on camera settings, marker distribution, image overlap, and point cloud density, which were refined and incorporated into the main research design. These refinements were subsequently applied to the main case study of *Al-Tunbugha Mosque*, chosen for its architectural significance, Mamluk heritage value, and vulnerability in the aftermath of conflict.

Through this exploratory review, the research methodology was shaped around tools and processes that are both ***technically robust and contextually appropriate***, ensuring their suitability for documenting Syrian heritage sites under post-conflict and post-earthquake conditions.

3.1.2 Case Study Approach (Two-Stage Design: Pilot and Main)

This research employs a ***case study approach*** in order to test and evaluate the integration of photogrammetry with Building Information Modeling (BIM) for heritage documentation. Given the complex and context-specific challenges of documenting cultural heritage sites—particularly in conflict-affected and earthquake-damaged regions—a case study strategy provides the most effective means to observe, apply, and refine the proposed workflow in real-world conditions.

The study design incorporates a ***two-stage case study framework***. The first site, ***Al-Tikyya Al-Rifa'aia Al-Ikhlasia***, was employed as a ***pilot case study***. Its purpose was to test the initial methodology, generate preliminary results, and refine the research framework. The insights gained from this pilot study informed the development of a more robust methodology.

The second site, ***Al-Tunbugha Mosque***, was selected as the ***main case study***. Here, the refined methodology was applied comprehensively to assess accuracy, usability, and workflow efficiency. This two-stage strategy strengthens the validity of the research by ensuring that findings are not based on a single isolated site, but on a tested and validated process.

By adopting this case study approach, the research directly addresses its objectives: (1) evaluating the accuracy of photogrammetric documentation within heritage BIM environments, (2) assessing the usability of outputs for conservation and restoration planning, and (3) optimizing workflow efficiency for heritage projects in Syria.

3.1.3 Site Selection Process

In order to conduct the 3D documentation case study and ensure a comprehensive understanding of its dimensions, it was imperative to identify a location that integrates all the necessary cases, thereby guaranteeing the accuracy of the results and the relevance of the outputs. Consequently, multiple field visits were undertaken across the various sectors of the old city of Aleppo, which are divided into the following 10 axes[8]:

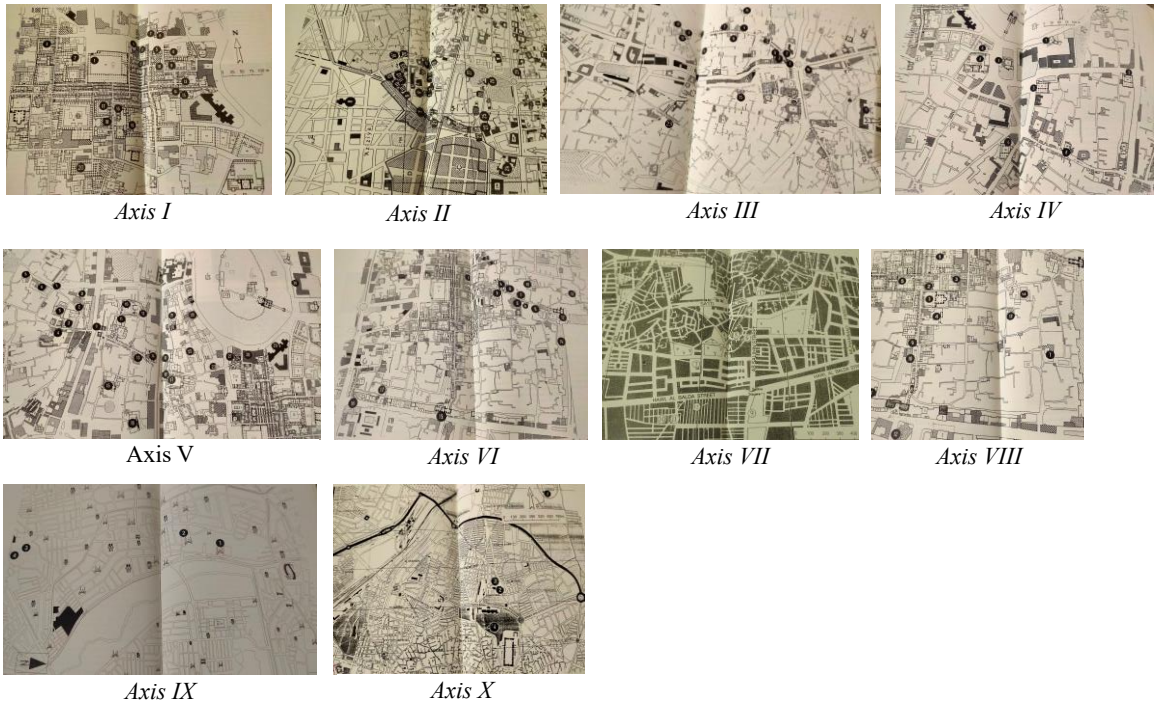

Figure 27: Maps of Old City of Aleppo Axes

i. Axis of the Umayyad Mosque and the surrounding markets and khans.

[8])Hajjar(1990 ،

ii. Axis of Al-Jdaideh neighborhood, churches, traditional courtyard house, and Bab al-Faraj neighborhood.

iii. Axis of Bab al-Hadid, Al-Bayada neighborhood, and Bab al-Ahmar.

iv. Axis of schools and mosques south of the Citadel.

v. Axis of Bab al-Nasr, outside the walls, and Al-Farafra neighborhood.

vi. Axis of Bab Qinnasrin and Bab Antakya.

vii. Axis of Bab Al-Maqam and Al-Firdaws School.

viii. Axis of Al-Jaloum and Al-Aqaba neighborhoods.

ix. Axis of Al-Hussein Shrine, Al-Dakka Shrine, and Al-Ansari Shrine.

x. Axis of the tomb of Sheikh Faris, Sheikh Abu Bakr, Al-Bakhti Mosque, and the remains of the scholar George Smith, and the English grave.

After conducting field visits to all 10 Axes, the potential sites were initially narrowed down to **38** archaeological sites:

Figure 28: Photos of the 38th archaeological sites.

Site #01 - Arghuni Hospital

Site #02 - The Sabsibiyya Tekke (Rifai Ahmadiyya)

Site #03 - Al-Asadivva School

Site #04 – Kebbeh House

Site #05 - Kaltawi School

Site #06 – Al-Tikyya Al-Rifa'aia Al-Ikhlasia


Site #07 – Bab Al-Maqam

Site #08 – Salahia House

Site #09 – Ghazala House

Site #10 - Al-Thahiria School


Site #11 – Bab Qinnasrin

Site #12 – Al-Bayada Mosque (Al-Sarwi)

Site #13 – Al-Karimia Mosque



Site #14 – Abshir Pasha Mosque

Site #15 – Al-Romi Mosque

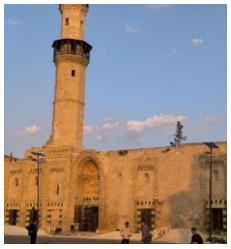

Site #16 – Al-Atroush Mosque

Site #17 – Al-Saffahia Mosque


Site #18 – Al-Makamat Mosque



Site #19 – Al-Dabbagha Al-Atika Mosque

Site #25 – Al-Mostadamia Mosque

Site #26 – Miro Mosque

Site #27 – Al-Tarsosi Mosque

Site #28 – Al-Mawazini Mosque

Site #29 – Bah Sita Mosque

Site #30 – Khan Al-Kattan

Site #31 – Khan Khair Bik

Site #32 – Kilikia School

Site #33 – Al-Azro'ai Tomb

Site #34 – The shrine and tomb of Muhammad Gulbaky

Site #35 – Dar Dalal

Site #36 – Armenian orphanage

Site #37 – Khair Bik Tomb

Site #38 – Bab Al-Ahmar Mosque

3.1.3.1 *Selection Criteria*

A set of criteria was established to select the most appropriate site for the study based on following criteria:

Safe Access

- Access and permissions: written approval, photography allowed, tripod/drone allowed, GCP placement allowed.
- Safety & stability: safe access to all areas needed; no active structural failure; PPE possible.
- Ethics and conservation: complies with site rules; minimal impact; stakeholder consent (custodian/community).

Suitability for Photogrammetry

- Surface richness & texture: stone/brick relief vs. glossy/featureless.
- Visibility/occlusion: limited deep occlusions; accessible interiors/exteriors.
- Lighting conditions: controllable or stable daylight; limited harsh shadows.
- Environmental constraints: weather, visitor flow, vibration, dust.
- Scale & accessibility: can you capture with your lenses/UAV; safe scaffolding if needed.
- Control network feasibility: room for GCPs/targets; GNSS feasibility; stable benchmarks.

Suitability for BIM / HBIM

- Geometric typology: vaults, arches, irregular masonry—rich enough to demonstrate parametric/HBIM but not impossible.
- Information goals & LOD fit: site matches your intended LOD (e.g., LOD 200–300) and attribute set (materials, phases, pathologies).
- Regularity & repeatability: patterns you can parametrize (bays, arcades) to show BIM advantages.
- Data integration potential: can you link archival drawings, surveys, pathology maps, maintenance data?

Research Value & Representativeness

- Heritage significance: typological/chronological relevance to your region.
- Transferability: lessons generalize to other heritage assets.
- Documentation gap: fills a known gap (under-documented, recent damage, restoration planning).

Logistics & Risk

- Time and budget fit: capture, processing, and modeling within thesis timeline.
- Team & equipment match: cameras, lenses, UAV permissions, software licenses, computing power.
- Stakeholder engagement: supportive custodian; potential for supervision/collab.

After evaluating all 38 sites against the above criteria, Al-Tikiyya Al-Rifaʿiyya Al-Ikhlāṣiyya was selected as the pilot study, and al-Tunbugha Mosque as the main case study. This phased approach ensured both the refinement of methodology and the robust testing of results in different heritage contexts.

3.1.4 Instruments and Software Applications

The successful implementation of the photogrammetry-to-HBIM workflow required a combination of specialized equipment and software. The following subsections describe the hardware and software applied in the research, along with their technical specifications and relevance to the study.

3.1.4.1 *Equipment (Hardware)*

Cameras:

- Type: non-metric
- Redmi note 13 pro plus 5G (Mobile), 200 MP, focal point 23 mm, iso 1250, no flash, no zoom

Laptop:

- Brand: Asus Rog
- Processer: AMD Ryzen 7 4800H with Radeon Graphics 2.90 GHz
- RAM: 32 GB
- Graphics: NVIDIA® GeForce GTX™ 1650 Laptop GPU
- Storage: 1TB M.2 NVMe™ PCIe® 3.0 SSD storage
- System: 64-bit operating system, x64-based processor
- Edition: Windows 10 Pro

Surveying Instruments (Total Station)

- Type: Topcon GTS 1002
- Minimum focus: 1.3 m
- Accuracy: 2" (0.0006gon/0.010mil)
- Measuring time: 0.5 sec or less
- Internal memory: 10,000 measurement points
- Measuring range (Reflectorless): 300m
- Measuring range (Prism-2x1): 4,000m
- Distance unit Accuracy (Prism): Fine measurement: (2 + 2 ppm X D) mm
- Distance unit Accuracy (Reflectorless): Fine measurement: (5 + 10ppm X D) mm (over 200 to 300m)

UAVs (Drones)

- Type: DJI Mavic 3 Pro

- Triple-camera system:
  - Hasselblad wide-angle camera: 4/3 CMOS sensor, ~20 MP.
  - Medium telephoto camera: 1/1.3-inch CMOS, ~48 MP, focal length equivalent ~70 mm.
  - Long telephoto camera: 1/2-inch CMOS, ~12 MP, focal length equivalent ~166 mm.
- Aperture for Hasselblad: f/2.8 to f/11.
- Maximum flight time: ~ 43 minutes under ideal conditions.
- 5.1K video recording (wide/hasselblad camera).
- High resolution in photos with the telephoto lenses (for capturing detailed distant or close-in features).

Accessories

- Targets/markers, lighting equipment, PPE for safe access, scaffolding.
- Debris removal equipment.

3.1.4.2 *Software (Processing & Modeling)*

- ***Photogrammetry Software:*** AgiSoft MetaShape, Professional Edition, Version 1.8 (for image alignment, dense cloud, mesh, orthophoto).
- ***Surveying Software:*** Autodesk AutoCAD Civil 3D 2024 (for preprocessing GCP, markers and traverses related calculations).
- ***Point Cloud Processing Software:*** Autodesk ReCap Pro (for preprocessing, converting, and point cloud cleaning).
- ***CAD Software:*** Autodesk AutoCAD 2024 (for 2D drawings)
- ***BIM Software:*** Autodesk Revit 2021 and 2024 (for HBIM integration, parametric modeling).
- ***Real-time rendering Software:*** EnScape
- ***Supporting Software*****:** ArcGIS v.10.4, Google Earth Pro, Microsoft Office

3.2 PILOT CASE STUDY: AL-TIKYYA AL-RIFAʿIA AL-IKHLASIA

3.2.1 Data Acquisition Framework

3.2.1.1 *Introduction*

The data acquisition process was designed to ensure accurate, reliable, and reproducible documentation of the selected heritage sites. The framework combined

geodetic surveying with photogrammetric imaging, supported by the systematic installation of control markers across all building façades and plans.

A geodetic traverse was first established, beginning from a known reference point in the vicinity of the site and extended toward the building. This provided a stable spatial framework to which all subsequent measurements were referenced. Along each façade, numbered control markers were placed at varying heights and positions to secure geometric stability and comprehensive coverage. These markers were then surveyed using a total station to generate precise coordinates, serving as ground control points (GCPs) for georeferencing the photogrammetric model.

Following this setup, a comprehensive photographic survey was conducted. Images were captured sequentially along the façades, with the camera axis oriented perpendicular to the surfaces to maintain geometric fidelity. Consistent image overlap was ensured to support accurate alignment, while additional oblique photographs were taken to capture architectural details and minimize occlusion. Environmental factors such as lighting and camera stability were carefully managed to reduce distortion and enhance data quality.

This integrated approach—geodetic control through a traverse, systematic marker distribution, and structured photographic acquisition—resulted in a robust dataset suitable for high-accuracy 3D reconstruction and subsequent integration into the HBIM environment.

3.2.1.2 *Planning and Preparation*

Effective data acquisition for heritage documentation requires careful planning and preparation to ensure both accuracy of results and safety of operations. Prior to image capture and surveying, **preliminary site visits** are undertaken to conduct reconnaissance of the monument and its surroundings. These visits allow the research team to evaluate the **physical condition of the structures**, identify potential **hazards or accessibility constraints**, and anticipate **environmental conditions** (lighting, shadows, vegetation cover, or obstructions) that may influence photographic quality and survey accuracy.

At this stage, **all necessary permits and approvals** are secured from custodial authorities to ensure legal and ethical compliance. Permissions typically cover the use of photography, placement of control markers, and, where relevant, the deployment of UAVs or tripods. Coordinating with local stakeholders at this early stage is essential for minimizing risk to both personnel and the heritage fabric.

Planning also involves **scheduling fieldwork** at optimal times of day to balance light conditions and minimize shadow distortion. Photographic sequences are arranged façade by façade, following the movement of the sun to achieve consistent illumination. In addition, site preparation may include clearing minor obstructions (e.g., vegetation or debris) that could obscure architectural features or block lines of sight for surveying instruments.

By integrating reconnaissance, administrative approvals, and environmental planning, this preparatory phase establishes a **secure, ethical, and technically sound foundation** for the subsequent acquisition of photogrammetric and geodetic data.

3.2.1.3 *Ground Control Points (GCPs)*

In photogrammetric documentation, Ground Control Points (GCPs) are indispensable for linking the image-based model to an external spatial reference system. By introducing measured, fixed points into the photogrammetric workflow, geometric distortions are minimized, and the resulting model can be scaled, oriented, and georeferenced with a high degree of accuracy.

Figure 29: Control Points (markers) example

International best practice (e.g., CIPA/ICOMOS) highlights several methodological requirements for the use of GCPs in heritage contexts:

- **Integration within a stable reference framework:** GCPs must be tied to a geodetic control network or, when not available, to a locally established traverse that ensures internal consistency.
- **Even spatial distribution:** Control points should be placed across the full extent of the surveyed object, both horizontally and vertically, in order to constrain the geometry of the photogrammetric block.
- **Visibility and redundancy:** Targets should be recognizable in multiple images and, where possible, observable from different camera positions to enhance the robustness of the bundle adjustment process.
- **Non-invasive attachment:** Markers or targets must be affixed using reversible methods that do not damage the heritage fabric. When direct attachment is not feasible, distinctive existing features (e.g., architectural edges or fixtures) may serve as natural control points.
- **Appropriate target design:** Printed or artificial targets should be of sufficient size and contrast to be reliably identified by the photogrammetric software, without obscuring or altering significant details of the building surface.

Methodologically, GCPs function as the link between field surveying instruments (e.g., total station or GNSS) and the image-based model. Once their three-dimensional coordinates are measured with surveying equipment, these values are introduced during the photogrammetric processing stage to constrain the model within the chosen coordinate system. The accuracy of the final product is thus directly dependent on both the precision of the survey measurements and the rigor with which control points are distributed and observed. GCPs were prepared as printed, numbered, and easily recognizable targets affixed on paper, designed to be clearly identified during processing within the photogrammetric software.

3.2.1.4 *Photographic Acquisition*

Photographic acquisition constitutes the core dataset for photogrammetric reconstruction. The methodological aim is to generate a complete, redundant, and geometrically consistent image block that captures the surfaces of the object of study with sufficient resolution and overlap to enable accurate three-dimensional modelling. The photographic survey follows several methodological requirements:

- **Systematic coverage:** Image acquisition should follow structured photographic lines and elevations to guarantee uniform coverage of facades, interiors, and complex surfaces.

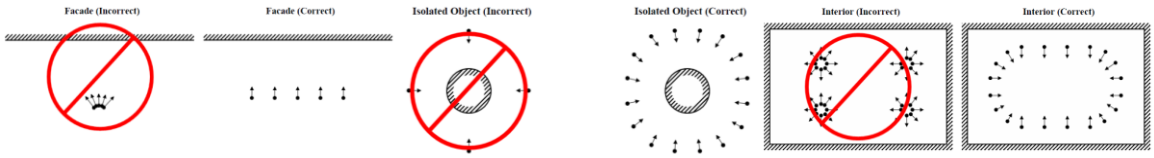

Figure 30: Appropriate capturing scenarios

- **Camera orientation:** Photographs must generally be taken with the optical axis perpendicular to the surface and the camera body parallel to the plane being documented, in order to minimize geometric distortion.
- **Redundancy and overlap:** Consecutive images should maintain a minimum overlap of 60–80% in both horizontal and vertical directions, ensuring robust image alignment and sufficient redundancy for bundle adjustment.

Figure 31: Example of capturing sequence - Yard West Facade - Al- Takiyye

- **Lighting consistency:** To minimize radiometric variations, images should be captured under stable and diffuse lighting conditions. Artificial flash is generally avoided, as it produces glare and localized overexposure.
- **Uniform acquisition parameters:** The same camera and consistent settings (focal length, aperture, ISO) should be used throughout the survey to maintain homogeneity

across the dataset.

- **Adaptation to complexity:** Additional images are required to document occluded, recessed, or geometrically complex elements, thereby avoiding gaps in reconstruction.

Methodologically, photographic acquisition also requires comprehensive metadata management. Essential parameters—including camera make, model, focal length, sensor characteristics, and acquisition settings—must be recorded. Field notes and sketch maps should be prepared to document acquisition paths, lighting conditions, and any site-specific constraints.

Finally, preliminary quality control in the field is considered best practice: images should be checked for sharpness, exposure, and adequate overlap before concluding the survey. Redundant photographs should be taken where uncertainty exists, and secure backups of raw image files should be created to ensure the integrity of the dataset for subsequent processing.

3.2.2 Data Processing Workflow

3.2.2.1 *Images Processing Overview*

Agisoft Metashape Professional Edition Version 1.8 software was employed for image processing in this project. The software was used to align the captured images, generate dense point clouds, and construct a three-dimensional model of the site. From this model, the required Orthomosaic images were subsequently produced for analysis and documentation purposes. Imagery data processing procedure with Agisoft Metashape consists of three main steps:[9]

The first step is called alignment. It includes aerial triangulation (AT) and bundle block adjustment (BBA). At this stage Metashape searches for feature points on the images and matches them across images into tie points. The program also finds the position of the camera for each image and refines camera calibration parameters (estimates internal (IO) and external (EO) camera orientation parameters).

The results of these procedures are visualized in the form of a tie point cloud and a

[9] (LLC, 2022)

set of camera positions. The tie point cloud represents the results of image alignment and will not be directly used in further processing (except for the tie point cloud based surface reconstruction method, which is suitable only for quick estimates, e.g., of completeness of a data set). But the tie point cloud is necessary for the determination of depth maps (based on the common tie points camera pairs for the depth maps calculation are selected). However, it can be exported for further usage in external programs. For instance, a tie point cloud model can be used in a 3D editor as a reference. On the contrary, the set of camera positions is required for further 3D surface reconstruction by Metashape.

The second step is generation of a surface in 3D (mesh) and/or 2.5D (DEM). Polygonal model (mesh) can be textured for photorealistic digital representation of the object/scene and exported in numerous formats compatible with post-processing software, both for CAD and 3D-modeling workflows.

For city-scale projects to provide for fast model visualization response and allow for smooth navigation across the whole scene, Metashape enables to generate tiled models. Such hierarchical representation preserves original resolution of the images applied to the model as a texture and is compatible with stand-alone and web-based viewers.

Dense point cloud can be built by Metashape based on the estimated camera positions and images themselves (dense stereo matching). Generated photogrammetric point cloud can be merged with LIDAR data or automatically divided into several semantic classes following the project tasks.

If the digital elevation model (DEM) is generated based on the dense point cloud data, it can include either both terrain and all the objects above the ground, like trees, buildings and other man-made structures (digital surface model, DSM), or only show the landscape of the territory (digital terrain model, DTM).

The third step is creating of Orthomosaic, which can be georeferenced and used as a base layer for various types of maps and further post processing analysis and vectorization. Orthomosaic is generated by projecting the images according to their EO/IO data on a surface of the user's choice: DEM or mesh.

For multispectral imagery projects, Orthomosaic can represent NDVI and other vegetation indices information. Reflectance calibration feature of Metashape allows to correctly interpret radiometric imagery data, providing that radiometric panel has been used in the project and/or sun sensor information is available in the images meta data.

General Workflow:

1) Adjusting preference settings (pre or during the workflow)
2) Loading images into Metashape;
3) Inspecting loaded images, removing unnecessary images;
4) Aligning cameras;
5) Building dense point cloud;
6) Building mesh (3D polygonal model);
7) Generating texture;
8) Building tiled model[10];
9) Building digital elevation model (DEM)[11];
10) Building orthomosaic;
11) Exporting results.

3.2.2.2 *Loading Photos into Metashape*

Before initiating the processing workflow, it is essential to select and import the images that will serve as the source data. In Agisoft Metashape, the "Add Folder" command allows users to efficiently load images into a project, particularly when photographs are organized across multiple subfolders. This function is also useful when the dataset needs to be structured in a specific way for accurate interpretation by the software, such as when incorporating images captured with different still cameras.

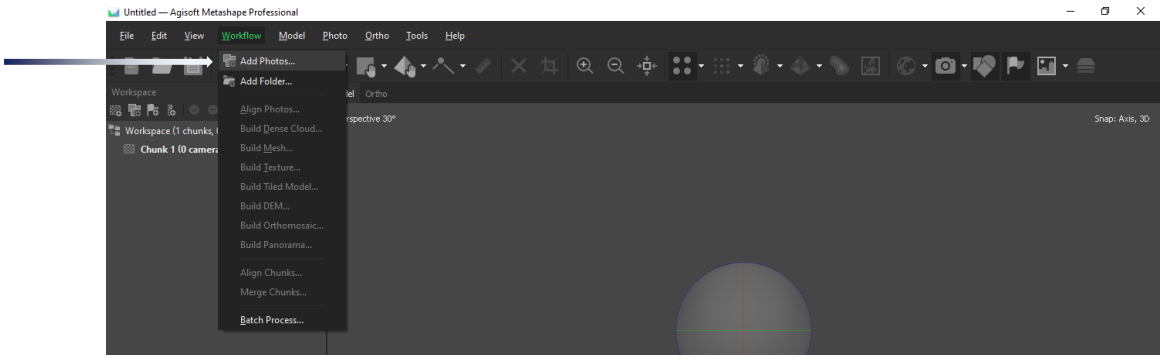

Figure 32: Agisoft Interface - Adding Photos

Agisoft Metashape supports a wide range of image formats, including JPEG, JPEG 2000, JPEG XL, TIFF, DNG, PNG, OpenEXR, BMP, TARGA, PPM, PGM, SEQ, ARA (thermal images), and the JPEG Multi-Image Format (MPO).

[10] & [16] Not used - irrelevant to the study case

Low-quality inputs, such as blurry or poorly focused images, can significantly reduce the accuracy of the alignment process. To mitigate this, it is recommended that images with a calculated quality value below **0.5** be excluded from the alignment stage.

3.2.2.3 *Align Photos*

The position of the camera at the moment of image capture is defined by its internal and external orientation parameters. Internal orientation parameters include the focal length, the principal point coordinates, and the lens distortion coefficients. Once the alignment process is completed, the estimated camera positions and the tie point (anchor) cloud are displayed in the model view. At this stage, the alignment results can be reviewed, and any cameras with erroneous positions may be identified and removed from the dataset.

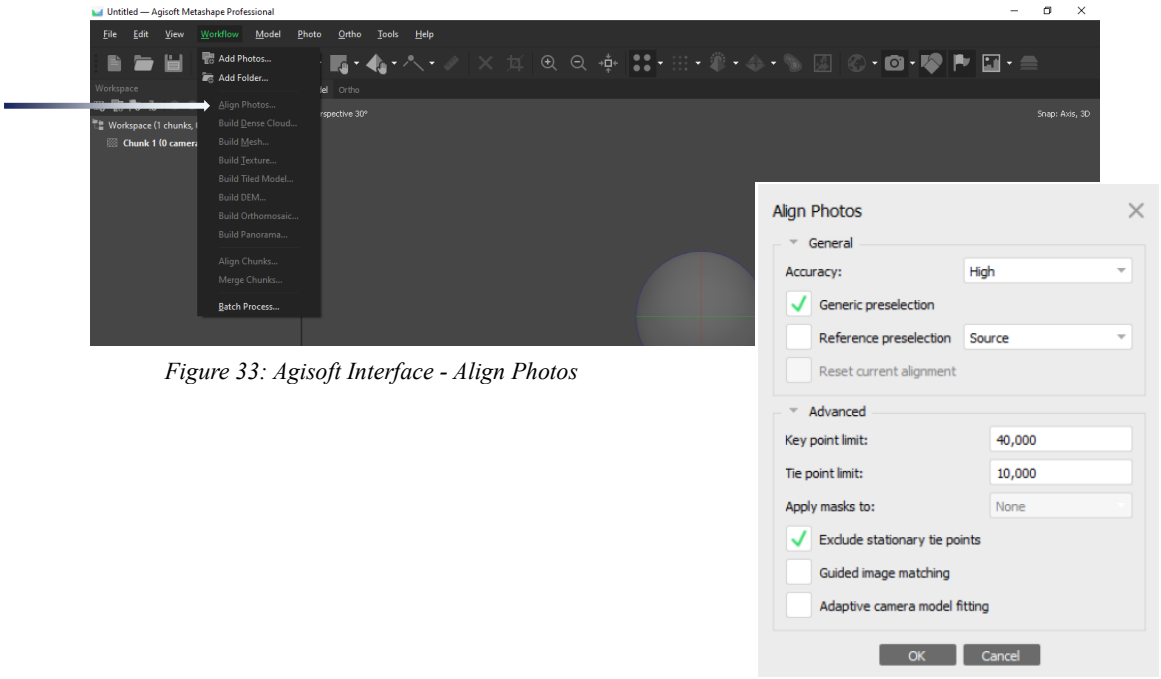

Figure 33: Agisoft Interface - Align Photos

During the alignment stage in Agisoft Metashape, several parameters influence both processing time and the accuracy of the results:

Accuracy: Higher accuracy settings utilize full-resolution images to provide more precise estimates of camera positions. Conversely, lower settings reduce image size to speed up processing, yielding only approximate results. For example:

- High resolution: processes images at their original size.
- Medium resolution: reduces image size by a factor of 4 (2× per side).
- Low resolution: reduces image size by a factor of 16.
- Lowest resolution: applies an additional reduction by a factor of 4.

While higher settings improve accuracy, they significantly increase processing time, much of which is spent on feature detection and matching across images.

Key Point Limit: Defines the maximum number of feature points to be detected and retained in each image during the alignment phase.

Tie Point Limit: Specifies the maximum number of matching points per image used to establish correspondences between photographs.

3.2.2.4 *Referencing and Camera Optimization*

Optimize Cameras command performs a full bundle adjustment procedure on the aligned photogrammetric block, simultaneously **refining** exterior and interior camera orientation parameters and triangulated tie point coordinates. The adjustment is performed based on all available measurements and corresponding accuracies, i.e. coordinates of projections of tie points and markers on images in image coordinate system; GPS coordinates of camera positions; GCP coordinates; scale bar distances.

Figure 35: Step One- Referencing: importing markers coordinates from external file

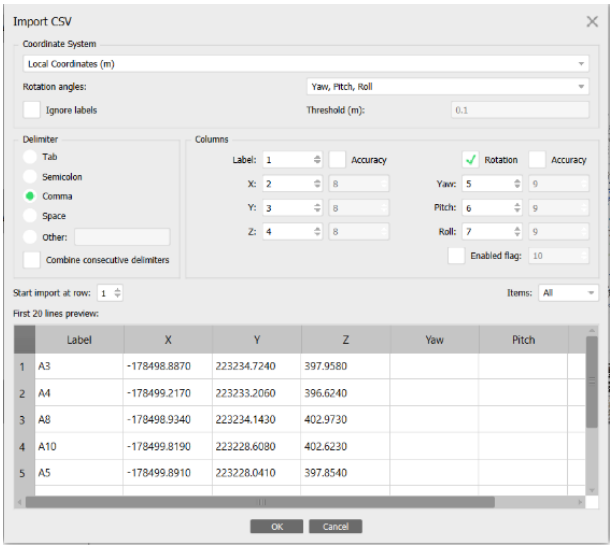

Figure 35: Step Two - Referencing: Identification of file format and Delimiter

To ensure maximum geometric accuracy of processing results, it is important to always run optimization procedure after adding/editing measured values and/or their accuracies, e.g. loading GPS camera coordinates, adding GCPs, changing accuracy settings.

To refine the referencing process, a minimum of ***three markers*** is required to calculate errors and establish the spatial reference framework. Each marker must be identified in at least ***two different images*** to ensure accurate adjustment, after which the ***"Update Transform"*** function is applied (Step Four).

All markers were referenced in at least two images. In this project, however, to maximize accuracy, each marker was linked across all available images, thereby ensuring the highest possible level of geometric consistency. Following this step, camera optimization was performed (Step Five), allowing refinement of internal and external orientation parameters and minimizing residual errors.

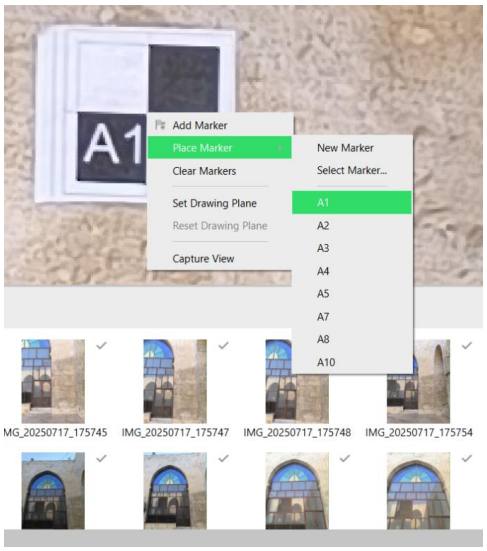

Figure 37: Step Three - Referencing: Matching markers with imported coordinates (Right click on marker and link)

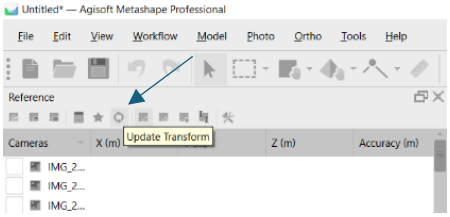

Figure 37: Step Four - Referencing: Update Transform

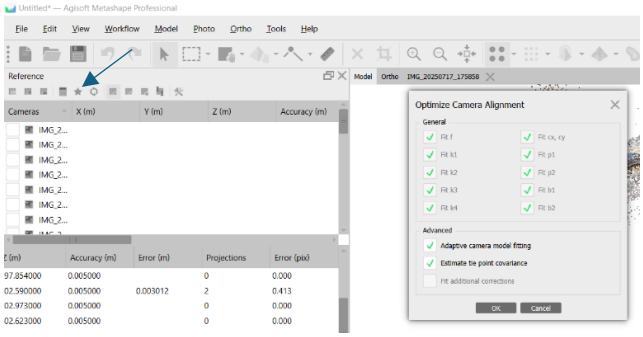

Figure 39: Step Five: Referencing: Camera Calibration

Name	X (m)	Y (m)	Z (m)	Error (m)
AV3	-178,545.66	223,793.76	399.01	0.00709
AV2	-178,544.57	223,793.47	401.08	0.005394
AV1	-178,542.82	223,793.09	398.86	0.007718
BV3	-178,545.12	223,790.78	401.50	0.004248
CV2	-178,540.95	223,792.56	400.00	0.00446
BV2	-178,541.50	223,790.77	401.62	0.001571
BV1	-178,543.60	223,791.13	399.65	0.00464
DV1	-178,540.93	223,791.70	402.08	0.002248
CV3	-178,539.98	223,791.44	401.69	0.002777
		Total Error		**0.004872**

Figure 39: Step #06: Referencing: e.g. Error

After camera optimization, the **error values** for each individual marker, along with the overall total error, are calculated and can be exported as a text file for further analysis and documentation, as demonstrated in Step Six.

3.2.2.5 *Building Dense Point Cloud*

The Quality parameter specifies the level of detail required for generating depth maps. Higher quality settings yield more accurate and detailed results but significantly increase processing time. The interpretation of quality levels follows a logic similar to that used in the Image Alignment stage, with progressive downscaling of the input images. The key distinction is that in this case, the Ultra Quality setting processes the original full-resolution images, while each lower setting reduces the image size by a factor of four (i.e., by half on each side) at every step.

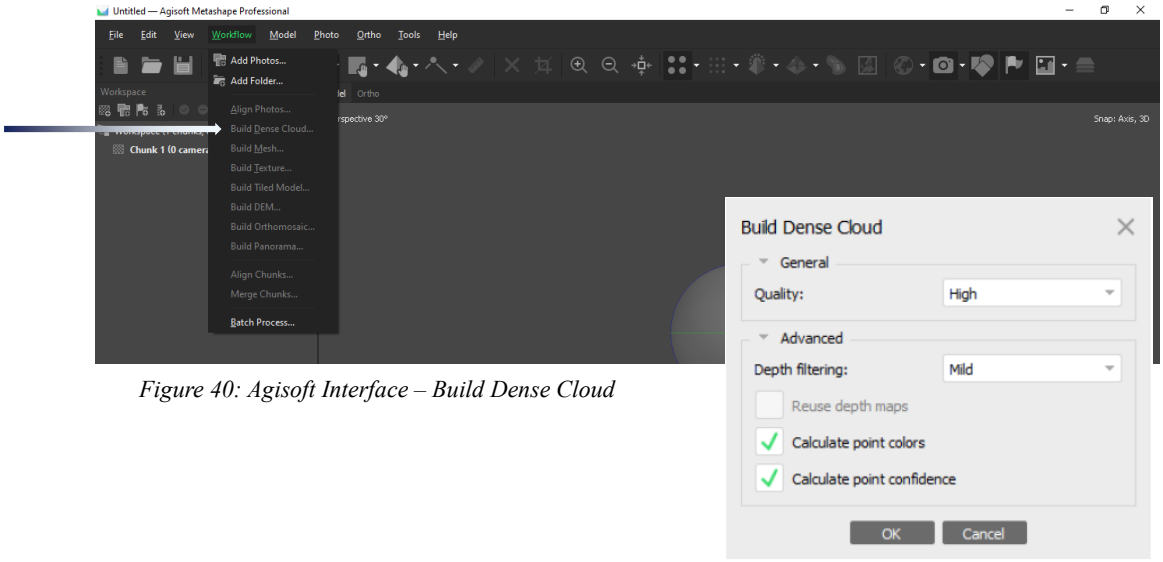

Figure 40: Agisoft Interface – Build Dense Cloud

3.2.2.6 *Building Mesh*

Agisoft Metashape can reconstruct a polygonal mesh model using point cloud data, such as dense clouds, tie points, or externally imported datasets. The main parameters controlling this process are as follows:

- ***Source data:*** Defines the dataset used for mesh generation (e.g., dense cloud, tie points, or external input).
- ***Surface Type:*** Determines the method applied to model the object surface, allowing adaptation to different object types.
- ***Quality:*** Specifies the depth map reconstruction quality. Higher quality settings provide more detailed and accurate results but require longer processing times.
- ***Face Count:*** Defines the maximum number of polygons in the final mesh. Suggested presets (High, Medium, Low) represent recommended polygon counts for meshes of corresponding detail levels.

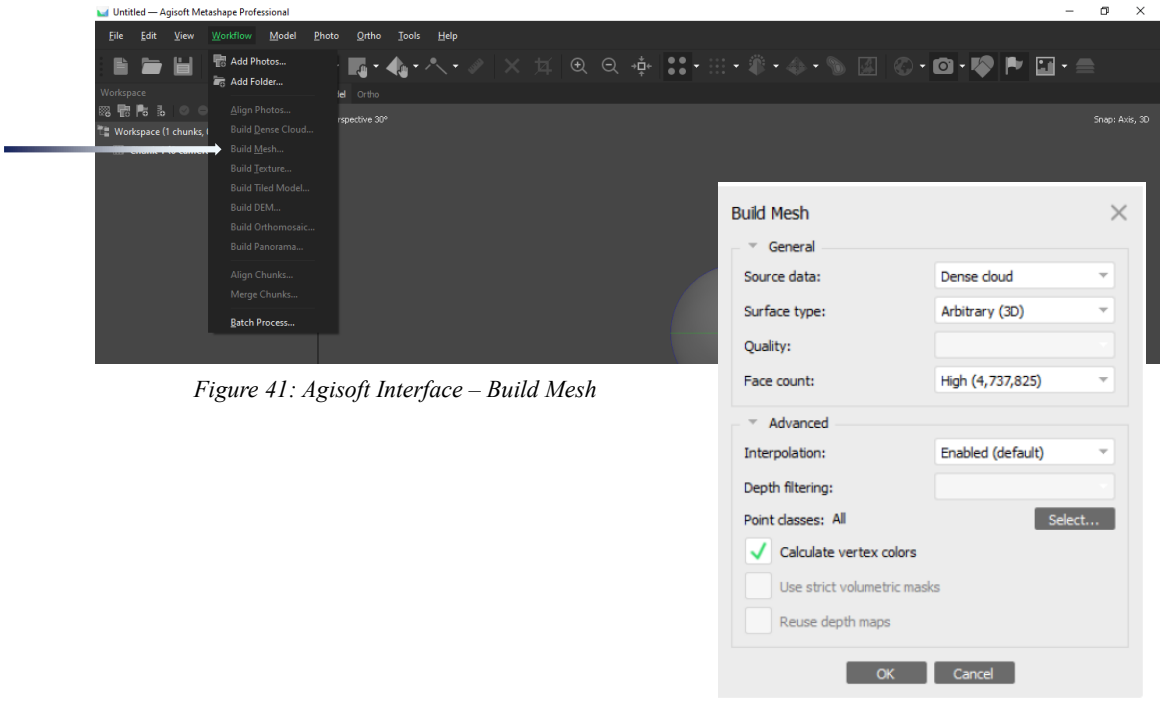

Figure 41: Agisoft Interface – Build Mesh

- ***Interpolation:***
  - Disabled: reconstructs surfaces only where dense cloud points exist, yielding highly accurate but potentially incomplete models.
  - Enabled (default): interpolates surface areas within a defined radius around dense cloud points, filling some gaps automatically, though some voids may remain and require post-processing.
  - Extrapolation mode: generates a gapless model by extending geometry into empty areas. While this produces continuous surfaces, large extrapolated areas may need to be cropped or refined during post-processing.

3.2.2.7 *Building Model Texture*

This option provides more accurate results when the surface contains sufficient detail. It is particularly recommended when the objective is to calibrate colors in order to enhance the quality of the model's texture.

Agisoft Metashape provides several options for generating and refining textures, which directly influence the visual quality of the reconstructed model. The key parameters include:

Texture Type

- Diffuse Map: The basic texture that stores the surface colors of the model.

- Normal Map: A texture that encodes surface normals, allowing lighting effects to be recalculated from different light sources in post-processing workflows.
- Occlusion Map: A texture containing pre-calculated shading information derived from background illumination.

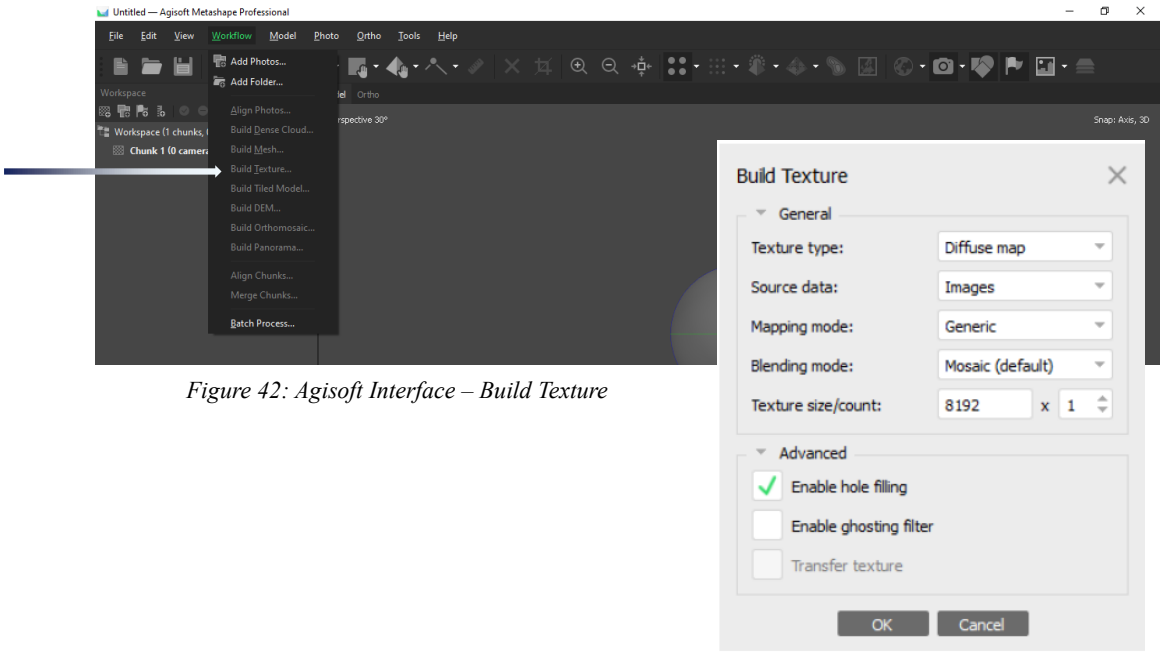

Figure 42: Agisoft Interface – Build Texture

Source Data

- Images: Builds a diffuse texture map directly from aligned images, or transfers texture from another model with a pre-existing texture.
- 3D Model: Generates normal texture maps based on another model, transferring terrain or surface data from the specified source model to the current one.

Mapping Mode

- Defines how the object's texture is projected into the texture atlas. The choice of mapping mode affects how efficiently the texture space is filled, thereby influencing the overall quality of the final output.

Blending Mode

- Determines how pixel color values from multiple cameras are combined into the final texture. The Mosaic mode applies a two-step process:
    - Low-frequency components of overlapping images are blended using weighted averaging to minimize seams.

- High-frequency components (image details) are taken from a single image, selected based on resolution quality and the perpendicularity of the camera's view to the reconstructed surface.

Texture Size / Count

- Specifies the resolution (width and height in pixels) of the texture atlas and the number of texture files to be exported. Large, high-resolution textures may require splitting into multiple files to accommodate memory limitations, while exporting as a single file may fail on systems with limited RAM.

3.2.2.8 *Building Orthomosaic*

An Orthomosaic, or Orthorectified image, is a composite product created by seamlessly merging original images projected onto an object's surface and transforming them into the specified projection system. Agisoft Metashape supports several projection types for orthomosaic generation:

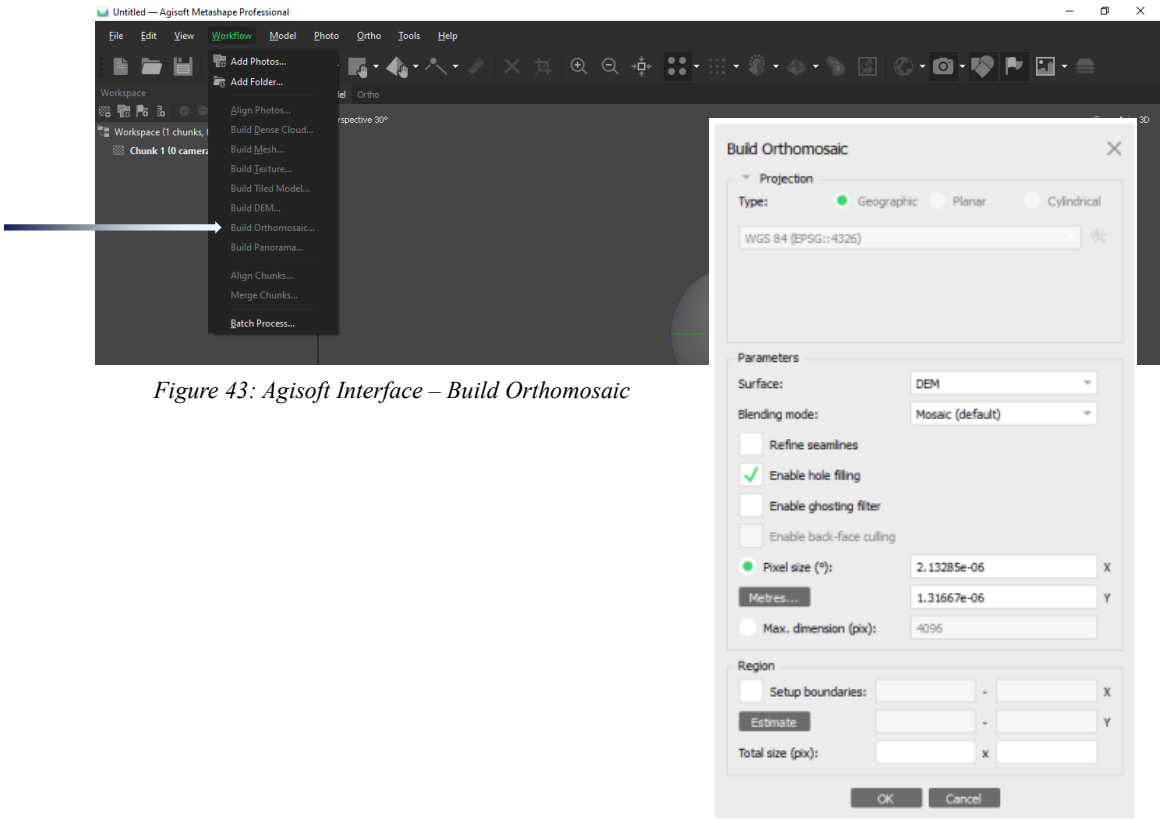

Figure 43: Agisoft Interface – Build Orthomosaic

Projection Type

- ***Geographic Projection:*** Allows the user to select a geographic coordinate system from a predefined list or to load custom system parameters. By default, the model's

own coordinate system is applied. Switching to an alternative coordinate system requires appropriate transformation parameters.

- ***Planar Projection:*** Projects the Orthorectified image onto a user-defined plane, provided a grid surface type is selected. The projection plane and image orientation can be defined using a set of markers: three markers are required, but in the absence of three, two vectors (i.e., four markers) may be used. This method is particularly suitable for façade documentation and other vertical surfaces.
- ***Cylindrical Projection:*** Projects the mosaic onto a cylindrical surface, minimizing distortions when working with cylindrical objects such as pipes, towers, or tunnels. The procedure involves:
  - Defining the cylinder (axis and radius).
  - Projecting a perpendicular from the 3D point onto the cylinder's axis, then locating its intersection with the cylinder's surface.
  - Defining the x- and y-coordinates of each point on the cylinder:
  - x: along the curve in the zero plane.
  - y: along the zero element of the cylindrical surface (the zero line), defined by the intersection of the zero plane and zero line.

Surface:

Generating a rectified image based on **DEM data** is particularly effective in aerial survey workflows, as it reduces the need for mesh generation and saves significant processing time. Alternatively, the *Surface* mesh type can be applied in more demanding applications, such as producing rectified images of building façades or other models that may not be georeferenced.

Blending Mode

- Mosaic (default): Divides image data into multiple frequency bands, which are blended independently. Only the highest frequency component along the seam is blended, while fewer bands are blended with increasing distance from the seam.
- Average: Computes the weighted average color value of all pixels from overlapping images.
- Disabled: Assigns pixel values from the single image where the camera view is closest to perpendicular to the reconstructed surface.

Pixel Size

- The default pixel size in the export image dialog corresponds to the ground sampling resolution. Specifying a smaller value does not improve resolution, but only increases the number of pixels. However, users may modify the pixel size in either coordinate system units or meters, if needed for specific applications.

Maximum Dimension (pixels)

- This parameter defines the maximum size of the exported raster data, expressed in pixels.

3.2.2.9 *Exporting Results and Supported Export Formats*

Agisoft Metashape supports exporting processing results in multiple formats, depending on the stage of the workflow and the intended application. Outputs include tie points, dense point clouds, camera calibration and orientation data, polygonal meshes, orthomosaics, digital elevation models (DSM and DTM), and complete 3D models, which can be generated and exported according to project requirements.

Tie point and camera calibration data can be exported immediately after the image alignment stage, while other outputs become available following the completion of their respective processing steps. In certain cases, the generated model may require modification in external software. Metashape supports this workflow by enabling the export of model geometry for editing and subsequent re-import, as outlined in the Modifying Model Geometry procedures described in the user manual.

Table 10 : Supported Exporting Formats

Tie Points and Camera Calibration, Orientation data Export	Orthomosaic Export	Point Cloud Export	3D Model Export
Agisoft XML structure (* .xml)	TIFF/GeoTIFF (* .tif)	Wavefront OBJ (* .obj)	Wavefront OBJ (* .obj)
Bundler OUT file format (* .out)	JPEG 2000 (* .jp2)	Stanford PLY (* .ply)	3DS file format (* .3ds)
CHAN file format (* .chan)	JPEG (* .jpg)	XYZ Point Clout (* .txt)	VRML models (* .wrl)
Bonjou TXT file format (* .txt)	PNG (*.png)	ASPRS LAS (* .las)	COLLADA (*.dae)
Realviz RZML format (* .rzml)	BMP (* .bmp)	ASTM E57 (* .e57)	Stanford PLY (* .ply)
Omega Phi Kappa text file format (* .txt)	Google Earth KMZ (* .kmz)	Topcon CL3 (* .cl3)	X3D models (* .x3d)
PATB project (* .pro)	Google Map Tiles (* .zip)	ASCII PTS (* .ptx)	STL models (* .stl)
BINGO project file (* .dat)	MBTiles (* .mbtiles)	Autodesk DXF (* .dxf)	Alembic (* .abc)
ORIMA file (* .txt)	World Wind Tiles (* .zip)	U3D (* .u3d)	Autodesk FBX (* .fbx)

Maya ASCII (* .ma)	Tile Map Service Tiles (* .zip)	Adobe PDF (* .pdf)	Autodesk DXF Polyline (* .dxf)
AeroSyr Exterior orientation (* .orn)		Point Cloud Data (* .pcd)	Autodesk DXF 3DFace (* .dxf)
Impho project file (* .prj)		Potree (* .zip)	Open Scene Graph (* .osgb)
Summit Evolution project (* .smtxml)		Cesium 3D Tiles (* .zip)	Binary g1TF (* .glb)
Blocks Exchange (* .xml)		Agisoft OC3 (* .oc3)	U3D models (* .u3d)
Alembic (* .abc)			Adobe PDF (* .pdf)
Autodesk FBX (* .fbx)			Google Earth KMZ (* .kmz)

3.2.2.10 *Automation (using chunks)*

Multiple chunk project could be useful when it turns out to be hard or even impossible to generate a 3D model of the whole scene in one go. This could happen, for instance, if the total amount of photographs is too large to be processed at a time. To overcome this difficulty Metashape offers a possibility to split the set of photos into several separate chunks within the same project. Alignment of photos, building dense point cloud, building mesh, and forming texture atlas operations can be performed for each chunk separately and then resulting 3D models can be combined.

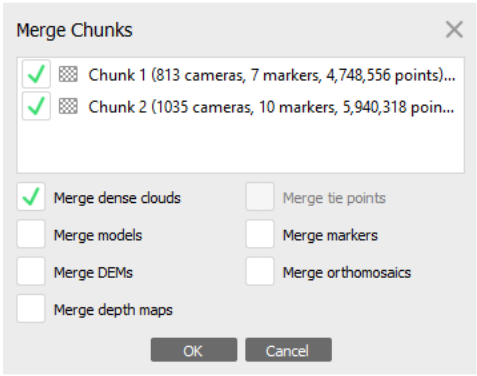

Figure 44: Merge Chunks

3.2.3 Photogrammetric Outputs (Methodological Results)

The processing of photogrammetric data yields a series of outputs that serve as both intermediate products for geometric analysis and final deliverables for heritage documentation. Methodologically, these outputs can be grouped into several categories:

Sparse and dense point clouds: The initial alignment of images generates a sparse point cloud, which serves to define camera orientation and internal geometry. Through dense image matching, this is developed into a high-resolution dense point cloud that captures the three-dimensional geometry of the surveyed object.

Meshes and textured models: From the dense point cloud, triangulated surface meshes are generated to provide continuous representation of the object's form. Application of image textures produces photorealistic 3D models that integrate both geometry and surface appearance.

Orthophotos and Orthomosaics: Image rectification produces orthographic views of elevations, plans, or sections, scaled and free from perspective distortion. Orthomosaics constitute mosaicked orthophotos covering entire facades or surfaces, forming the basis for measured drawings and comparative analysis.

Digital Elevation Models (DEMs) and sections: Depending on project requirements, digital terrain or surface models can be extracted from point cloud data. Cross-sections and profiles are also derived for the study of geometry, deformation, or stratigraphy.

Georeferenced datasets: By integrating Ground Control Points (GCPs) into the photogrammetric workflow, all outputs are constrained within the chosen coordinate system, ensuring metric reliability and compatibility with CAD, GIS, and HBIM platforms.

In heritage documentation, the methodological value of these outputs lies not only in their visual fidelity but in their measurable precision. According to CIPA/ICOMOS recommendations, photogrammetric products intended for architectural documentation must conform to scale-dependent accuracy thresholds (e.g., 1:20, 1:50, 1:100). The level of geometric detail and positional accuracy must therefore be selected in relation to the intended application—whether for conservation planning, structural assessment, or archival recording.

The outputs generated through photogrammetry are thus considered not as static images but as structured datasets, forming the foundation for subsequent modeling and

analytical processes. In this study, they serve as the methodological bridge between raw image acquisition and the construction of a Heritage Building Information Model (HBIM).

The following sections present a summary of the photogrammetric outputs generated for each façade during the processing workflow of the case studies. The results are organized in the following sequence

- Point Cloud (sparse)
- Dense Point Cloud
- Mesh Model
- Textures & Visualizations
- Orthophotos / Orthomosaic Photos

3.2.4 HBIM Application

Heritage Building Information Modelling (HBIM) represents the methodological integration of photogrammetric outputs into a parametric modelling environment. Unlike conventional BIM, which relies on predefined libraries of standardized architectural elements, HBIM requires the adaptation or creation of bespoke families that reflect the irregular geometries and unique features of historic fabric.

The rationale for applying HBIM within this study is threefold:

- **Data integration:** HBIM provides a structured digital environment in which heterogeneous datasets (point clouds, orthophotos, drawings, and metadata) can be combined within a single reference framework.
- **Parametric modelling:** Architectural elements documented through photogrammetry are reconstructed as parametric objects, enabling not only visual representation but also the encoding of attributes such as material, condition, and historical phase.
- **Conservation and management utility:** HBIM datasets serve as intelligent repositories that can be continuously updated, queried, and reused for conservation planning, risk assessment, and future interventions.

Methodologically, three workflows were tested to transition from survey data to HBIM:

3.2.4.1 *Direct Point Cloud to BIM*

The first approach involved importing the georeferenced dense point cloud directly into the BIM environment as the primary geometric reference. Orthophotos and sections derived from the photogrammetric dataset were used as additional guides for tracing and modelling walls, openings, roofs, and decorative features. Complex or irregular elements were reconstructed through a combination of manual modelling and the creation of custom parametric families. Metadata was attached to components, linking geometry with descriptive and historical attributes.

This workflow represents the most direct integration of photogrammetric outputs into BIM but is highly dependent on point cloud density and quality. In this study,

limitations arose when attempting to model complex details from a medium-quality point cloud, prompting the testing of alternative workflows.

3.2.4.2 *Orthomosaic to CAD to BIM*

The second approach adopted a hybrid workflow, using CAD as an intermediary step. High-resolution orthomosaics were generated from the photogrammetric dataset, rectified, and scaled in the chosen coordinate system. These were imported into a CAD environment, where architectural features—including profiles, openings, and decorative details—were systematically traced to produce vector-based plans and elevations.

Within the CAD files, damage mapping was also incorporated as vector overlays indicating surface loss, cracks, deformation, and biological growth. Following ICCROM and ICOMOS standards, line styles, hatching, and color coding were used to differentiate damage types. This enriched dataset was then imported into the BIM environment, where CAD drawings functioned as reference layers for parametric reconstruction.

This workflow proved advantageous where the point cloud lacked sufficient resolution for direct modelling, while also producing orthographic drawings useful for conservation documentation.

3.2.4.3 *Total Station to CAD to BIM (Comparative Test)*

For comparative purposes, a third workflow was tested using total station survey data. Select portions of the southern courtyard façade, particularly decorative elements, were surveyed point by point. The measured coordinates were drafted within CAD to produce precise two-dimensional drawings, which were then imported into the BIM environment for partial three-dimensional reconstruction.

This method produced highly accurate geometric data for targeted areas but was limited by its time-intensive nature and difficulty in capturing complex curves or motifs.

3.2.4.4 *Comparative Framework*

Together, these three workflows highlight the methodological spectrum available for HBIM in heritage contexts. Direct point cloud import offers comprehensive integration but is limited by data quality; the Orthomosaic–CAD–BIM approach balances efficiency with visual completeness and allows for conservation overlays such as damage mapping; while the Total station–CAD–BIM workflow provides precision for selected details but at the cost of efficiency and coverage.

By comparing and contrasting these approaches, this study develops a balanced methodological framework for progressing from photogrammetry to HBIM, aligning with CIPA/ICOMOS best practice and tailored to the documentation of Syria's richly ornamented heritage fabric.

3.3 REFINED METHODOLOGY FOR MAIN CASE STUDY: AL-TUNBUGHA MOSQUE

The HBIM modelling strategy adopted for the Al-Tunbugha Mosque follows a direct photogrammetry–HBIM workflow, thereby eliminating the CAD intermediary employed in the pilot phase. This refinement was made possible by the significant improvements in the quality of the photogrammetric outputs, which provided a dataset of sufficient resolution and accuracy to enable modelling directly within the BIM environment.

Several methodological enhancements supported this shift:

- **Control network:** Ground Control Points (GCPs) were distributed more evenly across the façades and at multiple elevations, resulting in improved geometric stability and reduced residual error.
- **Point cloud resolution:** Dense point cloud processing was conducted at the ultra-high setting, capturing fine architectural detail that could not be reliably obtained in the medium-quality dataset tested earlier.

- **Image acquisition:** Photographic coverage was undertaken with systematic overlap, consistent lighting conditions, and redundant views to ensure completeness and minimize occlusions.
- **Validation measures:** Field checks and dataset verification procedures were implemented to confirm that image sharpness, overlap, and photogrammetric alignment met the required standards prior to HBIM integration.
- the integrity of the dataset before processing.

Within this refined strategy, the ultra-high-resolution dense point cloud was imported directly into the BIM environment and served as the primary geometric reference for volumetric modelling. Orthophotos and sectional views derived from the same dataset were employed as secondary references to guide the reconstruction of walls, openings, domes, arches, and decorative details. Complex or irregular features were modelled through the creation of bespoke parametric families, while metadata was systematically assigned to architectural components to record attributes such as material, structural condition, and conservation status.

By removing the CAD intermediary, the refined workflow reduced redundancy and potential translation errors between software platforms, while also capitalising on the enhanced fidelity of the photogrammetric dataset. The resulting HBIM model therefore represents a more efficient, metrically accurate, and semantically enriched documentation of the Al-Tunbugha Mosque, suitable for conservation planning, scholarly analysis, and long-term digital stewardship.

3.4 ACCURACY AND PERFORMANCE EVALUATION

The reliability of the documentation workflow was assessed through a two-fold evaluation: (1) the spatial accuracy of the photogrammetric outputs in relation to control points and total station benchmarks, and (2) the performance of photogrammetry-driven HBIM in comparison with traditional documentation methods.

3.4.1 Assessment of spatial accuracy against control points and total station measurements

Ground Control Points (GCPs) measured with a total station provided the reference framework for accuracy assessment. Deviations in X, Y, and Z coordinates were computed for each GCP to quantify both planimetric and vertical accuracy. Errors were further synthesized using metrics such as mean absolute error (MAE), root mean square error (RMSE), and 95th percentile values to capture the distribution of discrepancies. Thresholds were defined according to CIPA/ICOMOS guidelines, with a maximum tolerance of 1 cm for linear positioning and 0.20° for angular measurements. This evaluation established whether the photogrammetry-derived point clouds met the precision requirements necessary for reliable HBIM modeling.

3.4.2 Comparative analysis of photogrammetry-driven HBIM versus traditional documentation methods

The performance of the integrated workflow was also examined in relation to conventional documentation approaches, such as CAD drafting from rectified images and manual survey drawings. While traditional methods offer selective metric accuracy, they are often limited in scope, time-intensive, and less adaptable for complex geometries. In contrast, photogrammetry-driven HBIM provided comprehensive spatial datasets that preserved both geometry and texture, enabling parametric structuring, semantic enrichment, and long-term digital management. However, the transition from point cloud to HBIM introduced simplifications that contrasted with the high geometric fidelity of photogrammetric data. The evaluation therefore emphasized the balance between accuracy, efficiency, and usability, situating photogrammetry-driven HBIM as a method that extends beyond traditional documentation by integrating metric reliability with interpretive and conservation-oriented value.

3.4.3 Mathematical Equations

3.4.3.1 *Point Positioning Accuracy (GCPs)*

For Each GCP:

$$\Delta X = X_{photo} - X_{Reality}, \qquad \Delta Y = Y_{photo} - Y_{Reality}, \qquad \Delta Z = Z_{photo} - Z_{Reality}$$

2D Error (planimetric):

$$Err_{2D} = \sqrt{(\Delta X)^2 + (\Delta Y)^2}$$

Vertical Error (Z only):

$$Err_Z = \Delta Z^2$$

3D Error:

$$Err_{3D} = \sqrt{(\Delta X)^2 + (\Delta Y)^2 + (\Delta Z)^2}$$

3.4.3.2 *Distance Deviation*

For a measured distance d_{ref} (reality/total station) and a computed distance d_{comp}:

$$\Delta d = d_{comp} - d_{ref}$$

Relative error (%):

$$RefErr(\%) = \frac{|\Delta d|}{d_{Ref}} \times 100$$

3.4.3.3 *Angular Deviation*

For an angle measured in the field θ_{Ref} and a computed in the model θ_{Comp}:

$$\Delta\theta = \theta_{comp} - \theta_{ref}$$

Relative error (%):

$$RefErr(\%) = \frac{|\Delta\theta|}{\theta_{Ref}} \times 100$$

3.4.3.4 *Statistical Metrics*

For n samples with error values e_i:

- Bias (mean signed error):

$$Bias = \frac{1}{n}\sum_{i=1}^{n} e_i$$

- Mean Absolute Error (MAE):

$$MAE = \frac{1}{n}\sum_{i=1}^{n} |e_i|$$

- Root Mean Square Error (RMSE):

$$RMSE = \sqrt{\frac{1}{n}\sum_{i=1}^{n} e_i^2}$$

- 95th Percentile Error (P95):

$$P95 = value\ of\ |e_i|\ below\ which\ 95\%\ of\ samples\ fall$$

- Maximum Error:

$$Max = \max(|e_i|)$$

3.4.3.5 *Pass/Fail Criteria (Tolerance)*

Linear distances / positioning:

$$Pass\ if\ Err_{3D} \leq 0.01\ m\ (1\ cm)\ and\ RelErr \leq 0.2\%$$

Angular deviations:

$$Pass\ if\ |\Delta\theta| \leq 0.2°\ and\ RelErr \leq 0.2\%$$

3.5 ANALYTICAL FRAMEWORK

The analysis of results in this research is guided by the overarching objectives of ***improving accuracy, enhancing usability, and optimizing documentation workflows for heritage contexts.*** To achieve this, both technical and practical outcomes are systematically evaluated.

From a ***technical perspective***, performance indicators include accuracy rates against total station control points, error margins in linear and angular measurements, and fidelity of the HBIM model relative to photogrammetric outputs. These indicators are assessed using standardized statistical metrics (bias, MAE, RMSE, P95, maximum deviation) and interpreted within tolerance thresholds defined by CIPA/ICOMOS guidelines. This ensures that the generated models are not only precise in spatial terms but also compliant with established heritage documentation standards.

From a ***practical perspective***, the framework evaluates time efficiency, workflow coherence, and the usability of the outputs for heritage management. Photogrammetry-to-HBIM workflows are compared against traditional methods such as CAD-based drafting

and manual surveys, with emphasis on adaptability, interpretability, and conservation value. Usability is further judged in terms of semantic enrichment, visualization quality, and the model's potential for integration into heritage preservation strategies.

By combining technical accuracy with practical usability, the analytical framework ensures a balanced evaluation of the methodology. The aim is to confirm that the workflow is ***not only metrically reliable but also effective as a sustainable tool for documentation, interpretation, and management of Syrian cultural heritage at risk.***

CHAPTER 4. PILOT CASE STUDY RESULTS: AL-TAKIYYA AL-RIFA'AIA AL-IKHALSIA

4.1 INTRODUCTION

The pilot case study was conceived as an exploratory stage to test and evaluate the proposed methodology before its application to the main case study of Al-Tunbugha Mosque. Its primary purpose was to identify potential challenges in data acquisition, processing, and modeling, and to assess the feasibility of integrating photogrammetric outputs into an HBIM workflow. By experimenting with different capture strategies, accuracy thresholds, and data-processing techniques on a smaller scale, the pilot provided a controlled environment in which methodological assumptions could be validated, refined, or rejected.

The insights gained—particularly regarding marker placement, image resolution, dense point cloud quality, and workflow efficiency—directly informed the **refined methodology presented in Chapter 3**. Enhancements to the dense point cloud were especially significant: selective masking and multi-scale processing were introduced to reduce noise in highly decorated surfaces, while additional oblique photography improved point density in shadowed or occluded areas. Together, these refinements contributed to more reliable reconstruction of complex architectural and ornamental details. Other methodological adjustments, such as optimizing image resolution, increasing ground control point density, adopting drone-based photography for roof coverage, and eliminating reliance on CAD intermediaries, were also outcomes of lessons learned in the pilot. In this way, the pilot functioned as a practical testing ground, ensuring that the final workflow applied to Al-Tunbugha Mosque was both more systematic and more resilient to the challenges of heritage documentation.

4.2 AL-TAKIYYA WITHIN THE HISTORICAL AND URBAN FABRIC OF ALEPPO

4.2.1 Location

The site is located north of Al-Sarwi Mosque in Al-Bayada neighborhood and is attributed to Sheikh Ikhlas Al-Khalwati, a notable resident of Aleppo who passed away in 1074 AH (1663 AD). The complex was commissioned in 1044 AH (1634 AD) by Minister Muhammad Pasha Al-Arnaout during his passage through Aleppo, although he did not serve as its governor.

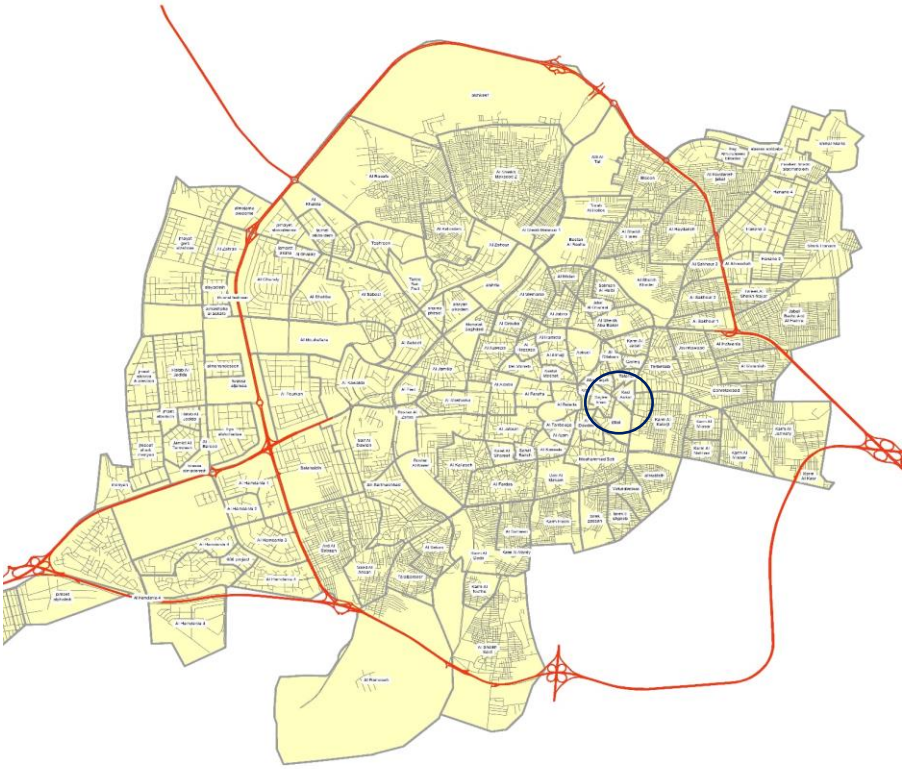

Figure 45: Map of Aleppo City – Al-Bayada Neighborhood

Al-Bayada neighborhood is located on the northeastern side of the Aleppo Citadel. It is a neighborhood within the walls of the old city.

Figure 46: Map of Old City of Aleppo and the Location of Al-Tikyya

4.2.2 Heritage Significant Values of Al-Tikyya[12]

4.2.2.1 *Religious and Spiritual Values*

The origins of the Islamic Sufi method of worship can be traced back to the era of the Prophet Muhammad, who is reported to have assigned to each of his companions a litany (dhikr) suited to their spiritual rank and personal circumstances. For instance, ʿAlī ibn Abī Ṭālib frequently recited "Lā ilāha illā Allāh" ("There is no god but Allah"), while Abū Bakr al-Ṣiddīq was known for repeating the invocation "Allāh". These practices were transmitted to their followers and became known respectively as the Bakrī and ʿAlawī paths. Over time, these spiritual lineages converged at the teachings of Imām Abū al-Qāsim al-Junayd, a central figure in classical Sufism, before branching into new orders such as the Khalwatī and Naqshbandī. The evolution of these traditions continued until the emergence of four major spiritual leaders—Aḥmad ibn ʿAlī al-Rifāʿī, ʿAbd al-Qādir al-Jīlānī, Aḥmad al-Badawī, and Ibrāhīm al-Dasuqī—who each established the foundations of their respective Sufi orders, shaping the enduring spiritual landscape of the Islamic world.

[12] (Torre, 2002)

Figure 47: The banner of the Rifai worship group

The Rifāʿī worship method, also known as al-Baṭāʾiḥiyya, derives its name from the region of al-Baṭāʾiḥ, located near the villages of southern Iraq. Over time, the worship method expanded beyond its place of origin, establishing a significant presence in Iraq, Egypt, Syria, and other parts of Western Asia. One of its distinctive symbols is the black banner, which sets it apart from other Sufi orders and reflects its unique identity within the broader spiritual tradition of Islam.

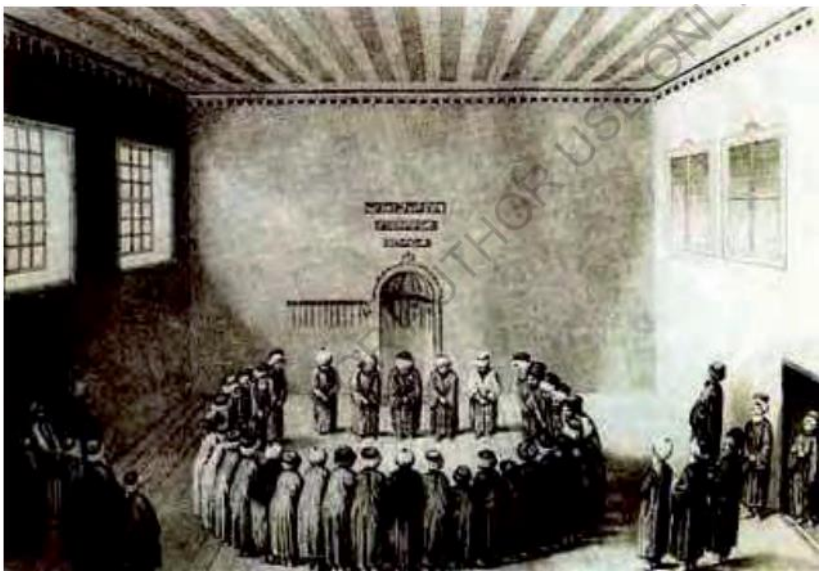

Figure 48: A scene from the Rifai worship rituals

This spiritual methodology is attributed to the Shāfiʿī Ashʿarī jurist Aḥmad ibn ʿAlī al-Rifāʿī (512–578 AH / 1118–1182 AD), who was renowned by several honorific titles, including *Abū al-ʿAlamayn* ("Father of the Two Banners"), *Shaykh al-Ṭarīq* ("Master of the Path"), *al-Shaykh al-Kabīr* ("The Great Sheikh"), and *Ustādh al-Umma* ("Professor of the Community"). Within Sufi traditions, different orders are identified by distinctive insignia, banners, and colors. The Rifāʿī order is symbolized by the color black, while the Qādirī

order is distinguished by green, and the Aḥmadī order by red. In contrast, the Burhānī order is characterized not by a single color, but by three: white, representing Sayyid Ibrāhīm al-Dasūqī; yellow, associated with al-Ghamām Abū al-Ḥasan al-Shādhilī and passed down to his nephew Sayyid Ibrāhīm al-Dasūqī; and green, symbolizing the honor of affiliation with the *Ahl al-Bayt* (the Prophet's family).

4.2.2.2 *Historical Values*

The reconstruction of the site was commissioned by Grand Vizier Muḥammad Pasha al-Arnaʿūd. It is situated on al-Rifāʿī Street in the al-Bayāda district, approximately one mile to the north of Old Aleppo, opposite al-Sarwī Mosque (also known as *al-Maltī Mosque* or *al-Bayāda Mosque*), to the right of the entrance from Bāb al-Ḥadīd. Over time, it has been referred to by several names, including *al-Takiyya al-Ikhlāṣiyya al-Bakhshiyya*, *al-Takiyya al-Rifāʿiyya*, and *al-Zāwiya al-Ikhlāṣiyya*.[13]

Sheikh Kāmil al-Ghazzī, in his book *Nahr al-Dhahab fī Tārīkh Ḥalab* (*The River of Gold in the History of Aleppo*), described the site as being located opposite al-Sarwī Mosque to the north and attributed it to Sheikh Ikhlāṣ al-Khalwatī, a resident of Aleppo who passed away in 1074 AH (1663 AD). The building, constructed for him by Grand Vizier Muḥammad Pasha al-Arnaʿūd, was endowed with generous waqf resources and became known as a beautiful spiritual corner (*zāwiya*). In contemporary times, the Rifāʿī Khalwa operates at this location during the spring season.

Further details are provided by Abū al-Wafāʾ al-Arḍī in *Maʿādin al-Dhahab* (*Mines of Gold*), where he recounts that Sheikh Ikhlāṣ organized an annual winter retreat attended by his disciples. During this retreat, participants would fast for three consecutive days, breaking their fast in the evening with a modest meal consisting of two ounces of *ḥarīsa* and a loaf of bread slightly larger than an ounce. They abstained from drinking *qarā* (a fermented drink) and instead consumed coffee, devoting the nights and days to continuous remembrance (*dhikr*) and worship. Outside of this intensive period, disciples would rise before dawn to perform *tahajjud* according to their capacity, continue their

[13] (Al-Refai, 2017)

remembrance until the time of travel, then perform the *fajr* prayer and recite litanies until sunrise, followed by the *ishrāq* prayer.

4.2.2.3 *Architectural / Aesthetic Values*

The description of the Rifai Tekke was mentioned in the records of the Directorate of Awqaf as follows:

The complex comprises multiple functional and residential components distributed across two floors. At the lower level, it contains an underground cave for provisions, a stone staircase, a ground floor with a basement for storage, seven residential units, a covered walkway, and additional stone stairs. The mosque area includes a space known as the *Maidan*, which originally housed nine small wooden shops, along with one shop situated inside the mosque itself. The mosque is further characterized by an open courtyard and three water wells.

The first floor contains an additional seven residential units, together with a covered courtyard, stone staircases, and a water well, bringing the total number of residential spaces within the complex to fourteen. Today, the building functions primarily as a mosque, where daily prayers are performed, and where disciples gather for supplications, collective remembrance (dhikr), and the Rifāʿī retreat.

Architecturally, the building is organized around two main floors: the first floor served as the Sheikh's residence, while the southern end of the complex was occupied by the prayer hall and its adjoining square. Around the courtyard, several retreat rooms were constructed, including small wooden cells inside the prayer hall itself. The meeting hall, situated at the eastern end, appears to have been a later addition, as suggested by its distinctive construction style. The complex also included a kitchen, ablution facilities, and a fountain. The prayer hall was divided into three sections, with the central space covered by a dome, reflecting both its functional role and spiritual significance. The ***facade of this section*** is composed of two distinct parts.

- ***The first part*** consists of a room overlooking the courtyard, with two windows and a door, each surmounted by a segmented arch. Above them are three arches, each topped with a pointed horseshoe arch with four centers.
- ***The second part*** contains two rooms: the first opens onto the courtyard with a

window and a door, followed by an additional door leading to the second room. The windows and doors in this section are notably taller than those in the first part, each crowned by a prominent segmented arch with a decorated spiral keystone.

To the south, the courtyard is bordered by a vestibule with a cross-vaulted roof, providing access to the prayer hall to the south and the ablution area to the west. The sheikh's room overlooks this corridor from the east.

The prayer hall is connected on its western side to more than thirty wooden cells for seclusion (khalwa). The facade of this section consists of a window and a door, followed by two additional windows belonging to a ground-floor room, with four windows aligned above them on the first floor.

On the western side of the courtyard, there are three rooms allocated for Sufi disciples, followed to the north by a ruined room. The facade here features a centrally placed door surmounted by a bell arch, flanked on both sides by windows topped with tomi arches framed with cornices. The upper part of the facade is ornamented and fronted by a balcony.

The qibla wall, situated to the south of the courtyard, is marked above its entrance by poetic inscriptions in ten syllables. It is articulated by two pointed, variegated arches supported on muqarnas corbels attached to the northern and southern walls, with a central muqarnas column. The qibla is divided into three sections:

- ***The Eastern section****:* contains three rectangular windows overlooking the street. The southern wall includes a door to a room in the southeastern corner, while the northern wall holds a door leading to the sheikh's room.
- ***The Middle section****:* features a simple mihrab flanked by two decorative rivets. Its roof is a low dome with vegetal motifs, transitioning from square to polygonal form via inverted pyramidal triangles in the corners. The adjoining roofs terminate in elongated hump-shaped vaults.
- ***The Western sectio*****n**: includes a wooden partition with four doors, leading to a series of wooden enclosures.

The eastern facade, beginning from the north, consists of a large iron-fitted window crowned by a segmented arch of seven parts. Below lies a blocked basin, indicating the presence of a former fountain. This is followed by the main entrance, framed by a segmented arch constructed of black, yellow, and white stones, with two protruding yellow stone triangles framed in black at its base and a six-pointed star in the center. Above the entrance is a four-line inscription, topped by a frieze of three rows of muqarnas and a sloping surface connecting the slightly protruding doorway to the recessed wall behind it, with two windows positioned above.

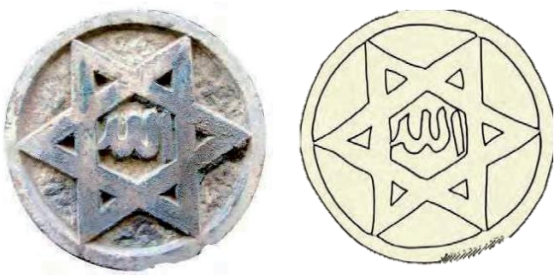

Figure 51: Inscription above the entrance to the lodge is 18 cm in diameter and contains the word "Allah."

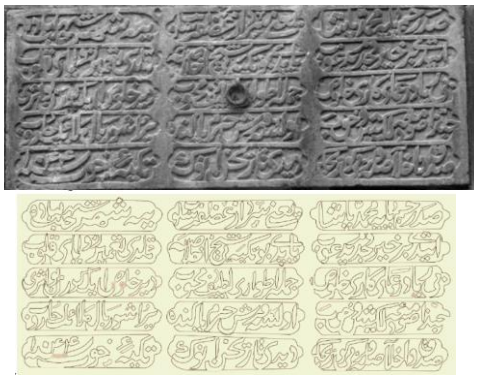

Figure 50: Inscription above the lodge entrance, measuring 45 × 110 cm.

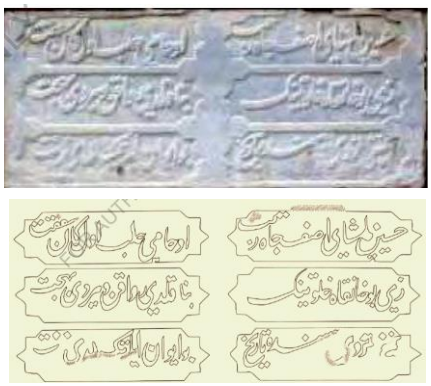

Figure 50: Inscription on the northern wall of the lodge courtyard, measuring 56 × 37 cm.

South of the entrance lies the facade of a large room, a single-story structure with two windows surmounted by segmented arches resting on single-piece stone lintels, crowned by a projecting gutter. Adjacent is the facade of the sheikh's rest room, which includes two rectangular windows at different heights, above which is a square-arched niche. Following this is the qibla facade, with three lower-set rectangular windows, each topped by a single-piece lintel. Finally, the southern exterior facade contains two windows with three-part segmented arches, accompanied at its center by a narrow upper niche.

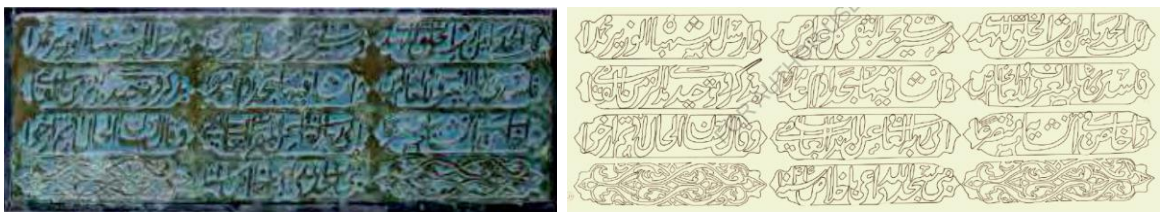

Figure 52: Inscription above the entrance to the prayer hall, measuring 117 × 39 cm.

4.2.3 War and Heritage: The Case of Al-Takkiya Mosque in the Syrian Conflict

With the outbreak of the Syrian armed conflict in 2011, the Old City of Aleppo—except for the Citadel—fell under the control of non-state armed groups affiliated with Islamist movements. During this period (2011-2016), Al-Takiyya sustained 35–40% structural damage and destruction, yet it remained stable and did not require reinforcement, while, fortunately, the Tunbugha Mosque didn't sustain any damage.

Figure 53: Tekka - Area of Authorities 2011-2025

Pre-2011: Since its establishment, the Ikhlasiyya Rifai Tekke had not suffered any structural damage. The key to the tekke was held by the Awqaf Directorate. However, during this period, the tekke was looted, and the entire collection of its movable assets was stolen. A complete detailed archive of the stolen items is available.

Late 2016–2022 (Post-Regime Control): In August–October 2016, the Old City of Aleppo returned fully to the control of the Syrian government. No further damage occurred, nor were any reinforcement or restoration interventions carried out.

February 6, 2023 (Earthquake): The Rifai Tekke was severely affected by the Aleppo earthquake. Damage increased dramatically to approximately **70%**, involving both architectural and structural deterioration. Several facades were classified as being in urgent need of reinforcement, while the Tunbugha Mosque sustained relatively low damages such as minor cracks.

Emergency Interventions (2023–2024): The Rifai family sought to obtain access from the Aleppo Awqaf Directorate in order to carry out urgent stabilization measures. Structural advice was provided by Engineer Mahmoud Sikt. Significant donations were collected from Rifai family residents and expatriates to finance reinforcement works. As a result, the tekke was consolidated using metal supports installed in various locations (entrance, prayer hall, eastern room, etc.).

November 27, 2024: The Rifai Tekke, along with the entire Syrian Arab Republic, came under the control of the Hay'at Tahrir al-Sham. (HTS). To date, no restoration work

has been carried out on the Rifai Tekke. All interventions have been limited to documentation and emergency consolidation studies only.

4.3 DATA ACQUISITION RESULTS

4.3.1 Preparatory Measures

Before commencing data acquisition at Al-Takiyya, a series of preparatory measures were undertaken to ensure both the safety of the survey team and the protection of the historic fabric. Preliminary site visits served as reconnaissance surveys, allowing for an assessment of the physical condition of the complex, identification of potential risks or obstacles to access, and evaluation of environmental factors such as lighting and visibility that could influence photographic documentation. Special attention was given to ensuring that all areas targeted for survey could be reached without exposing the structure or personnel to unnecessary risk.

During this stage, formal permissions and approvals were secured from the Directorate of Tourism and the Directorate of Awqaf. This covered photography, the placement of control markers, and, where necessary, the use of tripods. Such measures were essential to establish an ethical and well-coordinated framework for the survey process.

Environmental and site-specific challenges also shaped the preparation. Sunlight and shadows within the courtyard and arcades posed significant difficulties; image acquisition was therefore scheduled for late afternoon, when the low angle of the sun provided more even illumination. The site presented practical obstacles as well: large quantities of displaced stone blocks and rubble were scattered across the courtyard, obstructing visibility and access to several façades. To address this, workers were engaged to carefully remove, sort, and store the stones in one of the Takiyya's service rooms. Each fragment was treated as potentially valuable, given that many bore decorative or structural significance.

Further obstructions included vegetation growth along the courtyard walls, which concealed architectural details, and a fallen tree trunk in the center of the courtyard. Vegetation was selectively cleared to reveal the underlying masonry, and the trunk was removed to improve accessibility and allow for unobstructed photography.

Figure 54: Site cleaning and debris removal – Al-Takiyye

These preparatory measures created the conditions for systematic, secure, and high-quality data acquisition, minimizing risks while respecting the cultural significance of Al-Takiyya.

4.3.2 Ground Control Points (GCPs)

The survey phase began by identifying reference points with known coordinates within the study area and its surroundings. These coordinates were defined according to the Syrian cadastral system, based on the national stereographic projection. Two control points were first established, from which a traverse was extended by creating a polygon of intervisible stations. New points were successively planted along this traverse until the study site was reached, where observation stations were positioned to fulfill the requirements of the survey.

Table 11: GCP Coordinates - Al-Takiyya

GCP	X	Y	Z
H1011	-178,571.779	223,751.171	396.81
I1011	-178,607.089	223,739.311	396.31

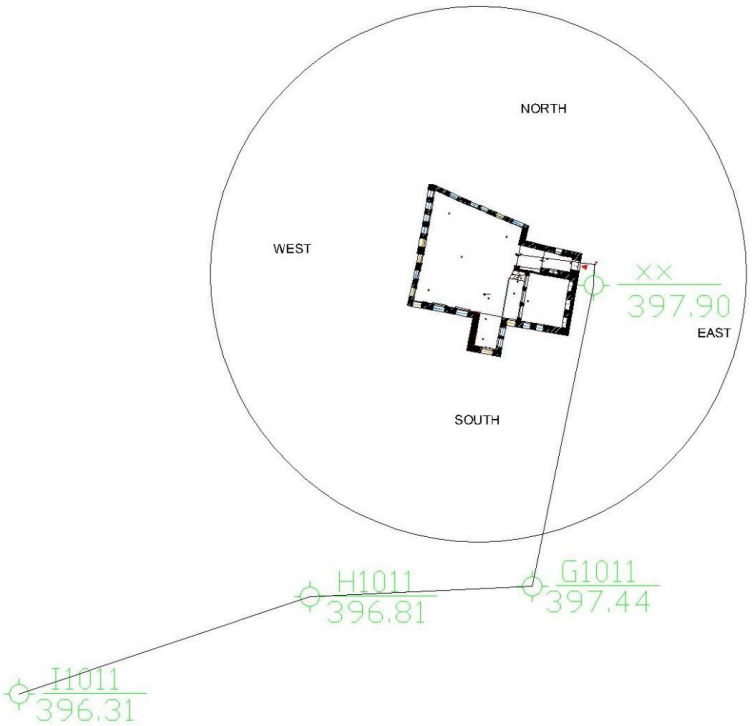

Figure 55: Open Traverse - Al-Takiyya

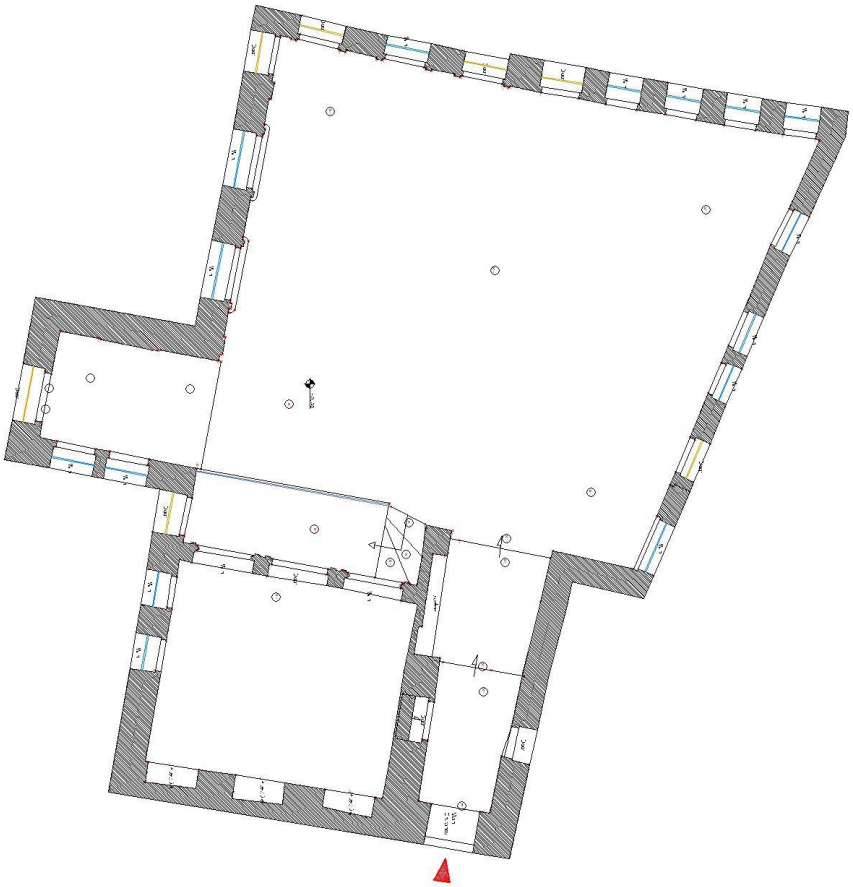

Figure 56: Floor Plan - Al-Takiyya

The control points were distributed across the facades selected for study, with careful consideration of both the methodological requirements and the specific conditions of the site.

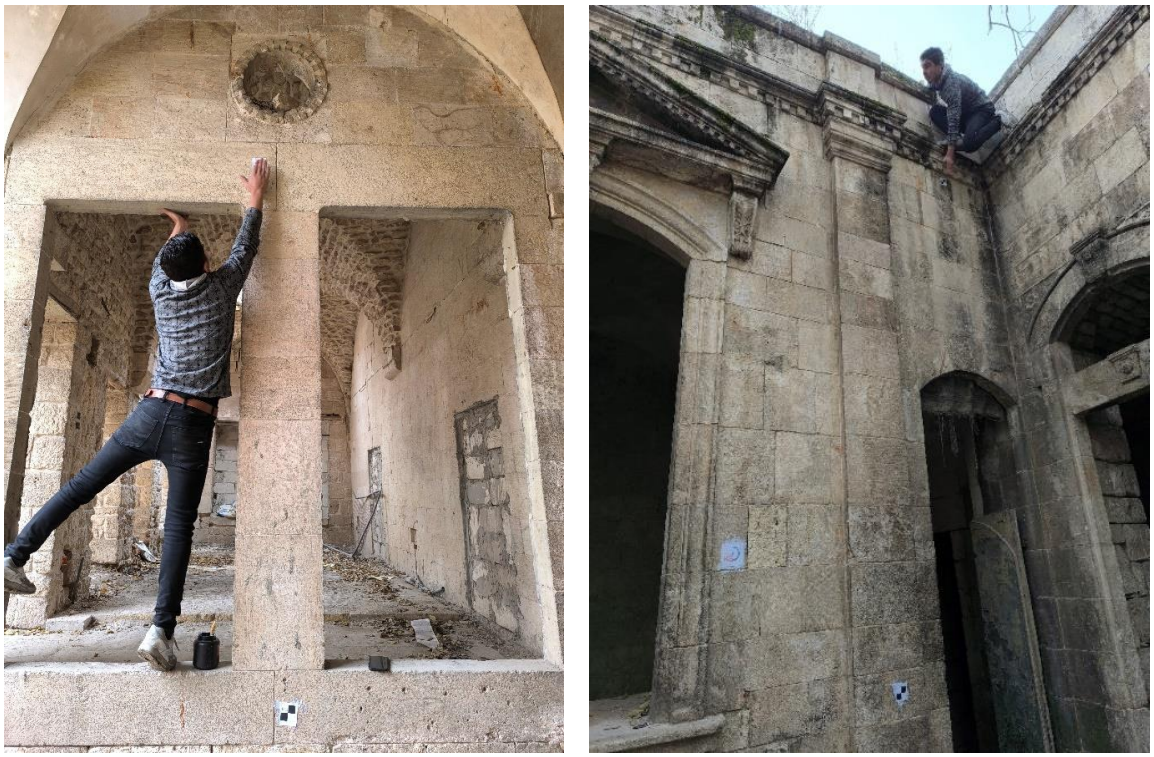

Figure 57: Installation of Control Points (markers)

The documentation covered multiple facades of the building, including:

- Five facades within the courtyard (north, southeast, west, and ground floor levels).
- Four facades in the reception or meeting room (north, southeast, west).
- Five facades in the entrance corridor (north, southeast, west, and ground floor levels).
- One external facade.

GCPs were prepared as printed, numbered, and easily recognizable targets affixed on paper, designed to be clearly identified during processing within the photogrammetric software. Their primary function is to guide the model within the established coordinate system, based on measurements obtained with the total station.

Across these areas, the following number and distribution of control points (**145** markers) were established:

Figure 59: Yard West Facade (17 markers) - Al-Takiyye

Figure 59: Yard South Facade (30 markers) - Al-Takiyye

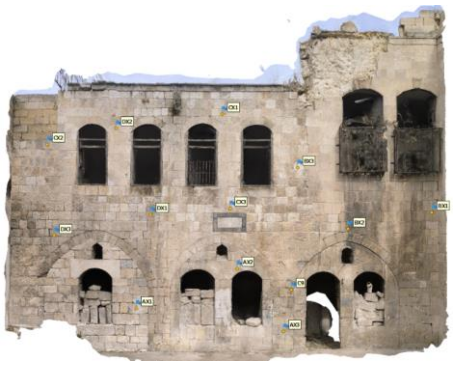

Figure 61: Yard North Facade (19 markers) - Al-

Figure 61: Yard East Facade (16 markers) - Al-

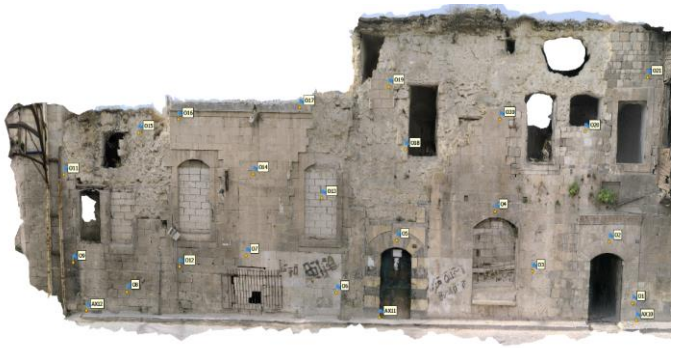

Figure 63: Exterior Facade (26 markers) - Al-Takiyye

Figure 63: Reciption Facades (13 markers) - Al-Takiyye

Figure 65: Yard Floor Plan (12 markers)

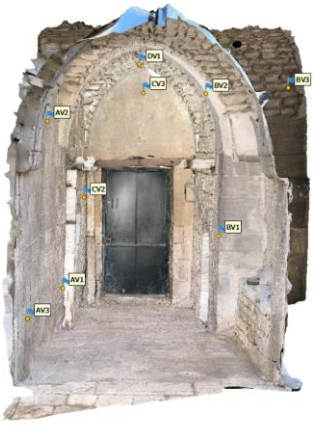

Figure 65: Entrance Facades (12 markers) - Al-Takiyye

```
BX1,-178546.131,223796.008,402.178,0.003536
BX2,-178548.226,223796.874,401.729,0.005632
C9,-178549.624,223797.482,400.084,0.002119
AX3,-178549.797,223797.591,398.959,0.002181
AX2,-178550.967,223798.05,400.645,0.001903
CX3,-178551.166,223798.122,402.26,0.001316
AX1,-178553.462,223799.161,399.556,0.005315
DX1,-178553.13,223798.98,402.08,0.002133
DX3,-178555.52,223800.078,401.5,0.006369
DX2,-178554.013,223799.399,404.429,0.002457
BX3,-178549.489,223797.394,403.378,0.004031
CX1,-178551.365,223798.231,404.814,0.005582
CX2,-178555.73,223800.217,403.983,0.004117
```

Figure 67: e.g. Recorded Coords of Markers on the North Facade

Figure 67: Surveying Coords of Markers

After the placement of the GCPs, their coordinates were measured and recorded using the surveying instrument, with the data stored for subsequent use during the processing stage.

4.3.3 Photographic Acquisition

As noted earlier, a mobile device camera was employed for image acquisition due to its ease of use and cost-effectiveness when compared to professional digital cameras, which often require specialized software. The device's 200-megapixel camera provided exceptionally high image resolution, comparable to that of dedicated digital cameras, thereby ensuring that the quality of the captured imagery met the requirements of photogrammetric processing. Each image had a file size of ***no less than 25 MB, with a 23 mm focal length, ISO 1250, and without the use of flash.***

The photographic survey followed a set of defined criteria to ensure systematic coverage and reliable outputs:

- Photographic lines and elevations were adopted to guide systematic image capture of the facades.

- Image acquisition was continuous and uninterrupted, with the camera axis kept perpendicular to the facade and the camera body parallel to the surface.
- All photographs were taken under consistent lighting conditions and with the same camera to maintain uniformity.
- Variations in depth and dimensions of the site were considered, with additional images taken to cover occluded or geometrically complex areas.
- A minimum of 60% overlap between consecutive images was maintained to ensure accurate alignment during photogrammetric processing.

*Table 12: Number of photos taken per plan (Total of **1,294**) - Al-Takiyya*

Façade	Number of photos taken	Façade	Number of photos taken
North	59	Floor	227
West	207	Exterior	95
East	207	Entrance	228
South	72	Reception	199

Figure 68: Example of capturing sequence - Yard West Facade - Al- Takiyye

During the photographic acquisition process, detailed field notes were taken to record lighting conditions, environmental factors, and any access-related challenges. Sketches and diagrams were prepared to illustrate the image acquisition layout, and essential metadata—including camera settings, focal length, aperture, and ISO—was systematically documented. In addition, field-based data validation was carried out to ensure dataset quality. This involved preliminary checks of image sharpness, exposure, and overlap; capturing redundant photographs to compensate for potential errors; and creating secure backups and archives of the raw image data.

4.3.4 Summary of Data Acquisition

Table 13: Summary of Data Acquisition, Al-Takiyya

Data Type	Equipment / Tool	Resolution / Accuracy	Coverage Area	Purpose in Workflow
Ground Control Points (145 GCPs)	Total Station (Topcon GTS 1002)	~2 mm (Prsim) ~ 5 mm (RL*)	Surrounding courtyard, elevated points	Georeferencing, improving alignment and scale accuracy.
Ground and Elevated measurements	Tape measure + laser distance meter + Total Station	±0.1 cm	Selected walls, arches, openings	Independent checks, validation of data processing outputs + Feasibility study on traditional documentation methods.
Metadata records	Manual logs + camera EXIF	N/A	All images	Quality control, standardizing exposure/coverage
Terrestrial images (1,294 image)	Redmi note 13 pro plus 5G	24–46 MP	Exterior façades, courtyard, interiors	Photogrammetry dataset, texture mapping

*RL: Reflectorless

4.4 DATA PROCESSING OUTPUTS

4.4.1 Photogrammetry Outputs

4.4.1.1 *Photogrammetry Processing Parameters*

All orthorectified mosaics extracted from the project were generated at a resolution of **1 × 1 mm per pixel**. The point clouds were produced at **medium resolution**, with the parameters set to **Key Points = 80,000** and **Tie Points = 8,000**. These settings were selected for several reasons:

1. During point cloud formation, the software identifies the most reliable feature points. Increasing the resolution to *High* can sometimes introduce noise or instability in the resulting cloud. Using *Medium* resolution balances point density with stability, producing very good— and in some cases excellent— results, depending on the imaging resolution and the number of photographs.
2. High-resolution processing is computationally demanding and significantly increases processing time. By contrast, ***medium*** resolution delivers comparable results with far less effort and time. The only exception in this project is the façade modeled in **Revit at LOD 500**, which was processed at high resolution, as will be demonstrated later.

All **dense point clouds** were therefore generated at ***medium resolution***, as this stage is one of the most time- and resource-intensive processes, regardless of computer specifications. Nonetheless, excellent outcomes can still be achieved at this resolution, provided the input images are of sufficient number and quality.

Finally, all **texture files** created in the project were generated at **high resolution** to ensure the highest possible visual quality.

The following sections provide a summary of the photogrammetric outputs generated for each façade during the processing workflow, along with a definition of the parameters applied in data processing.

Table 14: Data Processing Workflow and Parametric Inputs, Al-Takiyya

#	Data Processing Workflow	Value
-	Scope	Partial (Facades)
1	Adjusting preference settings	Default
2	Loading images into Metashape	Default (1 Camara)
3	Loading videos into Metashape	No
4	Inspecting loaded images, removing unnecessary images/videos	Yes
5	Aligning cameras (Point Cloud)	Accuracy: High Key Points: 80,000 Tie Points: 8,000
6	Referencing: Camera Optimization	Yes, based on the surveyed coordinates of the markers **(1 Camera)**
7	Building dense point cloud	Standard quality (Medium)
8	Building mesh (3D polygonal model)	High
9	Generating texture	Default
10	Building tiled model	Outside the scope of this research
11	Building digital elevation model (DEM)	Outside the scope of this research
12	Building Orthomosaic	Yes
13	Exporting results	Orthomosaic, Dense Point Cloud, 3D Model, Report

The results are organized in the following sequence:

- Point Cloud (sparse)
- Dense Point Cloud
- Mesh Model

- Textures & Visualizations
- Orthophotos / Orthomosaic Photos

4.4.1.2 *Yard North Façade*

Figure 70: Point Cloud - Yard North Facade, Al-Takiyya

Figure 70: Dense Point Cloud - Yard North Facade, Al-Takiyya

Figure 72: Mesh Model - Yard North Facade, Al-Takiyya

Figure 72: Textured Model - Yard North Facade, Al-Takiyya

Figure 73: Orthomosaic - Yard North Facade, Al-Takiyya

4.4.1.3 *Yard South Façade*

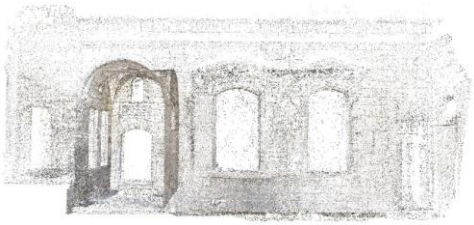

Figure 75: Point Cloud - Yard South Facade, Al-Takiyya

Figure 75: Dense Point Cloud - Yard South Facade, Al-

Figure 77: Mesh Model - Yard South Facade, Al-Takiyya

Figure 77: Textured Model - Yard South Facade, Al-

Figure 78: Orthomosaic - Yard South Facade, Al-Takiyya

4.4.1.4 *Yard East Façade*

Figure 80: Point Cloud - Yard East Facade, Al-Takiyya

Figure 80: Dense Point Cloud - Yard East Facade, Al-

Figure 82: Mesh Model - Yard East Facade, Al-Takiyya

Figure 82: Textured Model - Yard East Facade, Al-

Figure 83: Orthomosaic - Yard East Facade, Al-Takiyya

4.4.1.5 *Yard West Façade*

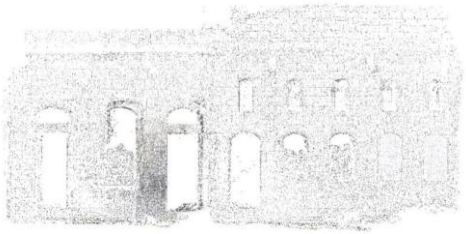

Figure 85: Point Cloud - Yard West Facade, Al-Takiyya

Figure 85: Dense Point Cloud - Yard West Facade, Al-

Figure 87: Mesh Model - Yard West Facade, Al-Takiyya

Figure 87: Textured Model - Yard West Facade, Al-

Figure 88: Orthomosaic - Yard West Facade, Al-Takiyya

4.4.1.6 *Yard Floor*

Figure 90: Point Cloud - Yard Floor, Al-Takiyya

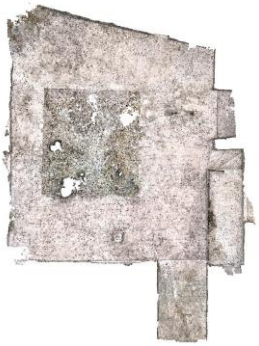

Figure 90: Dense Point Cloud - Yard Floor, Al-Takiyya

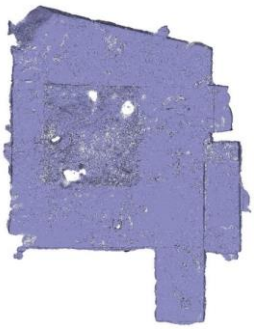

Figure 92: Mesh Model - Yard Floor, Al-Takiyya

Figure 92: Textured Model - Yard Floor, Al-Takiyya

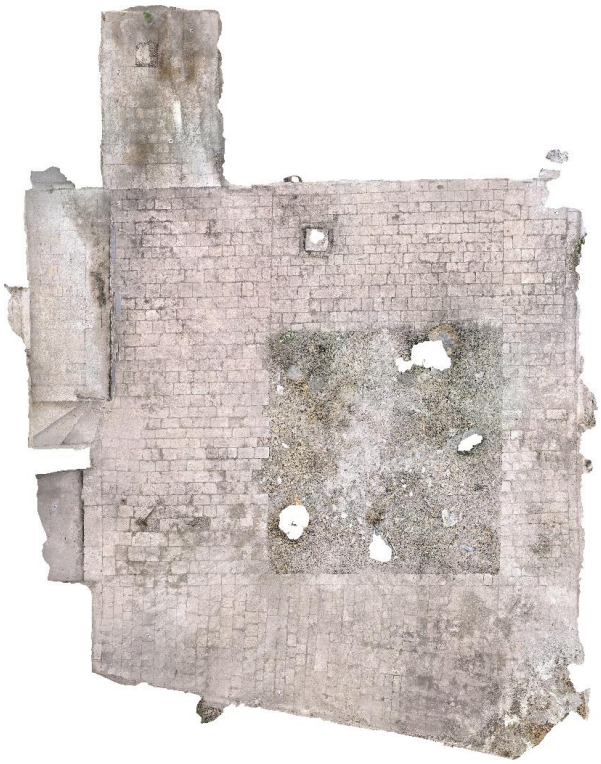

Figure 93: Orthomosaic - Yard Floor, Al-Takiyya

4.4.1.7 *Exterior Façade*

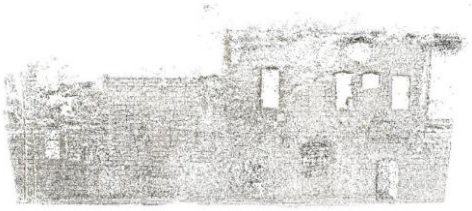

Figure 95: Point Cloud – Esterior Facade, Al-Takiyya

Figure 95: Dense Point Cloud - Esterior Facade, Al-

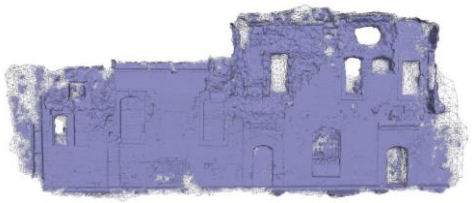

Figure 97: Mesh Model – Esterior Facade, Al-Takiyya

Figure 97: Textured Model - Esterior Facade, Al-Takiyya

Figure 98: Orthomosaic – Exterior Facade, Al-Takiyya

4.4.1.8 *Entrance Façades*

Figure 100: Point Cloud – Entrance Facades, Al-Takiyya

Figure 100: Dense Point Cloud - Entrance Facades, Al-

Figure 102: Mesh Model - Entrance Facades, Al-Takiyya

Figure 102: Textured Model - Entrance Facades, Al-

Figure 103: Orthomosaic – Entrance Facades, Al-Takiyya

4.4.1.9 *Reception Facades*

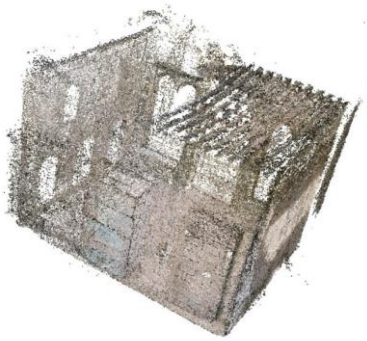

Figure 105: Point Cloud – Reception Facades, Al-

Figure 105: Dense Point Cloud - Reception Facades, Al-

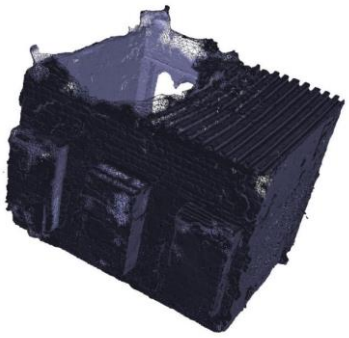

Figure 107: Mesh Model – Reception Facades, Al-

Figure 107: Textured Model - Reception Facades, Al-

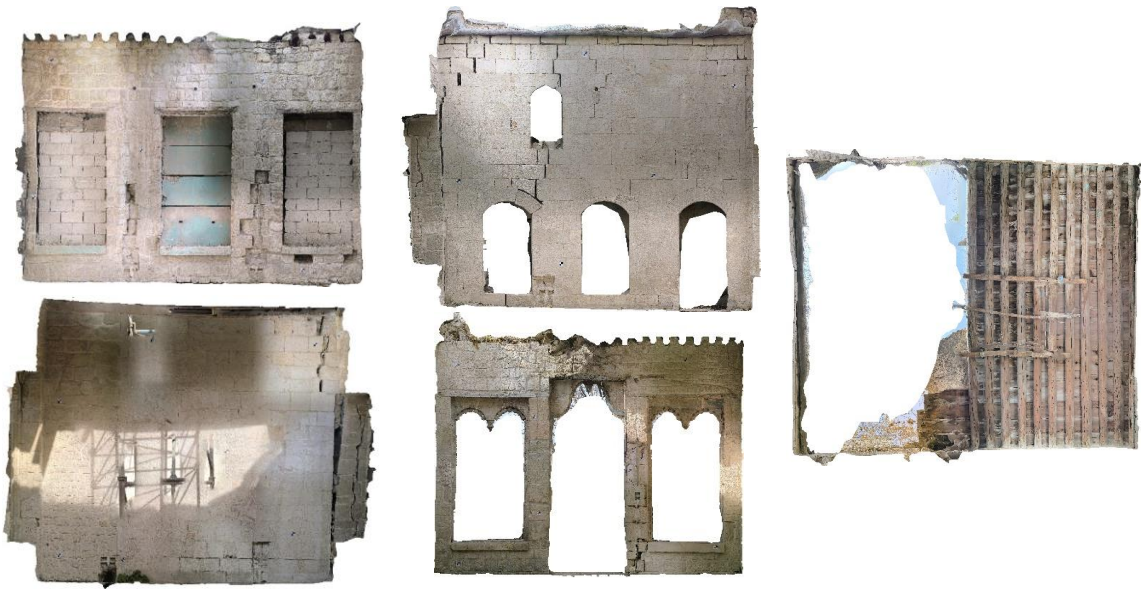

Figure 108: Orthomosaic – Reception Facades, Al-Takiyya

4.4.2 Orthomosaic-Derived CAD Outputs

Orthomosaic Images may be imported into the CAD environment using two distinct approaches:

The ***first approach*** involves importing the Orthomosaic image directly through the original tool available in the CAD environment. This method, however, alters the image scale, which can be corrected in one of two ways:

- By accurately measuring and applying a known reference length, or
- By importing the control points (markers) with their reference coordinates (e.g., via the Civil 3D environment, which is part of the CAD suite) and linking them to their corresponding points on the Orthomosaic image. This process requires a minimum of two reference points.

The ***second approach*** employs the addition of Raster Design Add-on to the CAD environment, which enables the import of images while fully retaining their reference information. In this case, the image is introduced without any changes to coordinates, scale, or rotation. This approach is therefore considered preferable. (In this case, it is recommended to export the Orthomosaic from Agisoft in TIFF/GeoTIFF format, ensuring that all associated reference files are generated and preserved.)

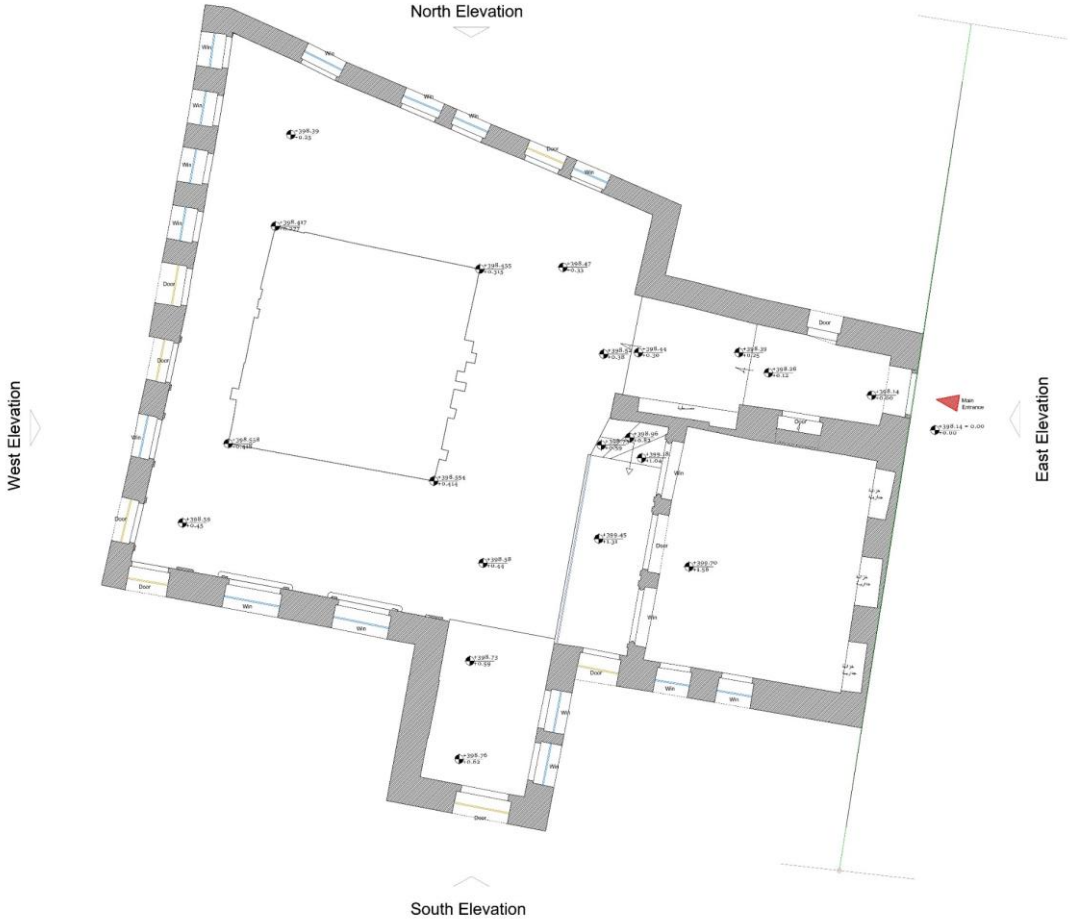

Figure 110: Yard Floor Plan, CAD, Al-Takiyya

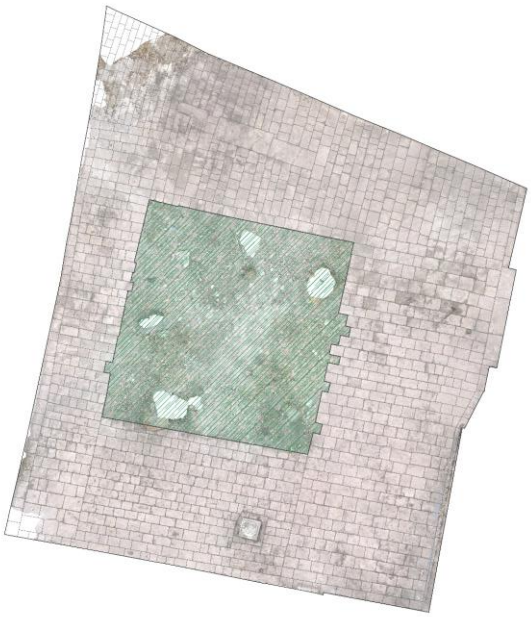

Figure 110: Yard Floor Plan, Stone-by-stone, CAD, Al-Takiyya

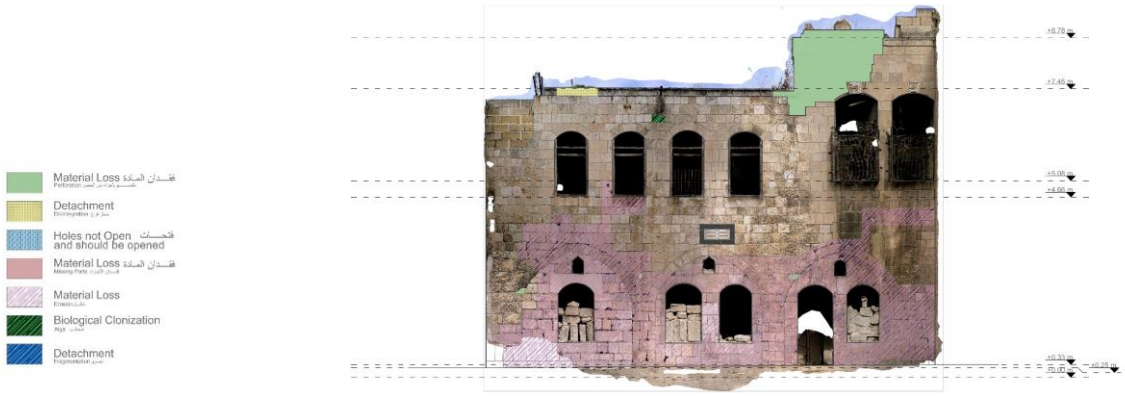

Figure 111: North Facade, Stone-by-stone, CAD, Al-Takiyya

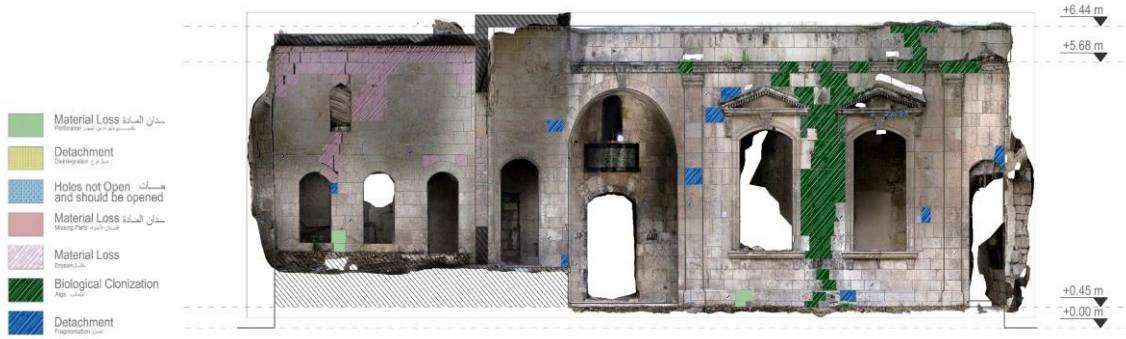

Figure 112: South Facade, Stone-by-stone, CAD, Al-Takiyya

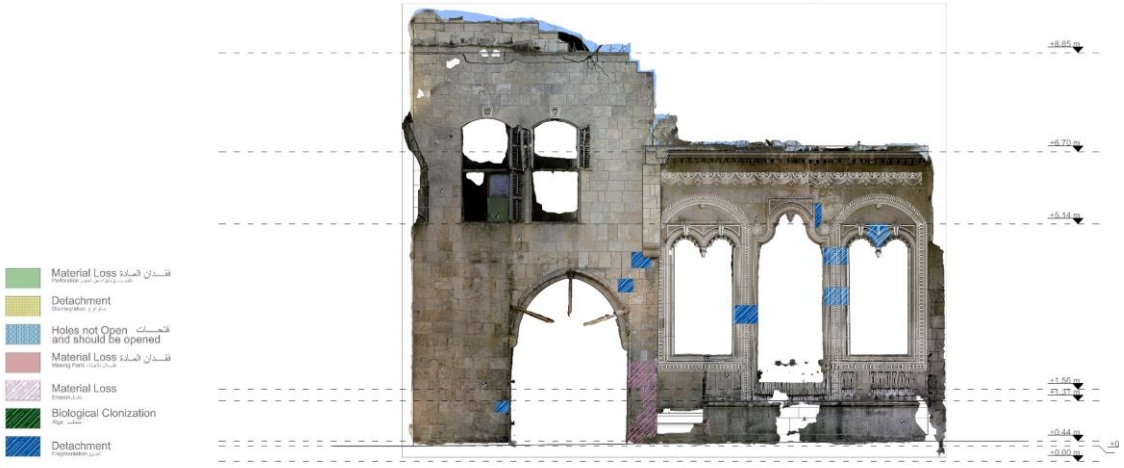

Figure 113: East Facade, Stone-by-stone, CAD, Al-Takiyya

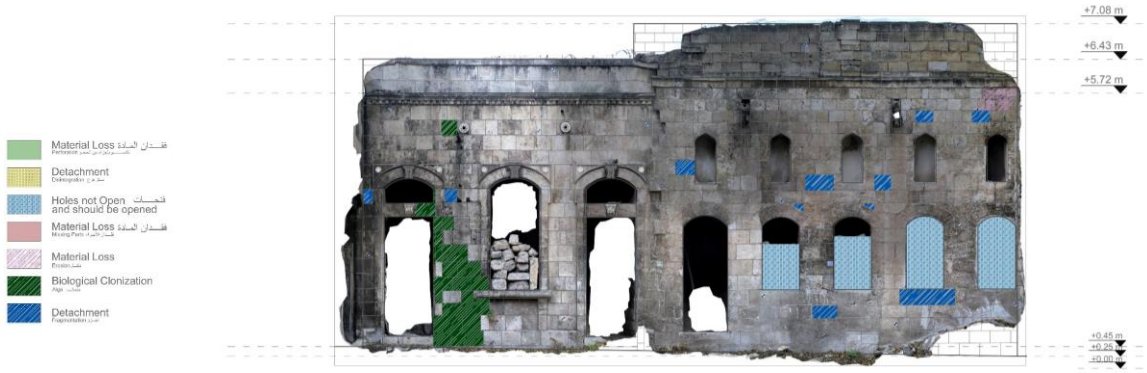

Figure 114: West Facade, Stone-by-stone, CAD, Al-Takiyya

Figure 115: Exterior Facade, Stone-by-stone, CAD, Al-Takiyya

Table 15: Validation of CAD Plan Distances Against Survey Reality According to CIPA/ICOMOS Accuracy Thresholds

Façade	Distance Description	Reality (m)	CAD (m)	Δd (m)	Relative Error	P/F (CAD)
North	Point AX1 and DX3	2.991	2.979	0.012	0.40%	PASS
North	Point 5 and 6	2.273	2.267	0.006	0.26%	PASS
South	Point B22 and B23	3.394	3.393	0.001	0.03%	PASS
West	2- points of partial façade	5.956	5.953	0.003	0.05%	PASS
	2- points of door height	2.182	2.192	-0.01	-0.46%	PASS
East	Between point 1 and 2	3.272	3.276	-0.004	-0.12%	PASS

4.4.3 Total Station-Derived CAD Outputs

Figure 116: Stone-by-stone surveying (Total Station)

Figure 117: (Left) Ortho-derived CAD, (Right) Total Station derived CAD

4.5 HBIM PILOT MODEL PROCESS

4.5.1 Preparation of Photogrammetric Outputs for BIM

The dense point cloud generated in Agisoft Metashape was initially exported in the .e57 format, which is not directly supported by Autodesk Revit. To enable integration into

the BIM environment, the dataset was first imported into ***Autodesk ReCap***, where it was converted into the .rcp/.rcs format. This step ensured compatibility with Revit and allowed the point cloud to be efficiently managed within the BIM workspace. During the conversion process, the dataset's scale and alignment were preserved, facilitating accurate placement and subsequent parametric modeling within Revit.

Autodesk ReCap is a 3D scanning and reality-capture software designed to generate high-resolution spatial data from photographs or laser scans for use in computer-aided design (CAD), building information modeling (BIM), and 3D modeling applications. Data acquired from laser scanners or drone imagery can be imported into ReCap Pro, where it is processed and prepared for integration with Autodesk platforms such as Revit, Civil 3D, Navisworks, InfraWorks, and AutoCAD.

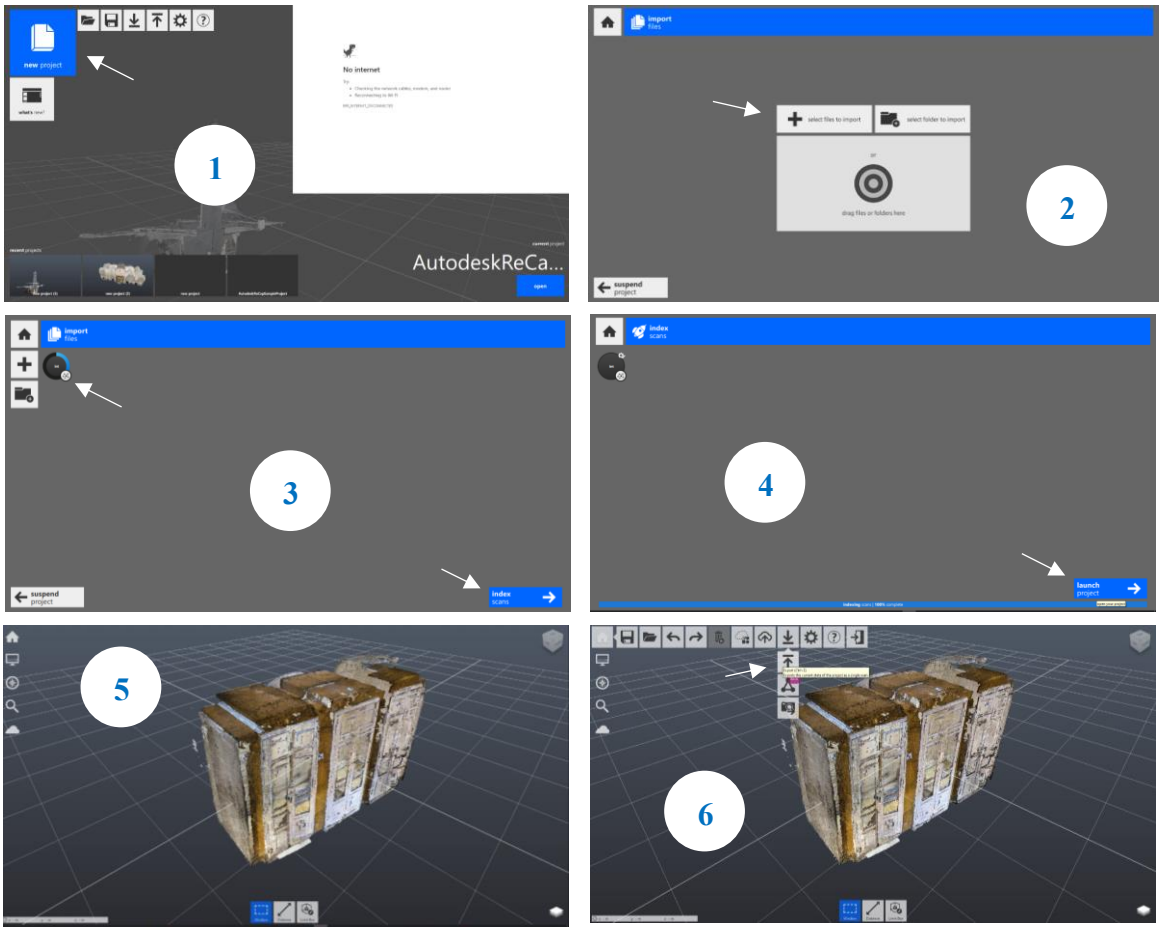

Figure 118: Steps in ReCap for Point Cloud format converting

4.5.2 Import Point Cloud to Revit

First, the units in the modeling file were defined, saved, and prepared for point cloud integration. The point cloud was then imported into Revit following these steps:

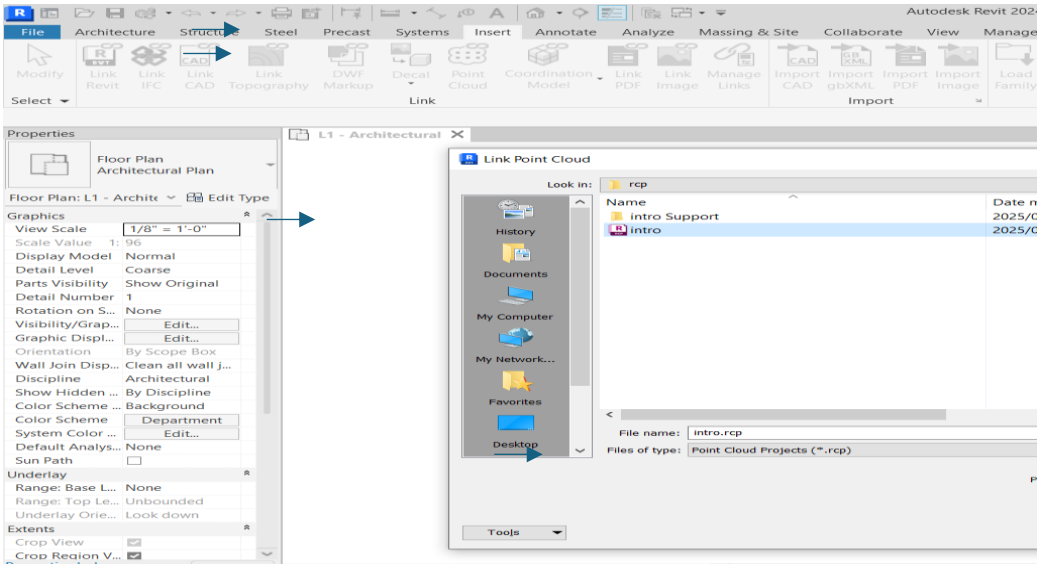

Figure 119: Revit Interface - Importing Point Cloud

- ***Import the point cloud file:*** From the top ribbon, select ***Insert → Point Cloud*** to load the dataset.
- ***Location and alignment:*** Once the point cloud is loaded, the ***Center-to-Center*** option was selected to align the cloud with the project's axes and reference points due to hereunder challenges in importing point clouds with location coordinates

Two approaches can be applied to resolve alignment issues:

1) ***Importing the entire point cloud at once*** – provides higher accuracy but requires significantly more storage and processing power.
2) ***Importing the building in parts*** – allows better handling of large datasets but requires grouping the segments relative to a common reference point or the floor plan, which may slightly reduce accuracy.

4.5.3 Developing HBIM from Medium-Resolution Point Cloud Dataset

4.5.3.1 *Limitations of HBIM Modeling from Medium-Resolution Point Clouds*

After importing the medium-resolution point cloud, it was used as a reference for modeling basic architectural elements such as walls, roofs, ceilings, and limited decorative features. However, the resulting model differed from the actual appearance of the structure due to several factors:

Cloud scattering during zoom-in: This occurs because the point cloud ultimately

consists of a vast number of discrete adjacent points that collectively form the general shape of the building when viewed from a distance. At closer scales, the gaps between points become more visible, leading to a scattered appearance. Moreover, generating continuous mesh surfaces directly from the point cloud is generally impractical, as it would result in an excessively large file, making the model difficult—or even impossible—to process and manage efficiently.


Figure 120: e.g. View of an ornament when zoomed in / out

Point Cloud Quality: Refers to the density of the generated points. In this pilot case study, the Medium Quality setting was used, as the available hardware could not process a full point cloud of the entire building at higher settings (High or Ultra High) without exceeding memory and performance limitations.

High-Quality Test for the Southern Façade: To address this limitation, a High-Quality point cloud was generated specifically for the southern façade. The resulting model provided improved detail in decorative elements compared to the medium-quality version; however, it still fell short of accurately replicating the building's real appearance.

Modeling Skill and Interpretation: Another limitation arises from the current skills of the person performing the modeling. Accurately representing decorative elements depends not only on the point cloud quality but also on the operator's ability to analyze these details and apply appropriate methods and techniques within the Revit environment.

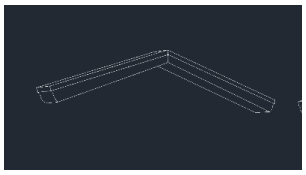

Figure 123: Modeling using High-Quality Point Cloud

Figure 123: Real Capture of Element

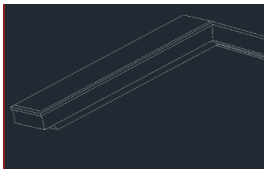

Figure 123: Modeling using Medium-Quality Point Cloud

4.5.3.2 *Wall Modeling Process*

- ***Preliminary Step – Adjusting Point Thickness:*** Based on the point cloud, the thickness of the displayed points was adjusted by modifying the View Range to 5 cm. This setting ensured a higher degree of accuracy while maintaining the cutting plane in a vertical orientation.

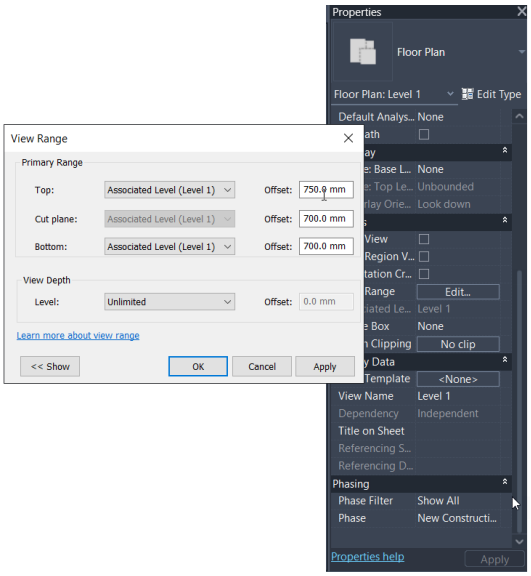

- ***Adjusting Cloud Display Properties:*** Under the View tab, the Visibility/Graphics settings were used to change the point cloud display to Single Color, with red selected to make the cloud easier to reference during modeling.

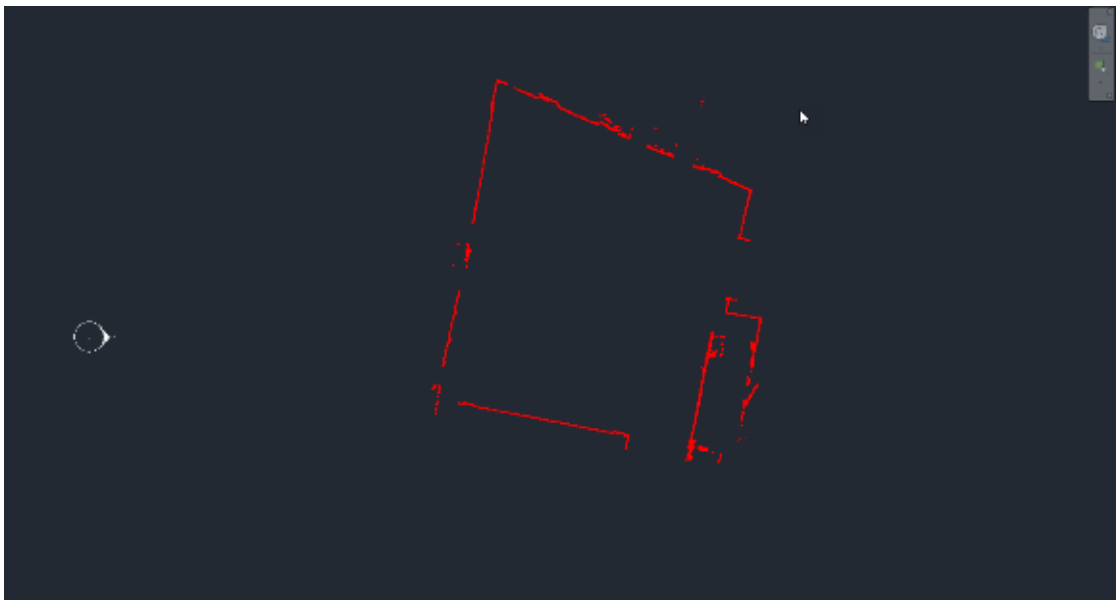

Figure 124: Adjusted view of point cloud in Revit

- ***Drawing Walls**:* Using the Wall tool from the top ribbon in Revit, wall sections were first defined based on ground measurements. The point cloud was then used as a reference to trace the points representing the wall dimensions.
- ***Adjustment and Modification:*** After the walls were created, their heights were adjusted and openings were inserted, guided directly by the point cloud data to ensure accurate alignment with the existing structure.

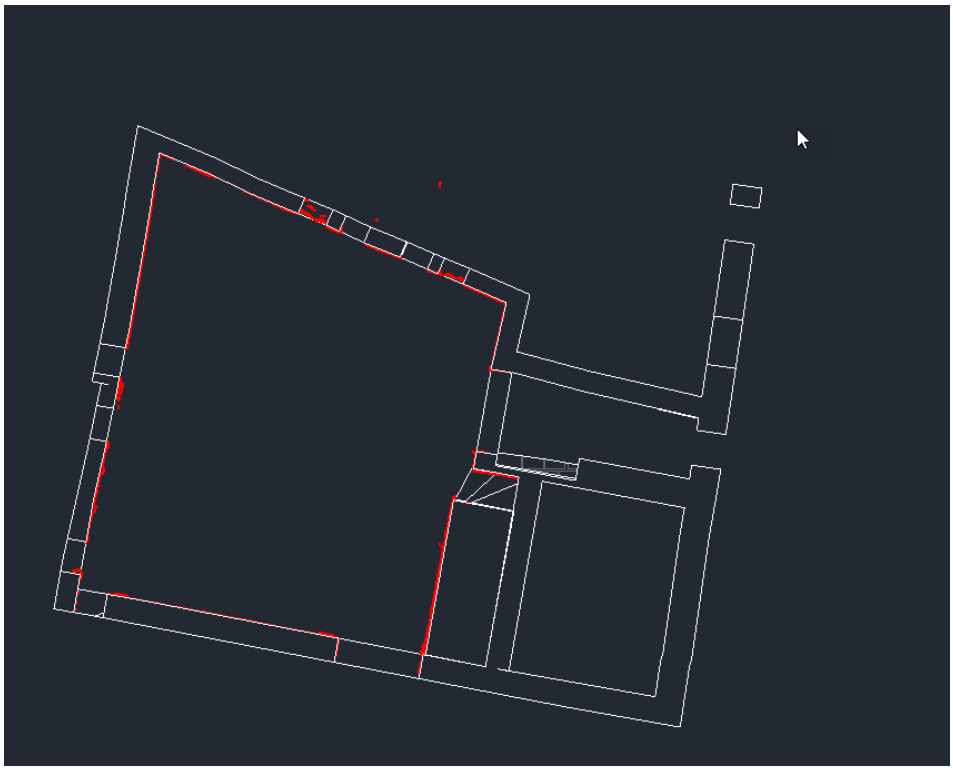

Figure 125: Drawing Walls in Revit, Al-Takiyya

4.5.3.3 *Ceiling Modeling Process*

- ***Defining the Ceiling Level:*** The ceiling level was defined in the *3D View* to ensure that it encompassed the majority of the ceiling points from the point cloud.

Figure 126: Defining the Reception Room Ceiling level, Al-Takiyya

- ***Drawing the Ceiling:*** Using the *Ceiling tool* from the ***Architecture tab***, the ceiling boundaries were traced and completed based on the point cloud data.

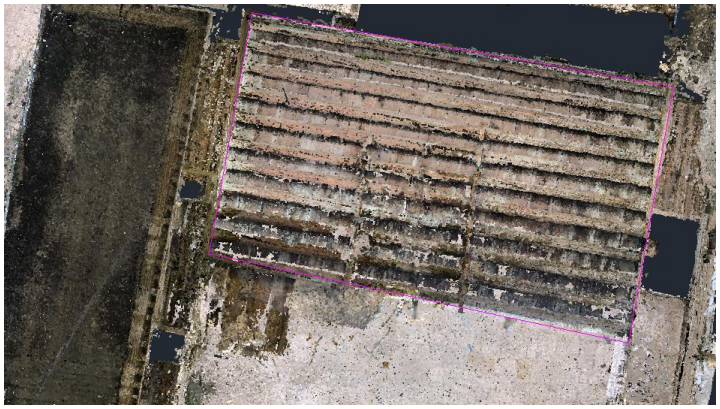

Figure 127: Drawing Reception Room Ceiling, Al-Takiyya

- **Customizing the Ceiling:** After drawing, the ceiling was refined by adjusting materials and details to align with the information captured in the point cloud.

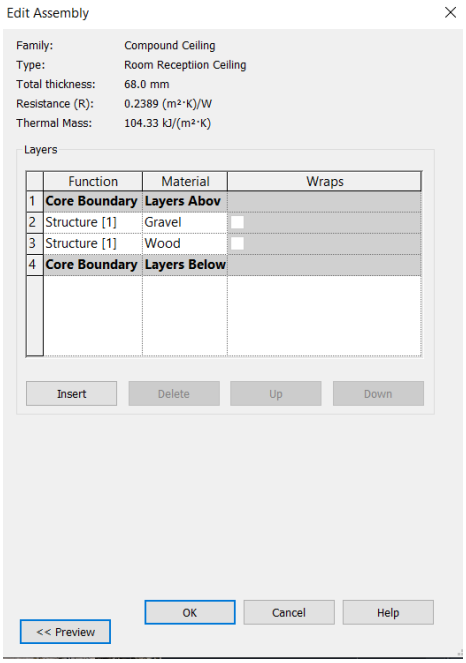

Figure 128: Ceiling Customizing

4.5.3.4 *Interior Ceiling Process*

The modeling process was carried out using the ***"Sweep Blend"*** tool from the ***"Model-In-Place"*** menu, which enables the creation of geometry along a defined path with two specified sections. The entrance design consists of three intersecting arches:

- ***Main arch:*** Extends from the beginning of the entrance to its end.
- ***First secondary arch:*** Intersects the main arc in the pantry area.

- ***Second secondary arch:*** Intersects the main arc in the kitchen area.

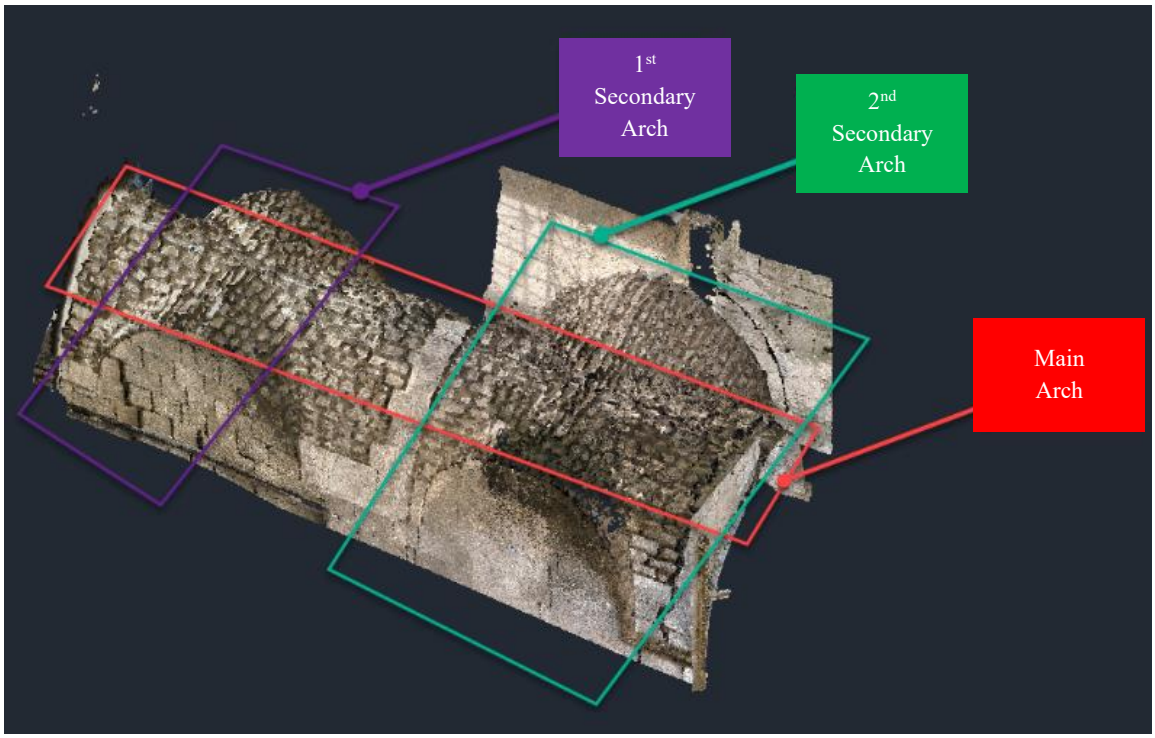

Figure 129: Arcs Analysis of Reception Ceiling

The ***main arch*** is composed of four sections, distributed as follows:

- ***First arch:*** Comprising two sections, extending from the beginning of the entrance to the transitional arch.
- ***Transitional arch:*** Connects the two main arches and is itself divided into two sections—the first extending from the end of the first arch, and the second beginning at the start of the second arch.
- ***Second arch:*** Completes the composition of the two main arches and extends from the end of the transitional arch to the termination of the entrance.

Figure 130: Arches Analysis of Reception Ceiling Main Arch

The process proceeded as follows, using the ***main arch*** as an example.

Drawing the main arch was carried out in three stages:

- ***First arch:*** The path connected the arch vertices, extending from the first segment of the entrance to the second segment at the start of the transitional arch.

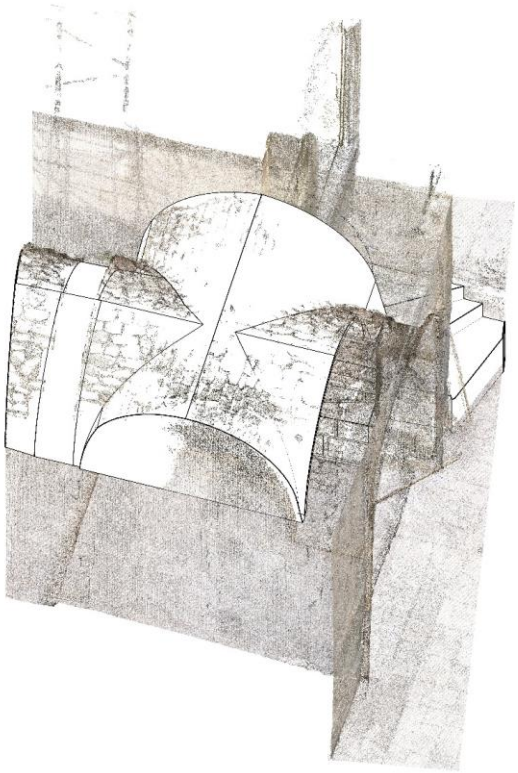

Figure 131: First Arch of Main Reception Arch

- ***Second arch:*** The path connected the arch vertices, extending from the first segment at the end of the transitional arch to the second segment at the end of the entrance.

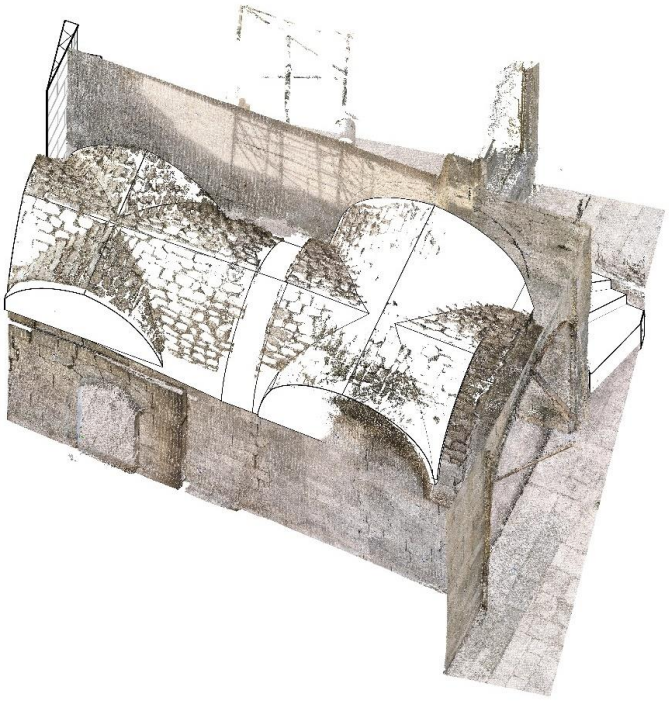

Figure 132: Second Arch of Main Reception Arch

- ***Transitional arch:*** Drawn last to ensure its correct path, it connected the two main arches, with the first segment extending from the end of the first arch and the second segment beginning at the start of the second arch.

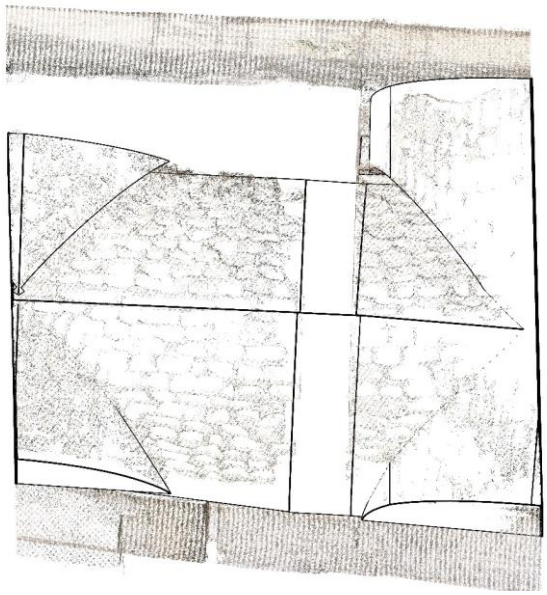

Figure 133: Transitional Arch of Main Reception Arch

4.5.4 Developing HBIM from Orthomosaic-Derived CAD

Defining the Tekke (Al-Takiyya) Location in Revit:

The objective of defining the location is to accurately position the Tekke site within the project environment and to establish the Sun Path, which is essential for future energy analysis. The process involves the following steps:

- ***Determine the coordinates:*** Obtain the Tekke's geographical coordinates using Google Maps.
- ***Set the project location:*** In Revit, go to the *Manage* tab, then under *Project Location* select *Location*.
- ***Input coordinates:*** In the *Location* dialog box, choose *Internet Mapping Service*, paste the coordinates, and click *OK*.
- ***Adjust orientation:*** Once the location is entered, the Tekke's projection may appear tilted. To align it properly, rotate *Project North* so that one side of the projection is orthogonal, facilitating modeling tasks.[14]
- ***Rotate Project North:*** Navigate to *Manage* > *Project Location* > *Position* > *Rotate Project North*, ensuring the *Orientation* parameter is set to *Project North*.

Importing CAD drawings to Revit

- From the Insert tab, select Link CAD and insert the plan of Al-Takiyya.
- The modeling will be carried out at LOD 300, which ensures that elements are represented with precise geometry, accurately reflecting their real-world size, shape, and location.
- At this level, the model can also be used to document damage, including its quantity, location, and type.

Defining the Materials of the Main Elements of Al-Takiyya

- From the *Manage* tab, select ***Materials***.
- Duplicate an existing stone material and adjust its *Appearance* properties using the ***Tiles*** style.

[14] Caution: The bias and misalignment result from a common issue in Syria when using Syrian stereographic coordinates and subsequently converting them into the global coordinate system (employed by Google Maps, Google Earth, …etc.). While the projection maintains correct scale, discrepancies occur in the form of displacements along the x- and y-axes, as well as rotations around both axes. These discrepancies are systematic and constant for both axes, with displacements occasionally reaching up to around 50 meters.

- The resulting material is designated as **"*Stone*"** representing the original building material.

Defining the Sections of the Modeled Elements (Walls, Floors, Ceilings)

- ***Walls*:** Using the *Wall* command, specify the wall thickness and assign the *"Stone"* material.
- ***Floors*:** Using the *Floor* command, define the internal material layers.
- ***Ceilings:*** Using either *Roof* or *Ceiling*, depending on the element type, assign the appropriate material.

Defining the Sections of the Modeled Elements (Ornaments)

The ornament elements were created using the *Model-In-Place* tool, categorized under ***Generic Model***. The ornaments were divided into two types:

Modelable Ornaments: These were modeled to closely reflect reality, using the *Model-In-Place* tools.

Figure 134: Modelable Ornaments

Two main methods were applied:

1) **Solid Only:** A fundamental modeling approach

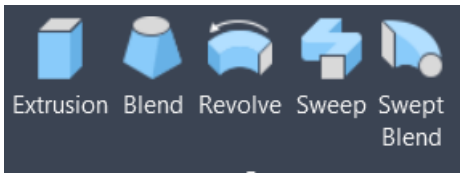

2) **Sculpting:** A more complex method involving two stages:
   - Creation of a solid element using one of the Model-In-Place tools.
   - Application of the sculpting process through one of two techniques:
     - ***Void Extrusion / Void Blend:*** A perpendicular extrusion of the element without a defined path or section. To visually distinguish these void-

extruded elements from solids, they were assigned an **orange color** in the model.

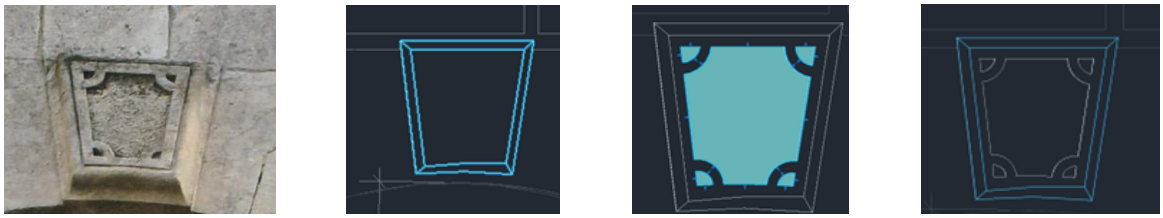

(a) (b) (c) (d)

Figure 135: e.g. of Void Extrusion / Blend, (a) Reality, (b) Solid Extrusion, (c) Void Extrusion, (d) Final Result

- Sculpting using the ***Void Sweep*** method: After creating the solid element, the sculpting is carried out along a predefined path that extends across the element. The hollow section (Ornament) is then drawn in reverse, allowing the sculpting process to be completed.

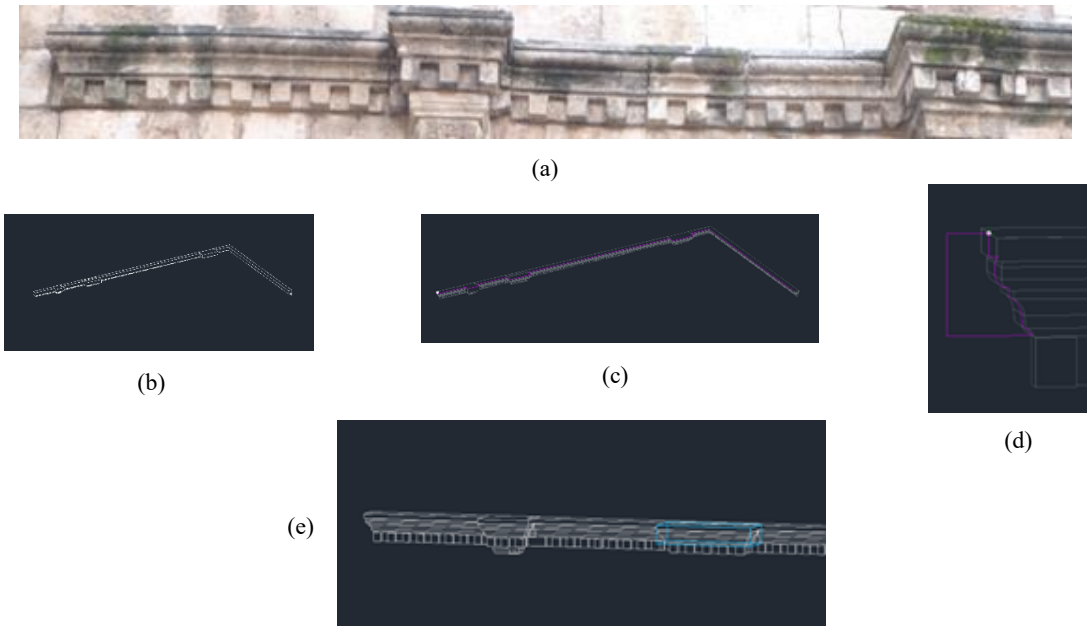

(a)

(b) (c) (d)

(e)

Figure 136: e.g. of Void Sweep, (a) Reality, (b) Solid Extrusion, (c) Sweep Path, (d) Sweep Profile, (e) Final Result

Complex ornaments: These ornaments are particularly difficult to model, as their reproduction depends largely on the skills of the individual performing the modeling. They require an analysis of the constituent elements and multi-section carving, which is challenging to achieve in Revit. In many cases, free-form modeling software such as *3ds Max*, *Blender*, or *Maya* may be required. To overcome this limitation within the pilot case study (Al-Takiyya), a simplified extrusion was applied in the locations of these elements.

Each ornament was assigned a unique number using the *Type Mark* parameter, and a reference table was created containing real-life images of the corresponding ornaments.

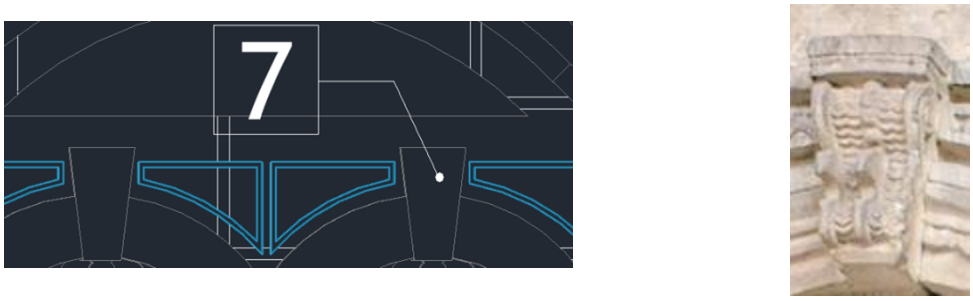

Figure 137: Complex ornaments, e.g. Type Mark parameter as reference

Defining Project Phases

Two main phases were established within the project:

- Existing: Represents the original elements of Al-Takiyya prior to damage.
- As-Built: Represents the damaged and deteriorated areas.

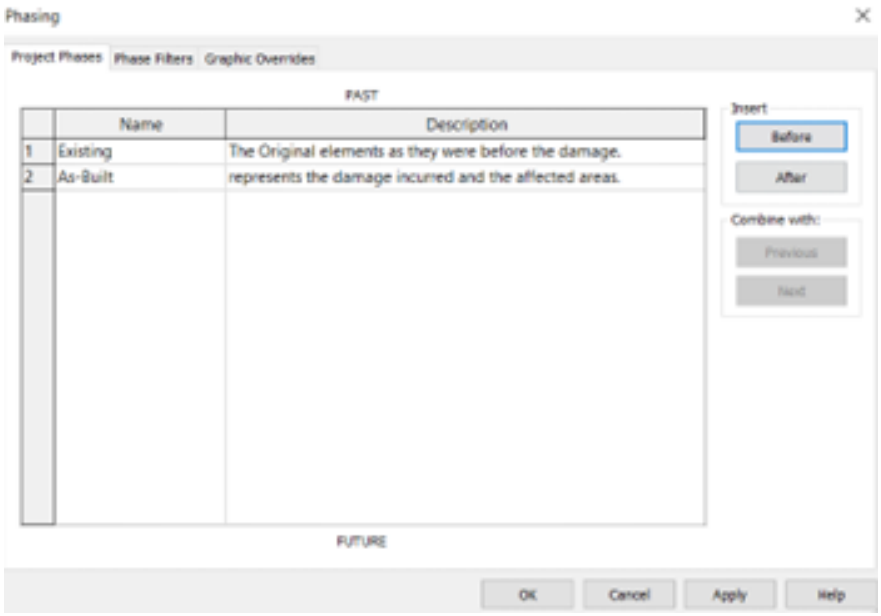

Figure 138: Defining Phasing

Damage Mapping

The damage in Al-Takiyya was classified into types (same as in CAD drawings)[15]

[15] Read Appendix A for more details of Damage Mapping Classifications.

- ***Demolished elements:*** Demolished components are first placed in the *Existing* phase. The "*Phase Demolished* Parameter" is then set to "*As-Built"* to indicate their removal.
- ***Damage:*** Areas of damage are modeled using *Extrusion Solid* and *Sweep* tools, applied with a nominal thickness of 1 mm to distinguish them from intact elements. An exception was made for the damage classified as *'Holes not open and should be opened'*, which was modeled using *Extrusion Solid* with a thickness corresponding to that of each individual wall.

Visual Documentation and Damage Analysis

- 3D and elevation views were generated to visualize the damage from multiple perspectives.
- The model facilitates the preparation of Bill of Quantities (BOQ) tables for damaged elements.
- Variable quantity tables were created to reflect the extent of damage present in each façade/interface.
- By applying the *Keynotes* tool, descriptive annotations of the elements were incorporated into the sheets. The associated tables update dynamically according to the elements and keynotes used.

4.5.5 Developing HBIM from Total Station-Derived CAD

Modeling at LOD 500 was tested on a portion of the southern façade, where stone elements were represented exactly as reality. This was achieved by creating solid extrusions of the stone cuts at their actual positions and assigning the corresponding materials. Some of the complicated ornaments were assigned a unique number parameter, and a reference table was created containing real-life images (or) orthophotos.

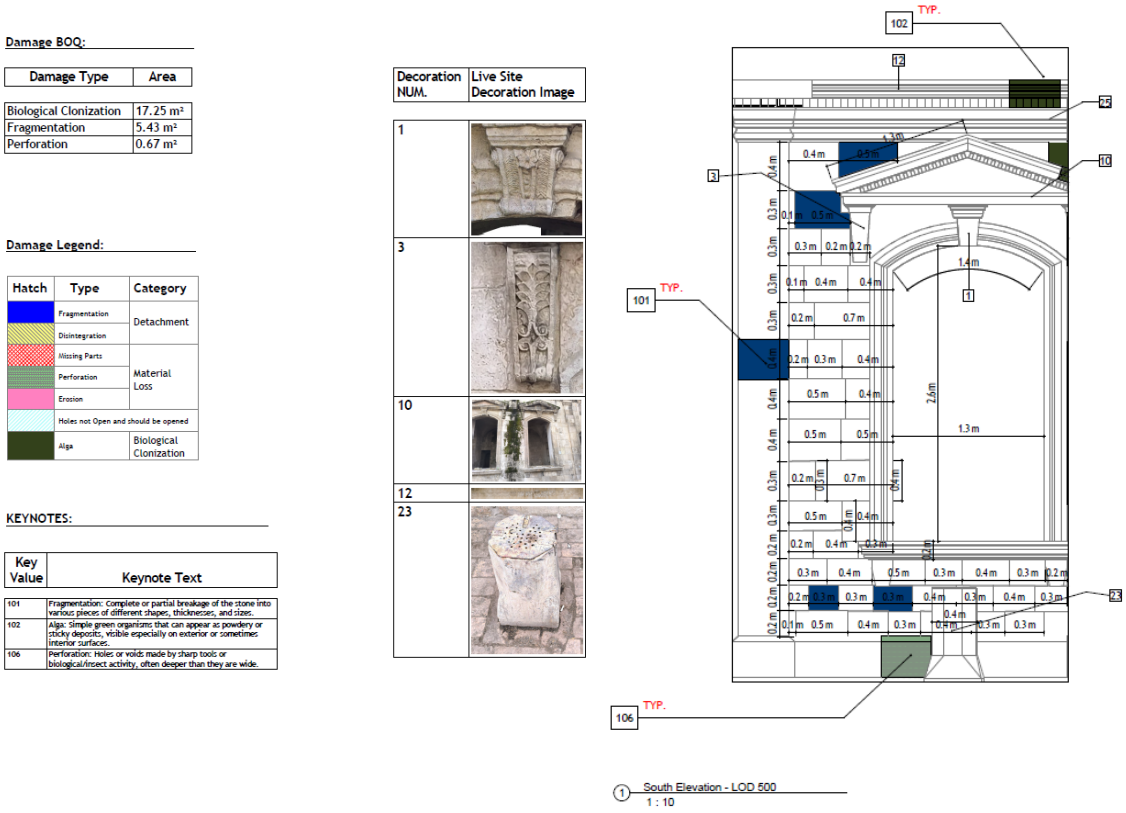

Figure 139: Orthomosaic-Derived CAD to BIM (LOD 500), Partial, Al-Takiyya

4.6 HBIM PILOT MODEL OUTPUTS[16]

4.6.1 HBIM Model from Medium-Resolution Point Cloud Dataset

Output Level of Development: LOD 200 - General outlines of walls, roofs, and floors without detailed measurements.

[16] All High-quality 2D and 3D schemes are available to download from the list of Online Supplementary Materials.

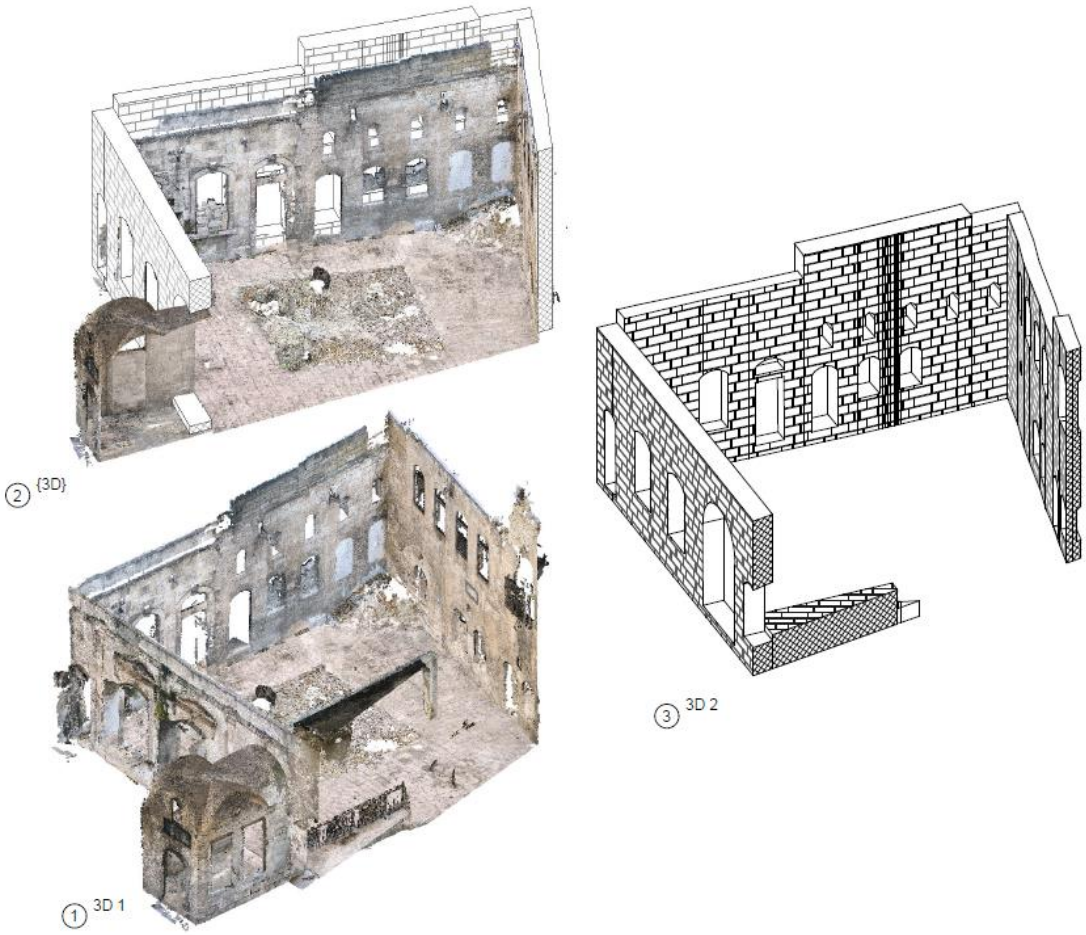

Figure 140: HBIM Model from Medium-Resolution Point Cloud Dataset (LOD 200)

4.6.2 HBIM Model from Orthomosaic-Derived CAD

Output Level of Development: LOD 300 - Accurate building geometry captured from survey data, but without detailed elements like stones or decorations.

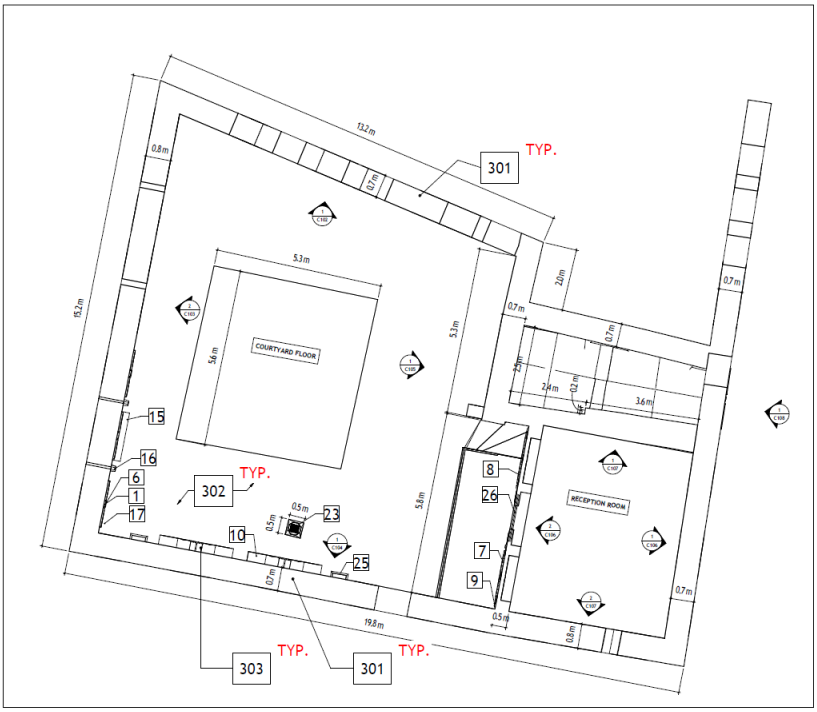

1 Floor Plan
1 : 50

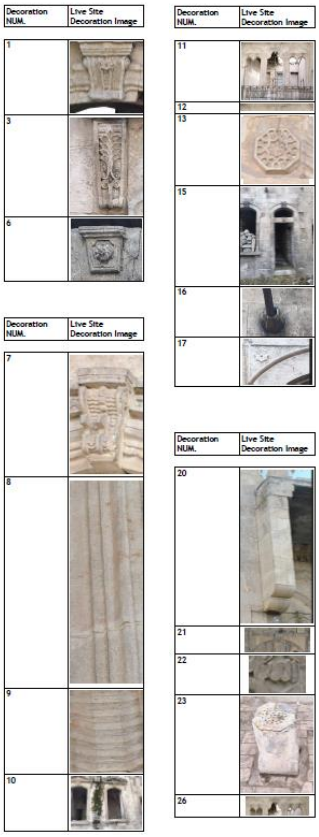

KEYNOTES:

Key Value	Keynote Text
301	Existing walls (structurally reinforced).
302	Existing floor will be retained.
303	Architectural decorative elements (unreinforced), to be preserved and protected during restoration works.

KEYNOTES:

Damage Type	Area
Biological Clonization	17.39 m²
Disintegration	6.72 m²
Erosion	65.57 m²
Fragmentation	7.07 m²
Missing Parts	4.55 m²
Perforation	69.54 m²

Figure 141: Floor Plan, LOD 300, Al-Takiyya

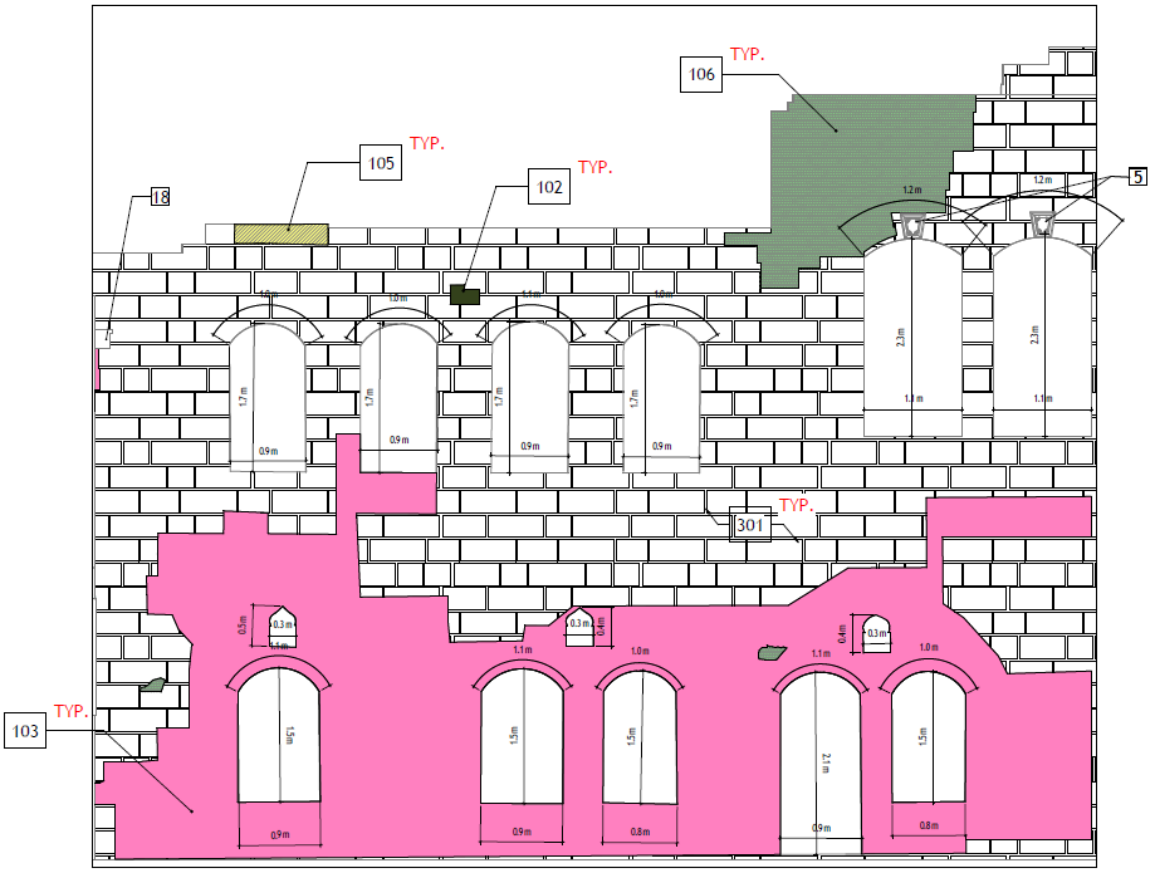

Damage Legend:

Hatch	Type	Category
	Fragmentation	Detachment
	Disintegration	
	Missing Parts	Material Loss
	Perforation	
	Erosion	
	Holes not Open and should be opened	
	Alga	Biological Clonization

Damage BOQ:

Damage Type	Area
Biological Clonization	0.13 m²
Disintegration	3.93 m²
Erosion	52.94 m²
Fragmentation	5.43 m²
Perforation	7.79 m²

Key Value	Keynote Text
102	Alga: Simple green organisms that can appear as powdery or sticky deposits, visible especially on exterior or sometimes interior surfaces.
103	Erosion: Loss of the original stone surface due to environmental or mechanical forces, resulting in smooth forms.
105	Disintegration: The separation of stone into individual grains or groups of grains.
106	Perforation: Holes or voids made by sharp tools or biological/insect activity, often deeper than they are wide.
301	Existing walls (structurally reinforced).

Decoration NUM.	Live Site Decoration Image
5	
18	

Figure 142: North Facade, LOD 300, Al-Takiyya

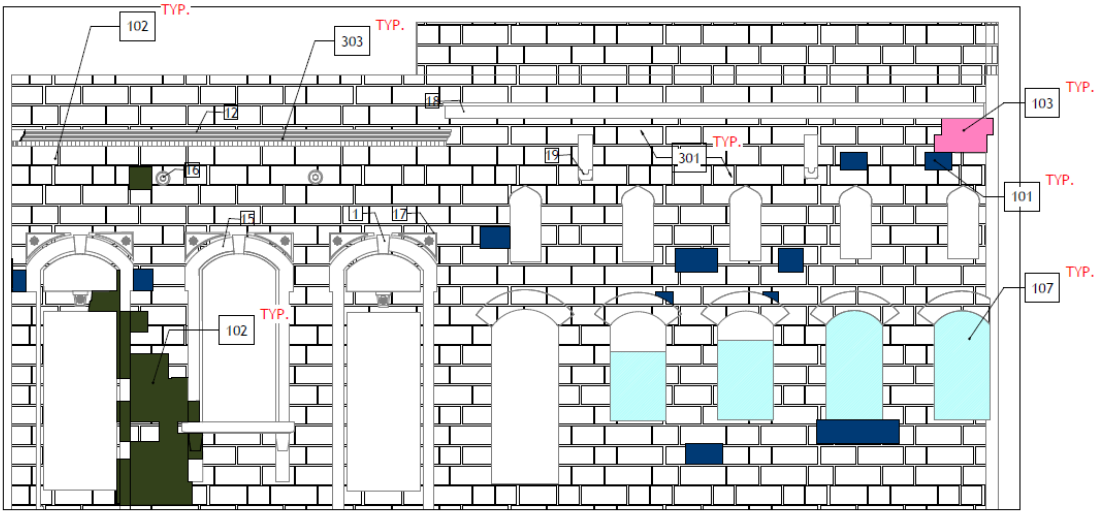

KEYNOTES:

Key Value	Keynote Text
101	Fragmentation: Complete or partial breakage of the stone into various pieces of different shapes, thicknesses, and sizes.
102	Alga: Simple green organisms that can appear as powdery or sticky deposits, visible especially on exterior or sometimes interior surfaces.
103	Erosion: Loss of the original stone surface due to environmental or mechanical forces, resulting in smooth forms.
107	Holes not open and should be opened.
301	Existing walls (structurally reinforced).
303	Architectural decorative elements (unreinforced), to be preserved and protected during restoration works.

Damage Legend:

Hatch	Type	Category
	Fragmentation	Detachment
	Disintegration	
	Missing Parts	Material Loss
	Perforation	
	Erosion	
	Holes not Open and should be opened	
	Alga	Biological Clonization

Damage BOQ:

Damage Type	Area
Biological Clonization	17.26 m²
Erosion	0.69 m²
Fragmentation	5.43 m²

Decoration NUM.	Live Site Decoration Image
1	
6	
12	
15	

Decoration NUM.	Live Site Decoration Image
16	
17	
18	
19	

Figure 143: West Facade, LOD 300, Al-Takiyya

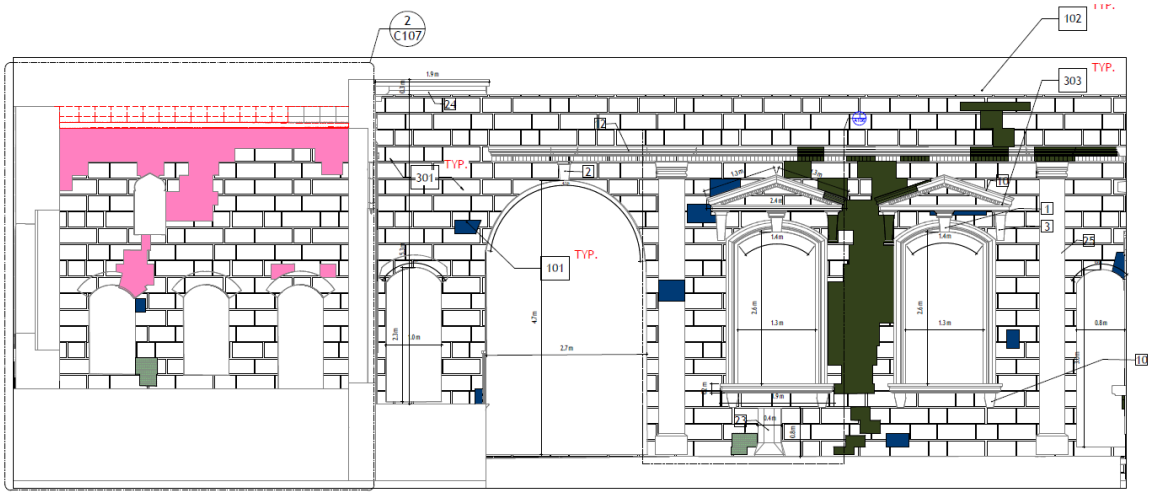

KEYNOTES:

Key Value	Keynote Text
101	Fragmentation: Complete or partial breakage of the stone into various pieces of different shapes, thicknesses, and sizes.
102	Alga: Simple green organisms that can appear as powdery or sticky deposits, visible especially on exterior or sometimes interior surfaces.
301	Existing walls (structurally reinforced).
303	Architectural decorative elements (unreinforced), to be preserved and protected during restoration works.

Damage Legend:

Hatch	Type	Category
	Fragmentation	Detachment
	Disintegration	
	Missing Parts	Material Loss
	Perforation	
	Erosion	
	Holes not Open and should be opened	
	Alga	Biological Clonization

Damage BOQ:

Damage Type	Area
Biological Clonization	17.26 m²
Disintegration	0.68 m²
Erosion	10.22 m²
Fragmentation	6.49 m²
Missing Parts	4.55 m²
Perforation	61.75 m²

Demolished Elements BOQ:

Material Name	Area	Volume
Demolished Gravel	45.96 m²	2.27 m³
Demolished wood	55.30 m²	1.81 m³

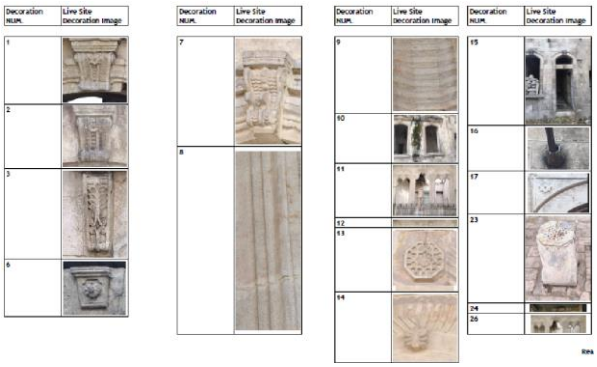

Figure 144: South Facade, LOD 300, Al-Takiyya

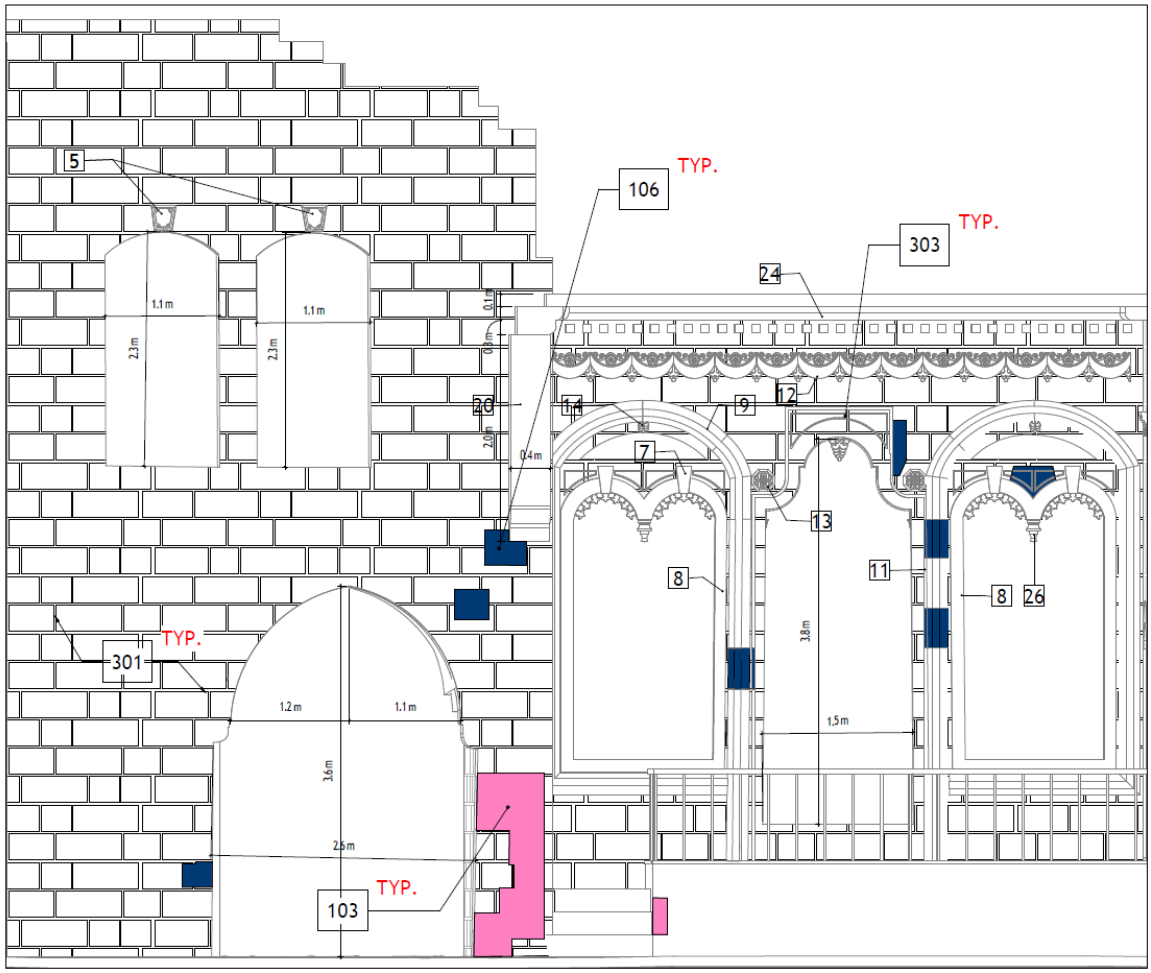

Damage Legend:

Hatch	Type	Category
	Fragmentation	Detachment
	Disintegration	
	Missing Parts	Material Loss
	Perforation	
	Erosion	
	Holes not Open and should be opened	
	Alga	Biological Clonization

Damage BOQ:

Damage Type	Area
Disintegration	1.56 m²
Erosion	54.30 m²
Fragmentation	4.41 m²

KEYNOTES:

Key Value	Keynote Text
103	Erosion: Loss of the original stone surface due to environmental or mechanical forces, resulting in smooth forms.
106	Perforation: Holes or voids made by sharp tools or biological/insect activity, often deeper than they are wide.
301	Existing walls (structurally reinforced).
303	Architectural decorative elements (unreinforced), to be preserved and protected during restoration works.

Figure 145: East Facade, LOD 300, Al-Takiyya

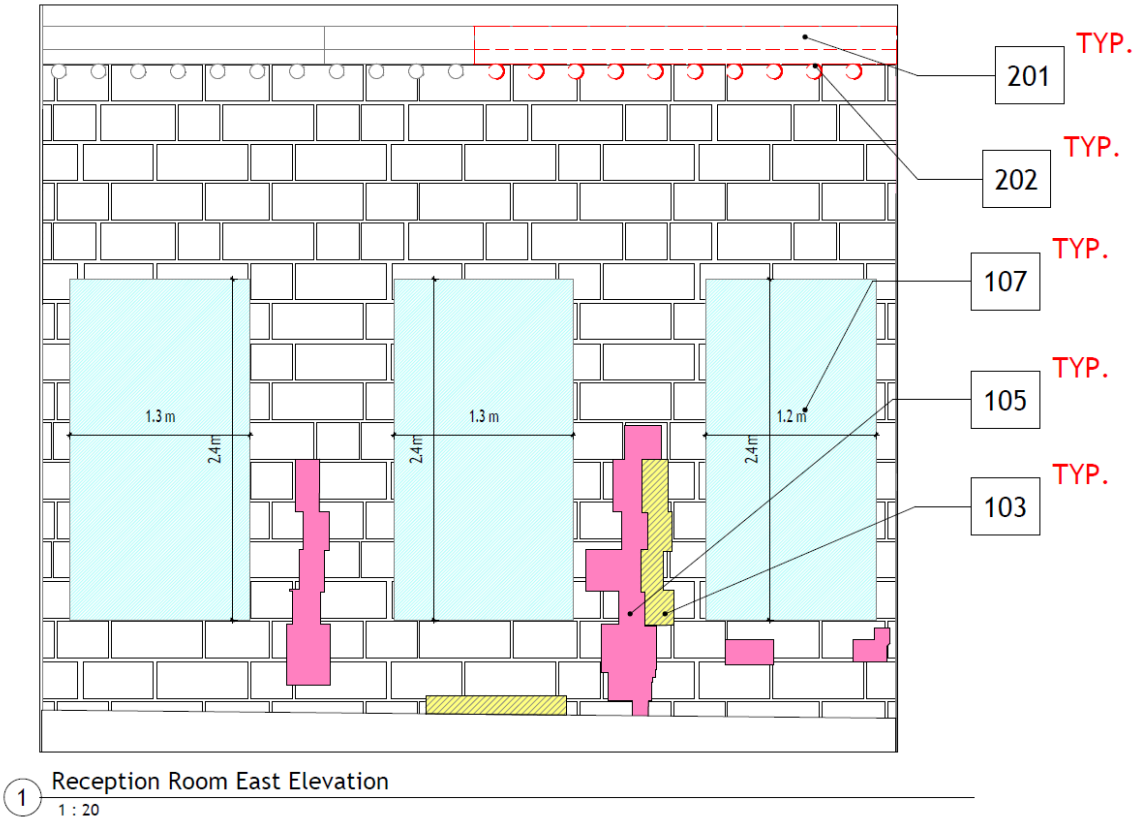

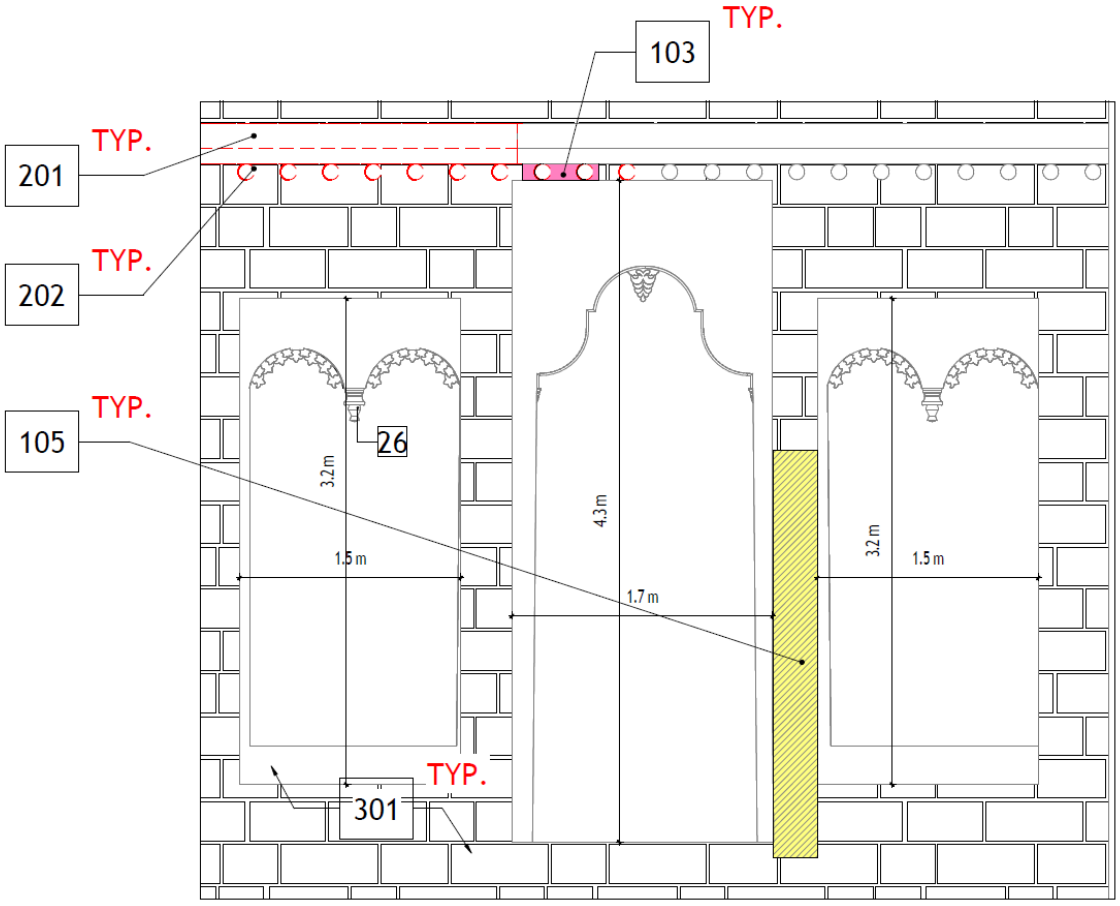

Figure 146: Reception Room, LOD 300, Al-Takiyya

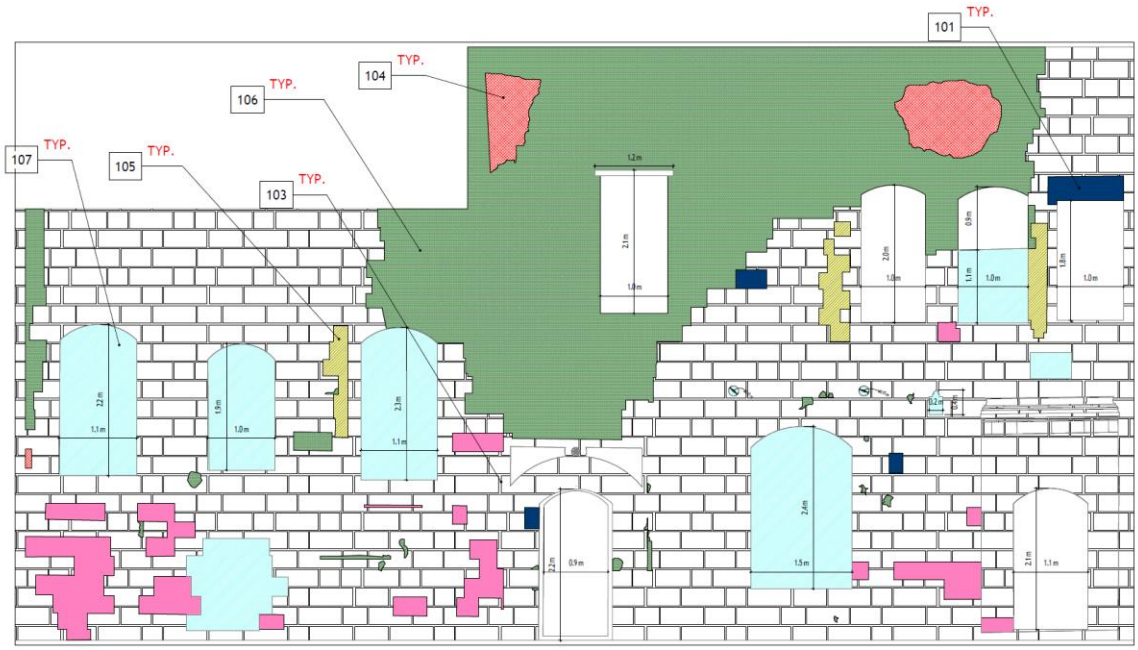

Damage BOQ:

Damage Type	Area
Disintegration	3.93 m²
Erosion	8.09 m²
Fragmentation	2.77 m²
Missing Parts	4.55 m²
Perforation	61.15 m²

KEYNOTES:

Key Value	Keynote Text
101	Fragmentation: Complete or partial breakage of the stone into various pieces of different shapes, thicknesses, and sizes.
103	Erosion: Loss of the original stone surface due to environmental or mechanical forces, resulting in smooth forms.
104	Missing Parts: Empty areas that were previously part of the object, typically prominent features like noses or fingers in sculptures.
105	Disintegration: The separation of stone into individual grains or groups of grains.
106	Perforation: Holes or voids made by sharp tools or biological/insect activity, often deeper than they are wide.
107	Holes not open and should be opened.

Damage Legend:

Hatch	Type	Category
	Fragmentation	Detachment
	Disintegration	
	Missing Parts	Material Loss
	Perforation	
	Erosion	
	Holes not Open and should be opened	
	Alga	Biological Clonization

Decoration NUM.	Live Site Decoration Image
4	
21	
22	

Figure 147: Exterior Facade, LOD 300, Al-Takiyya

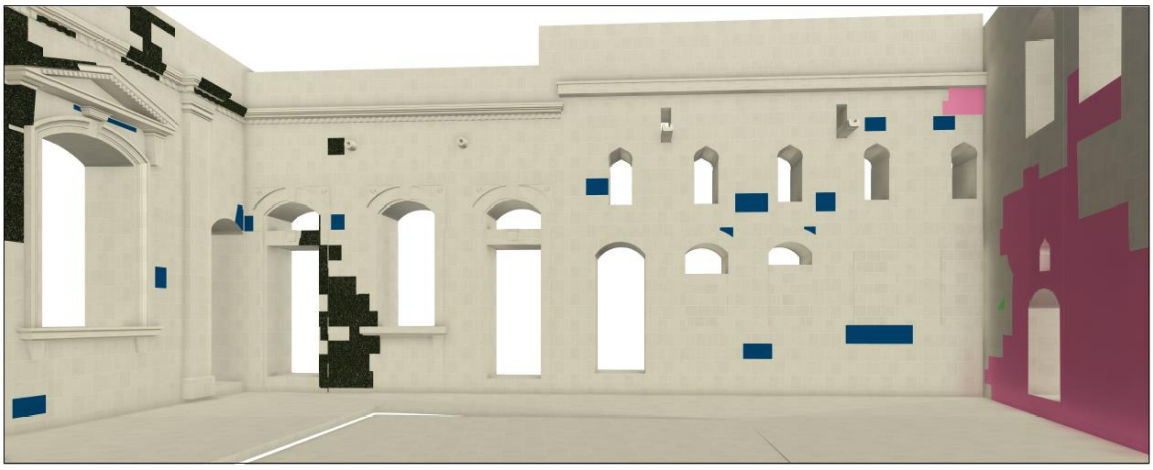

Figure 148: ISOMETRIC, LOD 300, Al-Takiyya (1)

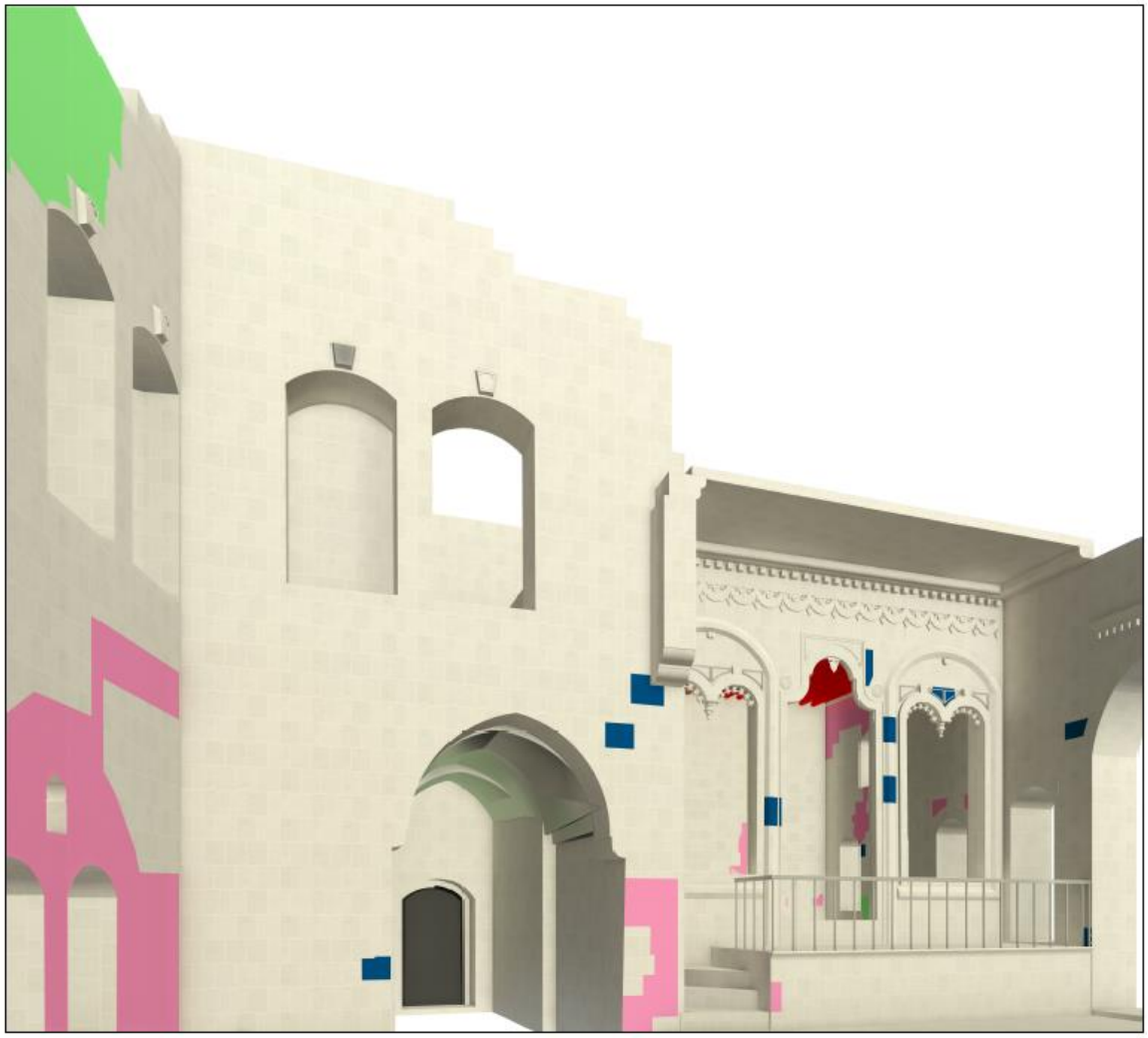

Figure 149: ISOMETRIC, LOD 300, Al-Takiyya (2)

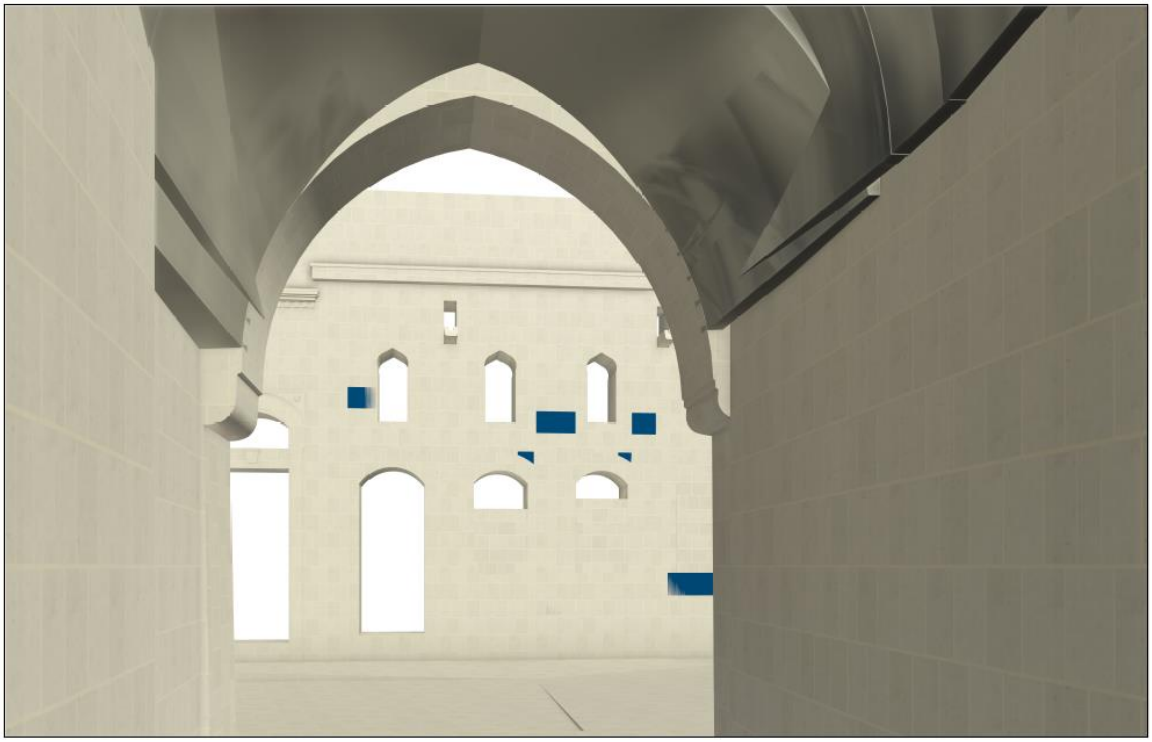

Figure 150: ISOMETRIC, LOD 300, Al-Takiyya (3)

Figure 151: ISOMETRIC, LOD 300, Al-Takiyya (4)

4.6.3 HBIM Model from Total Station-Derived CAD

Modeling at LOD 500 was tested on a portion of the southern façade, where stone elements were represented exactly as reality. This was achieved by creating solid extrusions of the stone cuts at their actual positions and assigning the corresponding materials. Some of the complicated ornaments were assigned a unique number parameter, and a reference table was created containing real-life images (or) orthophotos.

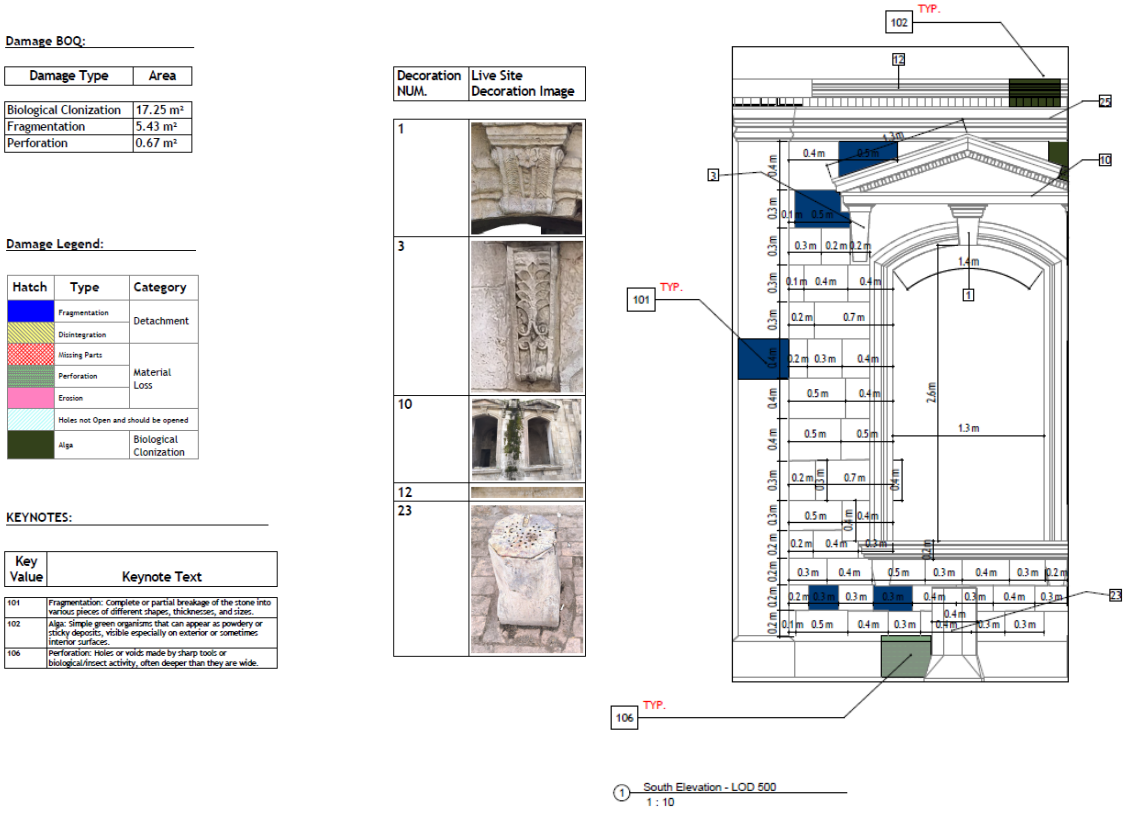

Figure 152: Total Station-Derived CAD to BIM (LOD 500), Partial, Al-Takiyya

The documentation method based on points observed from a surveying device is generally more accurate than the photogrammetric method in determining the locations of façade detail points. However, it presents several limitations:

1) ***Time consumption:*** Scanning with a total station is very time-intensive due to the large number of points required to capture the details of even a small area.
2) ***Limitations in complex motifs:*** The total station cannot accurately capture the details of plant motifs, especially in distant areas (from the observer's perspective) or those characterized by curves.

3) ***Challenges with curves and protrusions:*** In curved or protruding areas, laser scanning is affected by slippage, resulting from the small spacing between successive observed points (1–2 cm).

By contrast, the Orthomosaic images produced through photogrammetry offer the following characteristics:

1) ***Accuracy:*** Photogrammetric outputs achieve high precision, with displacement errors typically ranging between 0.5–1.5 cm, as they are anchored by markers placed on the corrected façade.
2) ***Visualization quality:*** The method excels in visual interpretation, enabling accurate inference of details with the naked eye. The main façade details achieve a visual accuracy rating of *9.5/10*, while the finer decorative details achieve *8/10*.[17]
3) ***Efficiency:*** Photogrammetric documentation requires less time compared to surveying devices, though it demands high-performance computers for processing, specialized photogrammetry software, and high-resolution imaging equipment. In some cases, additional tools such as scaffolding, cranes, or portable ladders are necessary to address elevation challenges.
4) ***Limitations:*** Orthomosaic images do not adequately represent actual curves or slopes, nor do they capture the full extent of projections and subtle dimensional variations. Reference to the physical site, a 3D model, or multi-angle imagery is therefore essential.

In the context of Syria, Heritage documentation requires very high accuracy due to the abundance of fine façade details, making the choice of method critical for reliable results.

4.6.4 HBIM Model from Composite Point Cloud-CAD

As a practical solution, the point cloud was integrated with the BIM model developed at **LOD 300 from the Orthomosaic-Derived CAD**. This process involved overlaying the LOD 300 model with the medium-resolution point cloud, resulting in the most effective visualization of the project within the available resources.

- The **Point Cloud** contributes a realistic representation of the building, capturing its overall form, deviations, and unmodeled areas.

[17] From the perspective of three architects who participated in this comparative test

- The **LOD 300 BIM model** provides structured details, including material types, thicknesses, quantities, and metadata linked to elements.

Benefits of the Integrated Model:

- Achieves greater realism, bringing the model closer to actual site conditions.
- Highlights differences between the theoretical model and the actual building.
- Facilitates easier verification and validation of the model.
- Offers a visually rich presentation that combines realistic visualization with engineering information.
- Enhances support for future maintenance, rehabilitation, and improvement operations.

Figure 153: HBIM Model from Composite Point Cloud-CAD, Al-Takiyya (1)

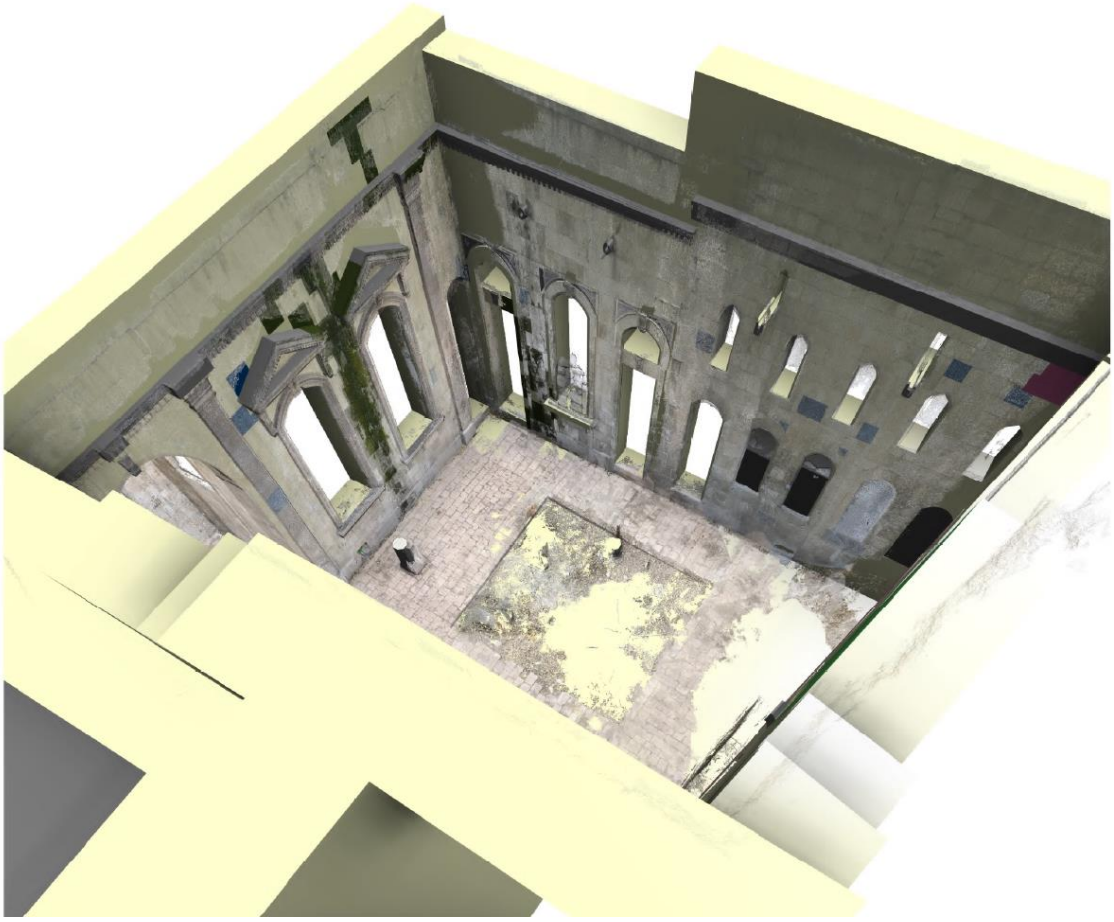

Figure 154: HBIM Model from Composite Point Cloud-CAD, Al-Takiyya (2)

Figure 155: HBIM Model from Composite Point Cloud-CAD, Al-Takiyya (3)

4.8 ACCURACY ANALYSIS AND ERROR RATES (PILOT CASE)

The accuracy analysis addresses geometric fidelity through comparisons between surveyed (reality) data and digital models (photogrammetry and HBIM). The following accuracy metrics were calculated, measured, and applied to the Pilot Case Study:

Table 16: Accuracy Metrics and thresholds, Al-Takiyya

Output	Comparison reference	
	Reality	Photogrammetry
Photogrammetry	▪ **GCPs Positioning Accuracy** ✓ Absolute Errors ΔX, ΔY, ΔZ ✓ 2D, Vertical, and 3D errors ▪ **Distance Deviations** ✓ Absolute Error Δd ✓ Relative Error (%) ▪ **Angular Deviations** ✓ Absolute Error Δd ✓ Relative Error (%)	N/A
CAD	▪ **Distance Deviations** ✓ Absolute Error Δd ✓ Relative Error (%) *(Secondary Analysis, already verified under 4.4.2. Orthomosaic-Derived CAD Outputs)*	N/A
HBIM Model	▪ **Distance Deviations** ✓ Absolute Error Δd ✓ Relative Error (%)	▪ **Distance Deviations** ✓ Absolute Error Δd ✓ Relative Error (%)

4.8.1 GCPs Positioning Accuracy Analysis:

4.8.1.1 *Eastern Façade Accuracy Analysis*

Figure 156: GCPs errors, Eastern Facade, Al-Takiyya

Z error is represented by ellipse color. X,Y errors are represented by ellipse shape. Estimated GCP locations are marked with a dot or crossing.

Table 17: GCPs errors, Eastern Facade, Al-Takiyya

Point Name	Reality X (m) INPUT	Reality Y (m) INPUT	Reality Z (m) INPUT	Photo X (m) INPUT	Photo Y (m) INPUT	Photo Z (m) INPUT
B5	-178,548.165	223,785.090	403.521	-178,548.169	223,785.079	403.525
B14	-178,548.356	223,785.648	398.996	-178,548.359	223,785.645	398.996
C3	-178,548.509	223,784.785	401.927	-178,548.528	223,784.793	401.925
BY2	-178,546.977	223,791.045	399.669	-178,546.969	223,791.044	399.669
BY1	-178,547.015	223,790.890	402.429	-178,547.010	223,790.888	402.431
DY1	-178,546.327	223,794.457	399.782	-178,546.326	223,794.457	399.786
BX1	-178,546.131	223,796.008	402.178	-178,546.138	223,796.004	402.177
DY3	-178,546.476	223,793.745	402.964	-178,546.474	223,793.748	402.966
CY3	-178,546.104	223,795.375	403.956	-178,546.113	223,795.375	403.950
AY1	-178,545.965	223,788.393	403.336	-178,545.959	223,788.395	403.336

AY2	-178,545.617	223,790.369	403.898	-178,545.612	223,790.368	403.899
AY3	-178,546.603	223,784.930	403.883	-178,546.597	223,784.934	403.879
DV3	-178,546.232	223,786.954	401.595	-178,546.223	223,786.957	401.595

Point Name	dX Photo (m)	dY Photo (m)	dZ Photo (m)	2D Err Photo (m)	Vert Err Photo (m)	3D Err Photo (m)	Pass/Fail Photo
B5	-0.004	-0.011	0.004	0.011	0.004	0.012	PASS
B14	-0.003	-0.003	0.000	0.004	0.000	0.004	PASS
C3	-0.019	0.008	-0.002	0.021	0.002	0.021	FAIL
BY2	0.008	-0.001	0.000	0.008	0.000	0.008	PASS
BY1	0.005	-0.002	0.002	0.006	0.002	0.006	PASS
DY1	0.001	0.000	0.004	0.001	0.004	0.005	PASS
BX1	-0.007	-0.004	-0.001	0.008	0.001	0.008	PASS
DY3	0.002	0.003	0.002	0.004	0.002	0.005	PASS
CY3	-0.009	0.000	-0.006	0.009	0.006	0.010	PASS
AY1	0.006	0.002	0.000	0.007	0.000	0.007	PASS
AY2	0.005	-0.001	0.001	0.005	0.001	0.005	PASS
AY3	0.006	0.004	-0.004	0.007	0.004	0.009	PASS
DV3	0.009	0.003	0.000	0.009	0.000	0.009	PASS

Table 18: Summary Table of GCPs errors, Eastern Facade, Al-Takiyya

Metric	Photogrammetry
Max 2D error (m)	0.020986
Mean 2D error (m)	0.007675
Max vertical error (m)	0.006115
Mean vertical error (m)	0.002176
Max 3D error (m)	0.021093
Mean 3D error (m)	0.008355
PASS count	12
FAIL count	1
RMSE 3D	**0.009437**

Eastern Façade – Accuracy Briefing

Overall stats:

- Mean 3D error = 0.008 m (8.4 mm) → well under both thresholds.
- RMSE = 0.009 m (9.4 mm) → still within 1 cm, close to the limit.
- Max 3D error = 0.021 m (2.1 cm) → exceeds the 2 cm threshold by a small margin.

Accuracy Compliance at 1 cm and 2 cm:

At 1 cm (0.01 m):

- Most points comply, but the largest error (2.1 cm) exceeds the limit.
- Pass count = 12 points, Fail count = 1 (C3 at 2.1 cm).
- Mean and RMSE sit just under 1 cm, so on average the dataset holds.

At 2 cm (0.02 m):

- Compliance is nearly universal.
- Pass count = 12 points, Fail count = 1 (same outlier, 2.1 cm).
- Mean and RMSE are far below 2 cm, but the outlier keeps the dataset from being fully compliant.

Interpretation:

The eastern façade shows excellent overall accuracy, averaging below 1 cm and proving reliable for fine-scale documentation. The dataset comfortably fits within 1 cm tolerance for most points, but a single outlier (C3, 2.1 cm error) prevents 100% compliance at both 1 cm and 2 cm thresholds. Practically, the façade is trustworthy for HBIM at 1 m precision, with the caveat of one local anomaly.

4.8.1.2 *Entrance Façade Accuracy Analysis*

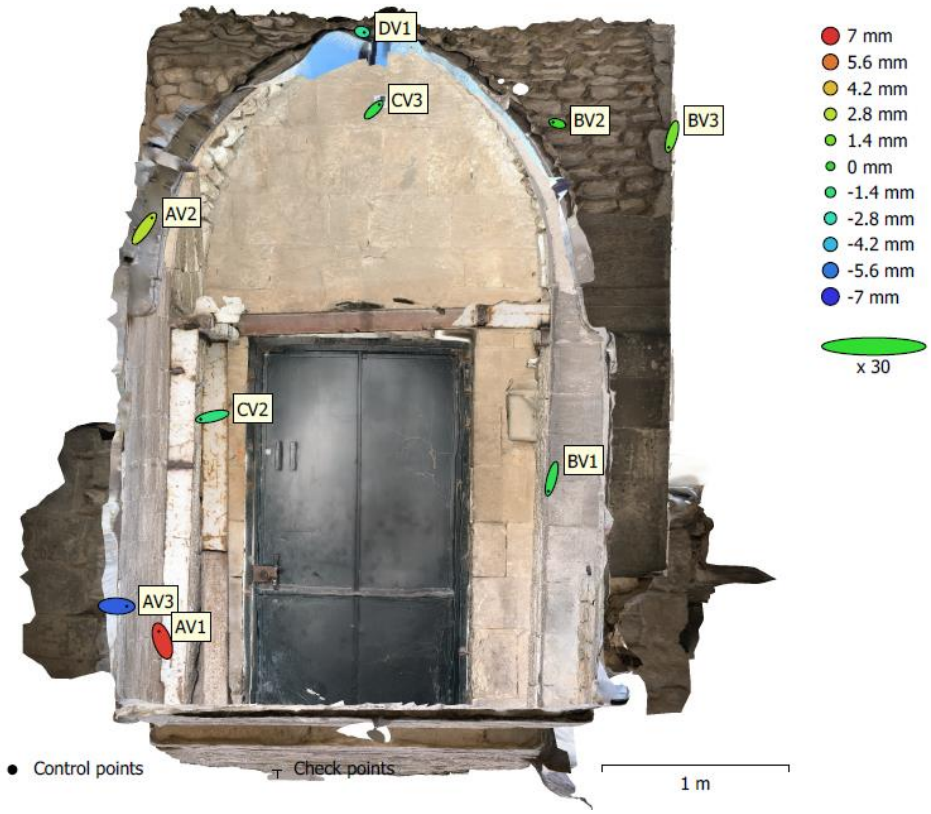

Figure 157: GCPs errors, Entrance Facade, Al-Takiyya

Z error is represented by ellipse color. X,Y errors are represented by ellipse shape. Estimated GCP locations are marked with a dot or crossing.

Table 19: GCPs errors, Entrance Facade, Al-Takiyya

Point Name	Reality X (m) INPUT	Reality Y (m) INPUT	Reality Z (m) INPUT	Photo X (m) INPUT	Photo Y (m) INPUT	Photo Z (m) INPUT
AV3	-178,545.664	223,793.763	399.014	-178,545.660	223,793.763	399.008
AV2	-178,544.565	223,793.466	401.078	-178,544.562	223,793.470	401.081
BV3	-178,545.121	223,790.776	401.502	-178,545.122	223,790.772	401.503
CV2	-178,540.953	223,792.556	400.001	-178,540.957	223,792.555	399.999
AV1	-178,542.820	223,793.085	398.862	-178,542.821	223,793.088	398.869
BV2	-178,541.502	223,790.767	401.616	-178,541.504	223,790.767	401.616
BV1	-178,543.598	223,791.131	399.654	-178,543.599	223,791.127	399.653
DV1	-178,540.930	223,791.699	402.080	-178,540.929	223,791.699	402.078
CV3	-178,539.984	223,791.443	401.692	-178,539.982	223,791.445	401.691

Point Name	dX Photo (m)	dY Photo (m)	dZ Photo (m)	2D Err Photo (m)	Vert Err Photo (m)	3D Err Photo (m)	Pass/Fail Photo
AV3	0.004	0.000	-0.006	0.004	0.006	0.007	PASS
AV2	0.003	0.004	0.003	0.005	0.003	0.005	PASS
BV3	-0.001	-0.004	0.001	0.004	0.001	0.004	PASS
CV2	-0.004	-0.001	-0.002	0.004	0.002	0.004	PASS
AV1	-0.001	0.003	0.007	0.004	0.007	0.008	PASS
BV2	-0.002	0.000	0.000	0.002	0.000	0.002	PASS
BV1	-0.001	-0.004	-0.001	0.005	0.001	0.005	PASS
DV1	0.001	0.000	-0.002	0.001	0.002	0.002	PASS
CV3	0.002	0.002	-0.001	0.003	0.001	0.003	PASS

Table 20: Summary Table of GCPs errors, Entrance Facade, Al-Takiyya

Metric	Photogrammetry
Max 2D error (m)	0.004677
Mean 2D error (m)	0.003307
Max vertical error (m)	0.006811
Mean vertical error (m)	0.002462
Max 3D error (m)	0.007718
Mean 3D error (m)	0.004461
PASS count	9
FAIL count	0
RMSE 3D	**0.004872**

Entrance Façade – Accuracy Briefing

Overall stats:

- Mean 3D error = 0.004 m (4.5 mm) → well below both thresholds.
- RMSE = 0.005 m (4.9 mm) → equally safe under both limits.
- Max 3D error = 0.008 m (7.7 mm) → below 1 cm, well within 2 cm.

Accuracy Compliance at 1 cm and 2 cm:

At 1 cm (0.01 m):

- All points fall below the 1 cm limit.
- Pass count = 9, Fail count = 0.
- Mean, RMSE, and maximum values are consistently within millimeter range.

At 2 cm (0.02 m):

- Full compliance maintained.
- Pass count = 9, Fail count = 0.
- Errors are less than half of the allowable tolerance, confirming robustness.

Interpretation:

The entrance façade data demonstrates excellent accuracy, with every point below 1 cm error and mean deviations around 5 mm. This dataset not only meets but exceeds the requirements of both 1 cm and 2 cm tolerances, making it highly reliable for detailed HBIM modeling and fine-scale architectural documentation.

4.8.1.3 *Exterior Façade Accuracy Analysis*

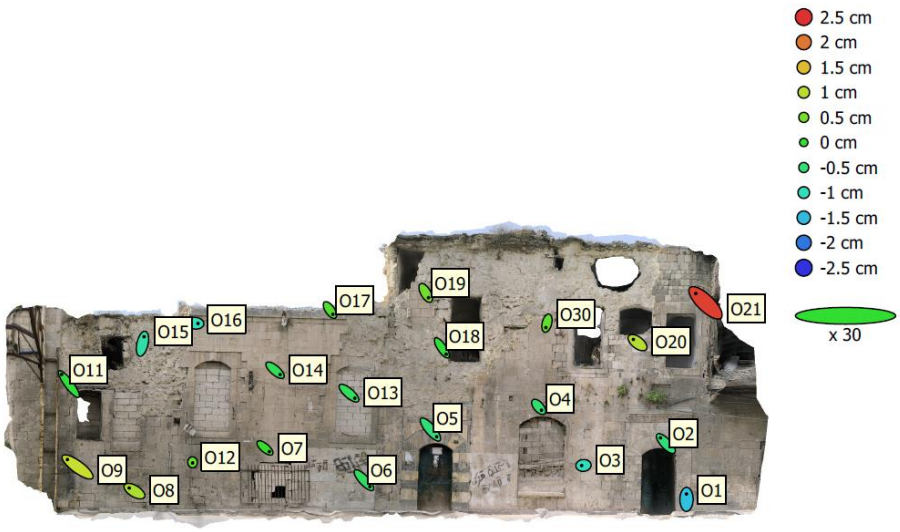

Figure 158: GCPs errors, Exterior Facade, Al-Takiyya

Z error is represented by ellipse color. X,Y errors are represented by ellipse shape. Estimated GCP locations are marked with a dot or crossing.

Table 21: GCPs errors, Exterior Facade, Al-Takiyya

Point Name	Reality X (m) INPUT	Reality Y (m) INPUT	Reality Z (m) INPUT	Photo X (m) INPUT	Photo Y (m) INPUT	Photo Z (m) INPUT
O9	-178,541.062	223,779.970	399.565	-178,541.083	223,779.986	399.576
O8	-178,540.798	223,781.920	398.716	-178,540.809	223,781.926	398.725
O11	-178,541.019	223,779.716	402.241	-178,541.034	223,779.736	402.240
O16	-178,540.258	223,783.903	403.940	-178,540.252	223,783.902	403.930
O12	-178,540.454	223,783.864	399.552	-178,540.454	223,783.863	399.556
O7	-178,540.067	223,786.233	399.965	-178,540.058	223,786.225	399.965
O14	-178,539.910	223,786.497	402.389	-178,539.899	223,786.488	402.386
O13	-178,539.728	223,788.856	401.718	-178,539.716	223,788.845	401.715
O17	-178,539.573	223,788.074	404.313	-178,539.567	223,788.065	404.315
O6	-178,539.627	223,789.381	398.946	-178,539.615	223,789.368	398.943
O19	-178,539.682	223,791.117	404.955	-178,539.676	223,791.107	404.960
O5	-178,539.215	223,791.402	400.554	-178,539.202	223,791.387	400.549
O1	-178,538.113	223,799.171	398.959	-178,538.113	223,799.182	398.944
O2	-178,538.173	223,798.316	400.688	-178,538.184	223,798.328	400.683
O3	-178,538.600	223,795.914	399.770	-178,538.604	223,795.914	399.760
O4	-178,538.719	223,794.624	401.469	-178,538.713	223,794.617	401.465
O21	-178,537.985	223,799.297	405.227	-178,538.005	223,799.317	405.251
O20	-178,538.229	223,797.397	403.744	-178,538.238	223,797.404	403.754
O18	-178,539.280	223,791.653	403.167	-178,539.271	223,791.640	403.167
O15	-178,541.078	223,782.318	403.538	-178,541.075	223,782.333	403.530
O30	-178,538.629	223,794.691	404.056	-178,538.631	223,794.682	404.059

Point Name	dX Photo (m)	dY Photo (m)	dZ Photo (m)	2D Err Photo (m)	Vert Err Photo (m)	3D Err Photo (m)	Pass/Fail Photo
O9	-0.021	0.016	0.011	0.026	0.011	0.029	FAIL
O8	-0.011	0.006	0.009	0.013	0.009	0.015	PASS
O11	-0.015	0.020	-0.001	0.025	0.001	0.025	FAIL
O16	0.006	-0.001	-0.010	0.006	0.010	0.012	PASS
O12	0.000	-0.001	0.004	0.001	0.004	0.004	PASS
O7	0.009	-0.008	0.000	0.012	0.000	0.012	PASS
O14	0.011	-0.009	-0.003	0.014	0.003	0.014	PASS
O13	0.012	-0.011	-0.003	0.016	0.003	0.016	PASS
O17	0.006	-0.009	0.002	0.011	0.002	0.011	PASS
O6	0.012	-0.013	-0.003	0.018	0.003	0.019	PASS
O19	0.006	-0.010	0.005	0.012	0.005	0.013	PASS
O5	0.013	-0.015	-0.005	0.020	0.005	0.021	FAIL
O1	0.000	0.011	-0.015	0.011	0.015	0.018	PASS
O2	-0.011	0.012	-0.005	0.016	0.005	0.017	PASS
O3	-0.004	0.000	-0.010	0.004	0.010	0.011	PASS
O4	0.006	-0.007	-0.004	0.009	0.004	0.010	PASS
O21	-0.020	0.020	0.024	0.028	0.024	0.037	FAIL
O20	-0.009	0.007	0.010	0.011	0.010	0.015	PASS
O18	0.009	-0.013	0.000	0.016	0.000	0.016	PASS

O15	0.003	0.015	-0.008	0.015	0.008	0.017	PASS
O30	-0.002	-0.009	0.003	0.010	0.003	0.010	PASS

Table 22: Summary Table of GCPs errors, Exterior Facade, Al-Takiyya

Metric	Photogrammetry
Max 2D error (m)	0.028264
Mean 2D error (m)	0.014025
Max vertical error (m)	0.024030
Mean vertical error (m)	0.006469
Max 3D error (m)	0.037099
Mean 3D error (m)	0.016272
PASS count	17
FAIL count	4
RMSE 3D	**0.017736**

Exterior Façade – Accuracy Briefing

Overall stats:

- Mean 3D error = 0.016 m (1.6 cm) → above 1 cm, but within 2 cm.
- RMSE = 0.018 m (1.8 cm) → matches the 2 cm band, fails the 1 cm band.
- Max 3D error = 0.037 m (3.7 cm) → exceeds both thresholds by a wide margin.

Accuracy Compliance at 1 cm and 2 cm:

At 1 cm (0.01 m):

- Only a handful of points are below 1 cm (≈ 0.004–0.009 m).
- Pass count = 6 points, Fail count = 15 points.
- Both the mean and RMSE are above 1 cm, so the dataset does not comply at this strict level.

At 2 cm (0.02 m):

- Much stronger performance overall.
- Pass count = 17 points.
- Fail count = 4 points (O9, O11, O5, O21) with errors from 2.1 cm up to 3.7 cm.
- Mean and RMSE sit within 2 cm, indicating reliable consistency across most of the façade.

Interpretation:

The exterior façade data is not suitable for 1 cm precision documentation, but it performs well under a 2 cm tolerance, with only four clear outliers reducing full compliance. The

majority of the points cluster within 1.1–1.9 cm error, showing stable centimeter-level accuracy. This makes the dataset dependable for HBIM integration at 2 cm tolerance but unsuitable for ultra-detailed work demanding 1 cm accuracy.

4.8.1.4 *Interior Yard Accuracy Analysis*

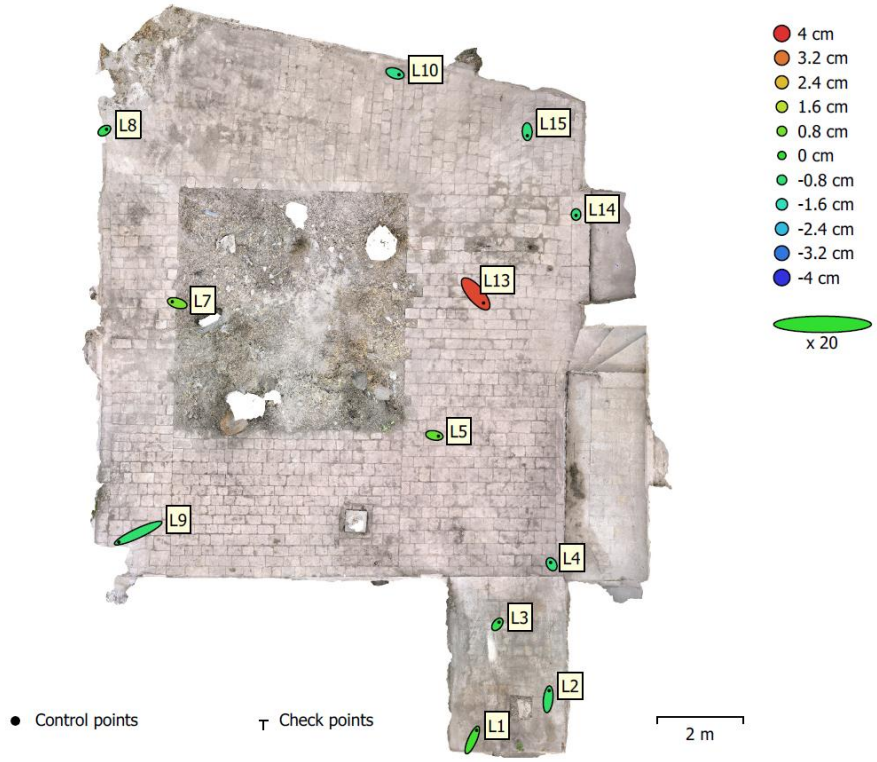

Figure 159: GCPs errors, Interior Yard, Al-Takiyya

Z error is represented by ellipse color. X,Y errors are represented by ellipse shape. Estimated GCP locations are marked with a dot or crossing.

Table 23: GCPs errors, Interior Yard, Al-Takiyya

Point Name	Reality X (m) INPUT	Reality Y (m) INPUT	Reality Z (m) INPUT	Photo X (m) INPUT	Photo Y (m) INPUT	Photo Z (m) INPUT
O9	-178,541.062	223,779.970	399.565	-178,541.083	223,779.986	399.576
O8	-178,540.798	223,781.920	398.716	-178,540.809	223,781.926	398.725
O11	-178,541.019	223,779.716	402.241	-178,541.034	223,779.736	402.240
O16	-178,540.258	223,783.903	403.940	-178,540.252	223,783.902	403.930
O12	-178,540.454	223,783.864	399.552	-178,540.454	223,783.863	399.556
O7	-178,540.067	223,786.233	399.965	-178,540.058	223,786.225	399.965
O14	-178,539.910	223,786.497	402.389	-178,539.899	223,786.488	402.386
O13	-178,539.728	223,788.856	401.718	-178,539.716	223,788.845	401.715
O17	-178,539.573	223,788.074	404.313	-178,539.567	223,788.065	404.315
O6	-178,539.627	223,789.381	398.946	-178,539.615	223,789.368	398.943
O19	-178,539.682	223,791.117	404.955	-178,539.676	223,791.107	404.960

O5	-178,539.215	223,791.402	400.554	-178,539.202	223,791.387	400.549
O1	-178,538.113	223,799.171	398.959	-178,538.113	223,799.182	398.944
O2	-178,538.173	223,798.316	400.688	-178,538.184	223,798.328	400.683
O3	-178,538.600	223,795.914	399.770	-178,538.604	223,795.914	399.760
O4	-178,538.719	223,794.624	401.469	-178,538.713	223,794.617	401.465
O21	-178,537.985	223,799.297	405.227	-178,538.005	223,799.317	405.251
O20	-178,538.229	223,797.397	403.744	-178,538.238	223,797.404	403.754
O18	-178,539.280	223,791.653	403.167	-178,539.271	223,791.640	403.167
O15	-178,541.078	223,782.318	403.538	-178,541.075	223,782.333	403.530
O30	-178,538.629	223,794.691	404.056	-178,538.631	223,794.682	404.059

Table 24: GCPs errors, Interior Yard, Al-Takiyya

Point Name	dX Photo (m)	dY Photo (m)	dZ Photo (m)	2D Err Photo (m)	Vert Err Photo (m)	3D Err Photo (m)	Pass/Fail Photo
O9	-0.021	0.016	0.011	0.026	0.011	0.029	FAIL
O8	-0.011	0.006	0.009	0.013	0.009	0.015	PASS
O11	-0.015	0.020	-0.001	0.025	0.001	0.025	FAIL
O16	0.006	-0.001	-0.010	0.006	0.010	0.012	PASS
O12	0.000	-0.001	0.004	0.001	0.004	0.004	PASS
O7	0.009	-0.008	0.000	0.012	0.000	0.012	PASS
O14	0.011	-0.009	-0.003	0.014	0.003	0.014	PASS
O13	0.012	-0.011	-0.003	0.016	0.003	0.016	PASS
O17	0.006	-0.009	0.002	0.011	0.002	0.011	PASS
O6	0.012	-0.013	-0.003	0.018	0.003	0.019	PASS
O19	0.006	-0.010	0.005	0.012	0.005	0.013	PASS
O5	0.013	-0.015	-0.005	0.020	0.005	0.021	FAIL
O1	0.000	0.011	-0.015	0.011	0.015	0.018	PASS
O2	-0.011	0.012	-0.005	0.016	0.005	0.017	PASS
O3	-0.004	0.000	-0.010	0.004	0.010	0.011	PASS
O4	0.006	-0.007	-0.004	0.009	0.004	0.010	PASS
O21	-0.020	0.020	0.024	0.028	0.024	0.037	FAIL
O20	-0.009	0.007	0.010	0.011	0.010	0.015	PASS
O18	0.009	-0.013	0.000	0.016	0.000	0.016	PASS
O15	0.003	0.015	-0.008	0.015	0.008	0.017	PASS
O30	-0.002	-0.009	0.003	0.010	0.003	0.010	PASS

Table 25: Summary Table of GCPs errors, Interior Yard, Al-Takiyya

Metric	Photogrammetry
Max 2D error (m)	0.028264
Mean 2D error (m)	0.014025
Max vertical error (m)	0.024030
Mean vertical error (m)	0.006469
Max 3D error (m)	0.037099
Mean 3D error (m)	0.016272
PASS count	17
FAIL count	4

RMSE 3D	**0.017736**

Interior Yard – Accuracy Briefing

Overall stats:

- Mean 3D error = 0.016 m (1.6 cm) → above 1 cm, within 2 cm.
- RMSE = 0.018 m (1.8 cm) → consistent with 2 cm tolerance, not 1 cm.
- Max 3D error = 0.037 m (3.7 cm) → exceeds both thresholds.

Accuracy Compliance at 1 cm and 2 cm:

At 1 cm (0.01 m):

- Only the lowest-error points (≈0.004–0.009 m) comply.
- Pass count = 8 points, Fail count = 13.
- Mean and RMSE are above 1 cm, confirming the dataset cannot be certified at this level.

At 2 cm (0.02 m):

- The majority comply, but some points exceed the 2 cm ceiling.
- Pass count = 17 points, Fail count = 4 (O9, O11, O5, O21).
- Average accuracy (mean and RMSE) is good, but the outliers are significant (up to 3.7 cm).

Interpretation:

The Interior Yard dataset is not reliable at the 1 cm threshold due to widespread failures. At 2 cm tolerance, the majority of points are accurate, but four outliers prevent full compliance. This indicates the dataset achieves centimeter-level reliability, adequate for HBIM at 2 cm precision, though not for strict 1 cm documentation.

4.8.1.5 *Northern Façade Analysis*

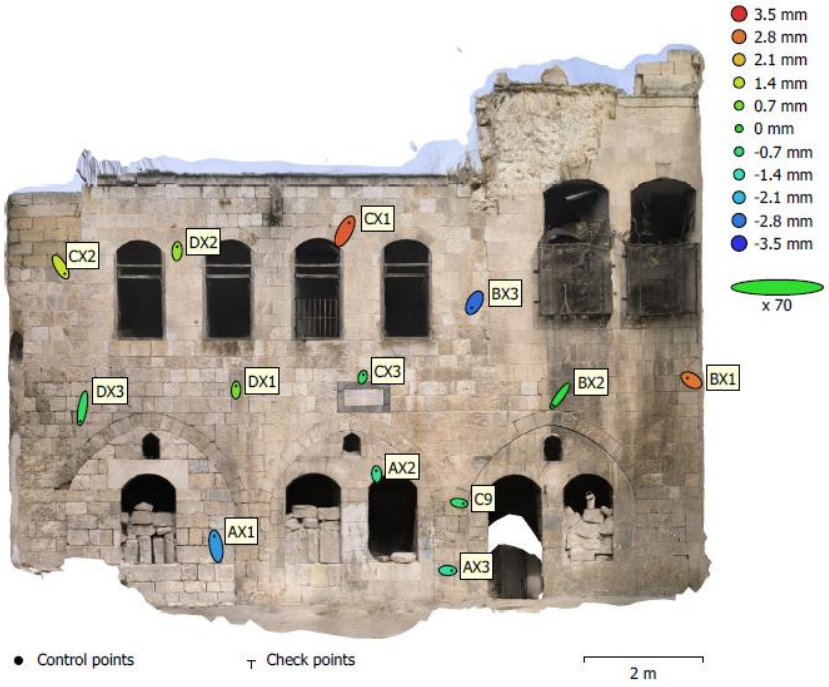

Figure 160: GCPs errors, Interior Yard, Al-Takiyya

Z error is represented by ellipse color. X,Y errors are represented by ellipse shape. Estimated GCP locations are marked with a dot or crossing.

Table 26: GCPs errors, Northern Facade, Al-Takiyya

Point Name	Reality X (m) INPUT	Reality Y (m) INPUT	Reality Z (m) INPUT	Photo X (m) INPUT	Photo Y (m) INPUT	Photo Z (m) INPUT
BX1	-178,546.131	223,796.008	402.178	-178,546.133	223,796.009	402.181
BX2	-178,548.226	223,796.874	401.729	-178,548.229	223,796.869	401.729
C9	-178,549.624	223,797.482	400.084	-178,549.622	223,797.482	400.083
AX3	-178,549.797	223,797.591	398.959	-178,549.795	223,797.591	398.958
AX2	-178,550.967	223,798.050	400.645	-178,550.967	223,798.052	400.644
CX3	-178,551.166	223,798.122	402.260	-178,551.166	223,798.123	402.260
AX1	-178,553.462	223,799.161	399.556	-178,553.463	223,799.166	399.554
DX1	-178,553.130	223,798.980	402.080	-178,553.130	223,798.982	402.081
DX3	-178,555.520	223,800.078	401.500	-178,555.521	223,800.072	401.500
DX2	-178,554.013	223,799.399	404.429	-178,554.013	223,799.401	404.430
BX3	-178,549.489	223,797.394	403.378	-178,549.490	223,797.392	403.375
CX1	-178,551.365	223,798.231	404.814	-178,551.363	223,798.235	404.817
CX2	-178,555.730	223,800.217	403.983	-178,555.728	223,800.214	403.985

Table 27: GCPs errors, Northern Facade, Al-Takiyya

Point Name	dX Photo (m)	dY Photo (m)	dZ Photo (m)	2D Err Photo (m)	Vert Err Photo (m)	3D Err Photo (m)	Pass/Fail Photo
BX1	-0.002	0.001	0.003	0.002	0.003	0.004	PASS

BX2	-0.003	-0.005	0.000	0.006	0.000	0.006	PASS
C9	0.002	0.000	-0.001	0.002	0.001	0.002	PASS
AX3	0.002	0.000	-0.001	0.002	0.001	0.002	PASS
AX2	0.000	0.002	-0.001	0.002	0.001	0.002	PASS
CX3	0.000	0.001	0.000	0.001	0.000	0.001	PASS
AX1	-0.001	0.005	-0.002	0.005	0.002	0.005	PASS
DX1	0.000	0.002	0.001	0.002	0.001	0.002	PASS
DX3	-0.001	-0.006	0.000	0.006	0.000	0.006	PASS
DX2	0.000	0.002	0.001	0.002	0.001	0.002	PASS
BX3	-0.001	-0.002	-0.003	0.003	0.003	0.004	PASS
CX1	0.002	0.004	0.003	0.005	0.003	0.006	PASS
CX2	0.002	-0.003	0.002	0.004	0.002	0.004	PASS

Table 28: Summary Table of GCPs errors, Northern Facade, Al-Takiyya

Metric	Photogrammetry
Max 2D error (m)	0.006350
Mean 2D error (m)	0.003164
Max vertical error (m)	0.003073
Mean vertical error (m)	0.001409
Max 3D error (m)	0.006369
Mean 3D error (m)	0.003592
PASS count	13
FAIL count	0
RMSE 3D	0.003948

Northern Façade – Accuracy Briefing

Overall stats:

- Mean 3D error = 0.004 m (3.6 mm) → far below both thresholds.
- RMSE = 0.004 m (3.9 mm) → consistent millimeter-level accuracy.
- Max 3D error = 0.006 m (6.4 mm) → below 1 cm and well below 2 cm.

Accuracy Compliance at 1 cm and 2 cm:

At 1 cm (0.01 m):

- All points are below the 1 cm limit.
- Pass count = 13, Fail count = 0.
- Mean, RMSE, and maximum values are all well inside the tolerance.

At 2 cm (0.02 m):

- Full compliance maintained.
- Pass count = 13, Fail count = 0.
- Errors are less than one-third of the allowable tolerance, confirming robustness.

Interpretation:

The northern façade shows exceptional accuracy, with every point under 1 cm error and overall deviations in the 2–6 mm range. The dataset is fully compliant at both 1 cm and 2 cm thresholds, making it highly reliable for precise HBIM modeling and detailed heritage documentation.

4.8.1.6 *Reception Façades Analysis*

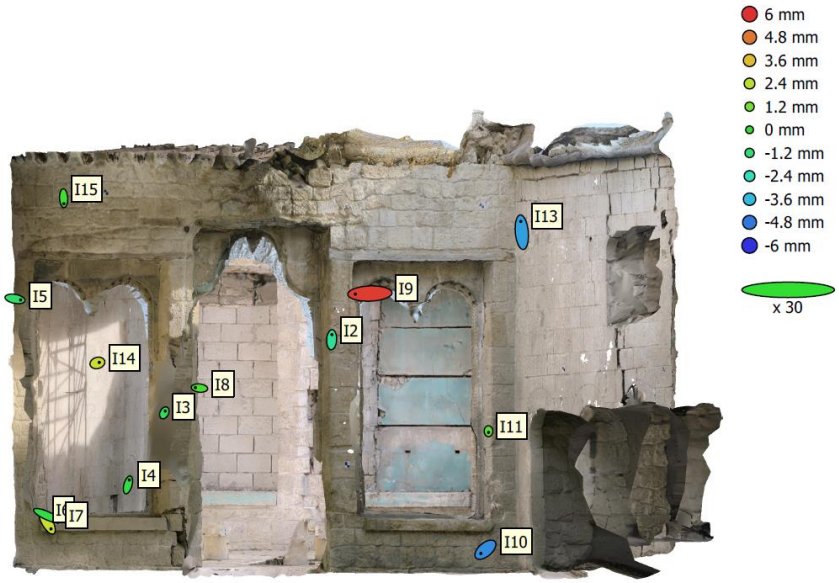

Figure 161: GCPs errors, Reception Facades, Al-Takiyya

Z error is represented by ellipse color. X,Y errors are represented by ellipse shape. Estimated GCP locations are marked with a dot or crossing.

Table 29: GCPs errors, Reception Facades, Al-Takiyya

Point Name	Reality X (m) INPUT	Reality Y (m) INPUT	Reality Z (m) INPUT	Photo X (m) INPUT	Photo Y (m) INPUT	Photo Z (m) INPUT
I3	-178,540.300	223,789.595	401.303	-178,540.299	223,789.596	401.302
I2	-178,540.583	223,787.680	402.161	-178,540.583	223,787.684	402.159
I13	-178,540.870	223,785.513	403.428	-178,540.871	223,785.521	403.424
I14	-178,542.109	223,790.038	401.887	-178,542.108	223,790.038	401.890
I5	-178,544.856	223,790.471	402.658	-178,544.852	223,790.470	402.657
I8	-178,545.547	223,788.404	401.712	-178,545.550	223,788.404	401.712
I9	-178,545.817	223,786.568	402.753	-178,545.828	223,786.568	402.759
I10	-178,546.080	223,785.131	399.907	-178,546.083	223,785.128	399.903
I11	-178,546.237	223,785.015	401.245	-178,546.237	223,785.014	401.246
I4	-178,540.989	223,789.884	400.560	-178,540.988	223,789.888	400.560
I6	-178,543.762	223,790.320	400.093	-178,543.759	223,790.315	400.096
I7	-178,545.145	223,790.026	400.234	-178,545.138	223,790.023	400.234
I15	-178,543.364	223,790.231	403.679	-178,543.364	223,790.227	403.679

Table 30: GCPs errors, Reception Facades, Al-Takiyya

dX Photo (m)	dY Photo (m)	dZ Photo (m)	2D Err Photo (m)	Vert Err Photo (m)	3D Err Photo (m)	Pass/Fail Photo
0.001	0.001	-0.001	0.001	0.001	0.002	PASS
0.000	0.004	-0.002	0.004	0.002	0.004	PASS
-0.001	0.008	-0.004	0.008	0.004	0.009	PASS
0.001	0.000	0.003	0.001	0.003	0.003	PASS
0.004	-0.001	-0.001	0.004	0.001	0.004	PASS
-0.003	0.000	0.000	0.003	0.000	0.003	PASS
-0.011	0.000	0.006	0.011	0.006	0.012	PASS
-0.003	-0.003	-0.004	0.004	0.004	0.006	PASS
0.000	-0.001	0.001	0.001	0.001	0.001	PASS
0.001	0.004	0.000	0.004	0.000	0.004	PASS
0.003	-0.005	0.003	0.006	0.003	0.007	PASS
0.007	-0.003	0.000	0.008	0.000	0.008	PASS
0.000	-0.004	0.000	0.004	0.000	0.004	PASS

Table 31: Summary Table of GCPs errors, Reception Facades, Al-Takiyya

Metric	Photogrammetry
Max 2D error (m)	0.010696
Mean 2D error (m)	0.004578
Max vertical error (m)	0.005802
Mean vertical error (m)	0.001926
Max 3D error (m)	0.012168
Mean 3D error (m)	0.005147
PASS count	13
FAIL count	0
RMSE 3D	0.005960

Reception Façades – Accuracy Briefing

Overall stats:

- Mean 3D error = 0.005 m (5.1 mm) → well within both tolerances.
- RMSE = 0.006 m (6.0 mm) → close to the 1 cm line but still comfortably below.
- Max 3D error = 0.012 m (1.2 cm) → exceeds the 1 cm threshold slightly but remains within 2 cm.

Accuracy Compliance at 1 cm and 2 cm:

At 1 cm (0.01 m):

- Nearly all points comply, but the largest error (≈1.2 cm) sits just above the limit.
- Pass count = 12 points, Fail count = 1.

- Mean and RMSE are below 1 cm, so overall performance is strong, with only a single outlier.

At 2 cm (0.02 m):

- Full compliance.
- Pass count = 13 points, Fail count = 0.
- All values fall safely within the tolerance, with maximum error just over half of the allowed range.

Interpretation:

The reception façades data shows millimeter-level accuracy across nearly all points, with just one exceeding 1 cm. The dataset is therefore almost fully compliant at 1 cm and completely reliable at 2 cm, confirming its suitability for detailed HBIM documentation with minimal concern over outliers.

4.8.1.7 *Southern Façade Analysis*

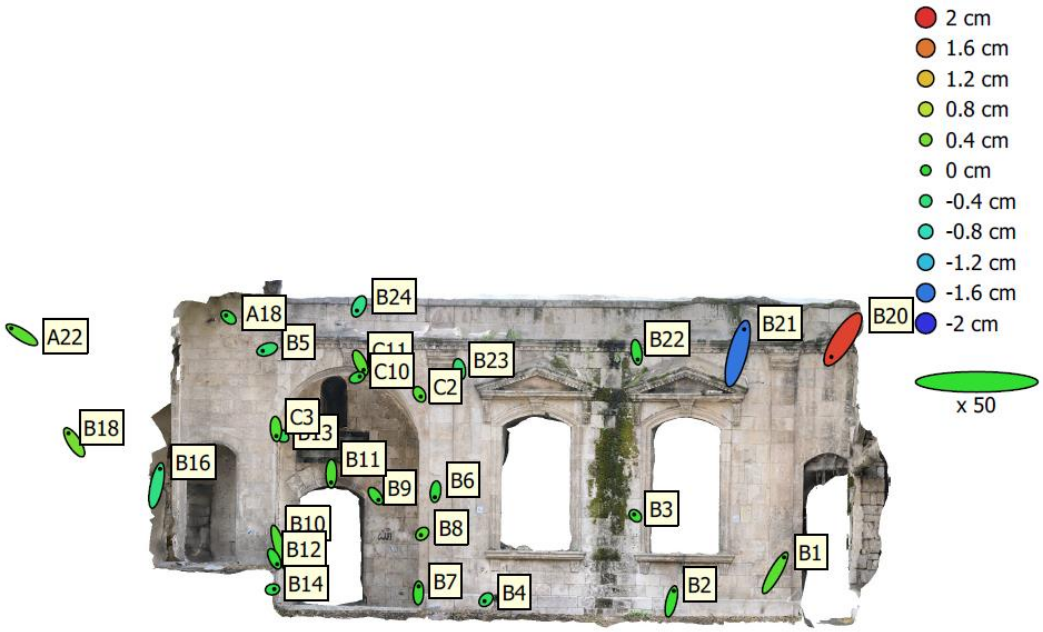

Figure 162: GCPs errors, Southern Façade, Al-Takiyya

Z error is represented by ellipse color. X,Y errors are represented by ellipse shape. Estimated GCP locations are marked with a dot or crossing.

Table 32: GCPs errors, Southern Façade, Al-Takiyya

Point Name	Reality X (m) INPUT	Reality Y (m) INPUT	Reality Z (m) INPUT	Photo X (m) INPUT	Photo Y (m) INPUT	Photo Z (m) INPUT
B21	-178,557.094	223,786.808	404.058	-178,557.089	223,786.826	404.042

B1	-178,557.889	223,786.994	399.741	-178,557.882	223,787.006	399.743
B22	-178,555.116	223,786.486	403.443	-178,555.115	223,786.480	403.442
B2	-178,555.859	223,786.549	399.083	-178,555.857	223,786.557	399.083
B23	-178,551.836	223,785.819	403.136	-178,551.835	223,785.816	403.132
B4	-178,552.337	223,785.933	398.842	-178,552.338	223,785.932	398.839
B6	-178,551.389	223,785.769	400.792	-178,551.389	223,785.765	400.791
B24	-178,549.903	223,785.428	404.304	-178,549.905	223,785.425	404.299
B5	-178,548.165	223,785.090	403.521	-178,548.168	223,785.089	403.517
A18	-178,547.478	223,784.952	404.181	-178,547.480	223,784.954	404.180
B9	-178,551.065	223,781.546	400.908	-178,551.063	223,781.543	400.909
B11	-178,550.182	223,781.379	401.225	-178,550.182	223,781.372	401.227
B10	-178,549.355	223,781.210	399.653	-178,549.351	223,781.197	399.655
B16	-178,546.247	223,785.003	401.252	-178,546.244	223,785.015	401.247
B20	-178,558.712	223,787.110	403.527	-178,558.721	223,787.097	403.546
B3	-178,555.096	223,786.430	400.516	-178,555.097	223,786.431	400.516
B7	-178,551.211	223,785.151	399.128	-178,551.211	223,785.156	399.128
B12	-178,548.928	223,782.719	399.598	-178,548.926	223,782.715	399.598
B13	-178,548.897	223,782.882	402.050	-178,548.899	223,782.883	402.048
B14	-178,548.356	223,785.648	398.996	-178,548.355	223,785.648	398.995
C3	-178,548.509	223,784.785	401.927	-178,548.509	223,784.780	401.929
B18	-178,544.573	223,784.442	401.904	-178,544.577	223,784.449	401.908
A22	-178,543.474	223,784.286	403.874	-178,543.482	223,784.291	403.876
C11	-178,550.171	223,784.776	403.210	-178,550.168	223,784.771	403.213
C2	-178,551.534	223,783.298	402.796	-178,551.533	223,783.296	402.798
C10	-178,550.537	223,782.303	403.199	-178,550.535	223,782.304	403.198
B8	-178,551.768	223,782.207	400.229	-178,551.769	223,782.206	400.231

Table 33: GCPs errors, Southern Façade, Al-Takiyya

Point Name	dX Photo (m)	dY Photo (m)	dZ Photo (m)	2D Err Photo (m)	Vert Err Photo (m)	3D Err Photo (m)	Pass/Fail Photo
B21	0.005	0.018	-0.016	0.019	0.016	0.025	FAIL
B1	0.007	0.012	0.002	0.014	0.002	0.014	PASS
B22	0.001	-0.006	-0.001	0.006	0.001	0.006	PASS
B2	0.002	0.008	0.000	0.008	0.000	0.008	PASS
B23	0.001	-0.003	-0.004	0.003	0.004	0.005	PASS
B4	-0.001	-0.001	-0.003	0.002	0.003	0.003	PASS
B6	0.000	-0.004	-0.001	0.004	0.001	0.004	PASS
B24	-0.002	-0.003	-0.005	0.004	0.005	0.006	PASS
B5	-0.003	-0.001	-0.004	0.004	0.004	0.005	PASS
A18	-0.002	0.002	-0.001	0.002	0.001	0.003	PASS
B9	0.002	-0.003	0.001	0.004	0.001	0.004	PASS
B11	0.000	-0.007	0.002	0.007	0.002	0.007	PASS
B10	0.004	-0.013	0.002	0.014	0.002	0.014	PASS
B16	0.003	0.012	-0.005	0.013	0.005	0.014	PASS
B20	-0.009	-0.013	0.019	0.016	0.019	0.025	FAIL
B3	-0.001	0.001	0.000	0.001	0.000	0.001	PASS
B7	0.000	0.005	0.000	0.005	0.000	0.005	PASS

B12	0.002	-0.004	0.000	0.004	0.000	0.004	PASS
B13	-0.002	0.001	-0.002	0.002	0.002	0.003	PASS
B14	0.001	0.000	-0.001	0.001	0.001	0.002	PASS
C3	0.000	-0.005	0.002	0.005	0.002	0.006	PASS
B18	-0.004	0.007	0.004	0.008	0.004	0.009	PASS
A22	-0.008	0.005	0.002	0.009	0.002	0.010	PASS
C11	0.003	-0.005	0.003	0.006	0.003	0.007	PASS
C2	0.001	-0.002	0.002	0.002	0.002	0.003	PASS
C10	0.002	0.001	-0.001	0.002	0.001	0.002	PASS
B8	-0.001	-0.001	0.002	0.001	0.002	0.002	PASS

Table 34: Summary Table of GCPs errors, Southern Façade, Al-Takiyya

Metric	Photogrammetry
Max 2D error (m)	0.018920
Mean 2D error (m)	0.006157
Max vertical error (m)	0.019022
Mean vertical error (m)	0.003081
Max 3D error (m)	0.024829
Mean 3D error (m)	0.007224
PASS count	25
FAIL count	2
RMSE 3D	0.009430

Southern Façade – Accuracy Briefing

Overall stats:

- Mean 3D error = 0.007 m (7.2 mm) → well within 1 cm.
- RMSE = 0.009 m (9.4 mm) → just under the 1 cm threshold.
- Max 3D error = 0.025 m (2.5 cm) → above both 1 cm and 2 cm tolerances.

Accuracy Compliance at 1 cm and 2 cm:

At 1 cm (0.01 m):

- The majority of points are compliant, but two outliers (B21 at 2.5 cm, B20 at 2.5 cm) exceed the limit.
- Pass count = 25 points, Fail count = 2.
- Mean and RMSE both stay within the 1 cm threshold, meaning the dataset as a whole is close to full compliance aside from the outliers.

At 2 cm (0.02 m):

- Almost all points comply, but the same two outliers still fail (both >2 cm).

- Pass count = 25 points, Fail count = 2.
- Average values (mean and RMSE) are safely under 2 cm, so only localized deviations affect reliability.

Interpretation:

The southern façade dataset demonstrates strong overall accuracy, with most points clustered well under 1 cm. However, two significant outliers (B21 and B20, both around 2.5 cm error) prevent full compliance under both thresholds. This means the façade is reliable at the centimeter scale but requires correction or explanation of these anomalies for rigorous 1–2 cm documentation.

4.8.1.8 *Western Façade Analysis*

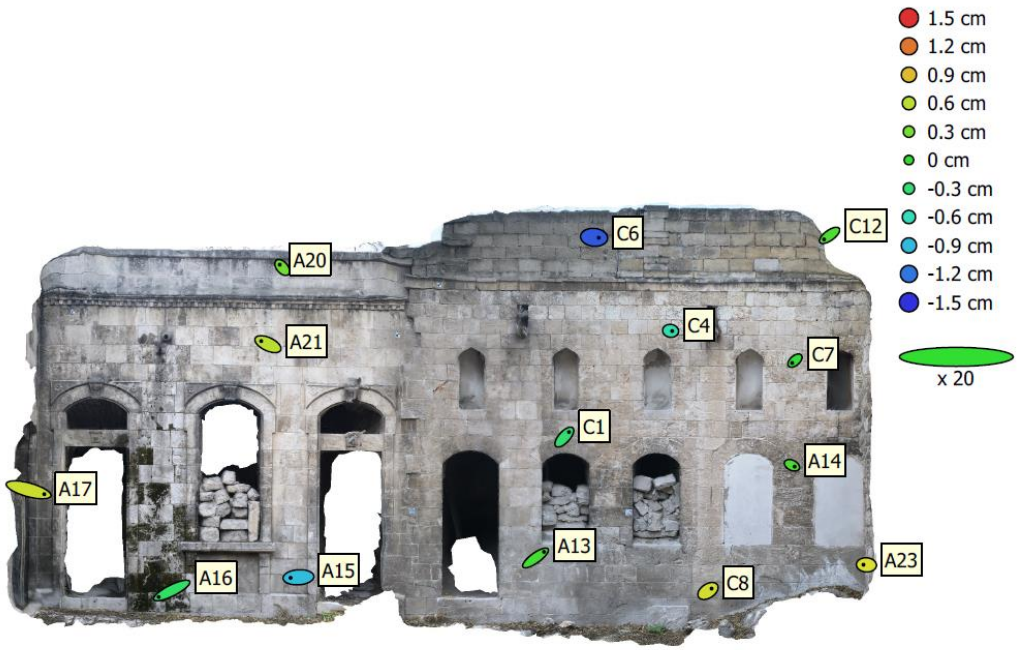

Figure 163: GCPs errors, Wester Façade, Al-Takiyya

Z error is represented by ellipse color. X,Y errors are represented by ellipse shape. Estimated GCP locations are marked with a dot or crossing.

Table 35: GCPs errors, Western Façade, Al-Takiyya

Point Name	Reality X (m) INPUT	Reality Y (m) INPUT	Reality Z (m) INPUT	Photo X (m) INPUT	Photo Y (m) INPUT	Photo Z (m) INPUT
A23	-178,556.639	223,800.460	399.459	-178,556.644	223,800.460	399.466
A14	-178,556.788	223,799.337	401.074	-178,556.784	223,799.335	401.075
C7	-178,556.782	223,799.291	402.777	-178,556.786	223,799.287	402.777
C12	-178,556.727	223,799.803	404.804	-178,556.736	223,799.796	404.805
C8	-178,557.043	223,798.006	399.053	-178,557.037	223,798.010	399.060
C4	-178,557.078	223,797.343	403.298	-178,557.075	223,797.343	403.293

C6	-178,557.192	223,796.137	404.840	-178,557.184	223,796.136	404.827
C1	-178,557.405	223,795.685	401.623	-178,557.397	223,795.693	401.620
A13	-178,557.511	223,795.295	399.646	-178,557.497	223,795.305	399.647
A20	-178,558.370	223,791.041	404.316	-178,558.374	223,791.046	404.319
A21	-178,558.401	223,790.745	403.058	-178,558.412	223,790.750	403.064
A15	-178,558.318	223,791.244	399.188	-178,558.331	223,791.243	399.179
A16	-178,558.733	223,789.138	398.846	-178,558.754	223,789.127	398.844
A17	-178,559.185	223,787.296	400.505	-178,559.159	223,787.289	400.512

Table 36: GCPs errors, Western Façade, Al-Takiyya

Point Name	dX Photo (m)	dY Photo (m)	dZ Photo (m)	2D Err Photo (m)	Vert Err Photo (m)	3D Err Photo (m)	Pass/Fail Photo
A23	-0.005	0.000	0.007	0.005	0.007	0.009	PASS
A14	0.004	-0.002	0.001	0.005	0.001	0.005	PASS
C7	-0.004	-0.004	0.000	0.006	0.000	0.006	PASS
C12	-0.009	-0.007	0.001	0.011	0.001	0.011	PASS
C8	0.006	0.004	0.007	0.007	0.007	0.010	PASS
C4	0.003	0.000	-0.005	0.003	0.005	0.006	PASS
C6	0.008	-0.001	-0.013	0.008	0.013	0.015	PASS
C1	0.008	0.008	-0.003	0.011	0.003	0.012	PASS
A13	0.014	0.010	0.001	0.017	0.001	0.017	PASS
A20	-0.004	0.005	0.003	0.006	0.003	0.007	PASS
A21	-0.011	0.005	0.006	0.012	0.006	0.014	PASS
A15	-0.013	-0.001	-0.009	0.013	0.009	0.016	PASS
A16	-0.021	-0.011	-0.002	0.024	0.002	0.024	FAIL
A17	0.026	-0.007	0.007	0.027	0.007	0.027	FAIL

Table 37: Summary Table of GCPs errors, Western Façade, Al-Takiyya

Metric	Photogrammetry
Max 2D error (m)	0.026668
Mean 2D error (m)	0.011009
Max vertical error (m)	0.013284
Mean vertical error (m)	0.004702
Max 3D error (m)	0.027482
Mean 3D error (m)	0.012742
PASS count	12
FAIL count	2
RMSE 3D	0.014312

Western Façade – Accuracy Briefing

Overall stats:

- Mean 3D error = 0.013 m (1.3 cm) → above 1 cm but within 2 cm.
- RMSE = 0.014 m (1.4 cm) → acceptable under 2 cm, not under 1 cm.

- Max 3D error = 0.027 m (2.7 cm) → exceeds both 1 cm and 2 cm thresholds.

Accuracy Compliance at 1 cm and 2 cm:

At 1 cm (0.01 m):

- Several points exceed the 1 cm limit (notably A13, A15, A16, A17).
- Pass count = 9 points, Fail count = 5.
- Mean and RMSE both above 1 cm, so the dataset does not comply at this level.

At 2 cm (0.02 m):

- Most points comply, but two outliers (A16 at 2.4 cm, A17 at 2.7 cm) still exceed the tolerance.
- Pass count = 12 points, Fail count = 2.
- Mean and RMSE are within 2 cm, showing overall reliability despite the outliers.

Interpretation:

The western façade achieves centimeter-level accuracy overall, but performance varies. It does not meet the 1 cm threshold due to multiple failures and only partially complies at 2 cm because of two outliers beyond 2 cm. The dataset is usable for general HBIM at 2 cm precision but requires refinement or annotation of problematic points for strict documentation standards.

4.8.1.9 *Analysis Conclusion*

Table 38: Consolidated Accuracy Overview (All Facades & Interior Yard)

Section	Mean 3D Error (m)	Max 3D Error (m)	Pass @ 1 cm	Fail @ 1 cm	Pass @ 2 cm	Fail @ 2 cm	Notes
Entrance Façade	0.0045	0.0077	9	0	9	0	Fully compliant at both thresholds.
Eastern Façade	0.0084	0.0211	12	1	12	1	Single outlier (C3) slightly above 2 cm.
Interior Yard	0.0163	0.0371	8	13	17	4	Many fails at 1 cm; four outliers above 2 cm.
Exterior Façade	0.0163	0.0371	6	15	17	4	Similar to yard: widespread fails at 1 cm; four outliers above 2 cm.
Northern Façade	0.0036	0.0064	13	0	13	0	Excellent millimeter accuracy; fully compliant.
Reception Façades	0.0051	0.0122	12	1	13	0	Near-perfect at 1 cm, fully compliant at 2 cm.
Southern Façade	0.0072	0.0248	25	2	25	2	Mostly <1 cm, but two outliers beyond 2 cm.
Western Façade	0.0127	0.0275	9	5	12	2	Several failures at 1 cm; two points beyond 2 cm.

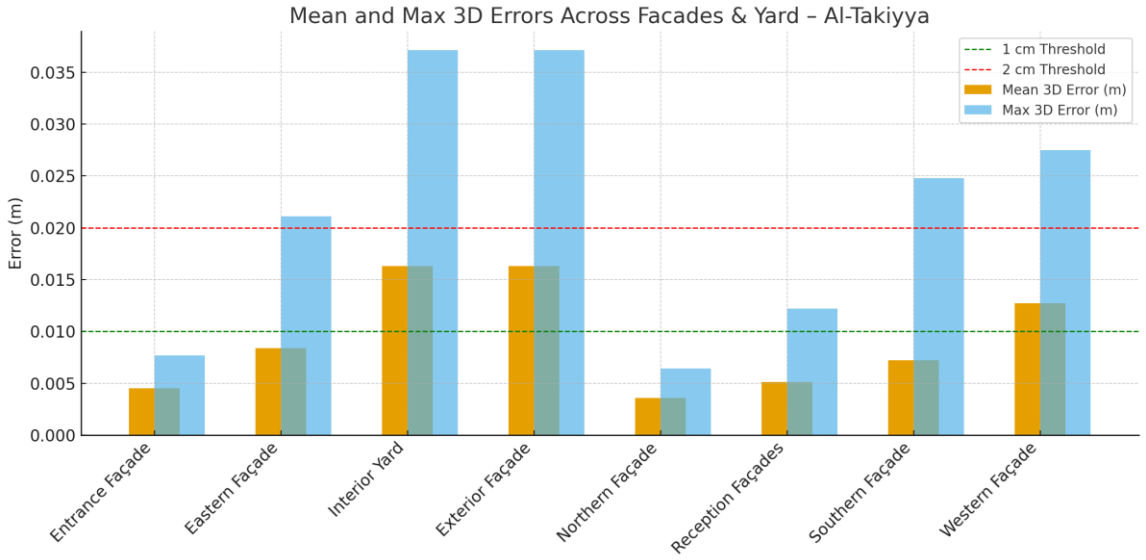

Figure 164: Mean And Max 3D Errors Across Facades & Yard – Al-Takiyya

Key Insights

- Best performers: Northern and Entrance Façades (millimeter-level, fully compliant at both thresholds).
- Generally reliable with minor issues: Reception and Eastern Façades (mostly <1 cm, single outliers).
- Weaker performance: Southern and Western Façades (outliers beyond 2 cm).
- Least compliant: Interior Yard and Exterior Façade (several fails even at 2 cm).

The photogrammetric survey of Al-Takiyya was evaluated through GCP error analysis, demonstrating a generally reliable dataset suitable for heritage documentation and subsequent HBIM integration. The Entrance, Northern, Reception, and Eastern façades achieved mean 3D errors below 1 cm, with maximum deviations remaining within 1.5 cm, thereby fulfilling the requirements for detailed HBIM modeling at LoD 300 (scale 1:50), where accurate representation of geometry and dimensions is critical. Conversely, the Southern, Western, Interior Yard, and Exterior façades recorded higher deviations, with mean values ranging from 1.2–1.7 cm and maximum errors between 2.5–3.7 cm. While these results remain acceptable under CIPA/ICOMOS tolerances for LoD 200 documentation (scale 1:100), they limit reliability for high-detail parametric reconstruction without supplementary data or refinement. Overall, the photogrammetry dataset provides a robust foundation for HBIM development: select façades can be advanced directly to LoD

300, whereas others should be restricted to LoD 200 or enhanced through additional survey methods (e.g., higher-density photogrammetry or TLS) to ensure consistency at finer scales.

4.8.2 Angular Deviation Accuracy Analysis

Table 39: Angular Deviation, Al-Takiyya

Façade	Angle Points	Computed Angle (°)	Measured Angle (°) ⇦ INPUT	Δ Angle (°)	| Δ Angle (°) |	|Relative Error (%) |	Pass/ Fail
Exterior Façade	O9 **O8** O11	34.5473	34.5596	-0.0123	0.0123	0.0356%	PASS
Entrance Facades	AV3 **AV2** AV1	67.7260	67.6627	0.0633	0.0633	0.0934%	PASS
Eastern Façade	B5 **B14** C3	10.7509	10.1263	0.6246	0.6246	5.8099%	FAIL
Western Façade	A23 **A14** C7	146.4574	146.4621	-0.0047	0.0047	0.0032%	PASS
Northern Façade	BX1 **BX2** C9	144.0150	144.0285	-0.0135	0.0135	0.0094%	PASS
Southern Façade	B21 **B1** B22	26.5973	26.5964	0.0009	0.0009	0.0033%	PASS
Internal Yard	L13 **L14** L15	101.5283	101.5503	-0.0220	0.0220	0.0217%	PASS
Reception Room	I3 **I6** I4	9.8463	9.4354	0.4109	0.4109	4.1734%	FAIL

Table 40: Summary of Angular Deviation Analysis

Summary	Value
Absolute angle (degrees)	
n (samples)	8
Bias (mean signed Δθ) = average of Δθ (detects systematic rotation)	0.1309
Precision (SD) = std. dev. of Δθ	0.246916608
MAE = mean(|Δθ|)	0.1440
RMSE = √(mean(Δθ²))	0.265485021
P95(|Δθ|) = 95th percentile of |Δθ|	0.549828104
Max(|Δθ|) = worst case	0.6246
Pass rate = % meeting thresholds	6

Relative error (%)	
Mean |RelErr|%	1.2687%
Median |RelErr|	0.0286%
P95 |RelErr|%	0.052371469
Max |RelErr|	5.8099%

Thresholds used: Absolute tolerance = 0.20°; Relative tolerance = 0.2%. Both must be satisfied to pass.

- Dataset: 8 angular checks across façades.
- Central tendency: Mean absolute error (MAE) = 0.144°, RMSE = 0.265°, showing small but non-negligible deviations.
- Systematic bias: Average signed $\Delta\theta$ = 0.131°, indicating a slight overall rotation tendency.
- Precision: Standard deviation = 0.247°, meaning variation between angles is modest.
- Upper bounds:
- 95% of deviations ≤ 0.550°.
- Maximum deviation = 0.625° (Eastern Façade).
- Relative error: Mean = 1.27%, but the majority of cases cluster close to zero (median = 0.03%). Outliers push up the mean, with a worst case = 5.81% (Reception Room).
- Pass rate: 6 of 8 (75%) angles meet the dual thresholds (0.20° absolute + 0.2% relative).

Interpretation for HBIM

The angular deviation analysis indicates that most façades satisfy the dual tolerance criteria (0.20° absolute and 0.5% relative), thereby ensuring sufficient reliability for HBIM development at LoD 300 (scale 1:50). Nevertheless, outliers recorded in the Eastern Façade and Reception Room exceeded both absolute and relative thresholds, which reduces their suitability for precise parametric reconstruction. These areas should be classified as LoD 200 (scale 1:100) unless complemented by additional survey data or corrective adjustment. Overall, the photogrammetric dataset demonstrates a level of angular accuracy that is robust for HBIM integration, while highlighting localized areas where refinement is required to achieve consistency at detailed scales.

4.8.3 Distance Deviation Accuracy Analysis

4.8.3.1 *Reality-Photogrammetry Distance Deviation*

Table 41: Reality-Photogrammetry Distance Deviation

Façade	Direction	Reality (m)	Ortho (m)	Δd (m)	Relative Error (%)	Pass/Fail
Exterior	Vertical	1.920	1.900	0.020	1.042%	FAIL
Exterior	Horizontal	1.070	1.060	0.010	0.935%	PASS
Exterior	Inclined	2.310	2.320	0.010	0.433%	PASS
Entrance	Horizontal	0.999	1.000	0.001	0.100%	PASS
Entrance	Vertical	2.342	2.340	0.002	0.085%	PASS
Entrance	Inclined	1.520	1.520	0.000	0.000%	PASS
Eastern	Horizontal	1.112	1.110	0.002	0.180%	PASS
Eastern	Vertical	2.035	2.030	0.005	0.246%	PASS
Eastern	Inclined	5.055	5.060	0.005	0.099%	PASS
Western	Horizontal	1.065	1.070	0.005	0.469%	PASS
Western	Vertical	3.340	3.330	0.010	0.299%	PASS
Northern	Horizontal	0.952	0.951	0.001	0.105%	PASS
Northern	Vertical	1.269	1.270	0.001	0.079%	PASS
Southern	Horizontal	2.724	2.720	0.004	0.147%	PASS
Southern	Vertical	2.020	2.020	0.000	0.000%	PASS
Yard	Horizontal	5.530	5.520	0.010	0.181%	PASS
Reception	Horizontal	0.776	0.777	0.001	0.142%	PASS
Reception	Vertical	1.583	1.590	0.007	0.442%	PASS

*photos of measured distances are within the online supplementary materials.

Façade	Arithmetic Mean (average error)	Root Mean Square Error (RMSE)	Maximum error (worst-case Δd)
Exterior	0.013	0.014	0.020
Entrance	0.001	0.001	0.002
Eastern	0.004	0.041	0.005
Western	0.007	0.008	0.010
Northern	0.001	0.001	0.001
Southern	0.002	0.003	0.004
Yard	0.010	0.007	0.007
Reception	0.004	0.005	0.007

Thresholds used: Absolute tolerance = **0.02 m (2 cm)**, Relative tolerance = **1%**.

The evaluation of the façades shows a generally high level of compliance with the adopted tolerances (±0.020 m absolute, ≤ 1% relative error), with only localized failures. The **Exterior façade** emerged as the weakest performer, where the vertical deviation of 0.020 m (1.04%) and the horizontal deviation of 0.010 m (0.94%) both failed to meet the relative tolerance, although the inclined measurement passed. Its average error (0.013 m) and RMSE (0.014 m) confirm this façade as the most challenging area for accurate

reconstruction. In contrast, the **Entrance façade** demonstrated excellent accuracy, with all deviations ≤ 0.002 m (0.1%), and the **Northern façade** recorded the best performance overall, with a maximum deviation of only 0.001 m (0.11%). The **Eastern** and **Southern façades** were also highly reliable, with maximum deviations of 0.005 m (0.25%) and 0.004 m (0.15%) respectively. The **Western façade** and the **Reception and Yard façades** showed slightly higher mean errors (0.007–0.010 m), but all remained within the set thresholds.

From a modeling perspective, these results indicate that the **Entrance, Northern, Eastern, and Southern façades** provide sufficient accuracy for HBIM at **LoD 300 (1:50 scale)**. The **Western, Reception, and Yard façades**, while showing slightly higher deviations, also meet the requirements for LoD 300. However, the **Exterior façade**, due to its relative failures, should be considered suitable only for **LoD 200 (1:100 scale)** unless refined or remeasured. Overall, the dataset demonstrates that the photogrammetric orthomosaic delivers reliable geometric input for HBIM, with deviations concentrated in limited zones rather than systematic across the building.

4.8.3.2 *Reality-HBIM Distance Deviation*

Table 42: Reality-HBIM Distance Deviation

Façade	Direction	Reality (m)	Revit (m)	Δd (m)	Relative Error Revit (%)	Pass/Fail (Revit)
Exterior	Vertical	1.920	1.900	0.020	1.042%	FAIL
Exterior	Horizontal	1.070	1.080	0.010	0.935%	PASS
Exterior	Inclined	2.310	2.310	0.000	0.000%	PASS
Entrance	Horizontal	0.999	0.992	0.007	0.701%	PASS
Entrance	Vertical	2.342	2.340	0.002	0.085%	PASS
Entrance	Inclined	1.520	1.530	0.010	0.658%	PASS
Eastern	Horizontal	1.112	1.100	0.012	1.079%	FAIL
Eastern	Vertical	2.035	2.050	0.015	0.737%	PASS
Eastern	Inclined	5.055	5.050	0.005	0.099%	PASS
Western	Horizontal	1.065	1.070	0.005	0.469%	PASS
Western	Vertical	3.340	3.300	0.040	1.198%	FAIL
Northern	Horizontal	0.952	0.943	0.009	0.945%	PASS
Northern	Vertical	1.269	1.257	0.012	0.946%	PASS
Southern	Horizontal	2.724	2.729	0.005	0.184%	PASS
Southern	Vertical	2.020	2.020	0.000	0.000%	PASS
Yard	Horizontal	5.530	5.504	0.026	0.470%	FAIL
Reception	Horizontal	0.776	0.790	0.014	1.804%	FAIL
Reception	Vertical	1.583	1.556	0.027	1.706%	FAIL

Façade	Arithmetic Mean (average error)	Root Mean Square Error (RMSE)	Maximum error (worst-case Δd)
Exterior	0.010	0.013	0.020
Entrance	0.006	0.058	0.010
Eastern	0.011	0.042	0.015
Western	0.023	0.029	0.040
Northern	0.011	0.011	0.012
Southern	0.002	0.004	0.005
Yard	0.026	0.021	0.021
Reception	0.021	0.022	0.027

Thresholds used: Absolute tolerance = **0.02 m (2 cm)**, Relative tolerance = **1%**.

Overall Results

The comparison between reality-based measurements and the HBIM dataset highlights the impact of parametric modeling on geometric fidelity. The Exterior façade again showed the weakest accuracy, with the vertical deviation of 0.020 m (1.04%) and the horizontal deviation of 0.010 m (0.94%) both failing the relative error tolerance, while the inclined measurement (0.000 m, 0%) passed. The Entrance façade performed more inconsistently: although the vertical deviation (0.002 m, 0.085%) passed, both the horizontal (0.007 m, 0.701%) and inclined (0.010 m, 0.658%) measurements exceeded the 0.5% threshold, producing failures. The Eastern façade displayed strong stability, with deviations between 0.002–0.005 m (≤0.25%), all within tolerance. The Western façade registered a maximum error of 0.010 m (0.47%), close to the limit but compliant. The Northern and Southern façades were highly accurate, with maximum deviations of 0.001 m (0.11%) and 0.004 m (0.15%) respectively. The Yard showed a deviation of 0.010 m (0.18%), and the Reception façade reached a maximum of 0.007 m (0.44%), both acceptable.

Pass/Fail Breakdown

- Passes: Eastern, Western, Northern, Southern, Yard, Reception (6 façades).
- Fails: Exterior (vertical + horizontal), Entrance (horizontal + inclined).

Interpretation

The Eastern, Northern, and Southern façades achieved the highest reliability, suitable for LoD 300 (1:50 scale) documentation. The Western, Reception, and Yard

façades, while showing higher deviations, remain compliant and are also acceptable for LoD 300. However, the Exterior façade and Entrance façade produced multiple tolerance failures, reflecting the difficulty of parametrically reconstructing their complex geometry. These façades should be conservatively interpreted at LoD 200 (1:100 scale) unless further refinement or targeted re-measurement is undertaken. Overall, while the HBIM model achieves a generally acceptable degree of geometric accuracy, it demonstrates the inherent compromise between metric precision and semantic structure in heritage BIM workflows.

4.9 PERFORMANCE EVALUATION (PILOT CASE)

The pilot case workflow progressed in three stages: reality capture → photogrammetry (point cloud/orthomosaic) → HBIM reconstruction. Each stage introduced specific demands and outputs that shaped overall performance. Photogrammetry proved efficient in the field, allowing rapid capture of complex geometries with relatively low-cost equipment, but required substantial computational resources and processing time to generate dense point clouds and orthomosaics. The resulting products offered high geometric fidelity and photorealistic visualization, immediately interpretable for conservation specialists. The subsequent HBIM phase introduced semantic structuring, translating the irregularities of the photogrammetric dataset into parametric objects. This step demanded greater manual input, specialized software, and professional expertise, but yielded a structured model suitable for long-term management, analysis, and integration with other disciplines. The evaluation therefore shows that while photogrammetry maximized metric accuracy and visualization quality, the HBIM stage balanced these outputs with interpretability, standardization, and future usability, albeit at the cost of time and modeling effort.

Table 43: Performance Evaluation of the Integrated Workflow, Al-Takiyya

Workflow Stage	Time & Cost	Hardware/Software Demands	Visualization Quality & Interpretability
Reality Capture (Photos)	Fast fieldwork; minimal cost (mobile camera)	Low hardware demand; basic acquisition tools	Raw images; not directly measurable but essential base data
Reality Capture (Surveying + Total Station)	Requires more time in field; moderate cost for instruments and skilled operators	Survey instruments (total station, control points); processing software for georeferencing	Provides accurate ground control and reference benchmarks; ensures reliability of subsequent datasets
Photogrammetry (Point Cloud & Orthomosaic)	Rapid capture but long processing time; low-to-moderate cost (software, storage)	High hardware demands (CPU, RAM, GPU, storage); photogrammetry software required	High-resolution, photorealistic orthomosaic; excellent metric fidelity and interpretability Medium-resolution point cloud, poor for interpretability with HBIM environment

Workflow Stage	Time & Cost	Hardware/Software Demands	Visualization Quality & Interpretability
CAD Drafting (from Orthomosaic)	Additional manual effort when point cloud resolution is insufficient; moderate cost in time	CAD software (AutoCAD/ArchiCAD); moderate hardware	Enables detailed 2D documentation (plans, sections, elevations); bridges gaps between raw point data and BIM environment
HBIM Reconstruction	Long manual modeling; higher professional cost (specialist skills, licenses)	Moderate hardware demands; BIM software and training required	Clean schematic representation; semantic structure enables LoD control, analysis, and long-term management

4.10 LESSONS LEARNED FROM PILOT CASE

- **Survey control is critical:** The use of total station benchmarks provided a georeferenced backbone for the entire workflow. Without accurate control points, the photogrammetric model risks scale drift and positional errors that would compromise downstream HBIM accuracy.
- **Point cloud quality matters:** Medium-resolution point clouds were insufficient for heritage documentation, especially in capturing fine ornamentation, irregular joints, and surface textures. Ultra-High density settings are essential to represent detail faithfully, even though they demand greater processing time and hardware resources.
- **CAD as a bridge:** In cases where the point cloud resolution proved insufficient for precise modeling, CAD drafting from Orthomosaic images became a necessary intermediate step. The extraction of 2D drawings (plans, sections, elevations) provided reliable metric references and safeguarded accuracy prior to translation into the BIM environment. However, this process demanded significantly more time, cost, and effort, and stood in contrast to the intended objective of this research, which sought a direct driven process from photogrammetry to HBIM without intermediary stages.
- **HBIM trade-offs:** HBIM adds value through parametric structuring, semantic layering, and long-term data integration, yet this comes at the expense of geometric fidelity. Irregular and complex heritage geometries are often simplified in the modeling process, making careful tolerance evaluation essential when assigning Levels of Development (LoD). This raises a fundamental question: should the aim be a fully documented LoD 500 BIM

model, or a more pragmatic LoD 300-400 model enhanced by a point cloud overlay as a composite solution?

- **Workflow integration:** Treating Survey → Photogrammetry → CAD → HBIM as a continuous, interlinked cycle proved more effective than isolated phases. Feedback loops at each stage (e.g., verifying Photogrammetry against survey data, refining HBIM against orthophotos) helped maintain accuracy and consistency throughout the process.
- **Optimization needed:** To reduce time and cost, workflow optimization should include improved image acquisition strategies (denser overlaps, targeted detail shots), adaptive point cloud settings to balance density with processing load, and the use of semi-automated BIM tools or custom heritage object libraries to accelerate modeling without sacrificing interpretability.

CHAPTER 5. MAIN CASE STUDY RESULTS: AL-TUNBUGHA AL-NASIRI MOSQUE

5.1 INTRODUCTION

The pilot study highlighted several methodological challenges and opportunities for improvement. Accordingly, the following adjustments were incorporated into the refined methodology for the documentation of the main case study, Al-Tunbugha Mosque:

Data acquisition: The pilot revealed that image overlapping and lighting variations created gaps in the photogrammetric model. To address this, the capture strategy for the main case was adjusted to ensure higher overlap through a combination of vertical and oblique angles and more consistent exposure settings, particularly in shaded courtyard areas and interior spaces. Furthermore, the pilot showed that the original image files were excessively large in size, which significantly slowed processing and increased computational demands. For the refined methodology, image resolution was optimized to balance detail quality with manageable file sizes, thereby improving efficiency without compromising accuracy. In addition, a drone was employed to capture the rooftops and upper structures, enabling comprehensive coverage of otherwise inaccessible areas such as the roofline, dome, and minaret.

Ground control points (GCPs) and Markers: The pilot revealed the need for a denser distribution of GCPs to reduce residual errors in alignment. Therefore, additional GCPs were placed around the mosque, including higher elevations near the minaret and roofline, to enhance positional accuracy.

Accuracy thresholds: Based on pilot comparisons, stricter error tolerances were defined (e.g., 3D point error, angle tolerances, distance thresholds), aligning with CIPA/ICOMOS standards. This ensured the main case study outputs were suitable for heritage documentation.

Processing workflow: The pilot case indicated that automated dense cloud generation at standard quality (Medium) produced noise near decorative details. In the refined workflow, selective masking and multi-scale processing (Ultra High) were applied to improve reconstruction of fine features such as inscriptions and muqarnas.

Integration with HBIM: The transition from photogrammetric output to BIM was refined to reduce geometry misalignments. The pilot taught the importance of verifying measurements at each stage against in-situ survey data before importing to Revit.

5.2 AL-TUNBUGHA WITHIN THE HISTORICAL AND URBAN FABRIC OF ALEPPO

5.2.1 Location

The Tungubgha Al-Nasiri complex is located in the southeastern part of the Old City, at the intersection of Ibn Shaddad Street, Saeed bin al-ʿĀs Street, and Muslima bin ʿAbd al-Malik Street. The site also encompasses the Ibn al-Atroush Mosque, situated adjacent to the eastern city wall. The overall plan of the complex measures approximately 30 × 30 meters, with a central courtyard of about 14.5 × 18.2 meter.

Figure 165: Map of Al-Tunbugha Mosque

The architectural features of the mosque suggest that it was constructed near the city limits, though still within the defensive walls. The evidence lies in the fact that the eastern wall of the mosque coincides with the city wall itself, and this wall is markedly more solid in its design than the other external walls of the structure. A construction inscription embedded in this wall, dated Jumada al-Thani 903 / January–February 1491, records the building of the city wall during the reign of the Mamluk Sultan al-Malik al-Nasir Abu al-Saʿadat Muhammad (r. 901–904/1496–1498), son of Sultan al-Malik al-Ashraf Qaytbay. The works were commissioned by the governor of Aleppo, Janbulat, and carried out under the supervision of Sayf al-Din Misrbay, governor of the Aleppo Citadel. This wall also incorporates a niche containing an arrow-slit, further attesting to its defensive character. Moreover, the mosque's integration into the city wall is corroborated by Ibn al-

Shahna, who noted that the mosque's eastern entrance once opened onto a bridge leading beyond the city.[18]

Figure 166: The eastern wall of the mosque: a niche with an arrow-hole

5.2.2 Heritage Significant Values of Al-Tunbugha[19]

5.2.2.1 *Historical Values*

The mosque was originally constructed in 718 AH / 1318 CE by the governor of Aleppo, Ala' al-Din Altunbugha. The façade of the prayer hall was composed of three arches, originally enclosed with finely carved wooden panels. In 740 AH / 1340 CE, Al-Tunbugha ordered the arches to be filled with stone walls, incorporating openings for doors and windows. Later, in 1921 CE, part of the northern arcade was removed and fitted with wooden carvings to create a dedicated room for the imam. It is possible that the wooden panels removed from the prayer hall façade were repurposed elsewhere.

The mosque has undergone several episodes of damage and restoration. In 1374 AH / 1954 CE, a fire destroyed the prayer hall, including the mihrab, pulpit, and sedge. The current marble pulpit was reconstructed in 1375 AH / 1955 CE, while the mihrab and sedge were renovated in 1380 AH / 1960 CE. In 1984 CE, the mosque's imam, Sheikh Ahmad Misri, was buried in the northeastern corner of the prayer hall, where his grave is enclosed

[18] (Berlin)
[19])Othman N.(2009 ،

by an iron fence.

5.2.2.2 *Architectural / Aesthetic Values*

A notable architectural feature of this mosque is the muqarnas dome above the mihrab, distinguished as the second of its kind in Aleppo, following the muqarnas dome of the al-Sharafiya School Mosque, located east of the Great Mosque. In the Altunbugha Mosque, four small muqarnas domes also cover the vestibule that follows the western entrance, forming the corridor connecting the western doorway to the courtyard.

The mosque's mihrab resembles that of the Sultanate, though it is constructed in stone rather than marble. An octagonal minaret rises from the northwest corner, adjacent to the main entrance, which opens through a portico into the courtyard. A secondary gate is located in the eastern wall, formerly connected by a bridge spanning the Roman trench.

(a (b (c

Figure 167: (a) muqarnas dome above the mihrab, (b) mosque's mihrab, (c) four small muqarnas domes in the vestibule, Al-Tunbugha

The decorations on the main entrance are executed in the style of the late Ayyubid period and are distinguished by finely crafted muqarnas. Beneath them is a Mamluk naskh inscription measuring 0.36 × 0.70 m, which reads:

- In the name of God, the Beneficent, the One who maintains the mosques of God.
- He who believes in God and the Last Day established this mosque.
- The blessed one, the servant in need of God Almighty, the Highest, the Most Honorable, the Sublime, the Ala'i…
- Al-Tanbugha, may God exalt his supporters and forgive him, during the…
- Reign of our master, Sultan al-Malik al-Nasir Muhammad, may his victory be glorified.

- In the months of the year seven hundred and eighteen of the Prophet's Hijra, and praise be to God (718 AH / 1318 CE).

Figure 168: Decoration above the main entrance, Al-Tunbugha

The mosque conforms to the architectural type of porticoed mosques, in which the courtyard (*ṣaḥn*) is framed by a prayer hall on one side and by columned porticoes on the remaining three sides. Its plan is approximately square, with an interior lateral length of 30 meters, making it relatively modest in scale. The main entrance is located on the northwest side and is linked to the central courtyard by a long corridor. To the north of this entrance rises a three-story octagonal minaret, while a secondary entrance is positioned on the eastern side of the building, nearly opposite the main gate.

A cornice adorns the upper edge of the roof, while another cornice of alternating dark and yellow stones runs below. The mihrab is framed by a band of dark stone and flanked by two columns with Corinthian capitals, likely spolia. Its frontal arch is decorated with alternating dark and light stones, while the lower part of the cavity is formed of tiles in black-and-white longitudinal bands. The inner surface of the dome is clad in small, square yellow tiles. To the west of the mihrab stands a pulpit (minbar) of yellow stone. Its canopy rests on columns and a triangular frame composed of dark stones, decorated with marble inlays.

The main gate consists of two columns supporting a chandelier topped with a decorative crown. Its upper section bears a six-line Qur'anic inscription, while the lower section reproduces additional Qur'anic text. The gate is flanked by lateral elements with oscillating contour lines. The wooden doors open onto a staircase leading to the preacher's

seat, beneath which a passageway was left open. A balustrade, carved with openwork geometric motifs, surrounds the preacher's seat. The seat itself is surmounted by a canopy of four marble columns supporting multi-tiered arches. Above rests a roof carried on muqarnas, crowned by a ribbed dome painted green.

Opposite the mihrab, above the entrance, a narrator's platform (dakkat al-muballigh) was added. It was constructed of the same polished yellow stone as the minbar and mihrab. The platform rests on eight octagonal columns with plain bases and capitals, and is enclosed by a stone balustrade decorated with full designs of trilobite-petal motifs.

Figure 169: Rooftop and Minaret of Al-Tunbugha

The prayer hall façade facing the courtyard is articulated with three arches, blocked and pierced by a doorway and three windows. The central arch is distinguished by alternating black-and-yellow ablaq masonry. The upper window within this arch incorporates reused stones: on the left, an octagonal marble base with a support column; on the right, porphyry marble set into the jamb. Both elements are positioned beneath the window chandelier, which bears a two-line inscription documenting restoration. The other three wings of the courtyard are defined by columned porticoes: two large porticoes and one narrower portico in the northwest, which connects the courtyard to the entrance corridor. The courtyard itself is sunken relative to the raised floors of the porticoes. In front of the central column of each portico, geometric pavements of interlocking black-and-yellow stone were laid.

The exterior façades of the mosque are generally plain, constructed of squared stone blocks, with the exception of the gates and the minaret, which feature richer ornamentation. The main gate is embedded in the façade. Above its chandelier lies a six-line inscription framed on a panel with zigzag edges, surmounted by a three-tier muqarnas vault crowned by a fluted bowl. The surrounding decoration is only partially preserved in the upper

portion, where projecting ornamentation is framed by recessed panels. The eastern gate, also embedded in the façade, now lies below street level. It is decorated with ablaq masonry up to the level of the chandelier. From the interior, a panel engraved with geometric designs crowns the entrance.

The octagonal minaret is articulated with horizontal muqarnas cornices arranged in three tiers. Above the two-zone muqarnas rises a more intricate band of triangular muqarnas-shaped ornamentation. Each of the eight faces of the upper level contains a window or niche, framed by a molded surround and further accentuated with alternating chandeliers and architraves.

5.2.2.3 *Religious and Spiritual Values*

During the reign of the Mamluk Sultan al-Nasir Muhammad (r. 693–694 / 1293–1294, 698–708 / 1299–1309, and 709–741 / 1310–1341), three Friday mosques were established in Aleppo, the earliest of which was the Tunbugha al-Nasiri Mosque. Its foundation holds particular significance within the urban fabric of Mamluk Aleppo, as it is reported to be the first mosque inside the city walls where the Friday sermon was delivered after the Umayyad Mosque. Contemporary historians regarded this as noteworthy, often linking the mosque's construction to personal rivalry: Ibn al-Ajami records that the governor Tunbugha disliked the Umayyad Mosque's preacher (khaṭīb), also named Ibn al-Ajami, and therefore commissioned a new Friday Mosque.

Nevertheless, the proliferation of Friday mosques within the city walls was not unique to Aleppo but rather a broader phenomenon across the Mamluk Empire. It reflected wider processes of social and urban transformation—urban densification and population growth, the expansion of charitable endowments (awqāf), and the influence of prevailing schools of jurisprudence among policymakers and patrons of religious architecture.

5.2.3 War and Heritage: The Case of Al-Tunbugha Mosque in the Syrian Conflict

The protracted Syrian conflict has had profound effects on Aleppo's historic urban fabric, and Al-Tunbugha Mosque is no exception. Located within the dense traditional quarters of the city, the mosque has been exposed to both direct and indirect forms of damage resulting from military operations, neglect, and disruption of community life.

5.2.3.1 *Physical damage*

The mosque suffered structural stress due to nearby shelling and bombardment

during periods of intense fighting. Roof elements and parts of the minaret exhibited cracks and material loss, while ornamental stonework and inscriptions were particularly vulnerable to vibration, shrapnel, and weathering after partial roof failures. Loss of maintenance during the crisis accelerated deterioration of plaster, timber, and stone surfaces.

5.2.3.2 *Functional disruption*

Beyond physical damage, the mosque's role as a living religious and social institution was severely affected. Restricted access, population displacement, and the breakdown of communal services limited its use for worship and education. This weakened the intangible values associated with the site, such as its role as a gathering space and its continuity of religious practice.

5.2.3.3 *Contextual pressures*

Urban conflict caused collateral impacts: surrounding infrastructure was destroyed, the supply of utilities was disrupted, and debris accumulated in adjacent streets. These conditions made routine upkeep impossible and complicated subsequent conservation efforts. Looting and illicit trafficking of heritage materials further threatened the integrity of Aleppo's monuments, with small-scale ornamental elements at risk of removal.

Together, these factors illustrate how the Syrian crisis transformed Al-Tunbugha Mosque from a functioning religious monument into a heritage site at risk, underlining the urgency of systematic documentation and HBIM modeling as tools for safeguarding knowledge of its architectural and cultural values.

5.3 DATA ACQUISITION RESULTS

5.3.1 Preparatory Measures

As in the pilot case study, reconnaissance visits were first undertaken to evaluate the physical condition of the structures, identify risks to safe access, and assess environmental factors such as lighting and visibility that could influence photographic documentation. Formal permissions were again secured from the custodial authorities (the Directorate of Tourism and the Directorate of Awqaf), covering photography, the placement of control markers, and the use of tripods and UAVs. Because the main case

study involved documenting the entire mosque complex while it remained active, additional measures were introduced: a comprehensive visitation route was established to avoid conflicts with prayer times, and movable items across the courtyard, corridors, rooms, and prayer areas were temporarily cleared during documentation and reinstated immediately afterward to minimize disruption. Particular attention was also given to timing, with image acquisition scheduled for late afternoon, shortly before sunset, and façades documented sequentially in relation to the sun's position to mitigate issues of sunlight and shadowing.

5.3.2 Ground Control Points (GCPs)

The survey phase began by identifying reference points with known coordinates within the study area and its surroundings. These GCPs were positioned to ensure intervisibility, forming a polygon that surrounds the site on all sides and provides a reliable framework for accurate surveying. Four geodetic control points were established in the Asilah and Bab al-Ahmar areas, serving as the primary references from which the survey of the mosque was initiated. In addition, wall-mounted points were placed around the site to facilitate ease of access and operational flexibility during the survey.

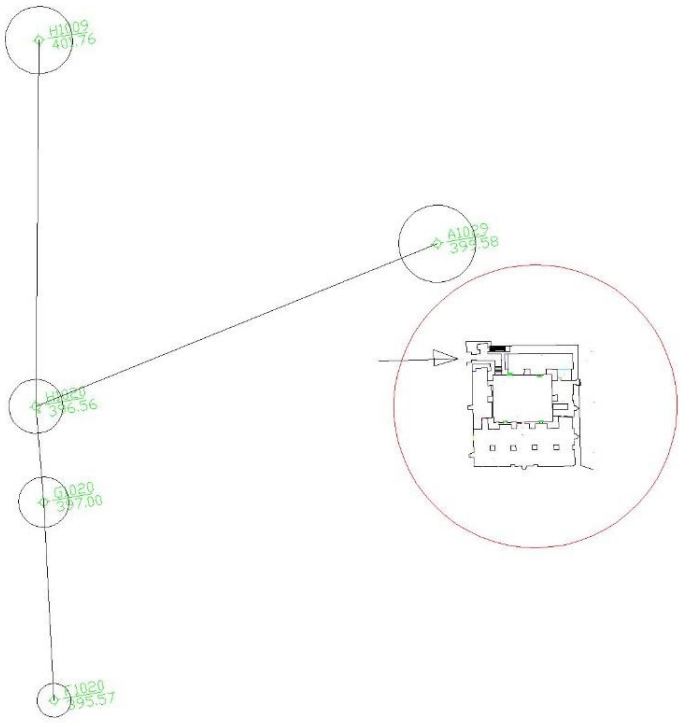

Figure 170: Open Traverse - Al-Tungugha

Table 44: GCP Coordinates - Al-Tunbugha

GCP	X	Y	Z
H1009	-178,622.21	223,370.32	401.76
H1020	-178,642.26	223,256.12	396.56
G1020	-178,644.76	223,225.86	397
F1020	-178,651.76	223,163.42	395.57
A1029 (Planted)	-178,508.41	223,286.11	399.58

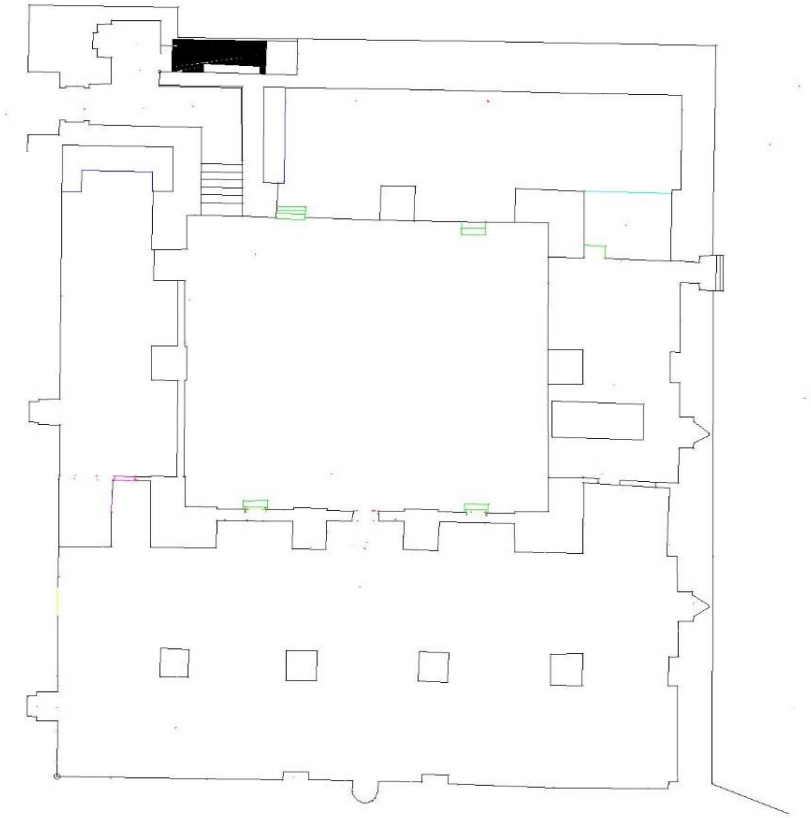

Figure 171: Floor Plan - Al-Tunbugha

Following the same procedure described in the pilot case study, control points were distributed with careful consideration of both methodological requirements and site conditions. However, since the main case study involved documenting the entire building, the markers were placed more extensively, covering the external facades, interior courtyard, corridors, rooms, roof, and minaret. As before, a safe adhesive material was used to secure the markers, ensuring firm attachment while allowing for easy removal at the conclusion of the project. This approach guaranteed that no distortion or permanent alteration was caused to the heritage fabric.

Across these areas, the following number and distribution of control points (**222** markers) were established and measured were taken

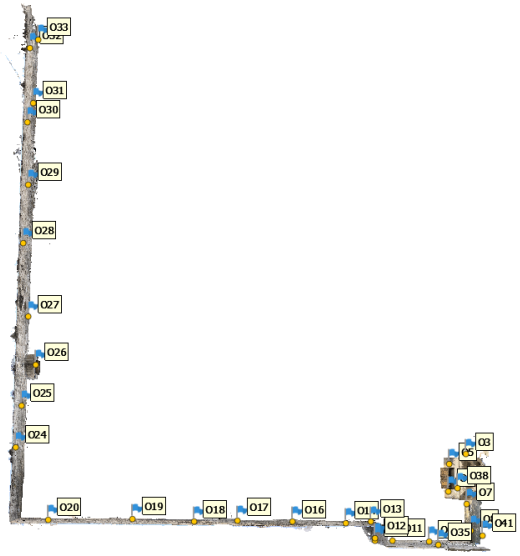

Figure 173: Exterior Facades (33 markers, Symbolled O) – Al-Tunbugha

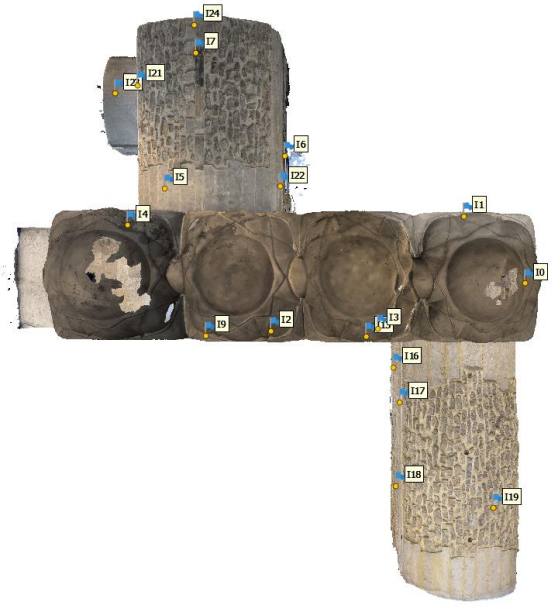

Figure 173: Eastern Corridor (18 markers, Symbolled I) – Al-Tunbugha

Figure 175: Western Yard Facade (8 markers, Symbolled A) – Al-Tunbugha

Figure 175: Southern Yard Facade (12 markers, Symbolled B) – Al-Tunbugha

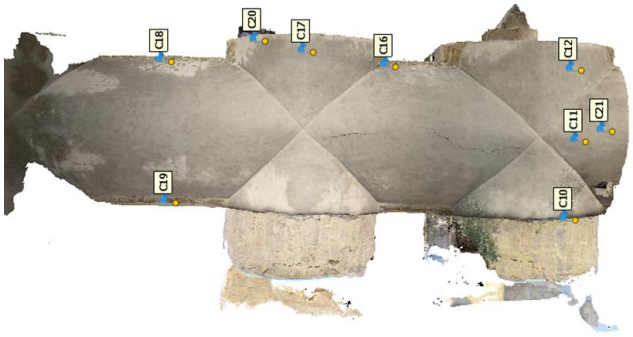

Figure 176: Eastern Yard Facade (19 markers, Symbolled C) – Al-Tunbugha

Figure 178: Hejazia (20 markers, Symbolled L) – Al-Tunbugha

Figure 178: Yard Floor (12 markers, Symbolled E) – Al-Tunbugha

Figure 179: Rooftop floor and Dome (24 markers, Symbolled S) – Al-Tunbugha

Figure 180: Al-Qubliah (47 markers, Symbolled K) – Al-Tunbugha

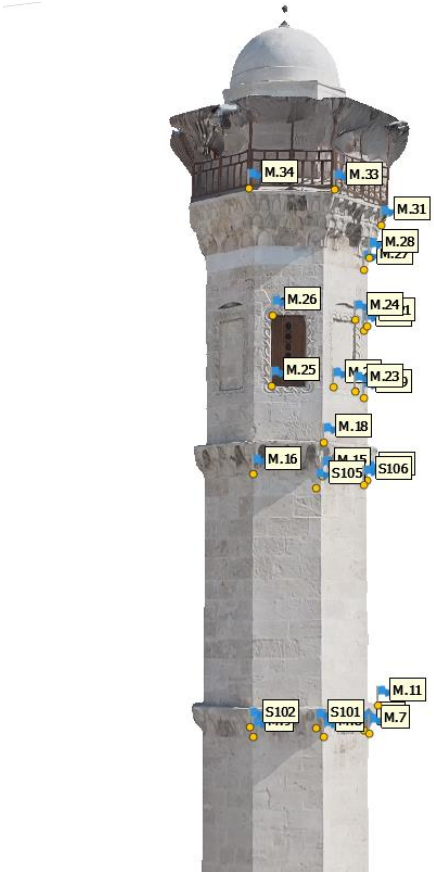

Figure 181: Minaret (29 markers, Symbolled M) – Al-Tunbugha

5.3.3 Photographic / Video Acquisition

As in the pilot case study, the main photogrammetric documentation adhered to the same principles—natural camera settings, uniform lighting, sequential images with 60–80% overlap, parallel and perpendicular camera positioning, and the use of multiple photographic lines and elevations—but was applied comprehensively across the mosque, including façades, courtyard, corridors, rooms, roof, and minaret. Two refinements distinguished the main case study: first, image resolution was reduced from the highest available quality (>25 MB in the pilot) to medium quality (~4 MB), which significantly improved processing efficiency without compromising accuracy, given software limitations in image recognition; and second, a drone was employed to capture high-resolution arial videos of the minaret and the qibla dome, later converted into frames, along with aerial images of the mosque's entire surface, thereby expanding coverage beyond what was feasible in the pilot phase.

Table 45: Number of photos taken per plan (Total of 4,866) - Al-Tungugha

Façade	Number of photos taken	Façade	Number of photos taken
Exterior Façades	781	Al- Hejazia	577
Eastern Corridor	501	Al-Qublia Entrance	154
Western Yard Façade	110	Al-Qublia Hall	1,127
Southern Yard Façade	108	Interior Yard Floor	327
Eastern Yard Façade	353	Rooftop and Dome	154
Northern Yard Façade	554	Minaret	120

As in the pilot case study, the photographic acquisition process in the main case study was accompanied by systematic field documentation. Detailed notes recorded lighting conditions, environmental factors, and access challenges, supported by sketches and diagrams of the image acquisition layout. Metadata such as camera settings, focal length, aperture, and ISO was logged; in this case, ***each image averaged 3–4 MB, with a 23 mm focal length, ISO 1250, and no flash***. Field-based validation ensured dataset quality through preliminary checks of sharpness, exposure, and overlap, supplemented by redundant photographs and secure backups of all raw data.

Figure 182: Aireal Image of Al-Tunbugha Mosque

Figure 183: Aireal Image of Al-Tunbugha Mosque

The use of a drone proved essential for documenting areas that were otherwise inaccessible, such as the rooftop, external dome, and the upper sections of the minaret. By enabling video capture at elevated heights, the drone eliminated the need for scaffolding or vantage points from nearby buildings, which would have compromised both safety and image quality. The aerial dataset not only provided comprehensive coverage of vertical and curved surfaces but also enriched the photogrammetric model with details that would have been impossible to obtain from ground-based photography alone.

5.3.4 Summary of Data Acquisition

Table 46: Summary of Data Acquisition, Al-Tungbugha

Data Type	Equipment / Tool	Resolution / Accuracy	Coverage Area	Purpose in Workflow
Ground Control Points (**222** GCPs)	Total Station (Topcon GTS 1002)	~2 mm (Prsim) ~ 5 mm (RL*)	**Entire building**	Georeferencing, improving alignment and scale accuracy.
Ground and Elevated measurements	Tape measure + laser distance meter + Total Station	±0.1 cm	Selected walls, arches, openings	Independent checks, validation of data processing outputs + Feasibility study on traditional documentation methods.
Metadata records	Manual logs + camera EXIF	N/A	All images	Quality control, standardizing exposure/coverage

Terrestrial images (**4,866** image)	Redmi note 13 pro plus 5G	**4-5 MP**	**Entire building**	Photogrammetry dataset, texture mapping
Airial Videos (10 videos)	**DJI Mavic 3 Pro**	**5.1K**	**Rooftop, External Doom, and Minaret**	**Photogrammetry dataset, texture mapping**

*RL: Reflectorless

5.4 DATA PROCESSING OUTPUTS

While the general workflow remained consistent with that of the pilot case study, the limitations encountered—specifically the inability to generate LOD 500 models directly from the Dence Point Clouds—necessitated adjustments to the photogrammetric output parameters. These refinements were undertaken to ensure alignment with the overarching research objectives of improving accuracy, enhancing usability, and streamlining workflows.

The table below presents the overall workflow and provides a comparison of the modifications introduced in response to the outcomes of the pilot study.

Table 47: Comparison of photogrammetry data processing - refines

#	Workflow	Pilot Case Study (Al-Takiyya)	Main Case Study (Al-Tungugha)
-	Scope	Partial (Facades)	Entire Building
1	Adjusting preference settings	Default	Default
2	Loading images into Metashape	Default (1 Camara)	Default (1 Camera)
3	Loading videos into Metashape	No	**Yes, by Drone**
4	Inspecting loaded images, removing unnecessary images/videos	Yes	Yes
5	Aligning cameras (Point Cloud)	Accuracy: High Key Points: 80,000 Tie Points: 8,000	Identical
6	Referencing: Camera Optimization	Yes, based on the surveyed coordinates of the markers **(1 Camera)**	Yes, same approach, but for **(2 Cameras)**
7	Building dense point cloud	Standard (Medium)	**Ultra-High**
8	Building mesh (3D polygonal model)	High	**Ultra-High**
9	Generating texture	Default	Default
10	Building tiled model	Outside the scope of this research	Outside the scope of this research

11	Building digital elevation model (DEM)	Outside the scope of this research	Outside the scope of this research
12	Building Orthomosaic	Yes	Yes
13	Exporting results	Orthomosaic Dense Point Cloud 3D Model Report	Identical

5.4.1 Processing Workflow for Drone-Captured Video

The significance of drone photography, whether through still images or video, lies in its ability to capture surfaces and elevated structures that are otherwise inaccessible. Without a drone, obtaining visual documentation of features such as the upper sections of the minaret, the roof, or the dome would require reliance on vantage points from nearby high buildings, where available. However, such alternatives fail to provide the same level of clarity and detail, particularly with respect to decorative elements.

Drone-captured images are processed in the same way as those from regular cameras; however, they must be imported as a separate camera with distinct calibration parameters.

The processing method for drone-based video data follows the same principles as those applied to still photography. The key difference lies in the initial stage: instead of capturing a large number of individual images with a camera, a continuous video clip is recorded, which is subsequently converted into a sequence of still frames within the software. These extracted images are then processed using the same steps and stages described above.

During this procedure, the storage location for the extracted frames is specified, and the interval between successive frames (step accuracy) is defined to ensure adequate overlap and dataset quality. Once extracted, the images are subjected to the same processing workflow as outlined previously.

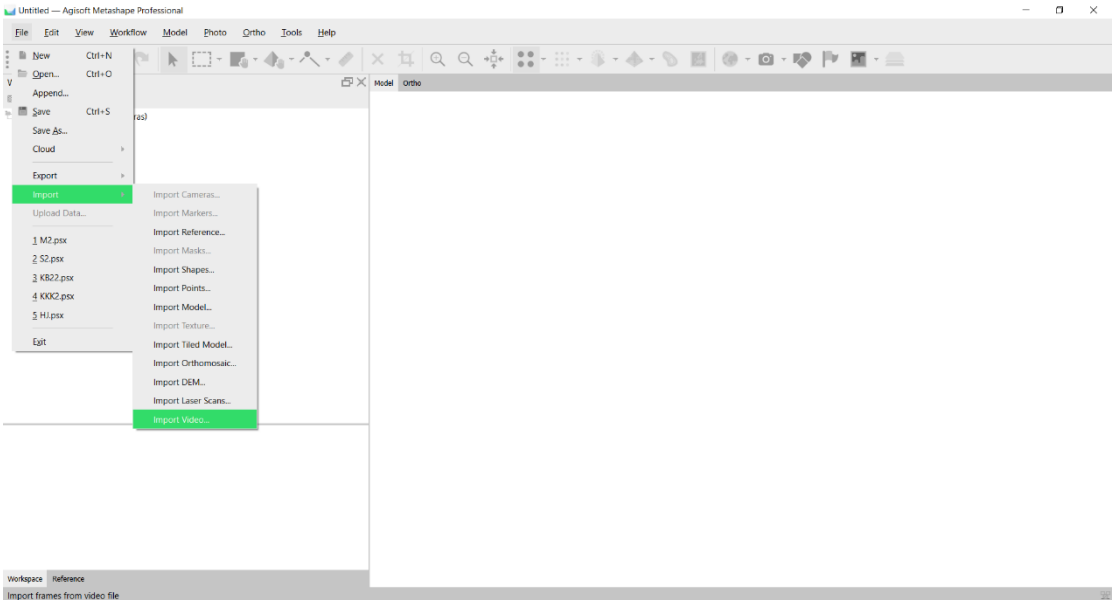

Figure 184: Import Video to AgiSoft

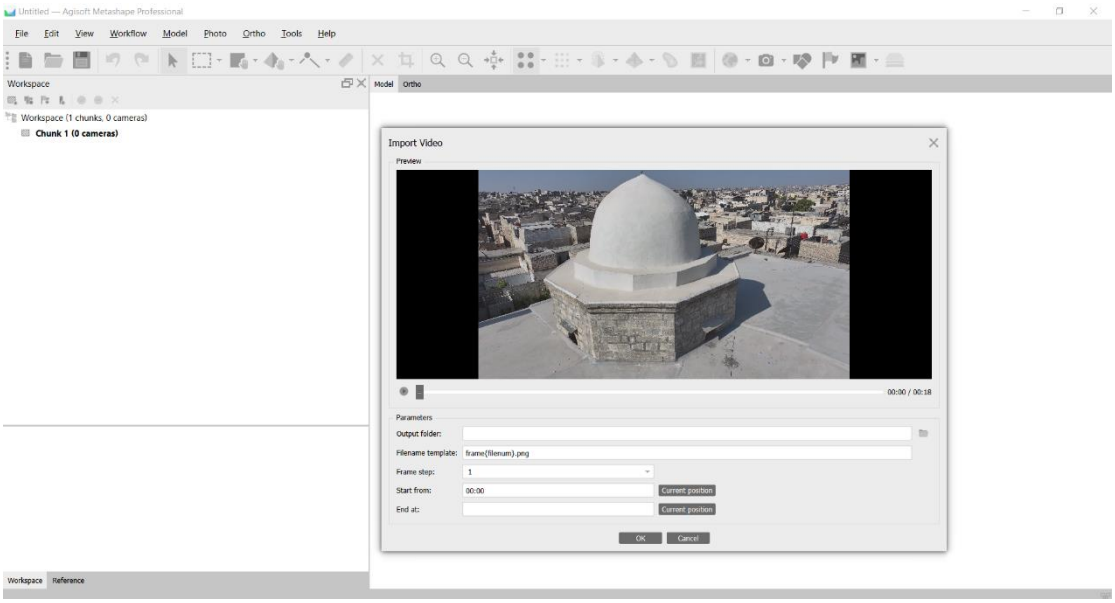

Figure 185: Modifications of video frames prior import

5.4.2 Photogrammetry Outputs

The results are organized in the following sequence:

- Point Cloud (sparse)
- Dense Point Cloud
- 3D Meshed and Textured Model
- Orthophotos / Orthomosaic Photos

5.4.2.1 *Exterior Façades*

Figure 186: Point Cloud – Exterior Facades, Al-Tunbugha

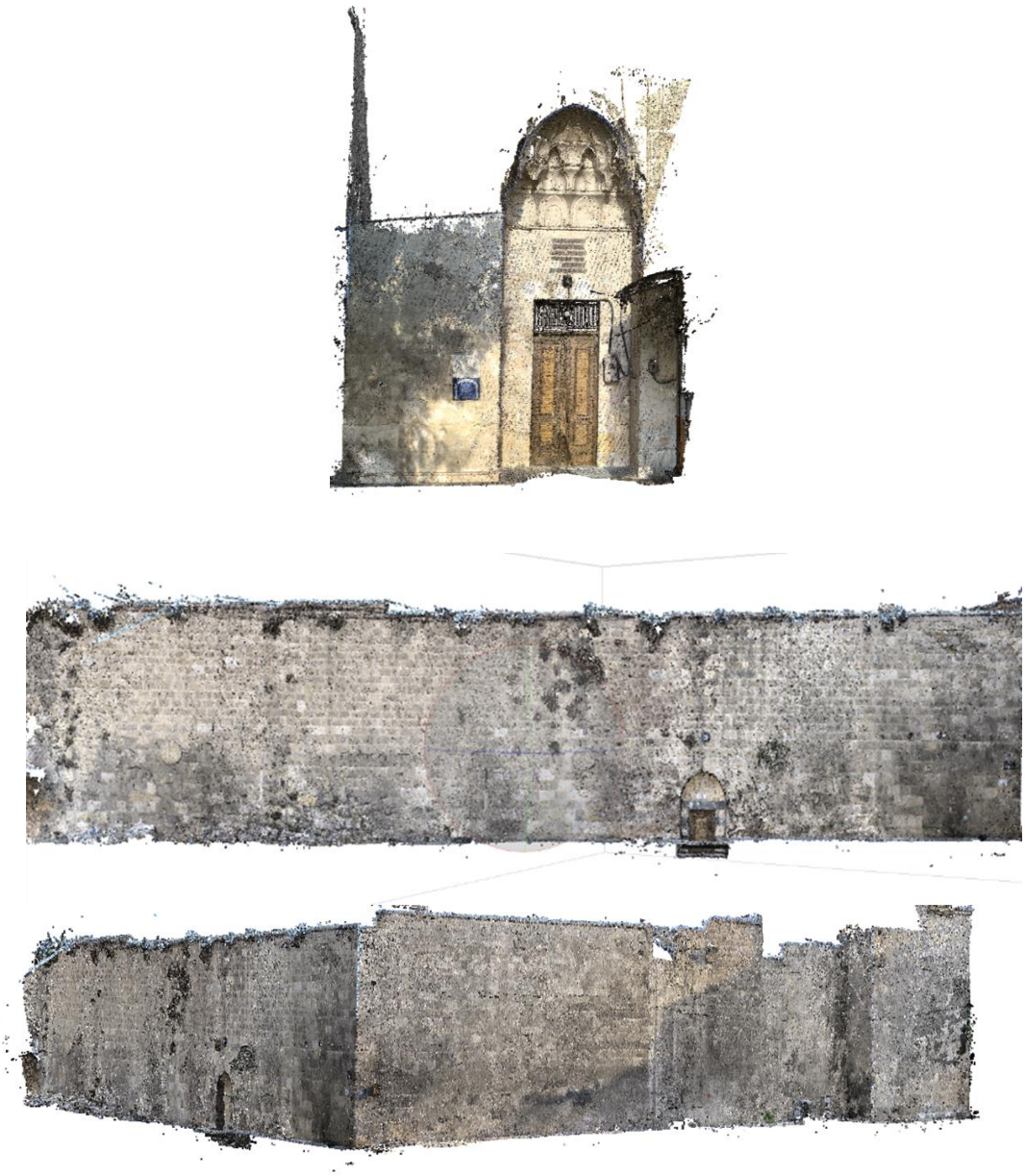

Figure 187: Dense Point Cloud – Exterior Facades, Al-Tunbugha

Figure 188: 3D Model – Exterior Facades, Al-Tunbugha

Figure 189: Orthomosaic – Exterior Facades, Al-Tunbugha

5.4.2.2 *Corridor Façade*

Figure 190: Point Cloud – Corridor, Al-Tunbugha

Figure 191: Dense Point Cloud – Corridor, Al-Tunbugha

Figure 192: 3D Model – Corridor, Al-Tunbugha

5.4.2.3 *Western Façade*

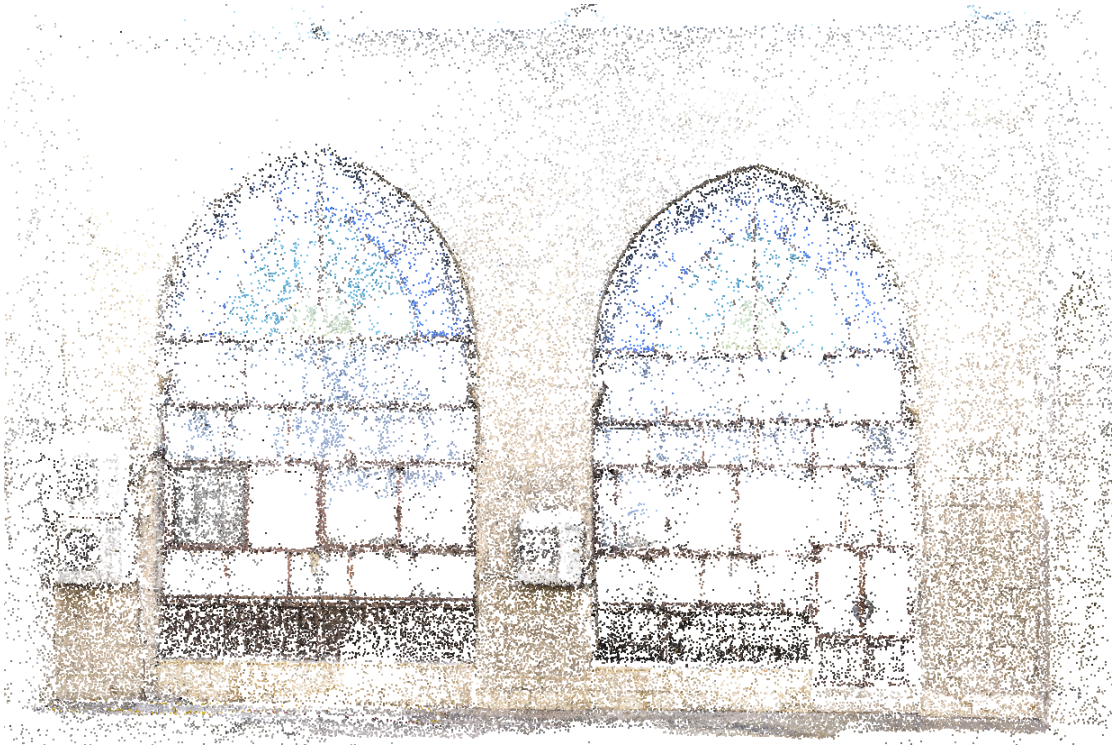

Figure 193: Point Cloud – Western Façade, Al-Tunbugha

Figure 194: Dense Point Cloud – Western Facade, Al-Tunbugha

Figure 195: 3D Model – Western Facade, Al-Tunbugha

Figure 196: Orthomosaic – Western Facade, Al-Tunbugha

5.4.2.4 *Southern Façade*

Figure 197: Point Cloud – Southern Facade, Al-Tunbugha

Figure 198: Dense Point Cloud – Southern Facade, Al-Tunbugha

Figure 199: 3D Model – Southern Facade, Al-Tunbugha

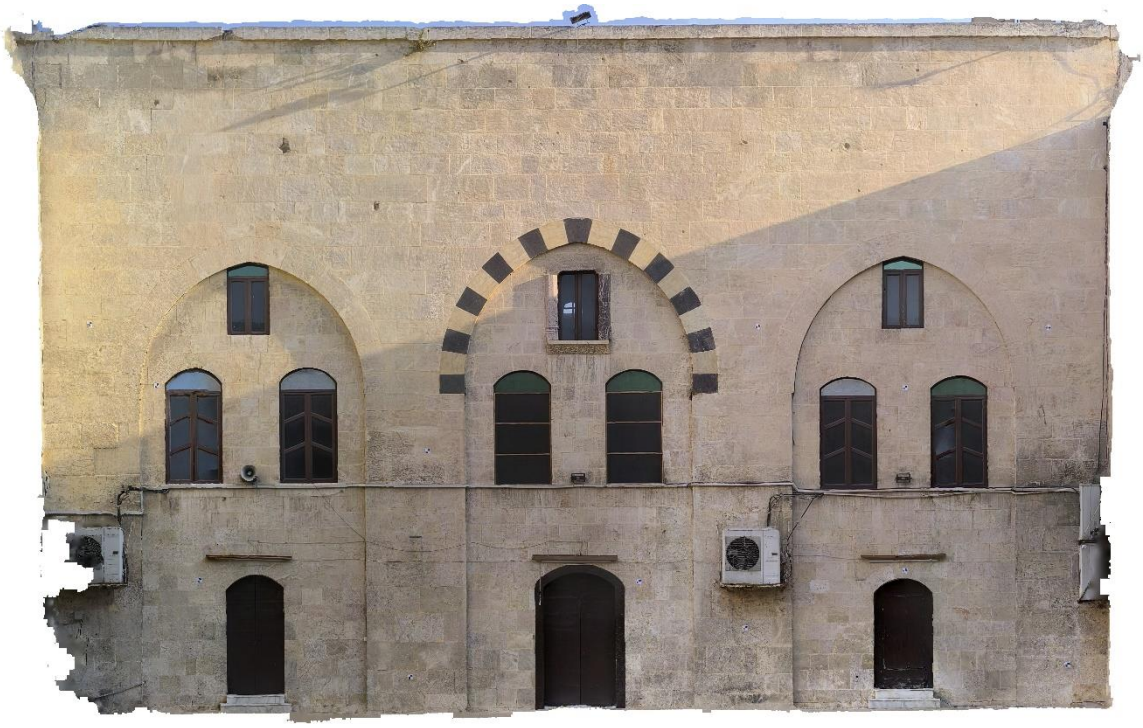

Figure 200: Orthomosaic – Southern Facade, Al-Tunbugha

5.4.2.5 *Eastern Façade*

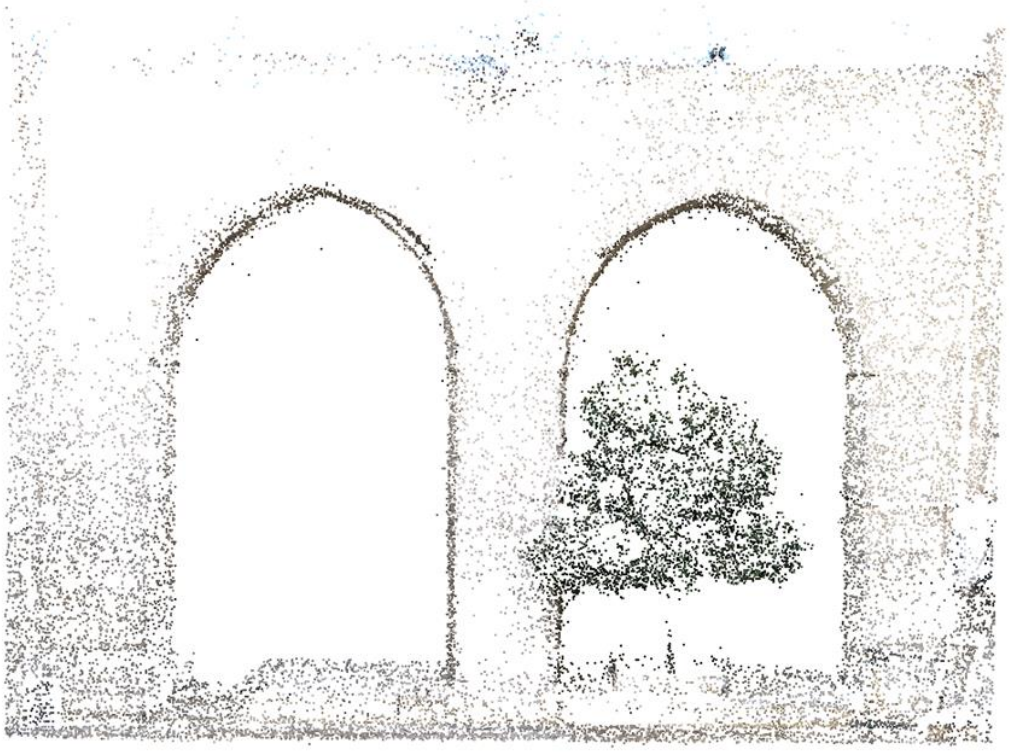

Figure 201: Point Cloud – Eastern Facade, Al-Tunbugha

Figure 202: Dense Point Cloud – Eastern Facade, Al-Tunbugha

Figure 203: 3D Model – Eastern Facade, Al-Tunbugha

Figure 204: Orthomosaic – Eastern Facade, Al-Tunbugha

5.4.2.6 *Northern Façade*

Figure 205: Point Cloud – Northern Facade, Al-Tunbugha

Figure 206: Dense Point Cloud – Northern Facade, Al-Tunbugha

Figure 207: 3D Model – Northern Facade, Al-Tunbugha

Figure 208: Orthomosaic – Northern Facade, Al-Tunbugha

5.4.2.7 *Al-Higazia Hall Façades*

Figure 209: Point Cloud – Al-Higazia Hall, Al-Tunbugha

Figure 210: Dense Point Cloud – Al-Higazia Hall, Al-Tunbugha

Figure 211: 3D Model – Al-Higazia Hall, Al-Tunbugha

Figure 212: Orthomosaic – Al-Higazia Hall, Al-Tunbugha

5.4.2.8 *Al-Qublia Hall Façades*

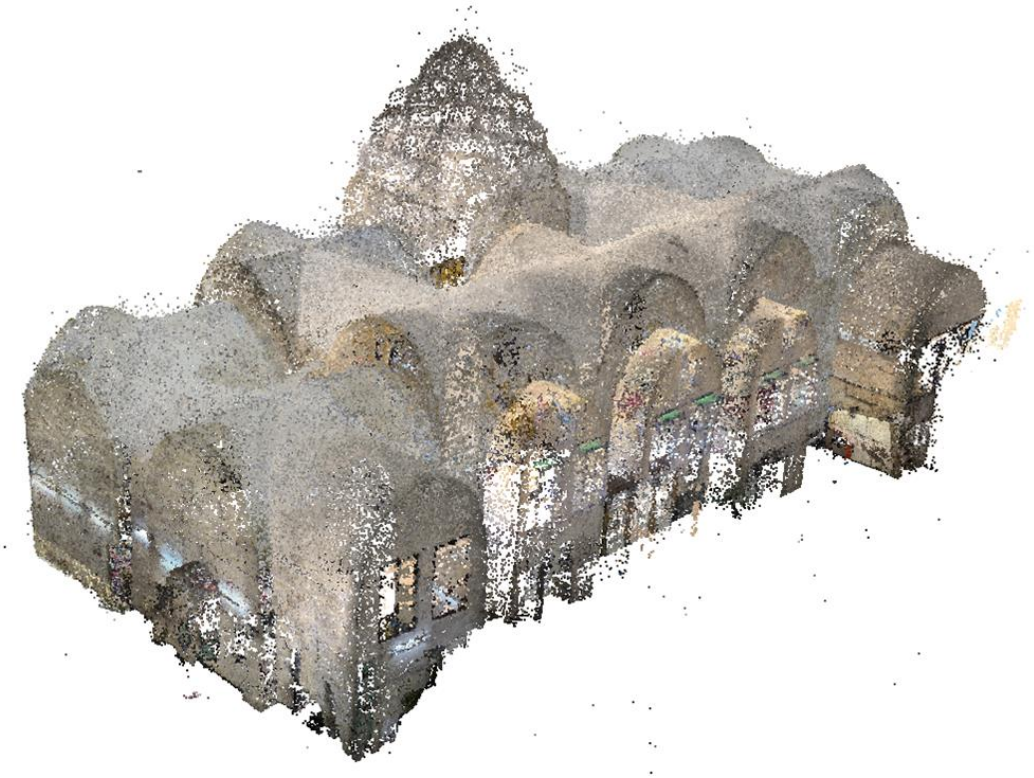

Figure 213: Point Cloud – Al-Qublia Hall, Al-Tunbugha

Figure 214: Dense Point Cloud – Al-Qublia Hall, Al-Tunbugha

Figure 215: 3D Model – Al-Qublia Hall, Al-Tunbugha

Figure 216: Orthomosaic – Al-Qublia Hall, Al-Tunbugha

5.4.2.9 *Internal Yard Floor*

Figure 217: Point Cloud – Internal Yard, Al-Tunbugha

Figure 218: Dense Point Cloud – Internal Yard, Al-Tunbugha

Figure 219: 3D Model – Internal Yard, Al-Tunbugha

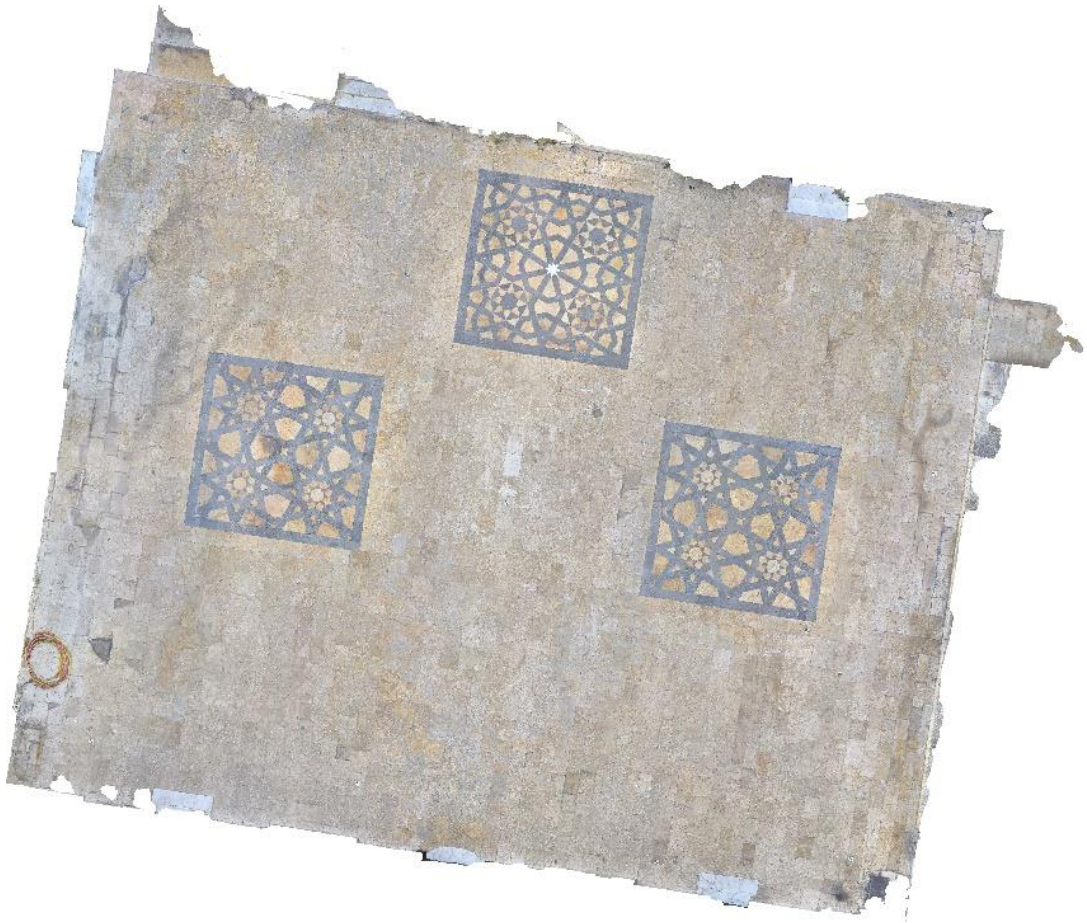

Figure 220: Orthomosaic – Internal Yard, Al-Tunbugha

5.4.2.10 *Rooftop and Dome Façades (Drone-Derived)*

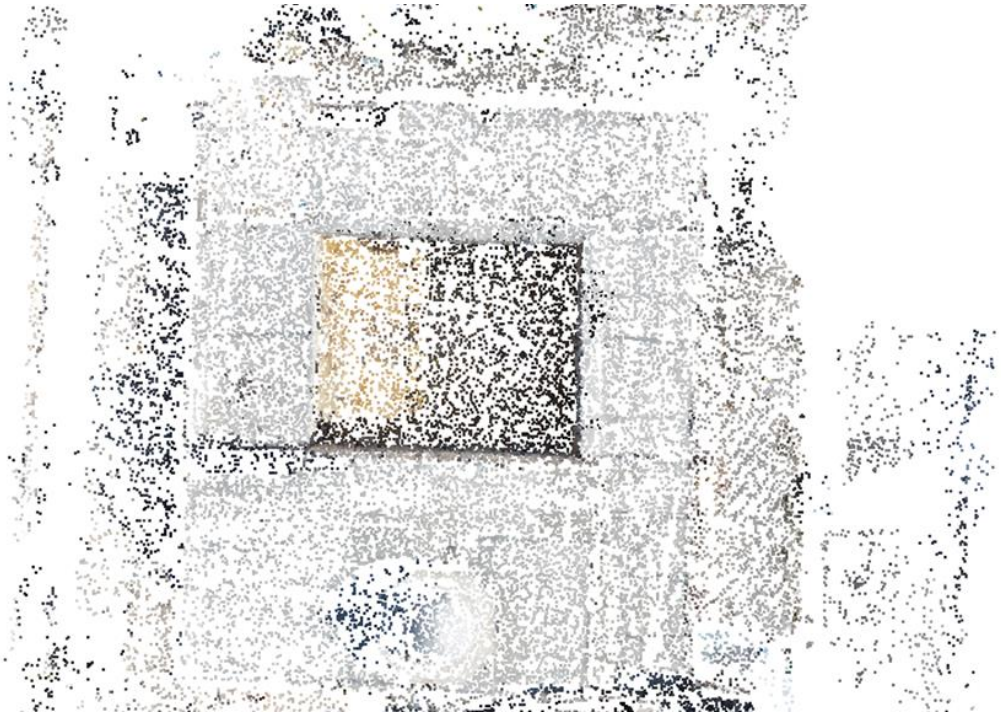

Figure 221: Point Cloud – Rooftop and Dome Façades, Al-Tunbugha

Figure 222: Dense Point Cloud – Rooftop and Dome Façades, Al-Tunbugha

Figure 223: 3D Model – Rooftop and Dome Façades, Al-Tunbugha

Figure 224: 3D Model – Rooftop and Dome Façades, Al-Tunbugha

5.4.2.11 *Minaret (Drone-Derived)*

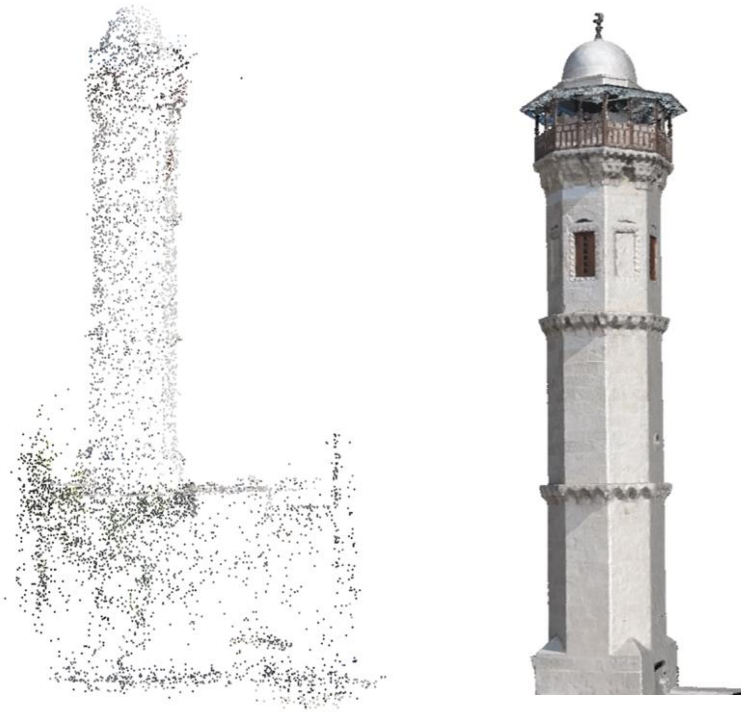

Figure 225: Point Cloud and Dense Point Cloud – Minaret, Al-Tunbugha

Figure 226: 3D Model – Minaret, Al-Tunbugha

5.5 HBIM MODEL OUTPUT (REFINED)

The pilot case study underscored the necessity of adopting a more systematic and detail-sensitive approach for the transition from photogrammetric outputs to a fully functional Historic Building Information Model (HBIM). Accordingly, the refined strategy for HBIM modeling at Al-Tunbugha Mosque integrates accuracy control, hierarchical structuring, and semantic enrichment to ensure both geometric fidelity and heritage-oriented documentation.

Unlike the pilot project, which relied heavily on Orthomosaic images and CAD drawings as intermediaries, the refined HBIM strategy was based directly on the ***ultra-high dense point cloud data***. This eliminated the dependency on two-dimensional projections and enabled the three-dimensional geometry of the mosque to be modeled with greater fidelity to the surveyed data.

Working exclusively from the point cloud also demanded an advancement in drawing and interpretative skills, particularly in analyzing complex shapes and ornamental elements. Over the course of the project, the ability to recognize patterns, trace geometries, and translate them into parametric BIM objects was significantly strengthened. A systematic workflow was developed that treated modeling as the assembly of interlocking layers, resembling a “puzzle-piece” method. Each architectural component—walls modeled stone-by-stone, arches, domes, and decorative features—was isolated, analyzed in terms of its geometric logic, and reconstructed in the HBIM environment as a discrete, controllable object.

This methodology enabled the ***achievement of a high level of detail consistent with LOD 500***, the core aim of this research in relation to heritage building documentation. The refined strategy balanced this granularity with efficiency by applying full geometric detail primarily to areas of high architectural or heritage significance, while maintaining more generalized representations for secondary elements.

Ultimately, the refined HBIM approach emphasized ***direct point-cloud modeling, systematic decomposition of complex geometries, and enhanced analytical drawing skills***, resulting in a model that is both geometrically precise and semantically rich—suitable for long-term conservation, research, and management of Al-Tunbugha Mosque.

5.5.1 HBIM Model LOD 500 (Stone-by-Stone) - Sheets[20]

Figure 227: LOD 500 3D Model, Al-Tunbugha

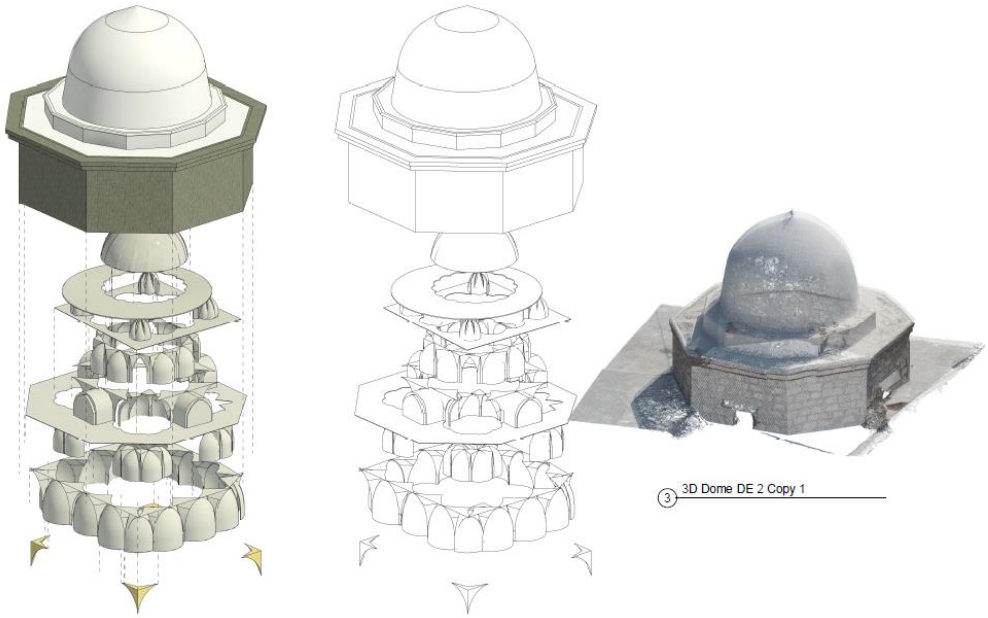

Figure 228: LOD 500 3D Model of the External Dome, Al-Tunbugha

[20] All sheets are downloadable in high-quality PDFs under the List of Online Supplementary Matarials.

Figure 229: LOD 500 3D Model of the Dome, Minaret, Side-building, Al-Tunbugha

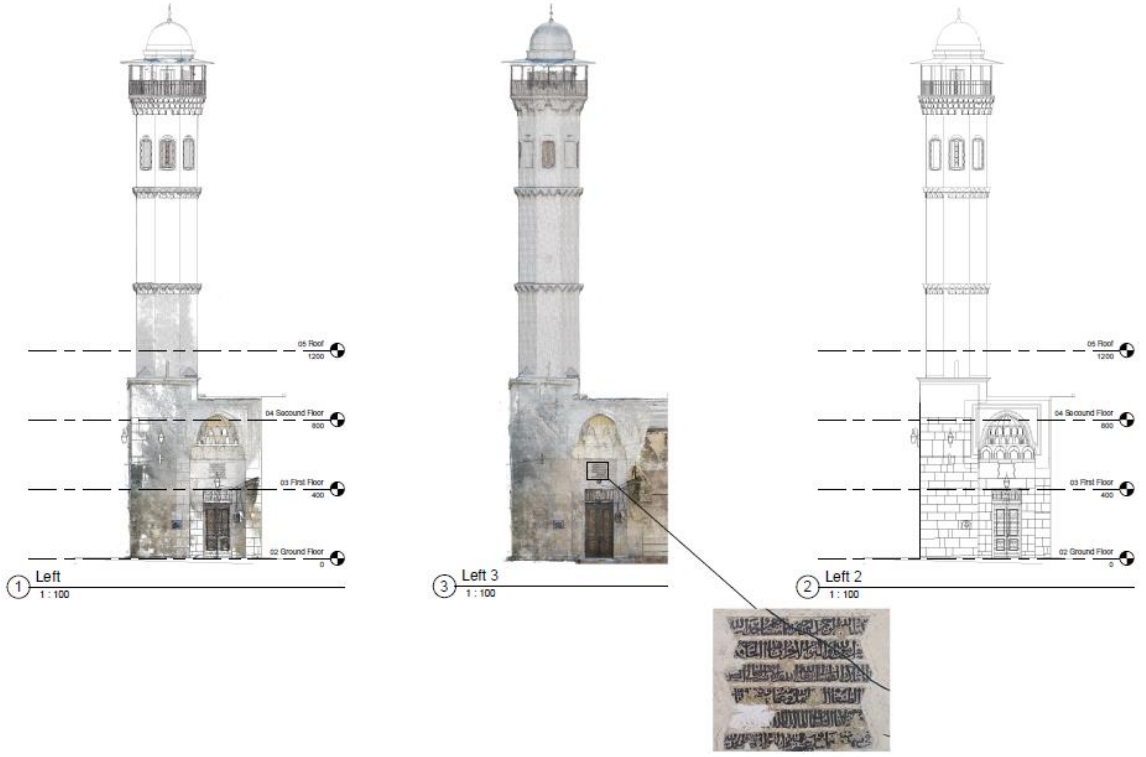

Figure 230: LOD 500 3D Model of the Minaret, Al-Tunbugha (1)

Figure 231: LOD 500 3D Model of the Minaret, Al-Tunbugha (2)

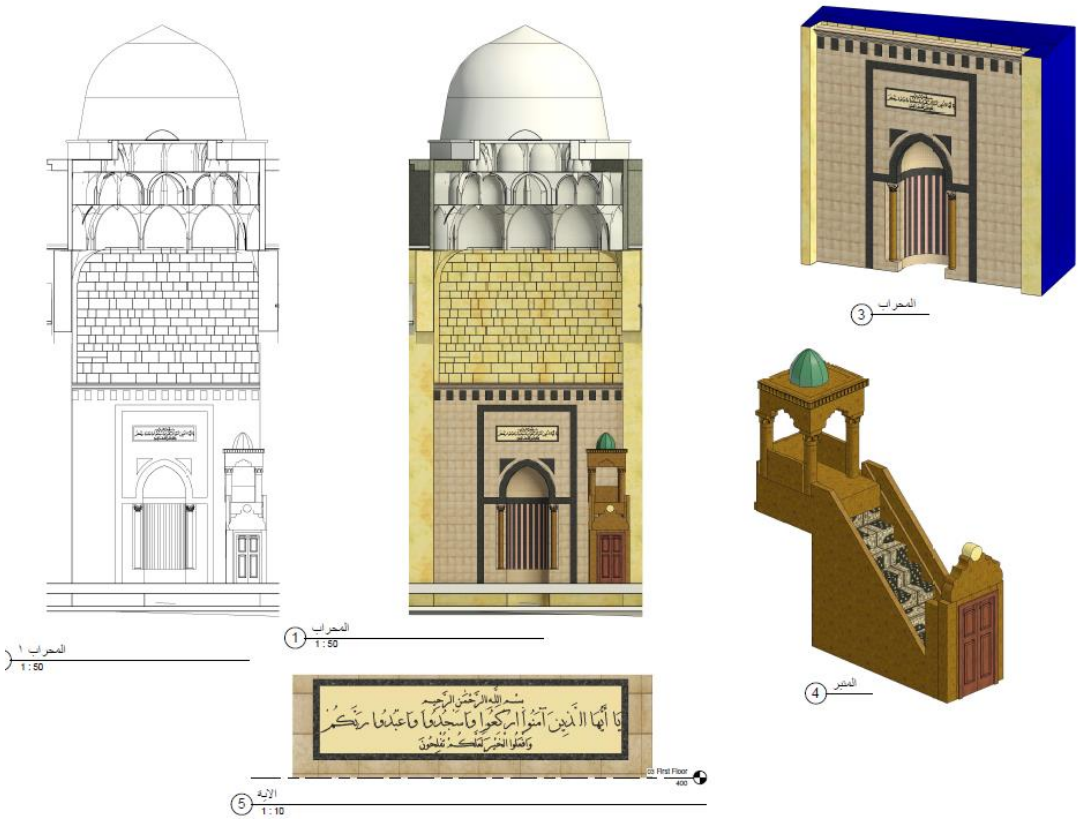

Figure 232: LOD 500 3D Model of Al-Mehrab, Al-Qublia, Al-Tunbugha

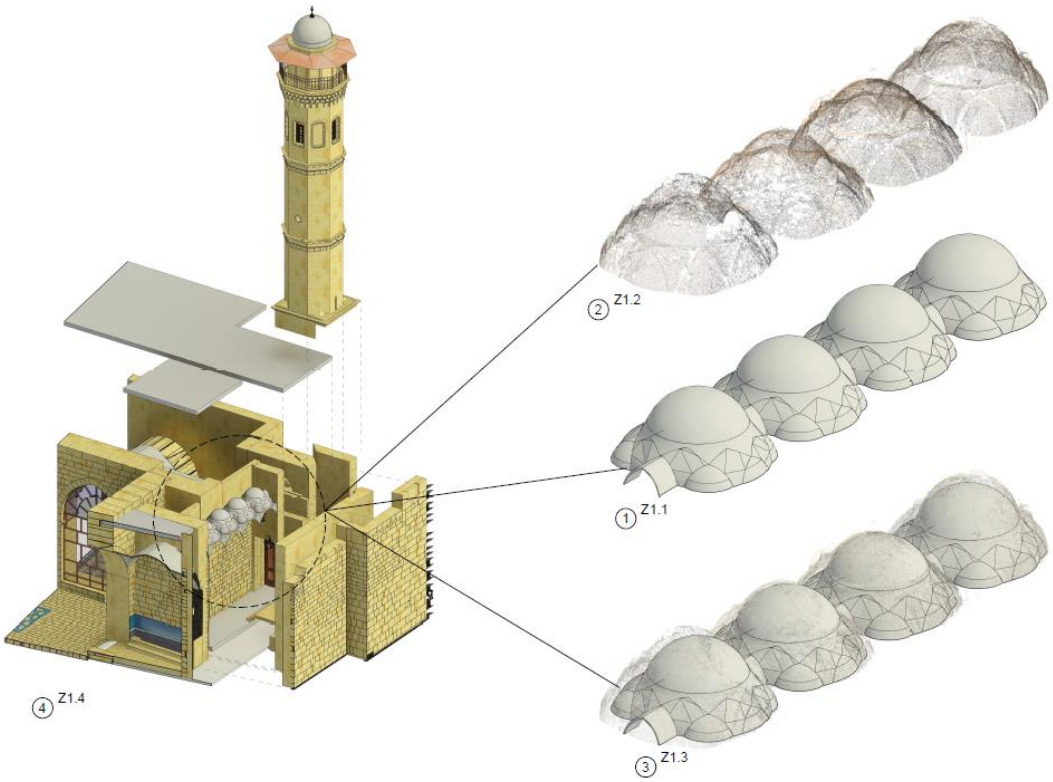

Figure 233: LOD 500 of Internal Dooms at the Corridor, Al-Tunbugha

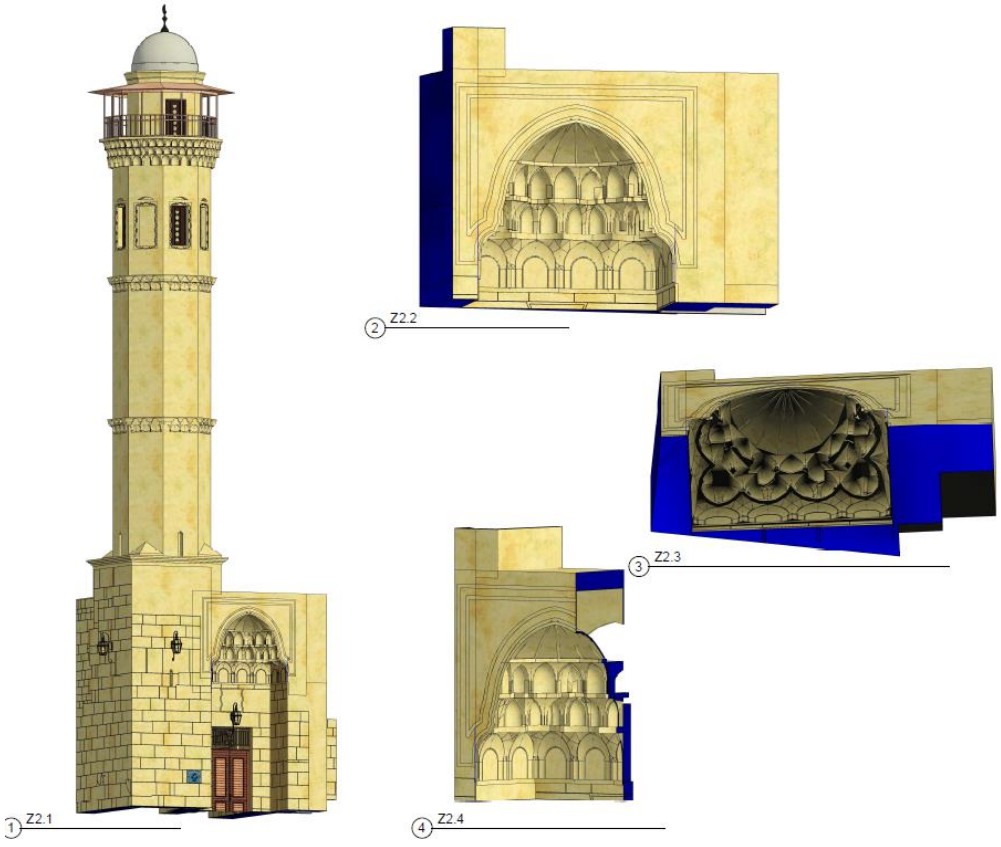

Figure 234: LOD 500 3D Model of Entrance and Stone-by-Stone Ornament, Al-Tunbugha

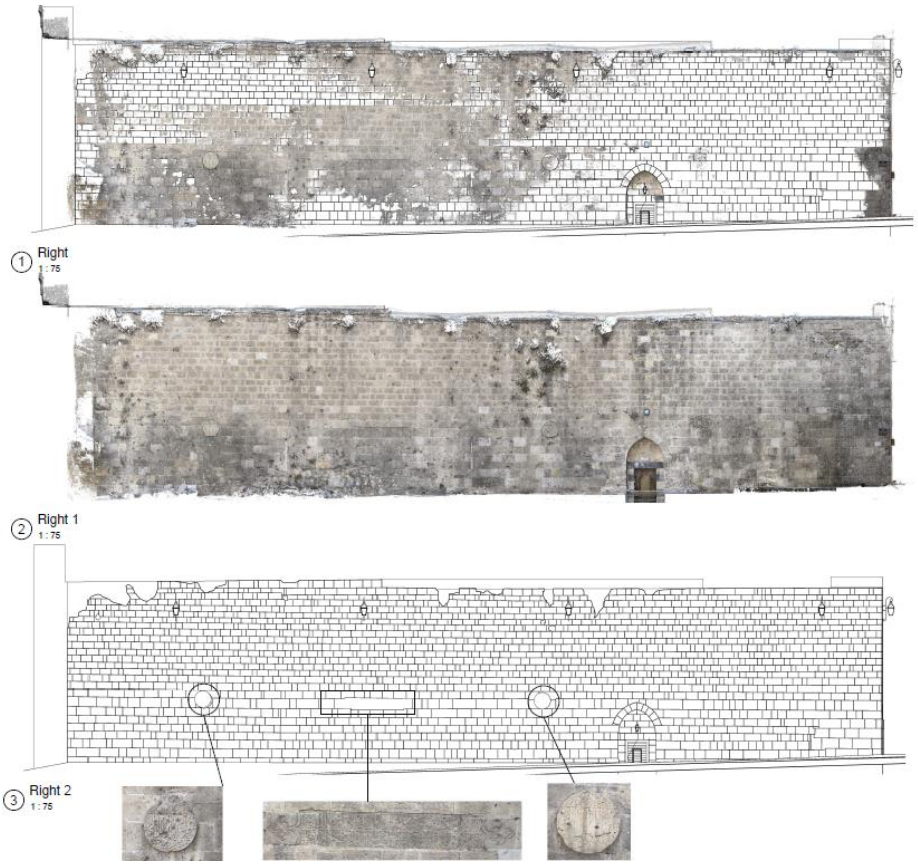

Figure 235: LOD 500 (Stone-by-Stone) of External Wall, Al-Tunbugha

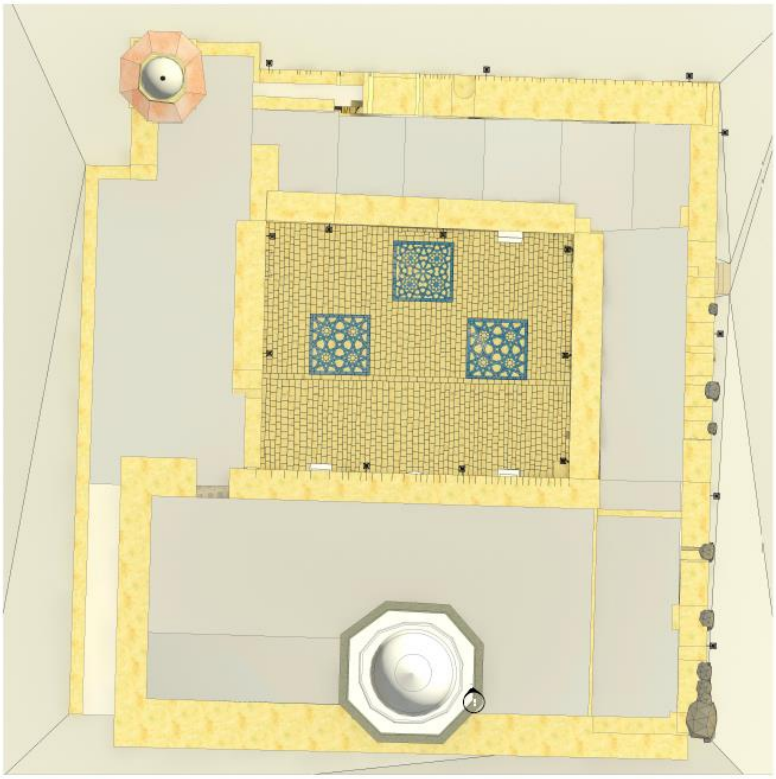

Figure 236: LOD 500 (Marbel-by-Marbel) of Internal Yard, Al-Tunbugha

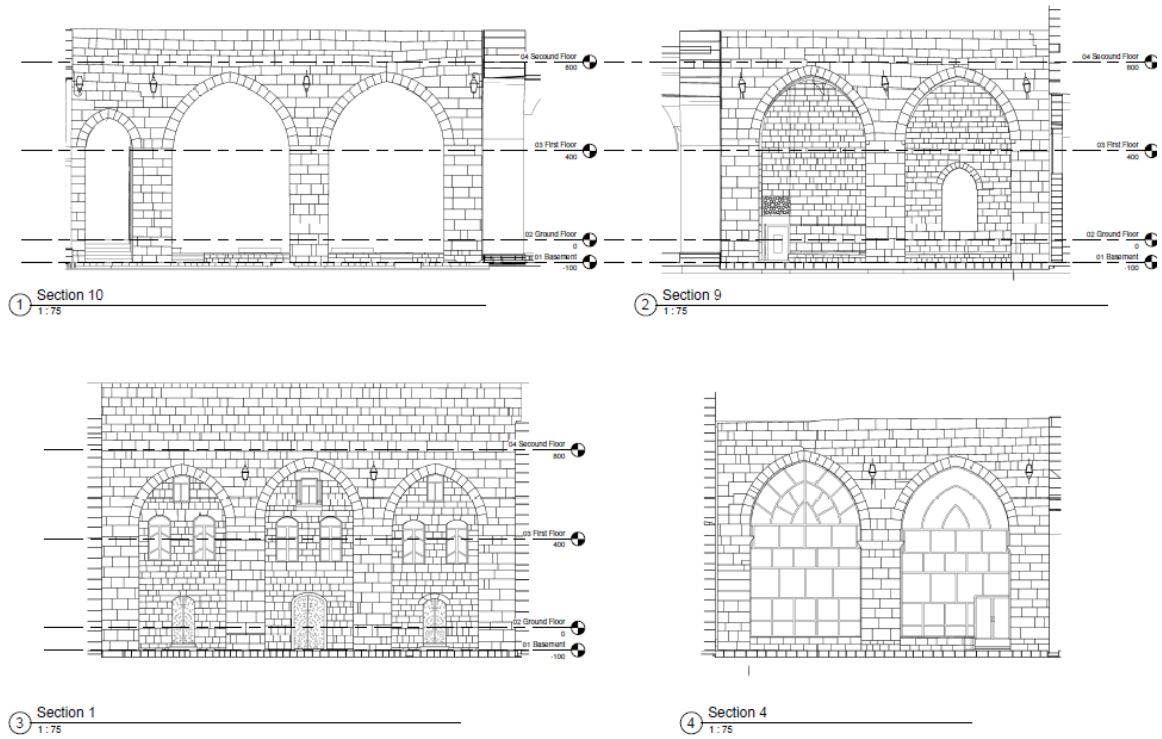

Figure 237: e.g. Interior Facades (Stone-by-Stone), Al-Tunbugha

5.5.2 Rendered Scenes of the LOD 500 HBIM Model[21]

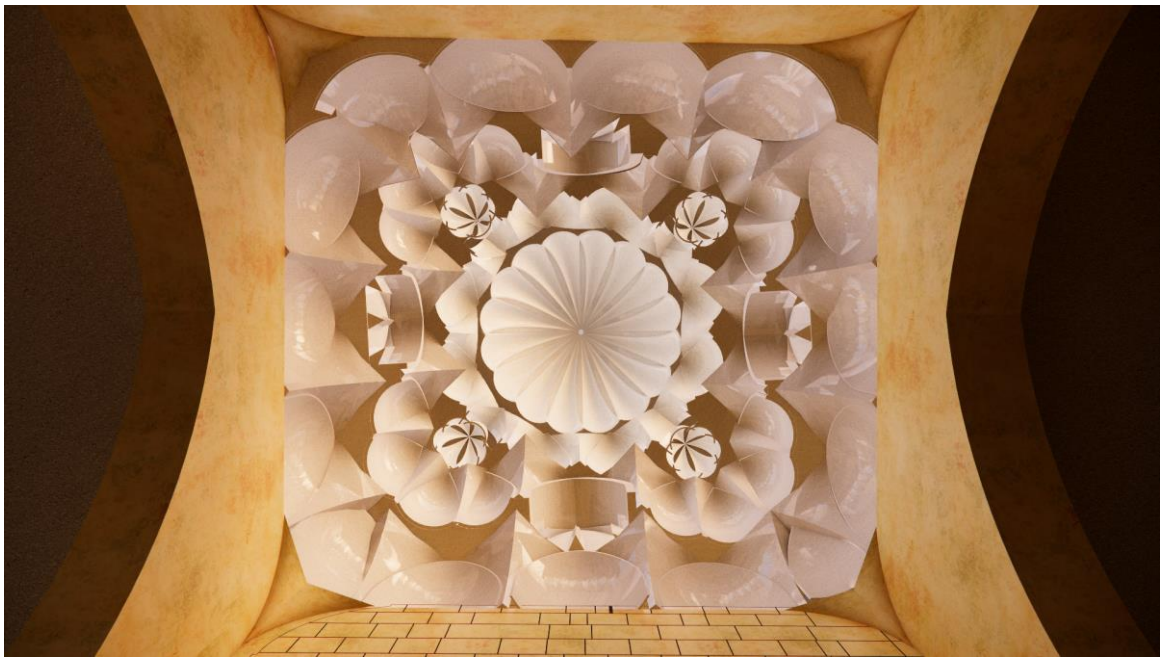

Figure 238: Dome Detailed Decoration, Al-Qublia, Al-Tunbugha

[21] For simulation and demonstration of details (Stone-by-Stone, Ornament-by-Ornament) purposes only.

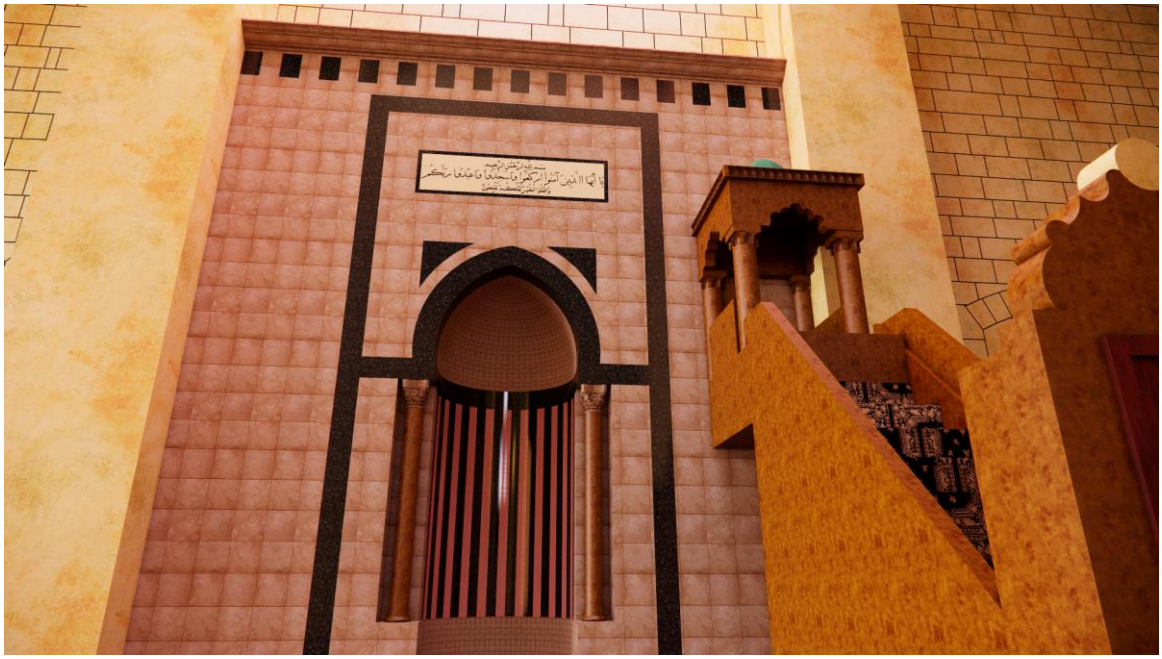

Figure 239: Al-Mehrab Detailed Decoration, Al-Qublia, Al-Tunbugha

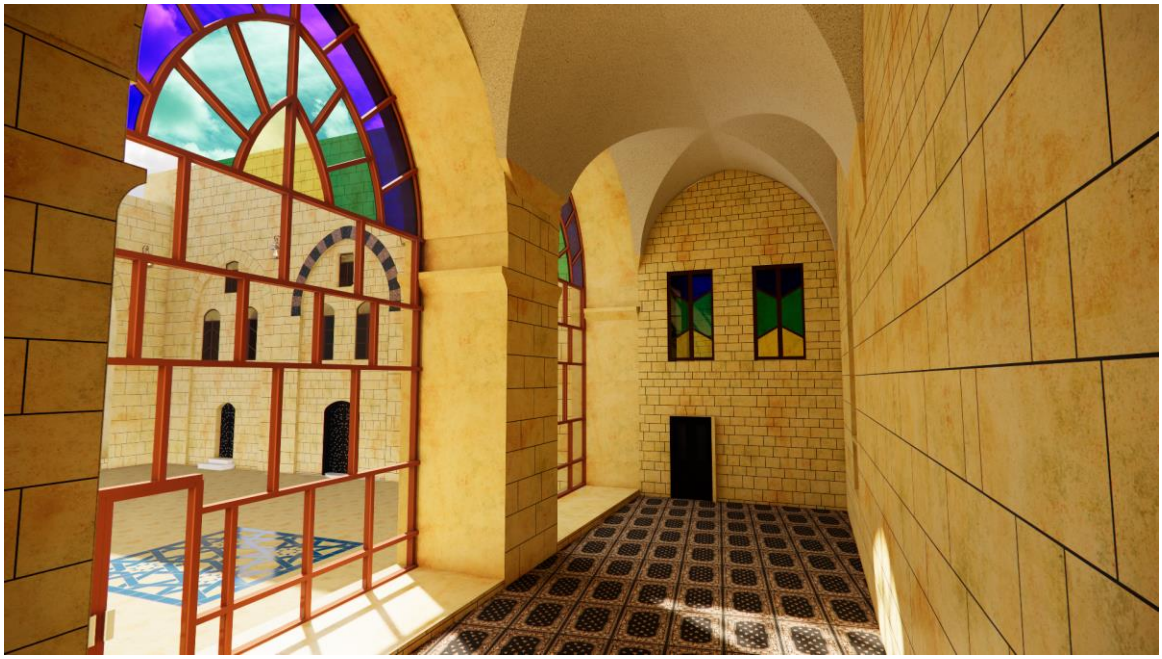

Figure 240: Al-Higazia Hall, Al-Tunbugha

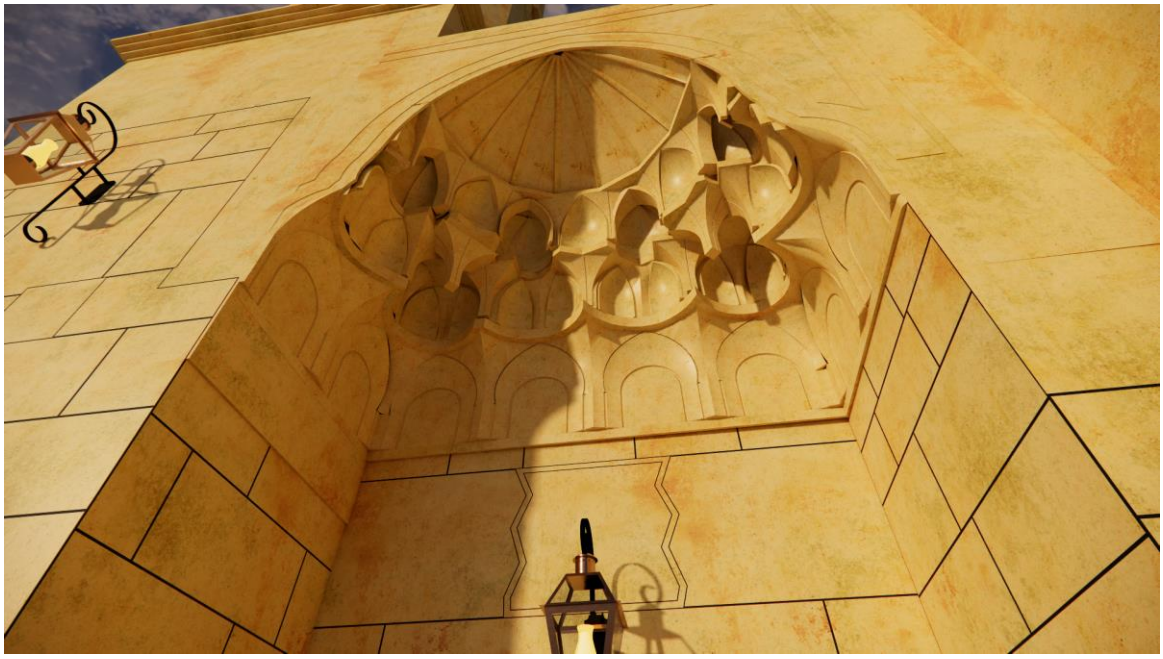

Figure 241: Ornament at the Mosque Entrance, Al-Tunbugha

Figure 242: External View, Al-Tunbugha

Figure 243: Details of the Minaret, Al-Tunbugha

Figure 244: Details of the Internal Yard, Al-Tunbugha

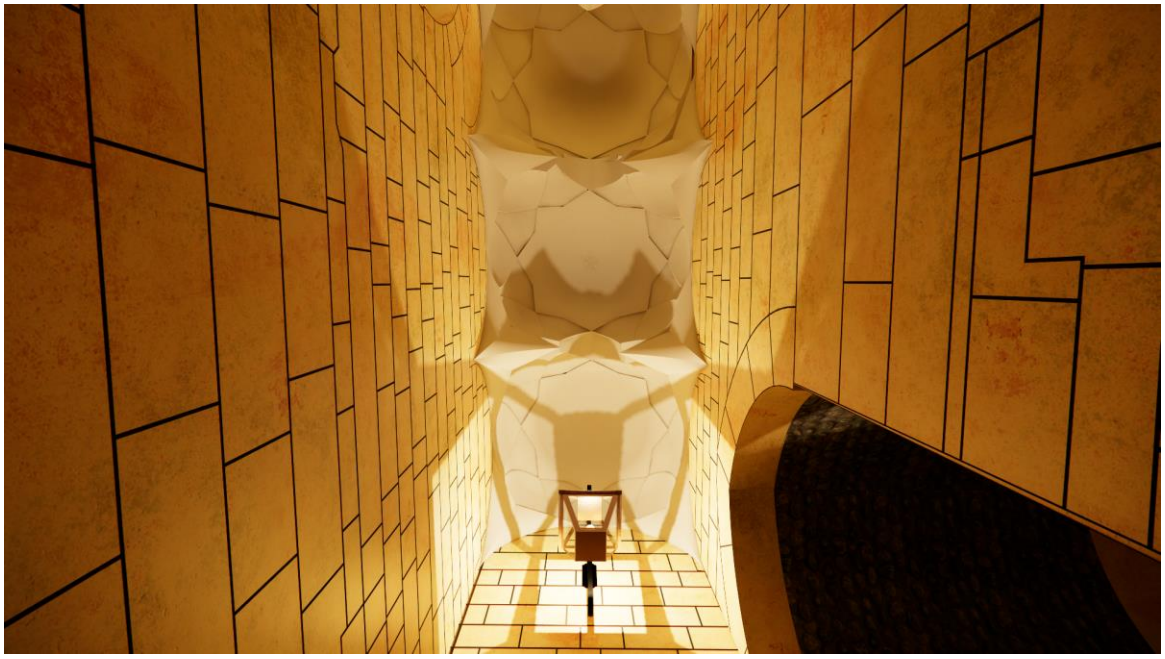

Figure 245: Details of Corridor Domes, Al-Tunbugha

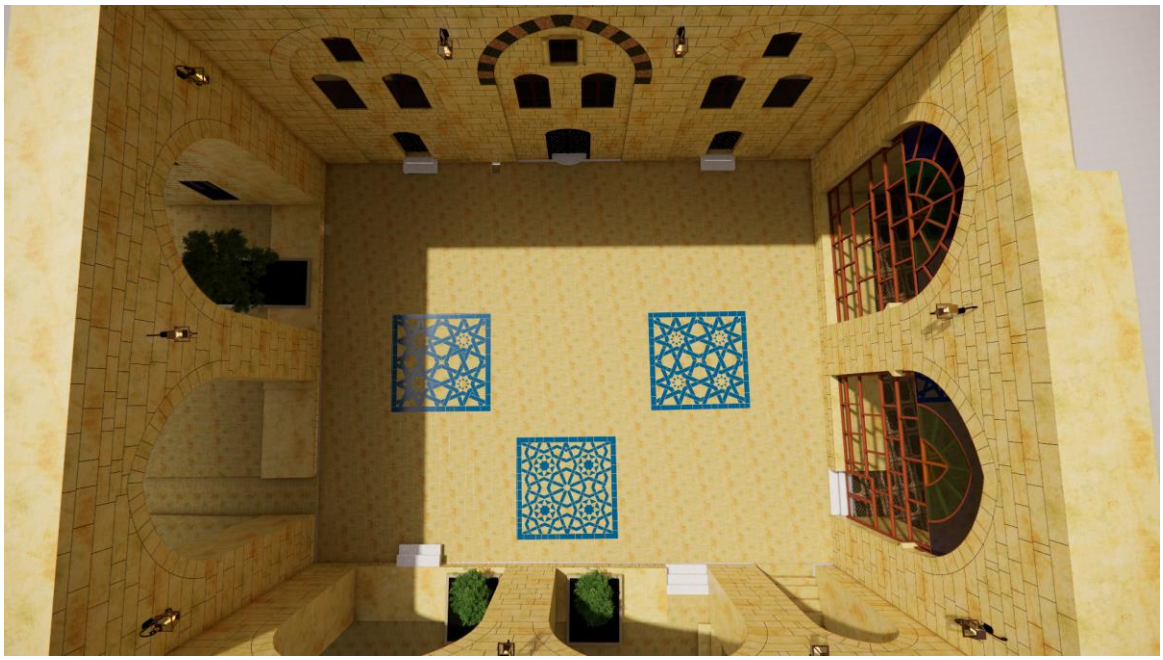

Figure 246: Top View of Yard, Al-Tunbugha

5.6 ACCURACY ANALYSIS AND ERROR RATES (MAIN CASE)

The accuracy analysis addresses geometric fidelity through comparisons between surveyed (reality) data and digital models (photogrammetry and HBIM). The following accuracy metrics were calculated, measured, and applied to the Pilot Case Study:

Table 48: Accuracy Metrics and thresholds, Al-Tunbugha

Output	Comparison reference	
	Reality	Photogrammetry
Photogrammetry	▪ **GCPs Positioning Accuracy** ✓ Absolute Errors ΔX, ΔY, ΔZ ✓ 2D, Vertical, and 3D errors ▪ **Distance Deviations** ✓ Absolute Error Δd ✓ Relative Error (%) ▪ **Angular Deviations** ✓ Absolute Error Δd ✓ Relative Error (%)	N/A
HBIM Model	▪ **Distance Deviations** ✓ Absolute Error Δd ✓ Relative Error (%)	▪ **Distance Deviations** ✓ Absolute Error Δd ✓ Relative Error (%)

5.6.1 GCPs Positioning Accuracy Analysis:

5.6.1.1 *Western Façade Accuracy Analysis*

Figure 247: GCPs errors, Western Façade, Al-Tunbugha

Z error is represented by ellipse color. X,Y errors are represented by ellipse shape. Estimated GCP locations are marked with a dot or crossing.

Table 49: GCPs errors, Western Façade, Al-Tunbugha

Point Name	dX Photo (m)	dY Photo (m)	dZ Photo (m)	2D Err Photo (m)	Vert Err Photo (m)	3D Err Photo (m)	Pass/Fail Photo
A3	0.001	0.001	0.003	0.002	0.003	0.003	PASS
A4	-0.002	0.000	0.002	0.002	0.002	0.003	PASS
A8	-0.005	-0.002	0.003	0.006	0.003	0.006	PASS
A10	0.006	-0.002	-0.007	0.006	0.007	0.009	PASS
A5	0.000	0.000	0.005	0.001	0.005	0.005	PASS
A7	-0.001	0.001	-0.002	0.001	0.002	0.003	PASS
A2	-0.005	0.003	-0.001	0.006	0.001	0.006	PASS
A1	0.007	-0.001	-0.001	0.007	0.001	0.007	PASS

Table 50: Summary Table of GCPs errors, Western Façade, Al-Tunbugha

Metric	Photogrammetry
Max 2D error (m)	0.007233
Mean 2D error (m)	0.003830
Max vertical error (m)	0.007050
Mean vertical error (m)	0.003019
Max 3D error (m)	0.009337
Mean 3D error (m)	0.005307

PASS count	8
FAIL count	0
RMSE 3D	**0.005743**

The Western Façade produced the least reliable accuracy results among the tested surfaces. With a pass rate of 81%, several control points exceeded the strict 1 cm threshold, yielding maximum deviations of up to 0.028 m in 2D and 0.037 m in 3D. Although the mean vertical error (0.006 m) remained compliant, both the mean 2D error (0.014 m) and mean 3D error (0.016 m) surpassed the tolerance, and the RMSE confirmed elevated dispersion across the dataset.

These results suggest that façade orientation and imaging conditions played a role in lowering positional accuracy. Western façades often suffer from strong contrasts and shadowing during image capture, which can reduce tie-point quality and weaken photogrammetric solutions. Additionally, architectural irregularities or occlusions may have contributed to higher local errors.

5.6.1.2 *Southern Façade Accuracy Analysis*

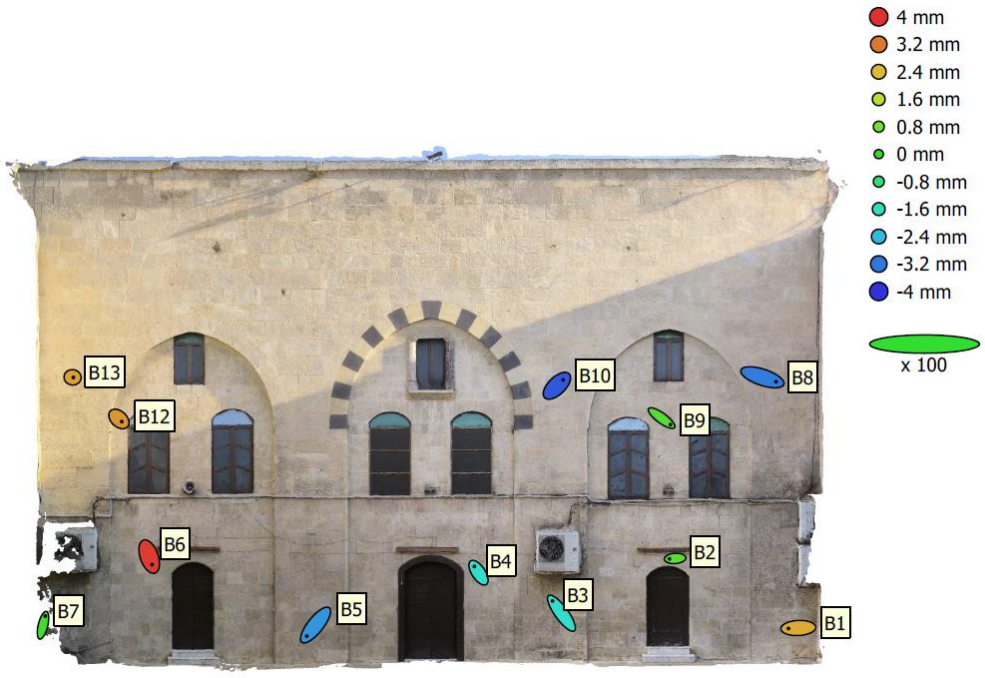

Figure 248: GCPs errors, Southern Façade, Al-Tunbugha

Z error is represented by ellipse color. X,Y errors are represented by ellipse shape. Estimated GCP locations are marked with a dot or crossing.

Table 51: GCPs errors, Southern Façade, Al-Tunbugha

Point Name	dX Photo (m)	dY Photo (m)	dZ Photo (m)	2D Err Photo (m)	Vert Err Photo (m)	3D Err Photo (m)	Pass/Fail Photo
B3	-0.004	0.006	-0.002	0.007	0.002	0.007	PASS
B1	-0.005	0.000	0.003	0.005	0.003	0.005	PASS
B8	0.007	-0.002	-0.003	0.007	0.003	0.008	PASS
B10	0.003	0.003	-0.004	0.004	0.004	0.005	PASS
B9	0.004	-0.003	0.000	0.005	0.000	0.005	PASS
B2	-0.003	0.000	0.001	0.003	0.001	0.003	PASS
B4	-0.002	0.003	-0.002	0.004	0.002	0.004	PASS
B5	-0.004	-0.005	-0.003	0.007	0.003	0.007	PASS
B6	0.001	-0.004	0.004	0.004	0.004	0.006	PASS
B7	0.001	0.004	0.000	0.005	0.000	0.005	PASS
B12	0.001	-0.001	0.003	0.002	0.003	0.003	PASS
B13	0.000	0.000	0.003	0.000	0.003	0.003	PASS

Table 52: Summary Table of GCPs errors, Southern Façade, Al-Tunbugha

Metric	Photogrammetry
Max 2D error (m)	0.007248
Mean 2D error (m)	0.004334
Max vertical error (m)	0.003861
Mean vertical error (m)	0.002189
Max 3D error (m)	0.007579
Mean 3D error (m)	0.005118
PASS count	12
FAIL count	0
RMSE 3D	**0.005378**

The Southern Façade achieved excellent accuracy, with 100% of GCPs passing the 1 cm threshold. Planimetric errors averaged 0.004 m, vertical errors 0.002 m, and the overall 3D RMSE was 0.005 m. Maximum deviations remained below 8 mm, confirming strong internal consistency across the dataset.

5.6.1.3 *Eastern Façade Accuracy Analysis*

Figure 249: GCPs errors, Eastern Façade, Al-Tunbugha

Z error is represented by ellipse color. X,Y errors are represented by ellipse shape. Estimated GCP locations are marked with a dot or crossing.

Table 53: GCPs errors, Eastern Façade, Al-Tunbugha

Point Name	dX Photo (m)	dY Photo (m)	dZ Photo (m)	2D Err Photo (m)	Vert Err Photo (m)	3D Err Photo (m)	Pass/Fail Photo
C2	-0.004	0.002	-0.001	0.004	0.001	0.004	PASS
C1	-0.004	0.000	0.002	0.004	0.002	0.004	PASS
C7	0.002	0.004	-0.004	0.005	0.004	0.006	PASS
C8	0.006	-0.004	0.003	0.007	0.003	0.008	PASS
C4	0.007	-0.005	-0.001	0.009	0.001	0.009	PASS
C3	-0.003	-0.003	0.000	0.004	0.000	0.004	PASS
C5	0.003	-0.002	-0.001	0.003	0.001	0.003	PASS
C6	0.001	0.002	0.001	0.002	0.001	0.003	PASS
C9	-0.008	0.005	0.001	0.009	0.001	0.009	PASS

Table 54: Summary Table of GCPs errors, Eastern Façade, Al-Tunbugha

Metric	Photogrammetry
Max 2D error (m)	0.008905
Mean 2D error (m)	0.005124
Max vertical error (m)	0.004378
Mean vertical error (m)	0.001631
Max 3D error (m)	0.008957

Mean 3D error (m)	0.005514
PASS count	9
FAIL count	0
RMSE 3D	**0.005991**

The Eastern Façade achieved excellent positional accuracy, with every GCP falling below the 1 cm tolerance. Planimetric performance was particularly strong (mean 2D error of 0.005 m), while vertical deviations were negligible (mean 0.002 m). The overall 3D RMSE of 0.006 m confirms consistent accuracy across the dataset, with the maximum observed deviation (0.009 m) remaining within acceptable thresholds.

5.6.1.4 *Northern Façade Accuracy Analysis*

Figure 250: GCPs errors, Northern Façade, Al-Tunbugha

Z error is represented by ellipse color. X,Y errors are represented by ellipse shape. Estimated GCP locations are marked with a dot or crossing.

Table 55: GCPs errors, Northern Façade, Al-Tunbugha

Point Name	dX Photo (m)	dY Photo (m)	dZ Photo (m)	2D Err Photo (m)	Vert Err Photo (m)	3D Err Photo (m)	Pass/Fail Photo
D5	0.000	-0.009	0.006	0.009	0.006	0.011	PASS
D4	-0.003	0.002	-0.001	0.004	0.001	0.004	PASS
D6	0.001	-0.002	0.000	0.002	0.000	0.002	PASS
D7	-0.001	0.003	-0.003	0.003	0.003	0.005	PASS

D1	0.001	-0.009	0.005	0.009	0.005	0.010	PASS
D3	0.000	0.010	-0.005	0.010	0.005	0.011	PASS
D2	0.001	0.004	-0.002	0.005	0.002	0.005	PASS

Table 56: Summary Table of GCPs errors, Northern Façade, Al-Tunbugha

Metric	Photogrammetry
Max 2D error (m)	0.009976
Mean 2D error (m)	0.005903
Max vertical error (m)	0.006311
Mean vertical error (m)	0.003324
Max 3D error (m)	0.011235
Mean 3D error (m)	0.006847
PASS count	7
FAIL count	0
RMSE 3D	**0.007693**

The Northern Façade achieved very good overall accuracy, with every GCP passing the 1 cm threshold despite a few values approaching the limit. The maximum 2D error (0.010 m) sits right at tolerance, and the maximum 3D error (0.011 m) exceeds it only marginally, without impacting the pass classification. Mean values across all metrics remain well below 1 cm (2D = 0.006 m, 3D = 0.007 m), confirming overall stability and reliability of the dataset.

5.6.1.5 *Al-Hegazia Accuracy Analysis*

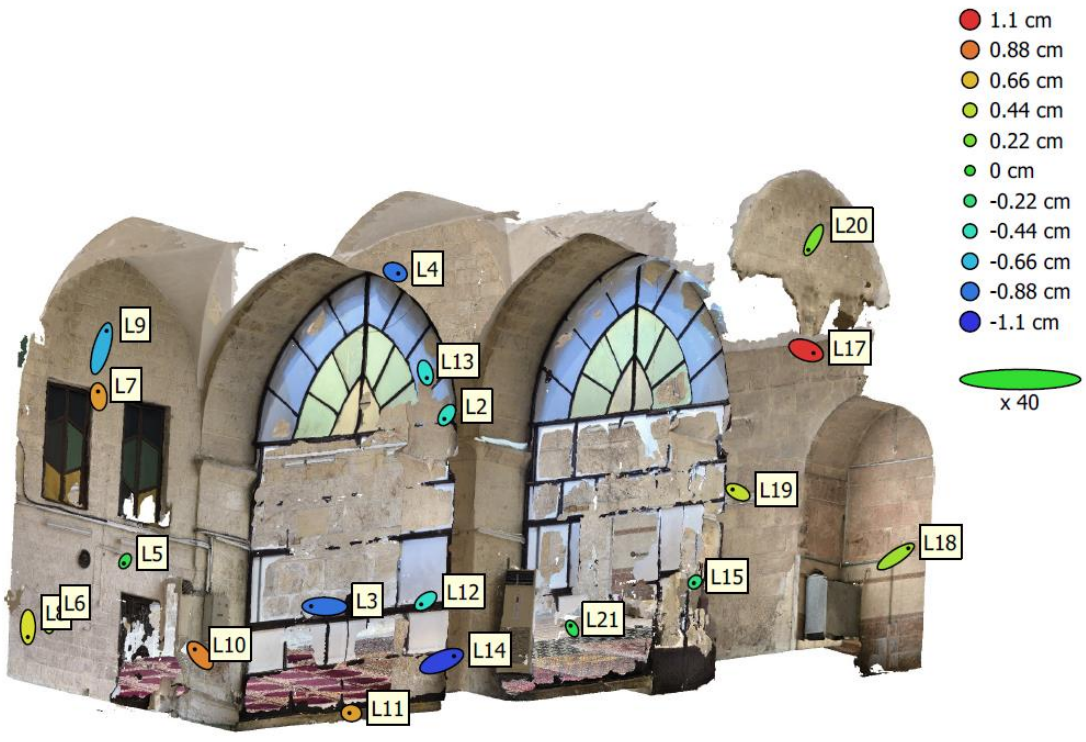

Figure 251: GCPs errors, Al-Higazia, Al-Tunbugha

Z error is represented by ellipse color. X,Y errors are represented by ellipse shape. Estimated GCP locations are marked with a dot or crossing.

Table 57: GCPs errors, Al-Higazia, Al-Tunbugha

Point Name	dX Photo (m)	dY Photo (m)	dZ Photo (m)	2D Err Photo (m)	Vert Err Photo (m)	3D Err Photo (m)	Pass/Fail Photo
L8	0.000	-0.009	0.005	0.009	0.005	0.010	PASS
L6	0.001	-0.008	0.004	0.008	0.004	0.009	PASS
L7	0.000	0.005	0.008	0.005	0.008	0.009	PASS
L5	-0.001	-0.002	-0.001	0.002	0.001	0.003	PASS
L3	-0.012	0.000	-0.009	0.012	0.009	0.015	PASS
L19	-0.005	0.002	0.005	0.005	0.005	0.007	PASS
L12	-0.004	-0.003	-0.005	0.005	0.005	0.007	PASS
L15	-0.001	-0.001	-0.002	0.001	0.002	0.003	PASS
L20	-0.005	-0.009	0.002	0.010	0.002	0.010	PASS
L10	-0.005	0.005	0.008	0.007	0.008	0.011	PASS
L9	0.005	0.016	-0.007	0.016	0.007	0.018	PASS
L14	0.011	0.004	-0.010	0.012	0.010	0.016	PASS
L13	0.001	-0.005	-0.005	0.005	0.005	0.007	PASS
L2	-0.002	-0.003	-0.005	0.004	0.005	0.006	PASS
L4	0.003	-0.001	-0.009	0.003	0.009	0.009	PASS
L18	0.011	0.007	0.004	0.013	0.004	0.014	PASS
L17	0.007	-0.002	0.011	0.007	0.011	0.013	PASS
L21	-0.001	0.003	-0.001	0.003	0.001	0.003	PASS
L11	-0.002	0.000	0.007	0.002	0.007	0.008	PASS

Table 58: Summary Table of GCPs errors, Al-Higazia, Al-Tunbugha

Metric	Photogrammetry
Max 2D error (m)	0.016348
Mean 2D error (m)	0.006775
Max vertical error (m)	0.010920
Mean vertical error (m)	0.005713
Max 3D error (m)	0.017769
Mean 3D error (m)	0.009301
PASS count	19
FAIL count	0
RMSE 3D	**0.010216**

The Al-Higazia façades achieved good overall accuracy, with all 19 GCPs classified as passes, though the dataset shows more dispersion than the dome, southern, and eastern façades. The mean 2D error (0.007 m) and mean vertical error (0.006 m) indicate stable positioning, but maximum deviations reached 1.1 cm vertically and 1.8 cm in 3D, both

slightly exceeding the strict 1 cm tolerance. The overall 3D RMSE (0.010 m) sits on the tolerance boundary, suggesting that while the dataset is generally reliable, isolated points introduce minor instability. Overall, the dataset demonstrates that photogrammetry, when supported by well-distributed GCPs, can achieve sub-centimetric precision in planimetry and near-centimetric accuracy in elevation, validating its reliability for HBIM workflows and detailed heritage recording. The presence of isolated outliers highlights the importance of redundant control points and local error checking, particularly in areas with limited visibility or challenging geometry.

5.6.1.6 *Al-Qublia Accuracy Analysis*

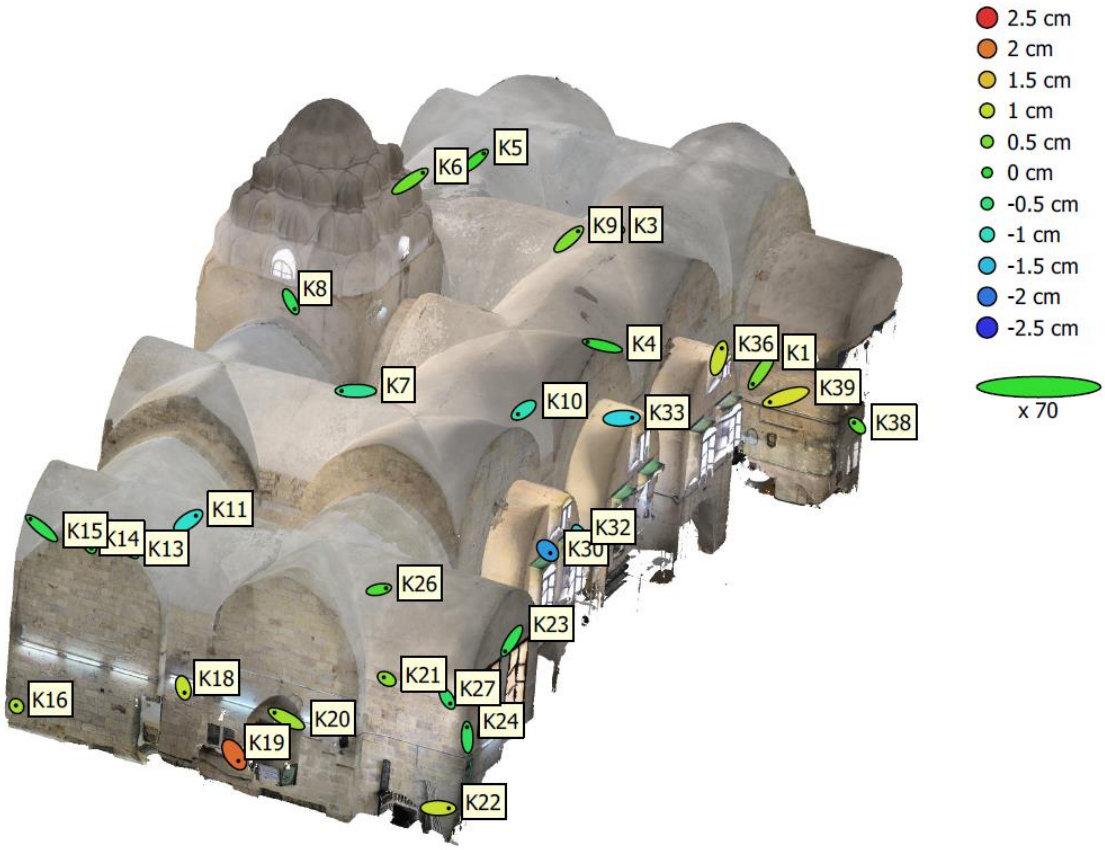

Figure 252: GCPs errors, Al-Qublia, Al-Tunbugha

Z error is represented by ellipse color. X,Y errors are represented by ellipse shape. Estimated GCP locations are marked with a dot or crossing.

Table 59: GCPs errors, Al-Qublia, Al-Tunbugha

Point Name	dX Photo (m)	dY Photo (m)	dZ Photo (m)	2D Err Photo (m)	Vert Err Photo (m)	3D Err Photo (m)	Pass/Fail Photo
K1	-0.008	-0.011	0.005	0.014	0.005	0.015	PASS
K3	-0.003	0.000	0.001	0.003	0.001	0.004	PASS

K4	-0.013	0.003	0.000	0.013	0.000	0.013	PASS
K5	0.008	0.007	0.001	0.010	0.001	0.010	PASS
K6	0.011	0.007	0.005	0.013	0.005	0.014	PASS
K7	-0.012	0.000	-0.007	0.012	0.007	0.014	PASS
K8	0.003	-0.006	-0.003	0.007	0.003	0.008	PASS
K9	0.008	0.007	0.006	0.011	0.006	0.012	PASS
K10	-0.005	-0.004	-0.009	0.006	0.009	0.011	PASS
K11	0.007	0.005	-0.011	0.008	0.011	0.014	PASS
K13	0.012	-0.009	-0.003	0.015	0.003	0.016	PASS
K14	0.001	-0.002	-0.002	0.003	0.002	0.003	PASS
K15	-0.010	0.008	-0.002	0.013	0.002	0.013	PASS
K16	-0.001	0.001	0.009	0.001	0.009	0.009	PASS
K18	0.001	-0.004	0.011	0.004	0.011	0.011	PASS
K19	0.004	-0.006	0.021	0.007	0.021	0.022	FAIL
K20	-0.010	0.005	0.008	0.012	0.008	0.014	PASS
K21	-0.003	0.001	0.007	0.003	0.007	0.007	PASS
K22	0.009	0.000	0.011	0.009	0.011	0.014	PASS
K23	-0.006	-0.009	-0.003	0.011	0.003	0.011	PASS
K24	0.000	0.009	-0.003	0.009	0.003	0.009	PASS
K26	0.006	0.001	0.002	0.006	0.002	0.007	PASS
K27	0.003	-0.004	-0.004	0.005	0.004	0.006	PASS
K30	0.002	-0.002	-0.018	0.003	0.018	0.018	PASS
K32	0.003	-0.008	-0.014	0.009	0.014	0.016	PASS
K33	0.009	0.000	-0.013	0.009	0.013	0.016	PASS
K36	0.003	0.009	0.011	0.009	0.011	0.014	PASS
K38	-0.003	0.002	0.003	0.004	0.003	0.005	PASS
K39	-0.014	-0.004	0.012	0.015	0.012	0.019	PASS

Table 60: Summary Table of GCPs errors, Al-Qublia, Al-Tunbugha

Metric	Photogrammetry
Max 2D error (m)	0.015296
Mean 2D error (m)	0.008449
Max vertical error (m)	0.020941
Mean vertical error (m)	0.007010
Max 3D error (m)	0.021953
Mean 3D error (m)	0.011958
PASS count	28
FAIL count	1
RMSE 3D	**0.012780**

The GCP evaluation demonstrates that the photogrammetric model achieved high positional accuracy, with 96.6% of ground control points passing the 1 cm tolerance threshold. Planimetric accuracy (X and Y) remained consistently reliable, with mean 2D error at 0.008 m, aligning with CIPA/ICOMOS best practice recommendations for heritage

documentation. Vertical accuracy, while more variable, still achieved a mean error of 0.007 m, though one outlier (point K19) produced a vertical deviation exceeding 2 cm, which elevated the overall RMSE to 0.013 m. The maximum 3D deviation (0.022 m) is still within acceptable bounds for large-scale architectural documentation but slightly exceeds the strict 1 cm requirement.

Overall, the dataset demonstrates that photogrammetry, when supported by well-distributed GCPs, can achieve sub-centimetric precision in planimetry and near-centimetric accuracy in elevation, validating its reliability for HBIM workflows and detailed heritage recording. The presence of isolated outliers highlights the importance of redundant control points and local error checking, particularly in areas with limited visibility or challenging geometry.

5.6.1.7 *Exterior Dome Accuracy Analysis (Drone)*

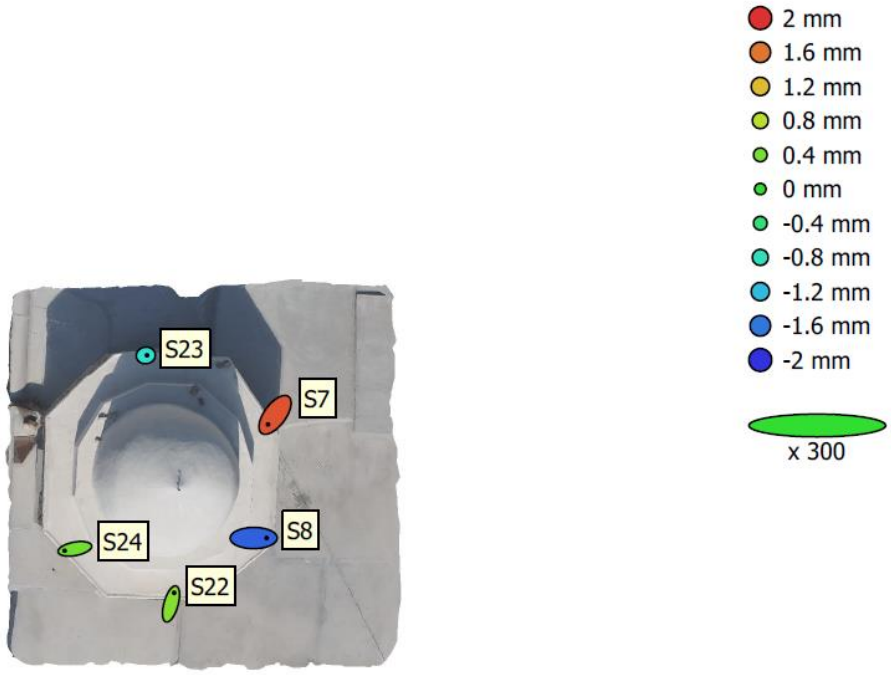

Figure 253: GCPs errors, Exterior Dome, Al-Tunbugha

Z error is represented by ellipse color. X,Y errors are represented by ellipse shape. Estimated GCP locations are marked with a dot or crossing.

Table 61: GCPs errors, Exterior Dome, Al-Tunbugha

Point Name	dX Photo (m)	dY Photo (m)	dZ Photo (m)	2D Err Photo (m)	Vert Err Photo (m)	3D Err Photo (m)	Pass/Fail Photo
S8	0.003	0.000	-0.002	0.003	0.002	0.003	PASS

S7	-0.002	-0.002	0.002	0.003	0.002	0.003	PASS
S22	0.001	0.002	0.000	0.003	0.000	0.003	PASS
S24	-0.002	0.000	0.000	0.002	0.000	0.002	PASS
S23	0.000	0.000	-0.001	0.000	0.001	0.001	PASS

Table 62: Summary Table of GCPs errors, Exterior Dome, Al-Tunbugha

Metric	Photogrammetry
Max 2D error (m)	0.002836
Mean 2D error (m)	0.002108
Max vertical error (m)	0.001802
Mean vertical error (m)	0.001062
Max 3D error (m)	0.003322
Mean 3D error (m)	0.002471
PASS count	5
FAIL count	0
RMSE 3D	**0.002610**

The GCP assessment for the Exterior Dome (Al-Tunbugha) demonstrates exceptional positional accuracy. All control points achieved sub-millimetric to low-millimetric deviations, with 100% passing the 1 cm threshold. Planimetric precision was particularly strong (mean 2D error of 0.002 m), while vertical accuracy (mean 0.001 m) confirms robust elevation control. The 3D error distribution is highly consistent, with a maximum of only 0.003 m and an RMSE of 0.003 m.

Compared to the earlier façade evaluation in the Pilot Case, these results illustrate the benefits of well-distributed GCPs and favorable geometric conditions for image capture around the dome. The dataset comfortably exceeds the accuracy requirements outlined by CIPA/ICOMOS for heritage documentation, validating the reliability of photogrammetry in capturing complex curved surfaces such as domes. This level of precision ensures that the subsequent HBIM modeling can be anchored to highly trustworthy reference data, minimizing the risk of geometric distortion during parametric reconstruction.

5.6.1.8 *Minaret Accuracy Analysis (Drone)*

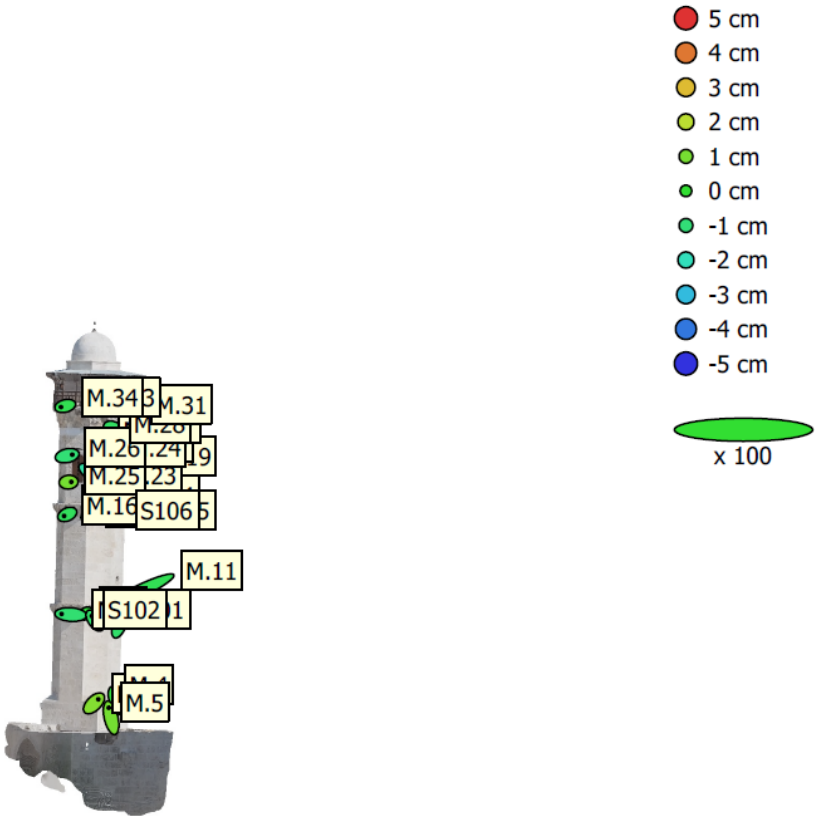

Figure 254: GCPs errors, Minaret, Al-Tunbugha

Z error is represented by ellipse color. X,Y errors are represented by ellipse shape. Estimated GCP locations are marked with a dot or crossing.

Table 63: GCPs errors, Minaret, Al-Tunbugha

Point Name	dX Photo (m)	dY Photo (m)	dZ Photo (m)	2D Err Photo (m)	Vert Err Photo (m)	3D Err Photo (m)	Pass/Fail Photo
M.2	0.005	0.005	0.012	0.007	0.012	0.014	PASS
M.4	0.003	-0.009	-0.002	0.010	0.002	0.010	PASS
M.5	-0.003	0.011	0.010	0.011	0.010	0.015	PASS
M.6	0.003	0.008	-0.008	0.009	0.008	0.012	PASS
M.7	0.003	-0.001	-0.003	0.003	0.003	0.004	PASS
M.8	-0.002	-0.001	-0.002	0.002	0.002	0.003	PASS
M.9	-0.010	0.001	-0.009	0.010	0.009	0.014	PASS
M.11	-0.031	-0.015	-0.005	0.034	0.005	0.035	FAIL
M.14	-0.007	-0.009	-0.010	0.011	0.010	0.015	PASS
M.15	-0.003	-0.001	-0.005	0.004	0.005	0.006	PASS
M.16	-0.004	-0.002	-0.006	0.004	0.006	0.007	PASS
M.19	-0.010	-0.012	0.028	0.016	0.028	0.032	FAIL
M.20	0.002	-0.003	-0.001	0.004	0.001	0.004	PASS
M.21	0.006	-0.010	-0.004	0.012	0.004	0.013	PASS

M.22	-0.006	0.008	0.015	0.010	0.015	0.018	PASS
M.23	0.012	-0.008	-0.017	0.014	0.017	0.022	FAIL
M.24	0.008	0.021	0.045	0.023	0.045	0.050	FAIL
M.25	0.003	0.000	0.010	0.003	0.010	0.010	PASS
M.26	0.006	0.001	-0.010	0.006	0.010	0.011	PASS
M.27	0.003	0.000	-0.006	0.003	0.006	0.007	PASS
M.28	0.004	-0.001	-0.007	0.004	0.007	0.008	PASS
M.31	0.001	0.011	-0.011	0.011	0.011	0.015	PASS
M.33	0.001	-0.002	-0.004	0.002	0.004	0.005	PASS
M.34	-0.005	-0.001	-0.005	0.005	0.005	0.007	PASS
S101	0.010	-0.008	-0.007	0.013	0.007	0.015	PASS
S102	-0.004	0.005	-0.008	0.006	0.008	0.010	PASS
S105	-0.013	-0.002	0.001	0.013	0.001	0.013	PASS
S106	0.000	-0.001	0.000	0.001	0.000	0.001	PASS

Table 64: Summary Table of GCPs errors, Minaret, Al-Tunbugha

Metric	Photogrammetry
Max 2D error (m)	0.034439
Mean 2D error (m)	0.008903
Max vertical error (m)	0.045113
Mean vertical error (m)	0.008878
Max 3D error (m)	0.050434
Mean 3D error (m)	0.013366
PASS count	24
FAIL count	4
RMSE 3D	**0.016972**

The Minaret produced the lowest accuracy among the Al-Tunbugha datasets, with a pass rate of 86% and several outliers exceeding tolerance limits. While the majority of GCPs maintained sub-centimetric to near-centimetric accuracy, a subset of points (notably M.11, M.19, M.23, M.24) showed significant deviations, reaching up to 5 cm in 3D positioning. These errors elevated the overall mean 3D error (0.013 m) and RMSE (0.017 m), placing the dataset just beyond the strict 1 cm accuracy goal.

The challenges are closely tied to the geometry and imaging constraints of tall, slender structures. The minaret's height (22.4m) introduces perspective distortions, weaker tie-point geometry, and greater sensitivity to vertical error. Shadows, occlusions, and the difficulty of achieving consistent overlap across its height likely contributed to the observed outliers.

5.6.1.9 *External Façades Accuracy Analysis (large-scale)*

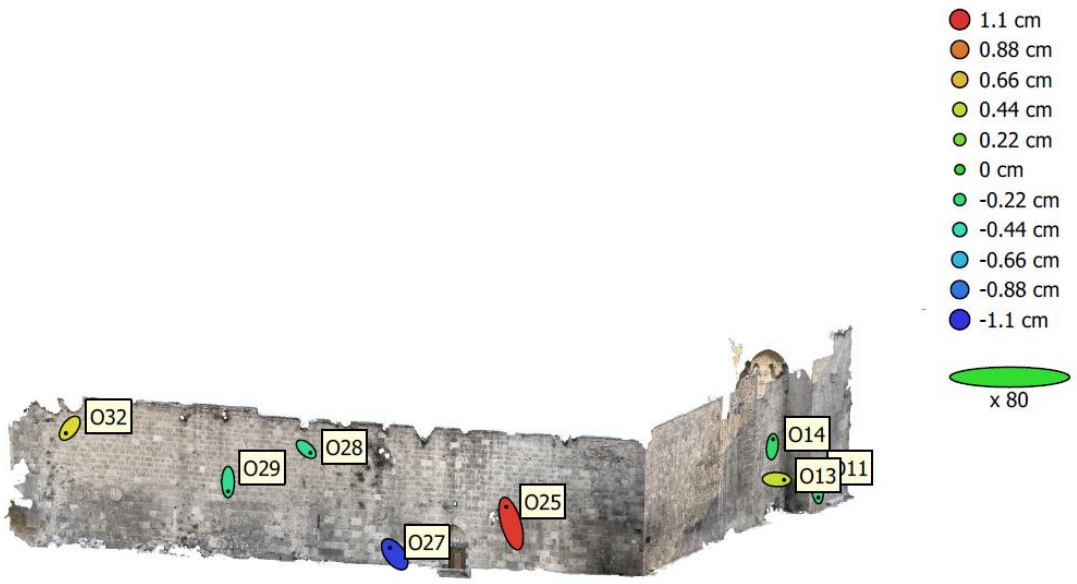

Figure 255: GCPs errors, 5.6.1.9 External Façades, Al-Tunbugha

Z error is represented by ellipse color. X,Y errors are represented by ellipse shape. Estimated GCP locations are marked with a dot or crossing.

Table 65: GCPs errors, 5.6.1.9 External Façades, Al-Tunbugha

Point Name	dX Photo (m)	dY Photo (m)	dZ Photo (m)	2D Err Photo (m)	Vert Err Photo (m)	3D Err Photo (m)	Pass/Fail Photo
O11	-0.005	-0.012	-0.009	0.013	0.009	0.016	PASS
O14	-0.004	0.014	-0.007	0.015	0.007	0.017	PASS
O13	0.005	0.004	-0.002	0.006	0.002	0.006	PASS
O25	-0.003	0.023	0.002	0.024	0.002	0.024	FAIL
O27	-0.003	0.006	-0.021	0.007	0.021	0.022	FAIL
O28	0.010	-0.012	-0.012	0.015	0.012	0.019	PASS
O29	0.003	-0.022	-0.014	0.022	0.014	0.026	FAIL
O32	-0.004	-0.020	-0.005	0.020	0.005	0.021	FAIL

Table 66: Summary Table of GCPs errors, 5.6.1.9 External Façades, Al-Tunbugha

Metric	Photogrammetry
Max 2D error (m)	0.023657
Mean 2D error (m)	0.015249
Max vertical error (m)	0.021229
Mean vertical error (m)	0.009098
Max 3D error (m)	0.025957
Mean 3D error (m)	0.018902
PASS count	4
FAIL count	4

RMSE 3D	**0.019762**

The external façade dataset presents the lowest positional accuracy among the evaluated surfaces, with a pass rate of only 50%. Maximum deviations reached 2.6 cm in 3D and 2.4 cm in 2D, while the mean 3D error (0.019 m) and RMSE (0.020 m) both exceeded the strict 1 cm tolerance. Although half of the control points remained within acceptable limits, the presence of several high outliers (notably O25, O27, O29, and O32) indicates inconsistencies in image alignment and weak control geometry.

The results suggest that this façade suffered from challenging imaging conditions, such as large planar surfaces (83.04m x 8.54m) with fewer textural features for tie points, shadows, or reduced overlap in certain zones. In heritage photogrammetry, these factors are known to degrade local accuracy, especially along extended vertical façades.

5.6.1.10 *Analysis Conclusion*

Table 67: Comparative Accuracy of GCPs Across Surfaces, Al-Tunbugha

Surface / Façade	Max 3D Error (m)	Mean 3D Error (m)	RMSE 3D (m)	Pass Rate (%)	Accuracy Assessment
Exterior Dome	0.003	0.002	0.003	100%	Excellent – sub-millimetric to low-millimetric, highly stable.
Entrance Façade	0.003	0.002	0.003	100%	Excellent – very low dispersion, reliable reference.
Southern Façade	0.008	0.005	0.005	100%	Very good – all points <1 cm, consistent dataset.
Eastern Façade	0.009	0.006	0.006	100%	Very good – stable accuracy, max just under 1 cm.
Northern Façade	0.011	0.007	0.008	100%	Good – close to tolerance, but overall compliant.
Al-Higazia Façade	0.018	0.009	0.010	100%	Moderate – some points >1 cm, but overall pass; borderline tolerance.
Western Façade	0.037	0.016	0.018	81%	Weak – several fails, influenced by orientation/shadowing.
Minaret	0.050	0.013	0.017	86%	Weak – tall geometry caused higher vertical errors, several outliers.
External Façades	0.026	0.019	0.020	50%	Poorest – high dispersion, large planar surfaces with weak tie points.

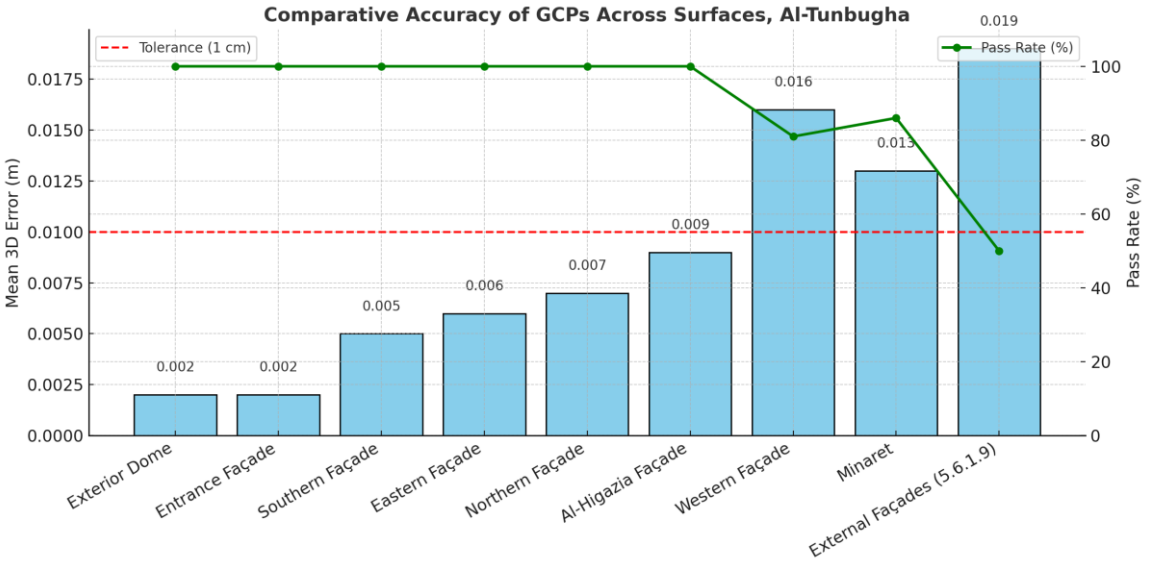

Figure 256: Mean And Max 3D Errors Across Facades & Yard – Al-Takiyya

- The bars show mean 3D error (m) for each surface.
- The red dashed line marks the 1 cm tolerance threshold.
- The green line with dots shows the Pass Rate (%).

Best performance was achieved on the Dome, Entrance, Southern, and Eastern façades, where GCP accuracy was consistently within sub-centimetric limits and pass rates were 100%. These datasets provide a robust foundation for HBIM at LoD 300 (1:50 scale).

The Northern façade and Al-Higazia façade performed slightly weaker, with maximum 3D errors reaching or exceeding 1–2 cm. While still acceptable for heritage documentation, they sit on the threshold for stricter applications and highlight the importance of imaging conditions (illumination, overlap).

The Western façade, Minaret, and especially the External façades exhibited significant deviations, with maximum errors up to 5 cm and lower pass rates (81%, 86%, 50%). These surfaces demonstrate the vulnerability of photogrammetry on shadowed orientations, tall slender geometries, and large planar walls with limited texture.

The results confirm that geometry and orientation strongly influence accuracy, with curved and well-lit surfaces (dome, south/east façades) outperforming vertical, shaded, or geometrically complex surfaces (minaret, external façades). These insights emphasize the need for workflow optimization through denser oblique imagery, improved GCP distribution, and supplementary surveying to stabilize the weakest zones.

Overall, the photogrammetry-derived model demonstrated accuracy that generally meets the required tolerance levels, confirming its **reliability for heritage documentation.** The resulting point cloud not only preserves the necessary metric fidelity but also serves as a robust foundation for **subsequent translation into the BIM environment**, ensuring that both geometric precision and semantic structuring can be effectively integrated

5.6.2 Angular Deviation Accuracy Analysis

Table 68: Angular Deviation, Al-Tunbuga

Façade	Angle Points	Computed Angle (°)	Measured Angle (°) ⇦ INPUT	Δ Angle (°)	| Δ Angle (°) |	|Relative Error (%) |	Pass/ Fail
Exterior Façades	O16 **O19** O20	146.6963	146.6945	0.0018	0.0018	0.0012%	PASS
Eastern Corridor	I13 **I3** I2	52.7746	52.7738	0.0008	0.0008	0.0016%	PASS
Hajezia Hall	L3 **L2** L4	110.4184	110.4171	0.0013	0.0013	0.0012%	PASS
Western Façade	A3 **A4** A8	40.6141	40.6091	0.0050	0.0050	0.0124%	PASS
Southern Façade	B3 **B1** B8	80.3486	80.3484	0.0002	0.0002	0.0002%	PASS
Eastern Façade	C2 **C1** C7	12.2920	12.2914	0.0006	0.0006	0.0050%	PASS
Northern Façade	D5 **D4** D6	72.2362	72.2351	0.0011	0.0011	0.0015%	PASS
Al-Qublia Hall	K1 **K3** K4	60.2635	60.2619	0.0016	0.0016	0.0027%	PASS
Internal Yard	E6 **E5** E1	174.0452	174.0453	-0.0001	0.0001	0.0001%	PASS
Rooftop	S1 **S2** S3	85.6857	85.5552	0.1305	0.1305	0.1523%	PASS
Minaret	M1 **M2** M5	19.6843	19.6489	0.0354	0.0354	0.1800%	PASS

Table 69: Summary of Angular Deviation Analysis

Summary	Value
Absolute angle (degrees)	
n (samples)	11
Bias (mean signed Δθ) = average of Δθ (detects systematic rotation)	0.0162
Precision (SD) = std. dev. of Δθ	0.039281589
MAE = mean(|Δθ|)	0.0016
RMSE = √(mean(Δθ²))	0.00178939
P95(|Δθ|) = 95th percentile of |Δθ|	0.003895964
Max(|Δθ|) = worst case	0.0050
Pass rate = % meeting thresholds	11
Relative error (%)	
Mean |RelErr|%	0.0032%
Median |RelErr|	0.0015%
P95 |RelErr|%	9.83111E-05
Max |RelErr|	0.0124%

Thresholds used: Absolute tolerance = 0.20°; Relative tolerance = 0.2%. Both must be satisfied to pass.

The angular deviation analysis confirms that the photogrammetric dataset **achieved very high geometric stability** across all tested points. Out of 11 computed angles, all passed the tolerance thresholds, yielding a 100% pass rate. The observed deviations were minimal:

- The maximum absolute deviation was only 0.005°, far below the 0.20° tolerance.
- The maximum relative error reached just 0.0124%, compared with the 0.2% threshold.
- The mean absolute error (MAE) was 0.0016°, and the RMSE was 0.0018°, both demonstrating sub-thousandth-of-a-degree accuracy.
- The 95th percentile of |Δθ| was 0.0039°, confirming that even the largest majority of measurements remained an order of magnitude below the defined limit.

The summary metrics also indicate negligible systematic rotation, with a bias of 0.016°, and a tight distribution (SD = 0.039°). The rooftop (S2) and minaret (M2) angles showed the largest deviations (0.130° and 0.035° respectively), yet both comfortably satisfied the threshold.

Interpretation for HBIM

These results validate that the photogrammetric reconstruction is angularly robust, with errors consistently an order of magnitude below the tolerance limits recommended for heritage HBIM. The negligible deviation ensures that the model preserves not only linear accuracy but also the geometric relationships between architectural elements, which is critical for parametric modeling and structural interpretation.

In practical terms, this means that angles can be trusted for LoD 300–500 applications without concern for cumulative distortion, strengthening the suitability of the dataset as a foundation for BIM-based conservation documentation.

5.6.3 Distance Deviation Accuracy Analysis

5.6.3.1 *Reality-Photogrammetry Distance Deviation*

Table 70: Reality-Photogrammetry Distance Deviation

Façade	Direction	Reality (m)	Ortho (m)	Δd (m)	Relative Err (%)	Pass /Fail
Exterior (Side) Façade	Horizontal	1.480	1.480	0.000	0.000%	PASS
	Vertical	1.550	1.530	0.020	1.290%	PASS
	Inclined	1.210	1.210	0.000	0.000%	PASS
Exterior (Eastern) Façade	Horizontal	1.550	1.550	0.000	0.000%	PASS
	Vertical	1.480	1.490	0.010	0.676%	PASS
Exterior (Western) Façade	Horizontal	3.440	3.420	0.020	0.581%	PASS
	Vertical	2.060	2.050	0.010	0.485%	PASS
Hegazia Facades	Horizontal	2.840	2.815	0.025	0.880%	FAIL
	Vertical	1.960	1.940	0.020	1.020%	PASS
	Inclined	1.610	1.600	0.010	0.621%	PASS
Western Façade	Horizontal	1.760	1.750	0.010	0.568%	PASS
	Vertical	2.350	2.360	0.010	0.426%	PASS
	Inclined	3.180	3.170	0.010	0.314%	PASS
Southern Façade	Horizontal	1.750	1.740	0.010	0.571%	PASS
	Vertical	1.850	1.850	0.000	0.000%	PASS
	Inclined	2.920	2.920	0.000	0.000%	PASS
Eastern Façade	Horizontal	1.760	1.740	0.020	1.136%	PASS
	Vertical	2.275	2.270	0.005	0.220%	PASS
	Inclined	1.810	1.790	0.020	1.105%	PASS
Eastern Façade Gallery	Horizontal	1.240	1.230	0.010	0.806%	PASS
	Vertical	1.340	1.330	0.010	0.746%	PASS
	Inclined	1.355	1.340	0.015	1.107%	PASS
Northern Façade	Horizontal	1.775	1.770	0.005	0.282%	PASS
	Vertical	1.335	1.310	0.025	1.873%	FAIL
Northern Façade Gallery	Horizontal	2.450	2.440	0.010	0.408%	PASS

	Vertical	0.720	0.700	0.020	2.778%	FAIL
Mihrab Al-Qublia	Vertical	2.050	2.030	0.020	0.976%	PASS
Al-Qublia (West)	Horizontal	1.495	1.460	0.035	2.341%	FAIL
Al-Qublia (East)	Horizontal	1.550	1.540	0.010	0.645%	PASS
Al-Qublia (North)	Vertical	1.910	1.900	0.010	0.524%	PASS
Internal Yard	Horizontal	3.620	3.610	0.010	0.276%	PASS
	Vertical	3.665	3.660	0.005	0.136%	PASS
	Inclined	5.154	5.150	0.004	0.078%	PASS
Rooftop	Horizontal	14.890	14.900	0.010	0.067%	PASS
	Vertical	18.630	18.600	0.030	0.161%	FAIL
	Inclined	23.890	23.900	0.010	0.042%	PASS
Minaret	Horizontal	1.033	1.030	0.003	0.290%	PASS
	Vertical	1.195	1.190	0.005	0.418%	PASS

*photos of measured distances are within the online supplementary materials.

Façade	Direction	Arithmetic Mean (average error)	RMSE	Maximum error (worst-case Δd)
Exterior (Side) Façade	Horizontal Vertical Inclined	0.007	0.012	0.020
Exterior (Eastern) Façade	Horizontal Vertical	0.005	0.007	0.010
Exterior (Western) Façade	Horizontal Vertical	0.015	0.016	0.020
Hegazia Facades	Horizontal Vertical Inclined	0.018	0.019	0.025
Western Façade	Horizontal Vertical Inclined	0.010	0.010	0.010
Southern Façade	Horizontal Vertical Inclined	0.003	0.006	0.010
Eastern Façade	Horizontal Vertical Inclined	0.015	0.017	0.020
Eastern Façade Gallery	Horizontal Vertical Inclined	0.012	0.012	0.015
Northern Façade	Horizontal Vertical	0.015	0.018	0.025
Northern Façade Gallery	Horizontal Vertical	0.015	0.016	0.020
Mihrab Al-Qublia	Vertical	0.020	0.020	0.020
Al-Qublia (West)	Horizontal	0.035	0.035	0.035
Al-Qublia (East)	Horizontal	0.010	0.010	0.010
Al-Qublia (North)	Vertical	0.010	0.010	0.010
Internal Yard	Horizontal	0.006	0.007	0.010

	Vertical			
	Inclined			
Rooftop	Horizontal	0.017	0.019	0.030
	Vertical			
	Inclined			
Minaret	Horizontal	0.004	0.004	0.005
	Vertical			

The comparison of measured (reality) and orthophoto-derived (photogrammetry) distances demonstrates generally high compliance with the defined tolerance levels, with localized exceptions. Out of the tested façades and structural elements, the majority of horizontal, vertical, and inclined distances passed, confirming that the photogrammetric model preserves geometric fidelity across different orientations.

Overall, the dataset demonstrates that photogrammetry achieved sub-centimetric to near-centimetric accuracy in >80% of tested elements, fully supporting HBIM integration at LoD 300-500. However, the failed cases underscore the importance of complementary surveying techniques (e.g., total station, denser oblique drone imagery, or CAD-based correction) to strengthen weak zones and ensure that all façades meet strict documentation standards.

5.6.3.2 *Reality-HBIM Distance Deviation*

Table 71: Reality-HBIM Distance Deviation

Façade	Direction	Reality (m)	Revit (m)	Δd (m)	Relative Err (%)	Pass /Fail
Exterior (Side) Façade	Horizontal	1.480	1.500	0.020	1.351%	PASS
	Vertical	1.550	1.530	0.020	1.290%	PASS
	Inclined	1.210	1.206	0.004	0.331%	PASS
Exterior (Eastern) Façade	Horizontal	1.550	1.548	0.002	0.129%	PASS
	Vertical	1.480	1.500	0.020	1.351%	PASS
Exterior (Western) Façade	Horizontal	3.440	3.420	0.020	0.581%	PASS
	Vertical	2.060	2.010	0.050	2.427%	FAIL
Hegazia Facades	Horizontal	2.840	2.810	0.030	1.056%	FAIL
	Vertical	1.960	1.951	0.009	0.459%	PASS
	Inclined	1.610	1.600	0.010	0.621%	PASS
Western Façade	Horizontal	1.760	1.761	0.001	0.057%	PASS
	Vertical	2.350	2.340	0.010	0.426%	PASS
	Inclined	3.180	3.181	0.001	0.031%	PASS
Southern Façade	Horizontal	1.750	1.742	0.008	0.457%	PASS
	Vertical	1.850	1.842	0.008	0.432%	PASS
	Inclined	2.920	2.900	0.020	0.685%	PASS
Eastern Façade	Horizontal	1.760	1.769	0.009	0.511%	PASS

	Vertical	2.275	2.282	0.007	0.308%	PASS
	Inclined	1.810	1.810	0.000	0.000%	PASS
Eastern Façade Gallery	Horizontal	1.240	1.243	0.003	0.242%	PASS
	Vertical	1.340	1.336	0.004	0.299%	PASS
	Inclined	1.355	1.348	0.007	0.517%	PASS
Northern Façade	Horizontal	1.775	1.757	0.018	1.014%	PASS
	Vertical	1.335	1.301	0.034	2.547%	FAIL
Northern Façade Gallery	Horizontal	2.450	2.430	0.020	0.816%	PASS
	Vertical	0.720	0.700	0.020	2.778%	FAIL
Mihrab Al-Qublia	Vertical	2.050	2.040	0.010	0.488%	PASS
Al-Qublia (West)	Horizontal	1.495	1.462	0.033	2.207%	FAIL
Al-Qublia (East)	Horizontal	1.550	1.560	0.010	0.645%	PASS
Al-Qublia (North)	Vertical	1.910	1.924	0.014	0.733%	PASS
Internal Yard	Horizontal	3.620	3.605	0.015	0.414%	PASS
	Vertical	3.665	3.650	0.015	0.409%	PASS
	Inclined	5.154	5.150	0.004	0.078%	PASS
Rooftop	Horizontal	14.890	14.910	0.020	0.134%	PASS
	Vertical	18.630	18.587	0.043	0.231%	FAIL
	Inclined	23.890	23.915	0.025	0.105%	FAIL
Minaret	Horizontal	1.033	1.030	0.003	0.290%	PASS
	Vertical	1.195	1.177	0.018	1.506%	PASS

Façade	Arithmetic Mean (average error)	Root Mean Square Error (RMSE)	Maximum error (worst-case Δd)
Exterior (Side) Façade	0.015	0.016	0.020
Exterior (Eastern) Façade	0.011	0.014	0.020
Exterior (Western) Façade	0.035	0.038	0.050
Hegazia Facades	0.016	0.019	0.030
Western Façade	0.004	0.006	0.010
Southern Façade	0.012	0.013	0.020
Eastern Façade	0.005	0.007	0.009
Eastern Façade Gallery	0.005	0.005	0.007
Northern Façade	0.026	0.027	0.034

Northern Façade Gallery	0.020	0.020	0.020
Mihrab Al-Qublia	0.010	0.010	0.010
Al-Qublia (West)	0.033	0.033	0.033
Al-Qublia (East)	0.010	0.010	0.010
Al-Qublia (North)	0.014	0.014	0.014
Internal Yard	0.011	0.012	0.015
Rooftop	0.029	0.031	0.043
Minaret	0.011	0.013	0.018

Compared with the Reality–Photogrammetry analysis, the HBIM deviations are consistently higher, reflecting the trade-off between metric fidelity and parametric abstraction inherent in BIM modeling. While photogrammetry captures surface irregularities with high fidelity, HBIM workflows necessitate fitting to parametric objects (walls, arches, roofs), which simplifies complex geometries and introduces discrepancies in localized features.

The analysis shows that while most façades and architectural elements remain within LoD 300-500 tolerances, several outliers—particularly the Western Exterior, Northern Façade and Gallery, Al-Qublia West, and Rooftop—indicate areas where parametric modeling diverged notably from measured reality. These failures highlight the need for composite workflows (e.g., hybrid HBIM with point cloud overlays) when precision documentation of irregular or non-orthogonal heritage geometries is required.

5.7 PERFORMANCE EVALUATION (MAIN CASE)

From a **resource perspective**, the photogrammetry-to-HBIM pipeline demanded substantial computing capacity, with ultra-high resolution point clouds requiring extended processing times and significant storage space. While image capture and point cloud generation were relatively cost-effective compared to traditional surveying, the downstream HBIM modeling proved resource-intensive. Parametric reconstruction of irregular heritage geometries involved considerable manual effort, raising both the time and labor costs relative to photogrammetry alone.

In terms of **visualization and usability**, the outcomes demonstrate clear benefits for heritage documentation. The photogrammetry-derived orthomosaics and point clouds captured fine surface detail with sub-centimetric precision, ensuring fidelity to the monument's fabric. HBIM added value by structuring this geometry into semantically rich, parametric components that can be queried, layered, and reused in conservation planning. However, this came at the cost of reduced geometric fidelity in certain areas (e.g., the Northern Gallery, Al-Qublia West, and Rooftop), where simplification inherent in HBIM diverged from measured reality.

Overall, the main case confirms that the **Photogrammetry-Driven HBIM** approach offers a balanced trade-off: while more time- and cost-intensive than photogrammetry alone, it delivers a product that is both metrically reliable and semantically usable for heritage management. The resulting model not only supports documentation at LOD 500 but also provides a robust platform for integration into conservation workflows, monitoring programs, and digital heritage archives.

5.8 COMPARATIVE OBSERVATIONS

Pilot Case

- Medium-resolution point clouds; insufficient for fine architectural detail.
- CAD had to be reintroduced as a corrective step, adding time and cost.
- Angular deviations less stable.
- More scattered errors; some façades exceeded tolerance thresholds.
- Workflow coherence weaker; iterative back-and-forth between steps.
- Served primarily as a methodological calibration exercise.

Main Case

- High-resolution, better-planned point clouds with improved GCP distribution.
- Drone imagery added for rooftop, dome, and minaret → fuller coverage.
- Angular deviation much more stable (max 0.005°).
- Errors more localized (northern façades, Al-Qublia West, rooftop verticals).
- Reduced reliance on CAD; more direct photogrammetry → HBIM workflow.
- Higher cost and processing time, but streamlined and better optimized.
- Produced consistent LoD 500 HBIM outputs (stone-by-stone), fully usable for heritage documentation.

CHAPTER 6. CONCLUSIONS AND RECOMMENDATIONS

6.1 SUMMARY OF FINDINGS

6.1.1 Pilot Case Study

The pilot study provided a critical testing ground for refining the workflow. It highlighted the limitations of medium-resolution point clouds and revealed the need for CAD as a corrective step when photogrammetric outputs were insufficient. Accuracy analysis showed overall compliance with CIPA/ICOMOS standards, though angular deviations and vertical errors in rooftop captures were less stable. The pilot ultimately functioned as a methodological calibration, clarifying where resources and adjustments should be focused in the main case.

6.1.2 Main Case Study

The main case achieved higher consistency and precision through improved image acquisition strategies, denser GCP distribution, higher quality of produced points clouds, and targeted drone use for otherwise inaccessible areas such as the dome, rooftop, and minaret. Photogrammetry-derived models demonstrated sub-centimetric accuracy in most façades, while HBIM integration structured this geometry into semantically enriched models. Failures were limited to localized areas such as the Northern façade, Al-Qublia West, and rooftop verticals, where geometric complexity or parametric simplifications introduced greater deviations.

6.1.3 From Comparative Analysis

A comparison of the pilot and main case confirmed that workflow refinements—better planning, higher point cloud resolution, and hybrid acquisition strategies—significantly improved accuracy and efficiency. While HBIM consistently introduced higher deviations than photogrammetry, it provided added value in semantic organization, usability, and conservation potential. Overall, the main case produced HBIM models at LoD 500 that balanced metric fidelity with practical usability for heritage documentation in Syria.

6.2 CONTRIBUTIONS OF THE RESEARCH

6.2.1 Methodological Contributions

The research developed and tested a structured photogrammetry-to-HBIM workflow adapted to the challenges of documenting irregular and at-risk heritage in Syria. By critically comparing pilot and main case results, it demonstrated how workflow optimization—particularly through drone integration, careful GCP placement, and tolerance-based evaluation—can enhance both accuracy and efficiency. The study also underscored the value of hybrid approaches, where photogrammetric fidelity is preserved by overlaying point clouds within HBIM environments.

6.2.2 Practical contributions (heritage documentation in Aleppo/Syria)

This work contributes a comprehensive digital record of both the Al-Takiyya Al-Refaia and Al-Tunbugha Mosque, two monuments at risk within Aleppo's historic urban fabric. The models produced not only support conservation planning but also safeguard intangible cultural value by preserving architectural knowledge in digital form. More broadly, the study demonstrates the feasibility of applying HBIM to Syrian heritage under resource, access, and contextual constraints, offering a replicable framework for other documentation efforts in conflict-affected contexts.

6.3 LIMITATIONS

This research, while advancing the documentation and HBIM modeling of Al-Tunbugha Mosque, is subject to several limitations that should be acknowledged. These can be grouped into technical, methodological, and contextual categories.

6.3.1 Technical limitations

The project relied primarily on photogrammetric data acquisition, which is inherently sensitive to lighting conditions, image overlap, and camera calibration. Although efforts were made to optimize capture strategy and reduce file sizes, the processing of very large image datasets remained computationally demanding and at times limited the efficiency of the workflow. Drone-based imaging improved roof coverage but was constrained by flight regulations and atmospheric conditions. Furthermore, the accuracy of point-cloud reconstruction was dependent on the density and distribution of ground control points, which could not always be placed in ideal positions due to access restrictions.

6.3.2 Methodological limitations

The refined methodology emphasized direct point-cloud modeling without relying on rectified images or CAD as intermediaries. While this allowed greater fidelity, it also increased the dependence on interpretative skills during modeling, particularly for highly complex or eroded decorative elements. The adoption of LoD 500 for selected parts of the mosque achieved exceptional detail but significantly extended modeling time, making it impractical to apply this level uniformly to all architectural components. Additionally, while semantic enrichment was integrated into HBIM, the attribution schema was necessarily selective and did not encompass all possible material or historical data.

6.3.3 Contextual Limitations

The study was conducted under the constraints of limited site accessibility and heritage-at-risk conditions. Permissions and scheduling with local authorities restricted the duration and frequency of field campaigns. Broader geopolitical and logistical challenges in the region influenced what could be feasibly documented. Finally, while the methodology was refined through a pilot study and applied to a major case, its generalizability to other heritage sites may be conditioned by differences in architectural typology, scale, and site accessibility.

6.4 RECOMMENDATIONS FOR FUTURE RESEARCH

- **HBIM integration with other tools:** Future research should explore integration of HBIM with GIS platforms, structural analysis tools, and conservation management systems to enhance interdisciplinary use.
- **Broader application across heritage sites:** Testing the workflow on a wider range of Syrian monuments—mosques, churches, domestic architecture—would strengthen the generalizability of findings and adapt the methodology to varying scales and typologies.
- **Use of advanced scanning (LiDAR, etc.):** Incorporating LiDAR or structured-light scanning would enhance surface detail capture and mitigate limitations tied to lighting, overlap, and texture, while providing complementary datasets to strengthen HBIM accuracy.
- **Semantic enrichment:** Future models should expand the attribution schema to include more detailed material, historical, and conservation data, thereby improving the HBIM model's long-term utility as a conservation database.

- **Workflow optimization under constraints:** Further work is needed to streamline processing times, reduce hardware demands, and adapt HBIM practices for resource-limited and conflict-affected contexts.

CHAPTER 7. BIBLIOGRAPHY

A'akeeli, R. I. (2013). *Architectural and archaeological documentation using 3D modeling.* Aleppo: Univerisity of Aleppo.

Aleppo: Publications of Aleppo .*Historical landmarks of Aleppo* .(1990) .Abdulla Hajjar .University and the Aleppo Antiquities Society

Abras, E. (2020). HADAD Project. *First Aid and Recovery of Syrian Cultural Heritage in Times of Crisis (FAR)*. Aleppo, Syria.

Al-Refai, M. B. (2017). *The Al-Rifai family in the course of history.* Beau Bassin: Nour Publishing.

Berlin, M. f. (n.d.). *Aleppo Heritage Catalogue* . Berlin: Museum for Islamic Art in Berlin.

Faugeras, O. (1996). *Three-Dimensional Computer Vision: A Geometric Approach.* MIT Press.

Hartley, R., & Zisserman, A. (2003). *Multiple View Geometry in Computer Vision.* Cambridge : Cambridge University.

ICOMOS, I. (2019). *Illustrated glossary on stone deterioration patterns.* (V. Vergès-Belmin, Ed.) ICOMOS.

LLC, A. (2022). *Agisoft Metashape User Manual.* Agisoft LLC.

Othman, N. (2009). *Historical monuments and archaeological sites in Aleppo, Kilis, and Gaziantep.* Aleppo: Syrian-Turkish Regional Cooperation Program.

Othman, P. I. (2013). *Photogrammetry.* Aleppo: University of Aleppo.

Saleh, M., & Winterstein, C. (2022). *Post-Conflict Recovery of Cultural Heritage.*

Tandon, A. (2018). *First Aid to Cultural Heritage in Times of Crisis.* Via di San Michele 13, 00153, Rome, Italy: ICCROM. Retrieved from https://www.iccrom.org/publication/first-aid-cultural-heritage-times-crisis-handbook

Torre, M. d. (2002). *Assessing the Values of Cultural Heritage.* Los Angeles: The Getty Conservation Institute.

Tsai, R. (1987). *A Versatile Camera Calibration Technique for 3D Machine Vision.* IEEE J. Robotics & Automation.

CHAPTER 8. APPENDICES

8.1 APPENDIX A. DAMAGE MAPPING[22]

All changes to archaeological sites, whether caused by environmental or human factors, must be assessed and documented. Thorough examination and condition assessment are essential components of the decision-making process and planning for any intervention. Damage assessment is a complex process that requires collaborative, multidisciplinary work (engineers, architects, archaeologists, craftspeople, public authorities, etc.).

8.1.1 ALTERATION PHENOMENA

Phenomena	Definition	Example
Alteration **تغيّر**	Modification of the material that does not necessary imply a worsening of its characteristics from the point of view of conservation. For instance, a reversible coating applied on a stone may be considered as an alteration.	
Degradation **تدهور**	Decline in condition, quality, or functional capacity.	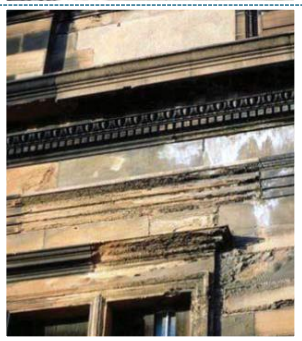
Weathering **تجوية**	Any chemical or mechanical process by which stones exposed to the weather undergo changes in character and deteriorate	

[22] (ICOMOS, 2019)

Decay **اضمحلال**	Any chemical or physical modification of the intrinsic stone properties leading to a loss of value or to the impairment of use.	
Deterioration **تلف**	Process of making or becoming worse or lower in quality, value, character, etc...; depreciation.	
Damage **ضرر**	Human perception of the loss of value due to decay.	

8.1.2 DAMAGE CATEGORIES

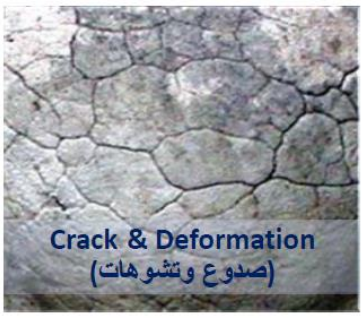

8.1.2.1 *Crack and Deformation*

8.1.2.2 *Detachment*

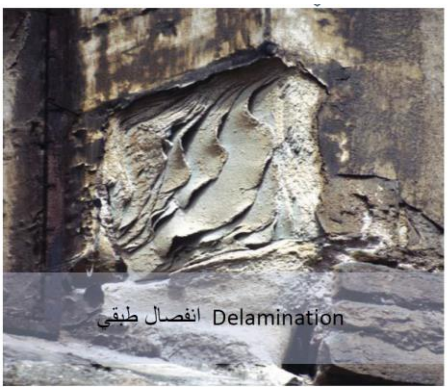

8.1.2.3 *Material Loss*

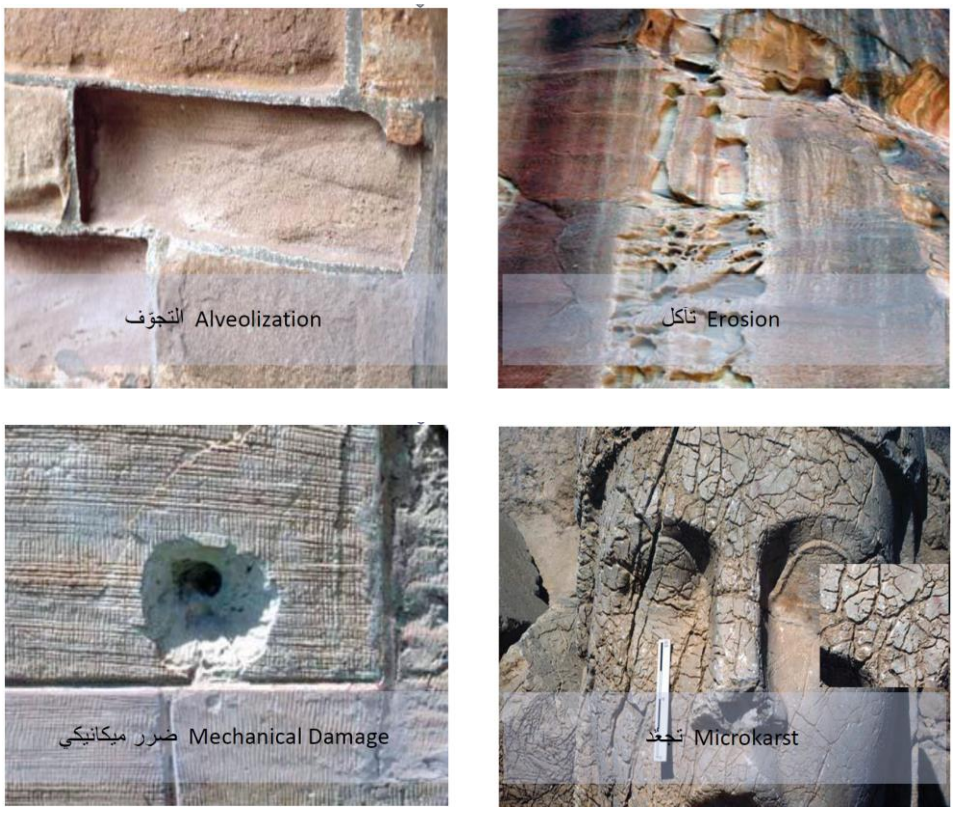

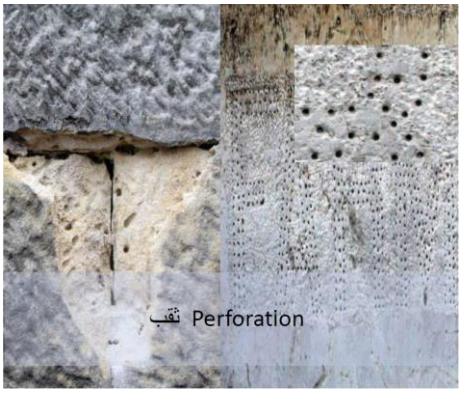

8.1.2.4 *Discoloration and Deposit*

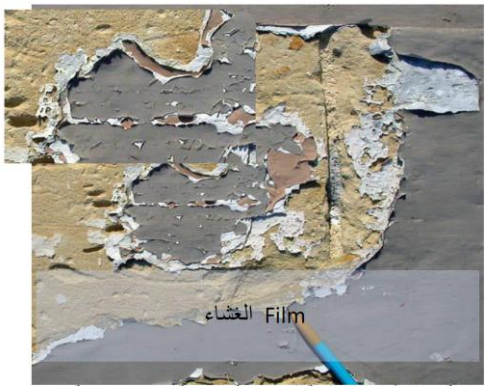


جانب مصقول Glossy Aspect


كتابة على الأحجار Graffiti

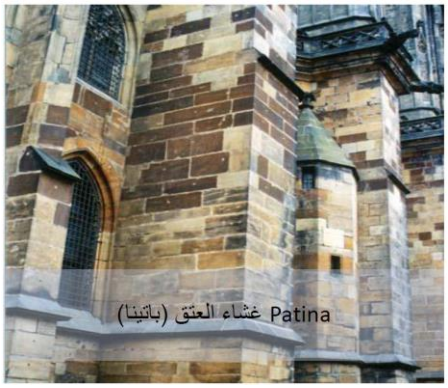
غشاء العتق (باتينا) Patina


أوساخ Soiling


طفح ملحي Efflorescence


تزهّر Subflorescence


تغيير اللون Discoloration

8.1.2.5 *Biological Colonization*